I. MATRIX ISOLATION OF 1,1-DIAZENES

II. DISTANCE, TEMPERATURE, AND DYNAMIC SOLVENT EFFECTS ON ELECTRON TRANSFER REACTIONS

Thesis by

James Edward Hanson

In Partial Fulfillment of the Requirements

for the Degree of

Doctor of Philosophy

California Institute of Technology

Pasadena, California

1990

(Submitted September 8, 1989)

Acknowledgements

I would like to thank my advisor, Peter Dervan , for his enthusiasm and support during my studies at Caltech. I would also like to thank Professor John Hopfield for his availability when I needed assistance with the theoretical complexities of the electron transfer work. I am deeply indebted to Lutfur "Zeta" Khundkar and Joe Perry for their expert assistance and collaboration in making measurements and understanding the implications of the results. Al Sylwester was extremely helpful in my first year as I began to work on 1,1-diazenes, and Alvin Joran and Burt Leland made my transition to the electron transfer project relatively simple. I should also thank those in the Dervan group who helped me with synthetic problems, especially John Griffin and Warren Wade. I appreciated discussions with some of the electron transfer experts at Caltech: Professor Rudy Marcus, Dave Beratan, Jose Onuchic, Dave Malerba, and Tad Fox. There were many times when the men in the chemistry shops provided invaluable assistance--you guys are the best! There are many who made my stay at Caltech enjoyable--I'll remember skiing with John and Linda Griffin and Heinz Moser, basketball (and marathons!) with Dave Kaisaki, tennis with Erich Uffelmann, and late night conversations with Kevin Luebke. There are also many outside Caltech who helped me keep a (tenuous) grip on reality. I appreciated weekends at the beach with Mike and Cathy Constantz or my cousins Jeff and Elizabeth Light. I am also grateful for the friendship of Ranjit Bhaskar, Joyce Stinson, Steve Burns, Dave Blakkolb, Bill Edmund, and many others. Finally, I must thank my parents for their love and support.

Abstract

Part I: Investigations of the reactive intermediates known as 1,1-diazenes or aminonitrenes are reported. These unstable species were generated by UV photolysis of appropriately substituted carbamoyl azides under matrix isolation conditions. Four systems were investigated: three cyclic dialkyl 1,1-diazenes (1,1-tetramethylene-diazene **1**, 1,1-trimethylenediazene **2**, and 3,4-dehydro-1,1-tetramethylenediazene **15**) and the first diaryl 1,1-diazene, 1,1-diphenyldiazene **22**. 1,1-Diazene **1** could be generated by broad band UV photolysis (200-400 nm) of the carbamoyl azide, but **2** and **22** required narrow band photolysis (290-310 nm) and gave poorer yields. 1,1-Diazene **15** could not be isolated even at 10 K. The chemical and spectroscopic properties of the 1,1-diazenes were investigated in some detail, and the results were analyzed with regard to the stability of the various 1,1-diazenes and the different reactive pathways available to 1,1-diazenes with different substituents.

Part II: The dependence of intramolecular electron transfer rates for porphyrin-quinone compounds on distance and temperature was studied. It was found that the rates depend exponentially on the edge-to-edge donor acceptor distance R_e as

$$k_{ET} = k_0 \exp [-\alpha R_e]$$

with α values of 1.10 to 1.25 in different solvents. The temperature dependence studies revealed that the electron transfer rates are not activated in a classical sense, but instead depend on the dynamic relaxation properties of the solvent. In 2-methyltetrahydrofuran, the rates are nearly independent of temperature at high temperatures (200-300 K), then begin to decrease with decreasing temperature. In toluene, the rates *increase* with decreasing temperature, while in deuterated toluene the rates initially increase with decreasing temperature, then go through a maximum

around 215 K, and finally decrease. Apart from the unusual *solvent* isotope effect in the toluene and toluene-d_8 data, this appears to be the first observation of the rate turnover with solvent "friction" predicted by Kramers. The results were analyzed in terms of theoretical predictions of the dependence of electron transfer rates on the longitudinal relaxation time of the solvent τ_L using the equation

$$k_{ET} = \frac{k_{NA}}{1.00 + \frac{\alpha}{k_{NA}\,\tau_L} + \gamma\, k_{NA}\,\tau_L}$$

where k_{NA} is a maximum rate and α and γ are fitted parameters. This equation gave reasonable fits to the data for all three solvents.

Table of Contents

List of Figures

List of Tables

Part I

Matrix Isolation of 1,1-Diazenes

Chapter 1

Introduction: 1,1-Diazenes

Nearly a century has elapsed since the chemical species now known as 1,1-diazenes were first proposed as reactive intermediates.[1] For many years knowledge of 1,1-diazenes was indirect, inferred from the product distributions of reactions believed to involve 1,1-diazene intermediates. These studies laid a foundation by delineating the reactive channels open to 1,1-diazenes and providing data on the mechanisms of these reactions and the influence of various substituents.[2] In recent years, it has become possible to perform theoretical calculations of sufficient precision to give reasonable values for chemical and physical properties of 1,1-diazenes that experiments had been unable to address. In the past decade, 1,1-diazenes have been studied directly, providing experimental data on their electronic states, molecular vibrations, and reactivity. This introduction is a summary of the 1,1-diazene literature that is relevant to the first part of this dissertation.

A Note on Nomenclature.

Two resonance structures can be drawn for 1,1-diazenes, as shown for the diethyl derivative in Scheme 1. Canonical structure **A**, with the double bond between the nitrogen

Scheme 1. 1,1-Diazene resonance structures.

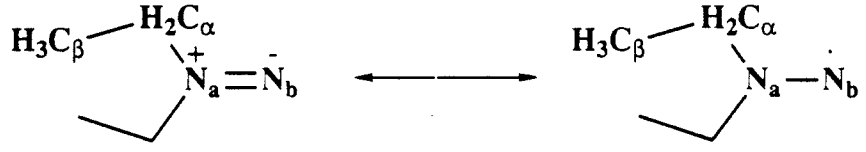

A **B**

centers, suggests the name *1,1-diazene*, and appears to be the best representation of this species based on current experimental and theoretical data. Structure **B** suggests the other name commonly used in the literature, *aminonitrene*.[3] This term has sometimes led to designation of N_a as the *amino nitrogen* and N_b as the *nitrene nitrogen*. Since this is misleading as regards the nature of these centers, the designations *central nitrogen* and *terminal nitrogen* will be used in this work. It is customary to label the carbon centers with Greek letters (α,β,γ, etc.) by analogy to carbonyls.

A. Chemistry of 1,1-Diazenes.

Before direct measurements on 1,1-diazenes, the strongest evidence for their existence was the observation of nearly identical products from different reactions that could be conceived as passing through a 1,1-diazene intermediate. These reactions included the oxidation of 1,1-disubstituted hydrazines, neutralization of diazenium ions, thermal or base induced decomposition of 1,1-disubstituted 2-sulfonylhydrazine salts, reaction of secondary amines with difluoramine or sodium nitrohydroxamate (Angeli's salt), and reduction of nitrosamines. The reactive intermediates generated in these reactions demonstrated nearly identical chemistry, and were identified as 1,1-diazenes. The most characteristic reactions observed for these 1,1-diazene intermediates were dimerization to form 2-tetrazenes, fragmentation to yield molecular nitrogen and radical products, rearrangement to hydrazones, and attack on unsaturated systems. Which reactive pathway was observed depended on the substituents and reaction conditions. Figure 1 collects the different methods of generation of 1,1-diazenes and their subsequent reactions.

Dimerization to 2-tetrazenes is probably the most general and fundamental reaction of 1,1-diazenes. 2-Tetrazene products are observed when the mildest reaction conditions are employed to generate 1,1-diazenes with weakly interacting substituents. For example,

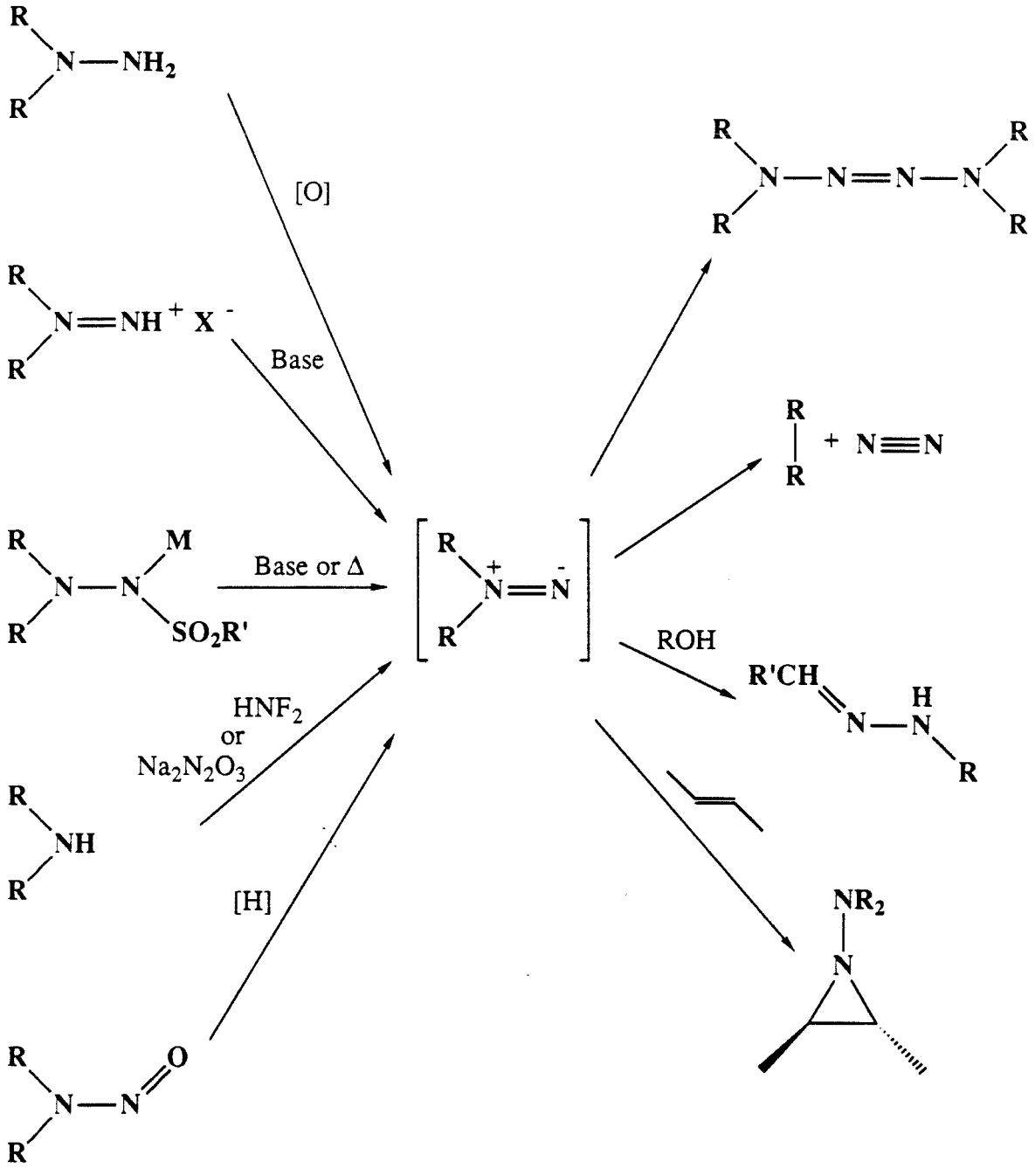

Figure 1. Generation and reactions of 1,1-diazenes.

mercuric oxide oxidation of 1,1-dimethylhydrazine in refluxing ether gives a good yield of 2-tetrazene.[4] The mechanism of tetrazene formation is not entirely clear, and undoubtedly depends on the method of 1,1-diazene generation. In many cases, 1,1-diazenes may react with the more abundant precursor compounds (e.g., hydrazines, diazenium ions) to give tetrazenes. In support of this, Rees was able to isolate an intermediate tetrazane from the oxidation of N-aminophthalimide with lead tetra-acetate.[5] This tetrazane gave the 2-tetrazene on further oxidation.

Although fragmentation could probably be induced for any 1,1-diazene under sufficiently strenuous conditions, it is commonly observed for certain structural types. These include small ring or strained 1,1-diazenes, 1,1-diazenes with an allowed concerted fragmentation pathway, and 1,1-diazenes which fragment to give stabilized radical centers. Fragmentation is in some cases the only observed reaction. The diazene to hydrazone rearrangement is also limited to 1,1-diazenes possessing a certain structural motif, and requires certain reaction conditions as well. Only 1,1-diazenes with α-hydrogens generated in a hydroxylic solvent will give hydrazone products. Addition of 1,1-diazenes to olefins is just as stringent, requiring electron withdrawing substituents and the presence of an appropriate unsaturated substrate.

The entire range of 1,1-diazene reactivity is demonstrated by derivatives of the four, five, and six membered ring cyclic 1,1-diazenes. Mercuric oxide oxidation of N-aminopyrrolidine **i** in refluxing diethyl ether gives the 2-tetrazene dimer.[6] 2-Tetrazene products are also obtained from the 2,5-dimethyl derivatives. Under different conditions,

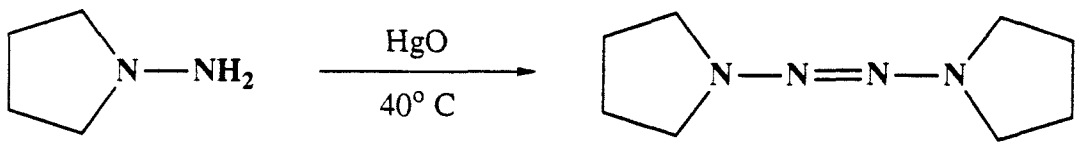

i ii

however, this same 1,1-diazene system can be induced to undergo fragmentation. Lemal found that thermal decomposition of the sodium benzenesulfonamide salt of N-aminopyrrolidine **iii** in refluxing diglyme gave high yields of ethene.[6] No cyclobutane

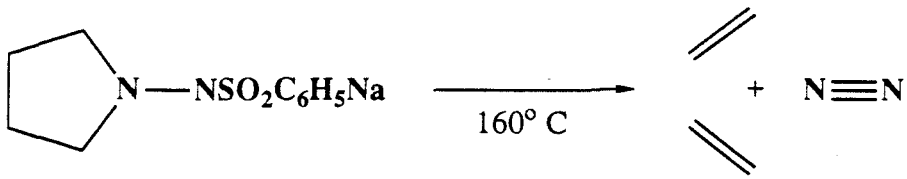

iii

was obtained from this reaction, which suggests that fragmentation of the 1,1-diazene is concerted. In support of this, the six membered ring compound dimerizes to tetrazene and does not lose nitrogen, even at temperatures near 200° C. Another 1,1-diazene which appears to undergo a concerted fragmentation is the 3-pyrroline derivative. Work by Lemal on this system showed that deamination of *cis* and *trans* 2,5-dimethyl-3-pyrrolines **iv** and

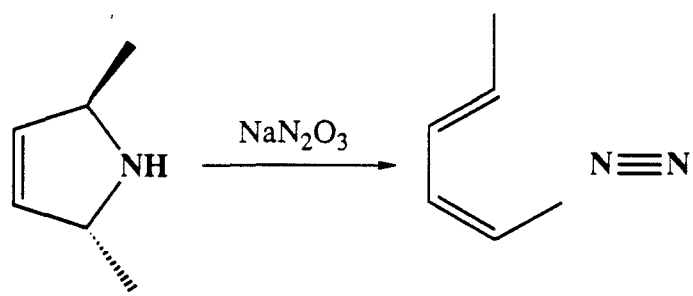

iv

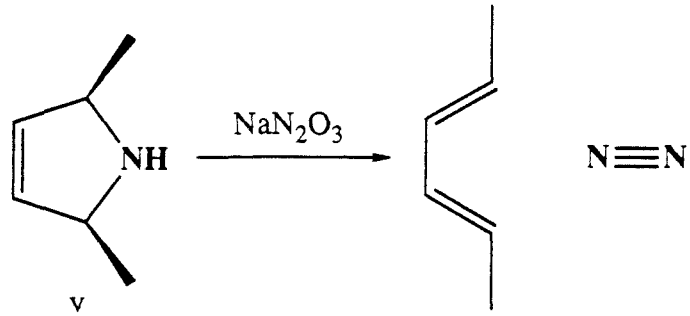

v

v with sodium nitrohydroxamate gave the products of disrotatory nitrogen extrusion exclusively, in accord with orbital symmetry considerations.[7]

Fragmentation can also be induced by radical stabilizing substituents on the α-carbons. Oxidation of 2,5-diphenyl-N-aminopyrrolidine **vi** gives 1,2-diphenylcyclobutane and styrene rather than 2-tetrazene.[8] The cyclobutane is formed with >90% retention of stereochemistry. It is not necessary to substitute both α-carbons, as shown by Overberger

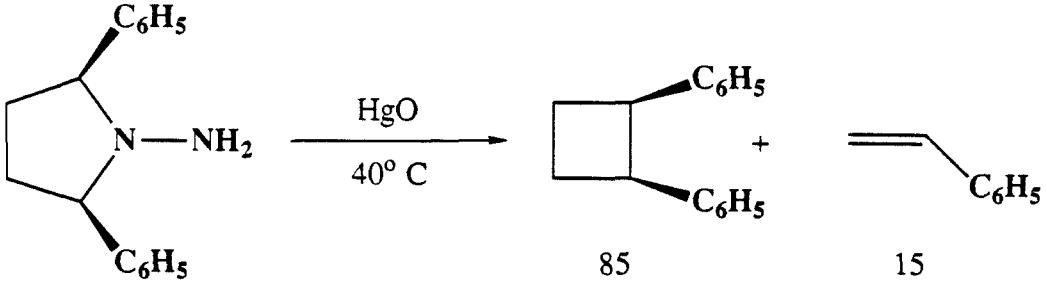

vi vii

in the case of 2-phenyl-N-aminopiperidine **viii**.[9] This compound gave cyclopentane and olefin products when added dropwise to mercuric oxide in refluxing ethanol. Rapid

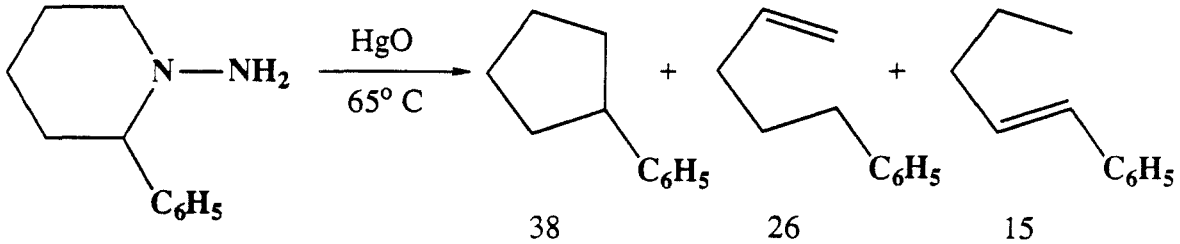

viii ix x xi

addition gave a significant yield of 2-tetrazene. These results are consistent with later observations on kinetically persistent 1,1-diazenes and with theoretical calculations on the strength of the remaining C-N bond after one bond cleavage (see below). Incorporation of the 1,1-diazene functionality into a smaller ring also leads to fragmentation, as

demonstrated by various azetidine systems. Deamination of azetidine with difluoramine gives cyclopropane.[10] Freeman studied the stereochemistry of this system and found that *cis* 2,4-dimethyl-N-aminoazetidine **xii** gave mostly *trans* 1,2-dimethylcyclopropane on oxidation, while the *trans* isomer gave mostly *cis* 1,2-dimethylcyclopropane. Similar ratios were observed using the nitrosamine reduction or difluoramine deamination reactions to generate the 1,1-diazene.[11] No olefins were found, providing a slight contrast to the

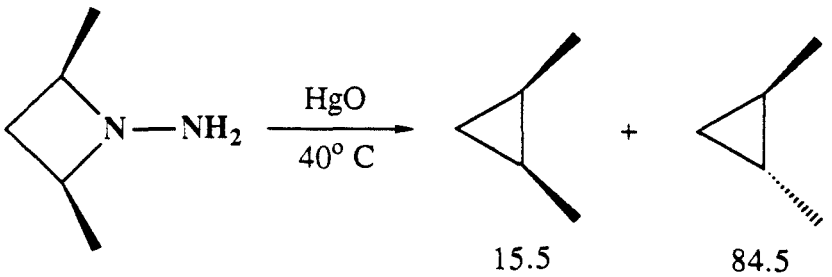

xii xiii xiv

1,2-diazene (pyrazoline) decompositions studied by Crawford and Mishra, where a small amount (2%) of 2-pentene was obtained.[12] The 2-tetrazene dimer was obtained by Kirste *et al* from N-aminoazetidine by extremely gentle oxidation.[13] The reaction conditions were quite unusual, and the yield was also low (31%).

The five membered ring 1,1-diazene will also undergo the diazene to hydrazone rearrangement. Treatment of tosyl-N-aminopyrrolidine **xv** with sodium methoxide in methanol results in formation of the cyclic hydrazone, 1,4,5,6-tetrahydropyridazine.[14]

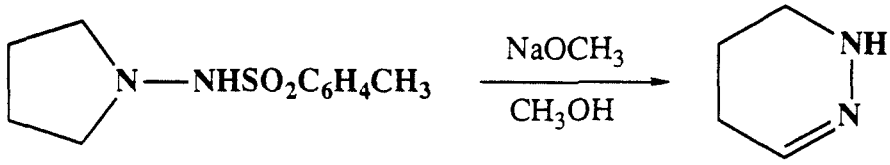

xv xvi

This rearrangement can also be induced by silica gel oxidation of the hydrazine in 98:2 chloroform/methanol.[15] The mechanism of the diazene to hydrazone rearrangement is poorly understood. It has been demonstrated that neither a 1,2-diazene nor a diaziridine intermediate is involved.[16] The requirement of hydroxylic solvents for the diazene to hydrazone rearrangement points to the azomethinimine tautomer as an intermediate. Azomethinimines are related to 1,1-diazenes in the same way enols are related to ketones, and have been shown to be involved in some 1,1-diazene reactions. Lemal found that

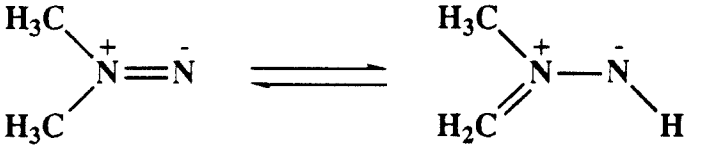

N-benzenesulfonamidopiperidine **xvii** gave the hexahydro-*s*-tetrazine when decomposed in hydroxylic solvents,[14] although 2-tetrazene products were observed in non-hydroxylic solvents. This product is the result of head to tail dimerization of the azomethinimine.

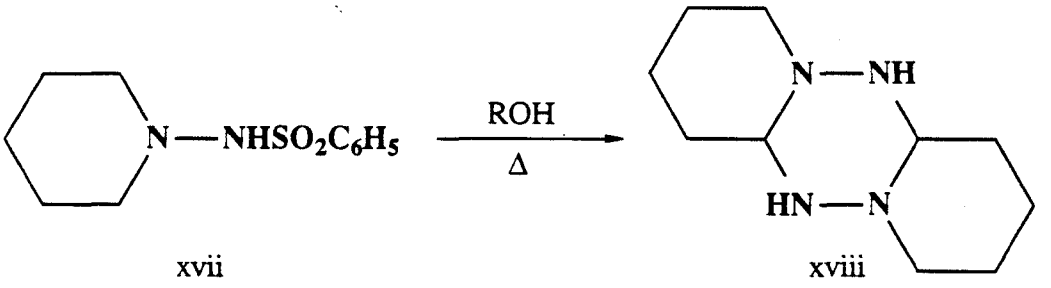

xvii xviii

Azomethinimines may be formed by tautomerization of 1,1-diazenes or directly from starting material by loss of a proton from the α-carbon instead of the terminal nitrogen. Huisgen found that azomethinimines could be intercepted with carbon disulfide and other dipolariphiles and the trapped products isolated.[17] A mechanism for the diazene to

hydrazone rearrangement involving the azomethinimine was proposed, as shown in Scheme 2.[16] Labelling studies, however, demonstrated that this mechanism is incorrect,

Scheme 2. Original mechanism proposed for the diazene to hydrazone rearrangement.[16]

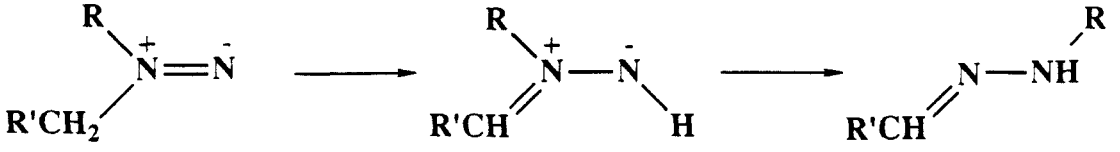

and that the actual mechanism is more complex. Lichter synthesized 1,1-diethyl-2-benzene-sulfonylhydrazine **xix** with a ^{15}N label incorporated at the terminal nitrogen, and decomposed it in dry diethylene glycol with diethylene glycol sodium salt. Degradation to acetonitrile and ethyldimethylamine and subsequent mass spectrometry revealed labelled acetonitrile.[18] This indicates that the terminal nitrogen becomes the doubly bonded nitrogen

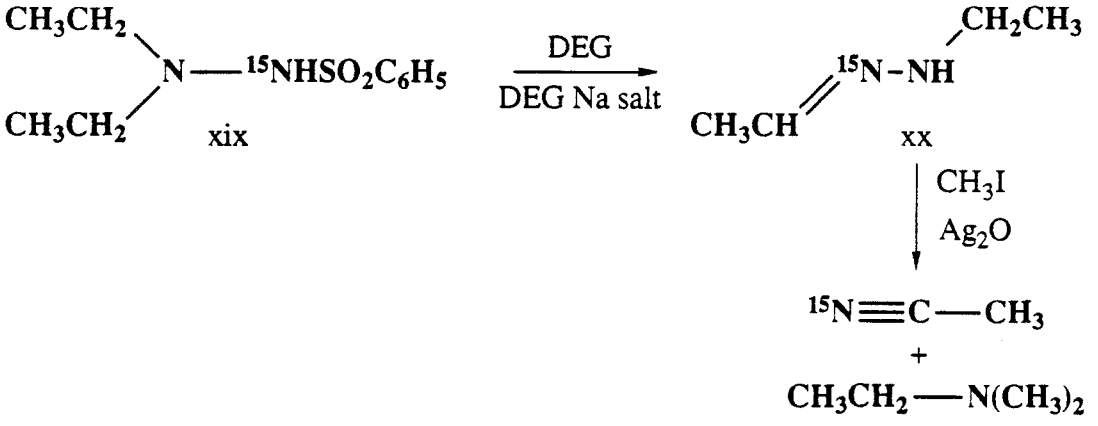

of the hydrazone, which contradicts the predictions of the mechanism in Scheme 2. Crossover experiments showed that the hydrazone products are the result of an intramolecular reaction, and excluded dimerization of the azomethinimine to the hexahydro-*s*-tetrazine followed by cleavage to hydrazone.[19] The experimental evidence points to a rather extraordinary mechanism in which the "alkylidene" substituent of the azomethinimine migrates to the terminal nitrogen. (Scheme 3) This requires extensive rearrangement of the

Scheme 3. Revised mechanism proposed for the diazene to hydrazone rearrangement.[2a]

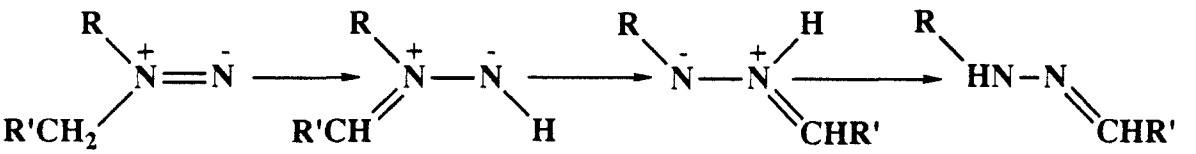

π and σ systems of the azomethinimine, yet the barrier to the reaction is not high, since in many cases rearrangement occurs readily at room temperature. At this point it should be noted that the dipolar structure commonly drawn for azomethinimines is only one of three reasonable resonance structures. Calculations on azomethinimines[20] indicate that a singlet

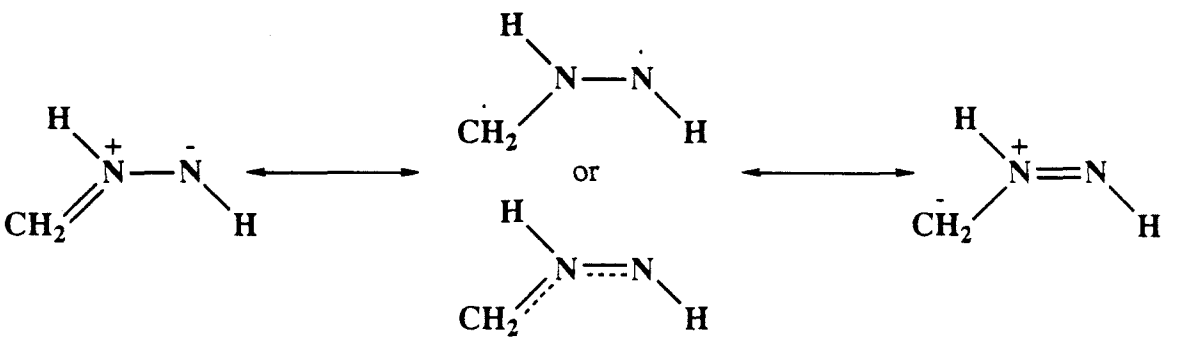

diradical electronic structure resembling isoelectronic ozone may be the best representation. It should also be noted that most of the work on this rearrangement was done over twenty

years ago, and new experimental and theoretical studies employing modern instrumentation (the labelling and crossover experiments should be especially suited for ^{15}N and ^{13}C NMR) and computational power might be able to cut through this mechanistic Gordian knot.

1,1-Diazenes with electron withdrawing substituents (especially carbonyls) will add to olefins to give N-aminoaziridine derivatives. N-Aminophthalimide is typical of hydrazine

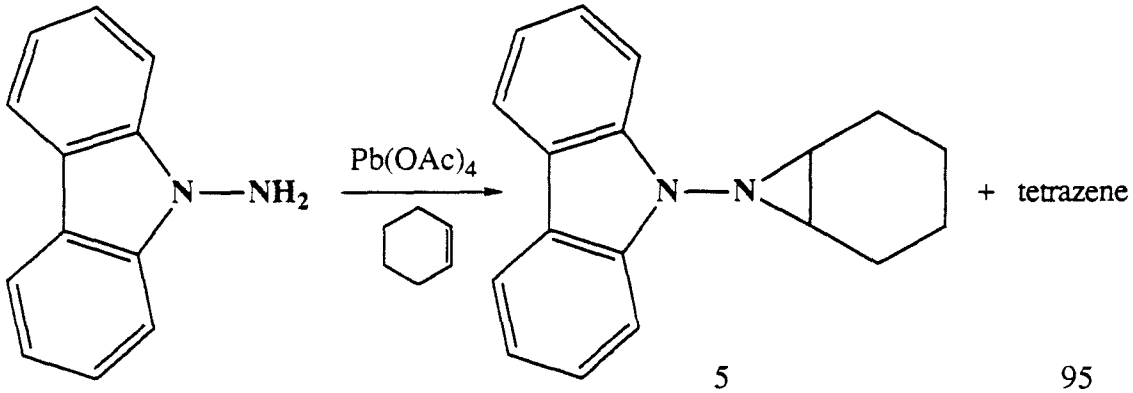

precursors for this reaction, but even N-aminocarbazole **xxi** gave some addition products along with 2-tetrazene.[2a] In other systems formation of N-aminoaziridines has been shown to be stereospecific, and this has been interpreted as an indication of a singlet ground state for the 1,1-diazenes.[21] Dialkyl 1,1-diazenes have not been observed to add to olefins.

The five membered ring 1,1-diazene demonstrates a remarkable change in mechanism with what appear to be fairly small changes in reaction conditions. In non-hydroxylic solvents, raising the temperature for decomposition from 40 to 160° C results in a switch from nearly complete dominance of dimerization to exclusively fragmentation. At room temperature, the addition of a small amount of a hydroxylic solvent results in rearrangement as the only observed reaction. This wide variability is a rather special case, since the six membered ring 1,1-diazene resists both fragmentation and rearrangement

while the four membered ring 1,1-diazene fragments preferentially. The availability of a low energy concerted fragmentation pathway and the formation of a six membered ring on rearrangement are probably responsible for this unique behavior of the five membered ring compound. The influence of structural effects on 1,1-diazene chemistry is underscored by the rather large differences in reactivity between these three compounds which would appear to be quite similar.

B. Theoretical Studies.

The chemistry of dinitrogen compounds has received considerable theoretical attention. The stability of many dinitrogen derivatives is low, requiring calculations to supplement sparse experimental data. The three isomers of diimide (H_2N_2) have been the subject of a number of theoretical studies. Only *trans* diimide was known prior to 1984, and several theorists worked to establish the relative energies of the less stable forms along with the energetics of their isomerization to *trans* diimide.[22] 1,1-Diimide (sometimes called *iso*diazene) is the simplest 1,1-diazene, and calculations also sought to describe its low-lying electronic states as a model for other 1,1-diazenes.

Most nitrenes possess a triplet ground state, but the chemical reactivity of *amino*nitrenes suggests a singlet ground state. Establishing the ground state multiplicity of 1,1-diimide was the objective of numerous calculations during the 1970's. The most complete study was performed over a decade ago by Davis and Goddard.[23] This work used the generalized valence bond (GVB) approach[24] with configuration interaction (CI) and employed a valence double zeta basis set with polarization functions. The most important findings of Davis and Goddard are summarized in Figure 2. The ground state is a planar singlet ($^1A_1$) with C_{2v} symmetry and considerable dipolar character. The lowest lying excited state is a triplet ($^3A_2$) 0.6 eV above the ground state. The lowest lying singlet

excited state ($^1A_2$) lies 2.2 eV above the ground state. These excited states correspond to the triplet ground state and lowest singlet state of nitrene (NH). The $^1A_1$ ground state corresponds to a higher excited state in nitrene, but in 1,1-diimide the delocalization of the central nitrogen lone pair into an empty orbital on the terminal nitrogen results in a large stabilization. This also results in substantial double bond character in the NN bond, as reflected in the short bond length (1.246 Å). In the $^3A_2$ state this delocalization is reduced

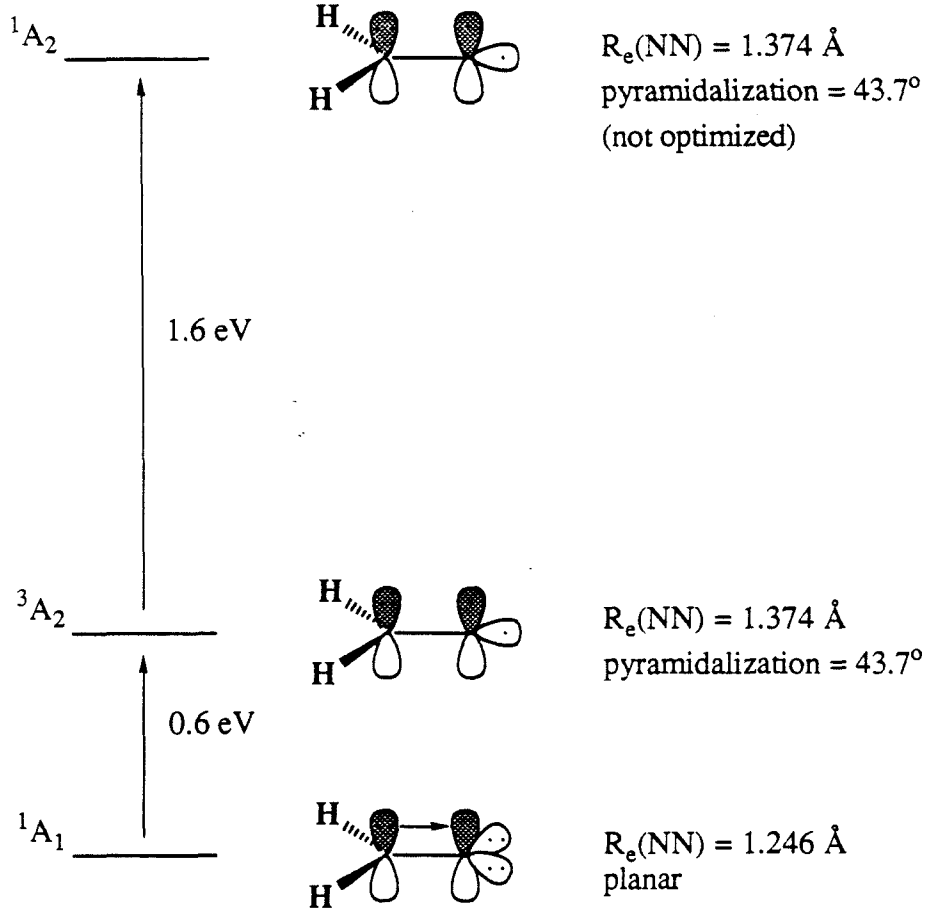

Figure 2. Calculated energies of low lying electronic states of 1,1-diimide.[23]

to two center three electron bonding, and the calculated bond length increases to 1.374 Å. For comparison, the NN bond length in hydrazine is 1.45-1.46 Å[25] and in trans diimide is 1.252 Å.[26] The $^3A_2$ state is also calculated to be pyramidalized to a considerable degree with a 43.7° angle between the HNH plane and the NN axis. The calculated geometry for the $^3A_2$ state was also used for the $^1A_2$ state. The 2.2 eV separation between the ground state and this first singlet excited state should correspond to an $n\rightarrow\pi^*$ transition at 565 nm, predicting that 1,1-diimide (and by analogy other 1,1-diazenes) should be a colored compound which could be detected by optical spectroscopy. Some other important predictions of these calculations for 1,1-diimide are a 9.4 eV ionization potential, a dipole moment of 4.036 D, and a 3.05 eV (70.4 kcal/mol) dissociation energy for the NN bond. Jensen et al., in calculating the H_2N_2 energy surface, found a slightly different geometry for 1,1-diimide.[27] They obtained an even shorter NN bond length (1.224 Å) and also calculated the NH bond lengths (1.038 Å) and the HNH angle (111.2°). This geometry was optimized more fully than the geometry used in the Davis and Goddard calculations.

The mechanism of nitrogen loss from dinitrogen compounds has also been a subject of interest.[28] Recently calculations have been performed to address the question of whether a concerted (two bond cleavage) or stepwise (one bond cleavage) is preferred.[29] The reaction coordinate for decomposition of the three isomers of diethyldiazene to molecular nitrogen and two ethyl radicals was calculated using the MNDO method[30] with 2x2 CI. A 24.3 kcal/mol activation energy was found for one bond cleavage of 1,1-diethyldiazene to ethyl and ethyldiazenyl radicals. The activation energies for recombination of these two radicals were 10.1 kcal/mol going to *cis* 1,2-diethyldiazene and 31.6 kcal/mol going back to 1,1-diethyldiazene. A second cleavage event to give molecular nitrogen and two ethyl radicals had an activation energy of 14.0 kcal/mol. Concerted two bond cleavage from 1,1-diethyldiazene to molecular nitrogen and ethyl radicals had an

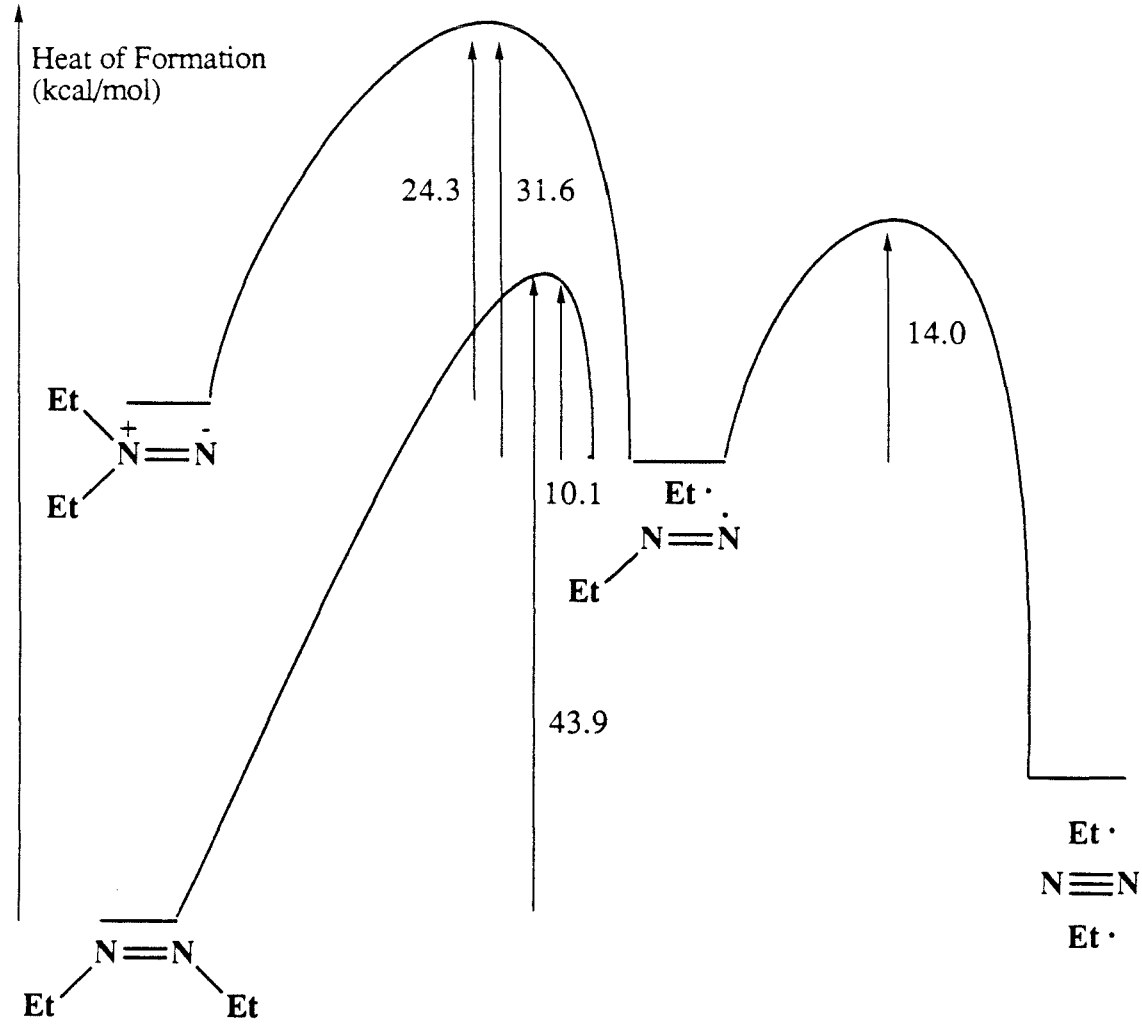

Figure 3. Partial reaction coordinate diagram for diethyldiazene systems.[29]

activation energy of 32.6 kcal/mol. An abbreviated version of the calculated reaction coordinate diagram for the diethyldiazenes is shown in Figure 3. This work predicts that closure of an alkyl/alkyldiazenyl radical pair to the *cis* 1,2-diazene is favored energetically over a second cleavage event. In real systems there would usually be a requirement for motion of the two radical centers after initial formation if recombination is to occur. 1,2-diazenes are not commonly observed from 1,1-diazene decompositions; however, under the conditions required for the first cleavage event to proceed thermally, the alkyldiazenyl radical may undergo the second cleavage faster than diffusion would bring the alkyl radical to a favorable position for recombination. Photochemical decomposition of a 1,1-diazene, on the other hand, could proceed at a temperature low enough that recombination could compete with the second cleavage event, especially if the dialkyl 1,1-diazene were cyclic and the two radical centers could not diffuse apart.

C. Direct Studies of 1,1-Diazenes.

1. Persistent 1,1-Diazenes.

The first direct observation of a 1,1-diazene was reported in 1978.[31] 2,2,6,6-Tetramethyl-1,1-pentamethylenediazene **xxiii** was generated by low temperature (below -78° C) oxidation of the corresponding hydrazine with *tert*-butyl hypochlorite in the presence of triethylamine. By analogy to stabilized free radicals,[32] the tetramethyl substitution presents a "steric blockade" which slows the dimerization reaction. Low temperature slows nitrogen extrusion, and the diazene-hydrazone rearrangement reaction is blocked by the lack of α-hydrogens. The combination of these effects is to render the 1,1-diazene *kinetically persistent*, allowing the application of spectroscopic techniques for characterization. The five membered 2,2,5,5-tetramethyl-1,1-tetramethylenediazene **xxiv**[33] and the acyclic 1,1-di-*tert*-butyldiazene **xxv**[34] were also prepared by this method.

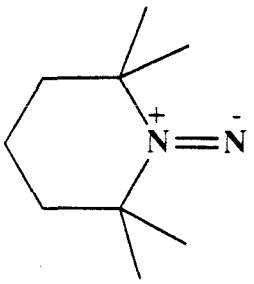

xxiii

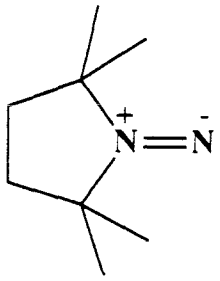

xxiv

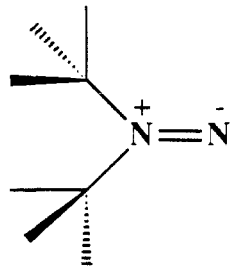

xxv

The techniques used to study these persistent 1,1-diazenes were electronic absorption and emission spectroscopy, infrared (IR) spectroscopy, and nuclear magnetic resonance (NMR) spectroscopy. Absorption and emission spectra of **xxiv** are shown in Figure 4. The 1,1-diazenes have $n \rightarrow \pi^*$ transitions in the visible, as predicted by Davis and Goddard,[23] with λ_{max} of 543, 497, and 506 nm for **xxiii**, **xxiv**, and **xxv** respectively. There is an expected blue shift in more polar solvents and fairly well resolved vibrational structure in the absorption spectra. This structure is associated with a vibration whose equilibrium position is significantly changed by the electronic transition (Figure 5).[35] The largest changes on excitation are lengthening of the N-N bond and pyramidalization. The spacing of the vibrational bands in the absorption spectra corresponds to the N-N stretch (ν_{NN}) of the S_1 state. The average vibrational spacings are 1040, 1238, and 1200 cm^{-1} for **xxiii**, **xxiv**, and **xxv** respectively. Emission occurs from the S_1 state with a quantum yield of 7 x 10^{-3} and a lifetime of 23 nsec.[36] Vibrational structure revealing the S_0 vibrational levels might be expected in the fluorescence spectra. Only **xxiv** shows any structure, with a spacing of 1640 cm^{-1} between the 0,0 and 0,1 bands in the emission spectrum.

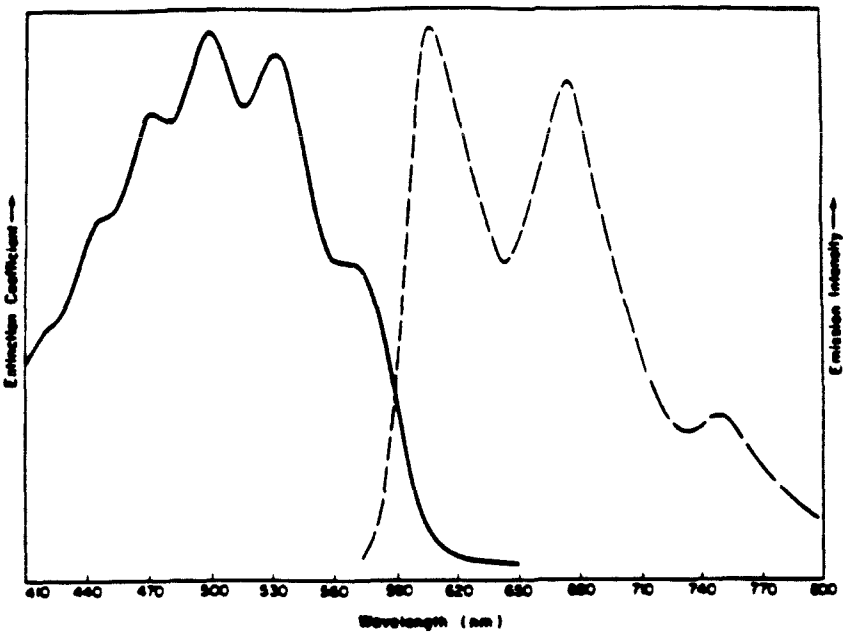

Figure 4. Electronic absorption (———) and emission (- - - -) spectra of 1,1-diazene xxiv in $CFCl_3$ at -78° and -196° C respectively.[36]

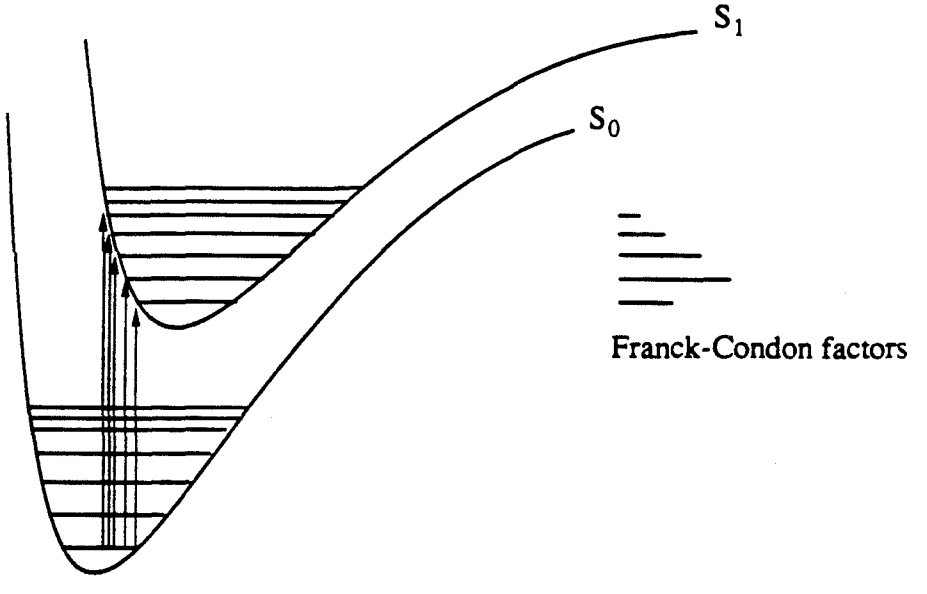

Figure 5. Vibrational structure in an electronic transition. The arrows represent excitation to different vibrational levels of the S_1 state. The Franck-Condon factors for the different vibronic transitions are shown on the right. These factors relate to intensities in the absorption spectrum.

Infrared spectra could be obtained for **xxiii** and **xxiv** in dichloromethane. Bands at 1595 cm^{-1} for **xxiii** and 1638 cm^{-1} for **xxiv** were characterized as the N=N stretches ($\nu_{N=N}$) by preparation of compounds with ^{15}N substitution at the terminal nitrogen, causing an isotopic (Hooke's law) shift to 1568 and 1612 cm^{-1} respectively (Figure 6). A doubly labelled isotopomer of **xxiii** was synthesized for characterization by ^{15}N NMR spectroscopy.[37] By using both singly and doubly labelled compounds, the central and terminal nitrogen resonances were assigned at 321.4 and 917.0 ppm downfield from $^{15}NH_3$ (anhydrous) (Figure 7). The terminal nitrogen resonance is among the most highly deshielded ever observed in a neutral organic compound.

Warming the solutions of 1,1-diazenes allowed analysis of their decomposition products and kinetics.[38] At low temperatures, dimerization is the main reaction pathway due to the low activation energy (E_a=6.4±0.9 kcal/mol, log A=3.8±0.7 for **xxiii**). At higher temperatures, nitrogen extrusion becomes the main pathway for decomposition due to the higher pre-exponential factor (E_a=20.0±0.4 kcal/mol, log A=13.7±0.3 for **xxiii**). The product ratios obtained from decomposition of **xxiv** are relevant to the present work, so they are listed in Table I. Photochemical decomposition of 1,1-diazene **xxiv** by direct and triplet sensitized photolysis gave 2-tetrazene and hydrocarbons in 4:1 and 9:1 ratios respectively.[36] The reaction of the nitrene-like S_1 and T_1 excited states with the S_0 state is very fast and accounts for the high yield of tetrazene from solution photolysis. Excited state parameters for **xxiv** are summarized in Figure 8. Direct and triplet sensitized photolysis of chiral 1,1-diazene **xxvi** demonstrates a spin-correlation effect.[36b]

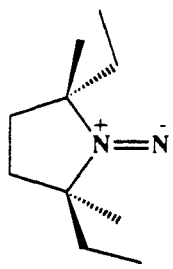

xxvi

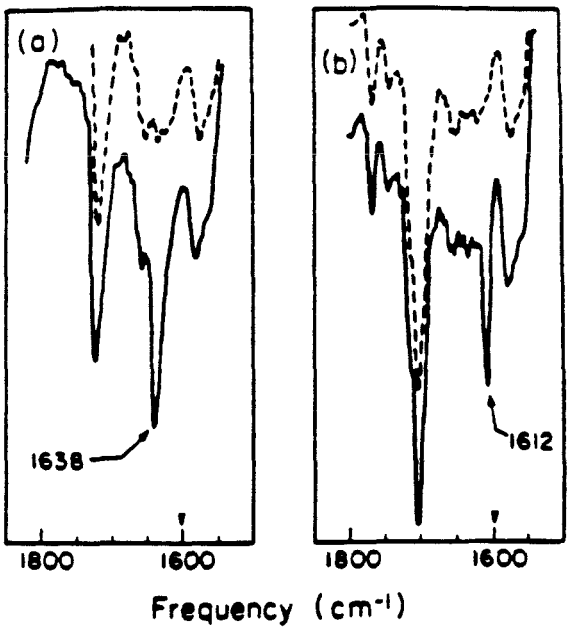

Figure 6. Infrared spectra of 1,1-diazene **xxiv** in CH_2Cl_2: (a) $\nu_{N=N}$ and (b) $\nu_{N=^{15}N}$ at -78° C (——) and after warming to 25° C (- - -).[38]

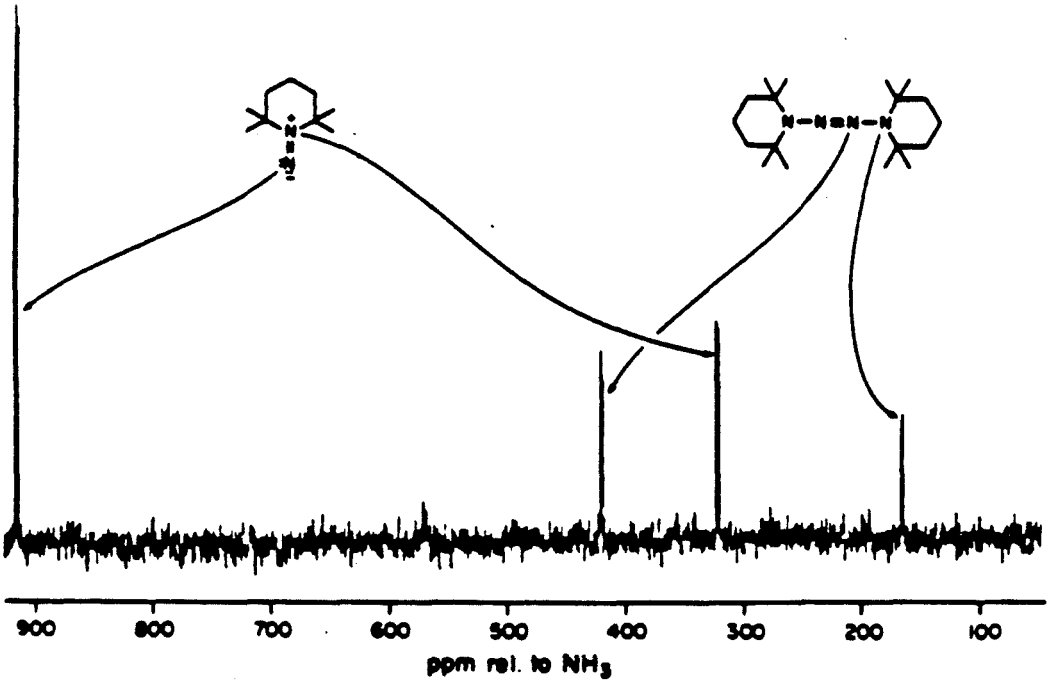

Figure 7. ^{15}N NMR spectrum of doubly labelled 1,1-diazene **xxiii** and 2-tetrazene in dimethyl ether at -90° C.[37]

Table I. Hydrocarbon Product Ratios from Decomposition of 1,1-Diazene **xxiv**.[36]

conditions	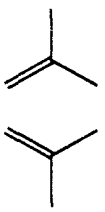	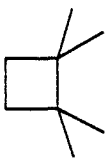	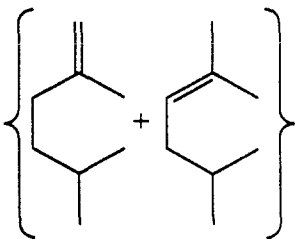
0° C, thermal	47	49	4.0
-10° C, thermal	53	44	3.0
-20° C, thermal	59	39	2.0
-78° C, hν (direct)	54	44	2.0
-78° C, hν (sensitized)	74	24	2.0

The characterization of kinetically persistent 1,1-diazenes **xxiii-xxvi** was a turning point in the study of 1,1-diazenes. They were removed from the realm of chemical speculation and became well-studied chemical entities with characteristic spectral data and known activation parameters. However, the technique used for preparing **xxiii-xxvi** was not capable of extension to 1,1-diazenes lacking the special structural elements which conveyed kinetic persistence to **xxiii-xxvi**. To prepare and characterize these more reactive species, the techniques of matrix isolation and cryochemistry would be required. The extreme low temperatures should shut down nearly all activated chemical reactions,

and immobilization in an inert gas matrix or organic glass would prevent all bimolecular chemistry. A method for generating 1,1-diazenes in an effusive molecular beam prior to deposition or *in situ* in the matrix would be required for the successful application of cryogenic techniques to the study of 1,1-diazenes.

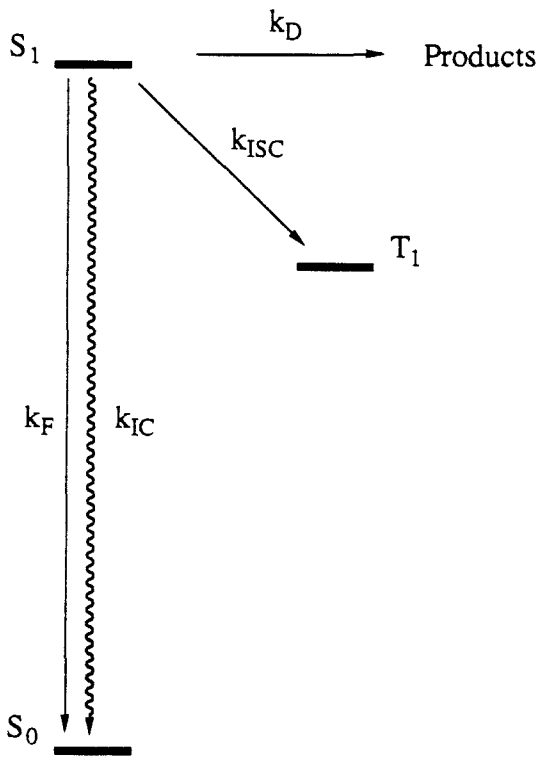

$E(S_1)$ = 2.17 eV (CH_2Cl_2)

$E(T_1)$ < 1.35 eV

τ_F = 2.3×10^{-8} sec (-196° C)

k_F ~ 3×10^5 sec^{-1}

k_{IC} = 1.5×10^8 sec^{-1} (-78° C)

k_D = $k_{DIM} + k_{FRAG}$

k_{DIM} > 4.2×10^7 $mol^{-1}sec^{-1}$ (-78° C)

k_{FRAG} > 3.4×10^5 sec^{-1} (-78° C)

k_{ISC} << k_{FRAG} or ~10^4 sec^{-1}

Figure 8. Photochemical Parameters for 1,1-Diazene **xxiv**.[36]

2. 1,1-Diimide: Matrix Isolation of a 1,1-Diazene.

In 1984 Sylwester and Dervan reported the observation of matrix isolated 1,1-diimide **xxvii**, the simplest 1,1-diazene.[39] The cornerstone of this discovery was the development of a photochemical route to generate 1,1-diimide from a stable precursor. The precursor molecule was carbamoyl azide **xxviii**, a compound first synthesized by Thiele in 1894.[40] On broad band UV photolysis (λ=200-400 nm), carbamoyl azide (λ_{max}=214 and 266 nm) undergoes the photo-Curtius rearrangement to give aminoisocyanate and nitrogen. Aminoisocyanate **xxix** (λ_{max}~350 nm) is subsequently photodecarbonylated to give 1,1-diimide and carbon monoxide (Scheme 4). This work built on the results of Lwowski and Reichen, who had studied the reactions of aminoisocyanates generated by photolysis and thermolysis of carbamoyl azides.[41] This implied that by using substituted carbamoyl azides, this route could be extended to a variety of 1,1-diazenes.

Scheme 4. Photochemical generation of 1,1-diimide.

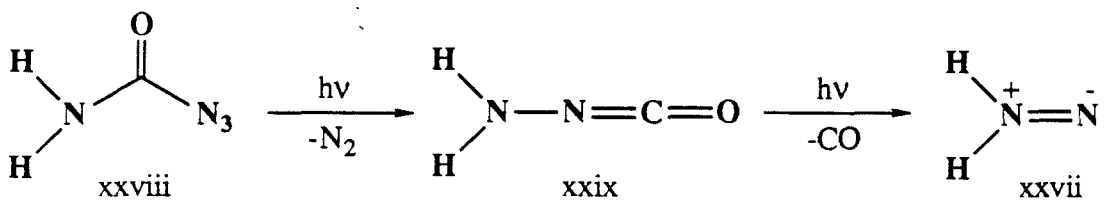

xxviii xxix xxvii

The studies of 1,1-diimide[39,42] showed it to be similar spectroscopically to the kinetically persistent dialkyl 1,1-diazenes that had been studied earlier. Electronic absorption spectroscopy of **xxvii** in a 2-methyltetrahydrofuran (2MTHF) glass at 80 K revealed a blue-violet species with λ_{max}=636 nm and an average vibrational spacing of 1315 cm^{-1} (Figure 9). No emission could be detected from **xxvii**. Infrared spectroscopy of 1,1-diimide and its isotopomers in an argon matrix at 10 K was very revealing. Five

bands were observed for both **xxvii** and **xxvii**-^{15}N, including $\nu_{N=N}$ at 1574.2 and 1547.6 cm^{-1} respectively (Figure 10). The observed spectrum corresponds fairly well with the calculations of Jensen et al., who calculated that $\nu_{N=N}$ should be at 1611 cm^{-1}.[27] 1,1-Diimide should have six molecular vibrations, rather than the five that are observed. According to Jensen et al., the "missing" band would be the rocking motion at 1375 cm^{-1}, however, the intensity is calculated to be quite small. The infrared spectra of the deuterated isotopomers were also studied. This is a reasonably complete set of vibrational data on 1,1-diimide and its isotopomers. NMR experiments were not pursued for **xxvii** since highly specialized equipment (magic angle spinning) is required to obtain NMR data on matrix isolated species.[43] Such experiments might be worth the effort, however, since they could provide structural data for 1,1-diimide.[44]

The thermal decomposition of 1,1-diimide in 2-MTHF is dominated by dimerization to 2-tetrazene and isomerization to 1,2-diimide. These compounds are also unstable at room temperature, and the final products derived from 1,1-diimide are hydrogen, nitrogen, ammonia, hydrazine, and ammonium azide. Photochemical decomposition of 1,1-diimide in a 2MTHF glass at 77 K results in nearly quantitative yields of hydrogen and nitrogen.

3. Simple Dialkyl 1,1-Diazenes.

The usefulness of carbamoyl azide photolysis as a general synthetic method for 1,1-diazenes was demonstrated in studies of several simple dialkyl derivatives.[42] The carbamoyl azide precursors for 1,1-dimethyldiazene **xxx** and 1,1-di-*iso*-propyldiazene **xxxi** were synthesized by standard techniques. Broad band UV photolysis (λ=200-400 nm) of these carbamoyl azides under matrix isolation conditions resulted in the formation of

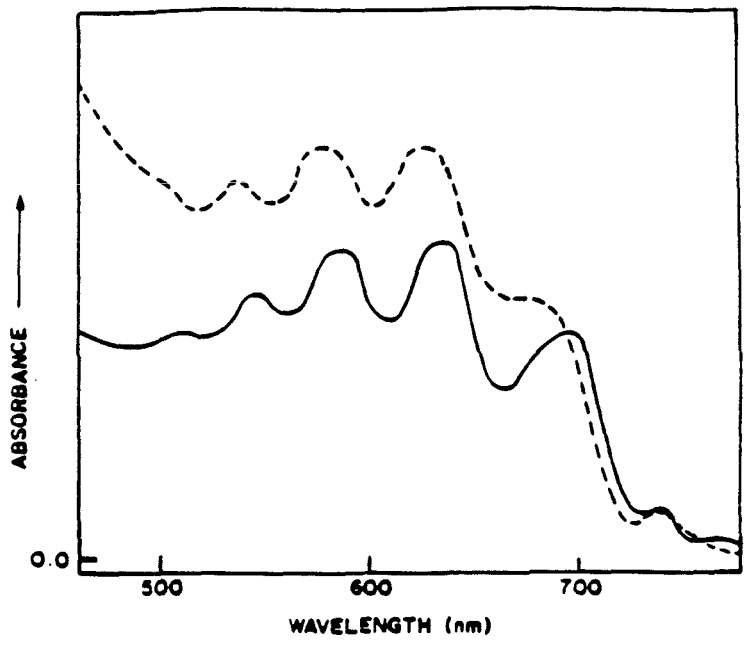

Figure 9. Electronic absorption spectrum of 1,1-diimide **xxvii** at 80 K in 2-MTHF glass (——) and in 1:1 2-MTHF/butyronitrile glass (- - -).[42]

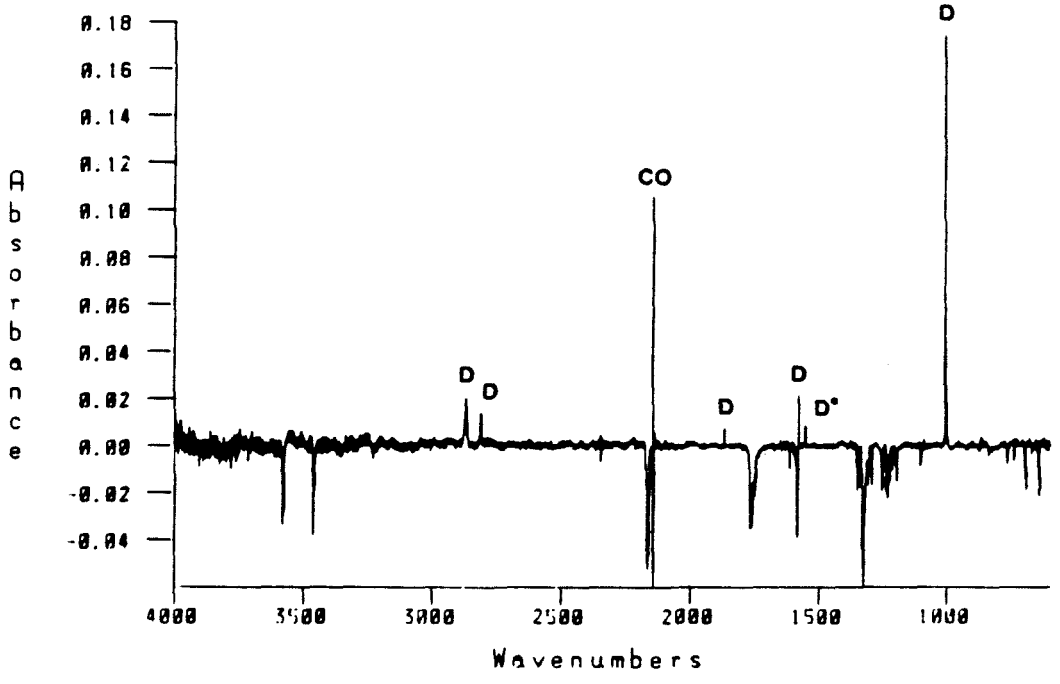

Figure 10. Difference FTIR spectrum of 1,1-diimide **xxvii** (D), ^{15}N labelled **xxvii** (D^*), and CO in an argon matrix at 10 K.[42]

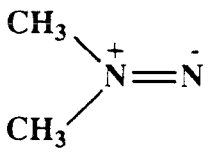

xxx

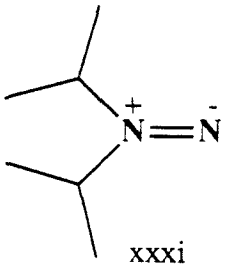

xxxi

the 1,1-diazenes. Electronic absorption spectroscopy (2MTHF glass, 80 K) revealed the characteristic structured absorptions of 1,1-diazenes with λ_{max} of 556 nm for **xxx** and 504 nm for **xxxi**. The average spacing of the vibrational bands was 1315 cm^{-1} for **xxx** and 1306 cm^{-1} for **xxxi**. Preparation of the dimethyl derivative by UV photolysis of (Z)-3,3-dimethyl-1-phenyltriazene-1-oxide **xxxii** in a 2MTHF glass at 80 K allowed estimation of an ε of 6 $M^{-1}cm^{-1}$ for **xxx**. Using the carbamoyl azide precursor, 1,1-dimethyldiazene **xxx** was never generated cleanly in a 2MTHF glass; there was always some contamination

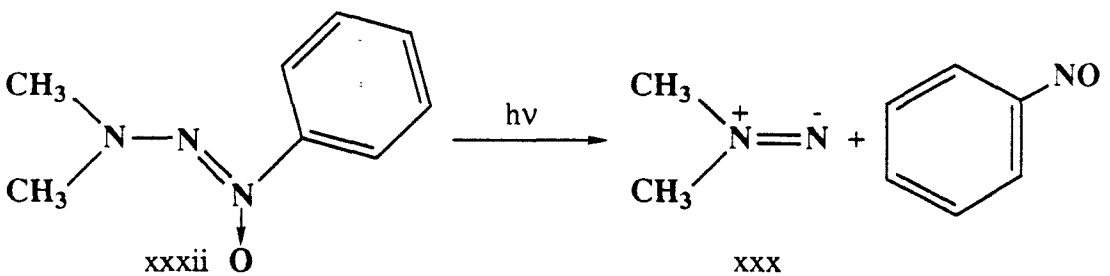

xxxii xxx

by another species with λ_{max}=464 nm. The proposed identity of this contaminant and its relevance to 1,1-diazene chemistry are discussed more fully below. Infrared spectroscopy of **xxx** and **xxxi** revealed $\nu_{N=N}$ of 1601 cm^{-1} for both molecules, with an isotopic shift to 1582 and 1579 cm^{-1} for the terminal ^{15}N derivatives of **xxx** and **xxxi** respectively. When combined with the studies of 1,1-diimide and the persistent 1,1-diazenes, these spectral data reveal a strong resemblance between 1,1-diazenes and the isoelectronic carbonyl

compounds. Similar structural perturbations (i.e., formaldehyde to acetone and 1,1-diimide to 1,1-dimethyldiazene) generally have similar effects on the spectra.

Thermal decomposition of these 1,1-diazenes was dominated by an apparent tautomerization to the azomethinimines. (See the discussion of the diazene to hydrazone rearrangement in section A above.) When a 2MTHF glass of either **xxx** or **xxxi** is warmed to the softening point of 2MTHF (90-92 K), the structured absorption of the 1,1-diazene disappears and is replaced by a strong, structureless absorption (λ_{max}=464 for **xxx**, λ_{max}=474 for **xxxi**). This strong absorption was tentatively assigned to the

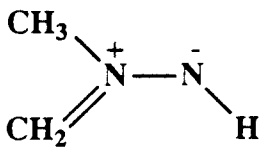

xxxiii

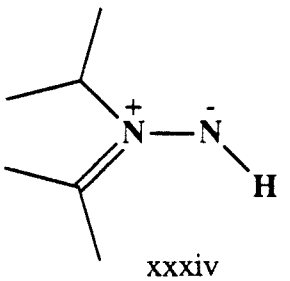

xxxiv

azomethinimine tautomers **xxxiii** and **xxxiv**. There are no reports of simple azomethinimines, but azomethinimines stabilized by aryl substitution or incorporation into a heterocyclic system are known. For example, **xxxv** is a deeply colored species (λ_{max}=460 nm, ε=10600).[45] The spectral similarity to the species observed from thermal

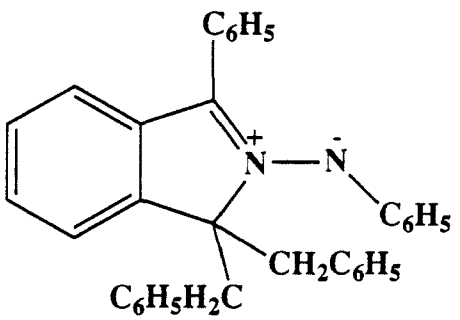

xxxv

decomposition of 1,1-diazenes is striking. Since azomethinimines are tautomers of 1,1-diazenes as enols are tautomers of ketones, studies of keto-enol systems are relevant. The

rate of ketonization of simple enols in water at 25° C is ~10^{-2} sec^{-1}, but acid or base catalysis increases the rate by more than three orders of magnitude.[46] The equilibrium constant is ~10^8 in favor of the ketone form, so the rate of enolization is considerably slower. For the 1,1-diazene/azomethinimine case, the stabilities must be reversed and the isomerization rates must be considerably greater for the transformation to occur at 90 K.

While no spectral evidence was found that the azomethinimines and 1,1-diazenes are in equilibrium, there is strong evidence from kinetic and product analyses that this is the case. Further warming of 2MTHF solutions of **xxxiii** and **xxxiv** derived from the 1,1-diazenes resulted in the loss of the azomethinimine absorption with measurable kinetics. The products obtained from these decompositions are the products expected from the corresponding 1,1-diazenes, however. The thermal decomposition kinetics of **xxxiii** are bimolecular with activation parameters E_a=8.2±0.5 kcal/mol, log A=1.8±0.6. Along with the predominance of tetrazene in the product analysis, this was interpreted as supporting a mechanism where dimerization occurs by reaction of a 1,1-diazene with its azomethinimine tautomer. The presence of a kinetic isotope effect for the perdeuterated isotopomer of **xxx** (and therefore of **xxxiii**) also supported such a mechanism. The thermal decomposition of **xxxiv**, on the other hand, is unimolecular with activation parameters E_a=16.2±0.5 kcal/mol, log A=11.8±0.3. These activation parameters, similar to the unimolecular decomposition parameters for the persistent 1,1-diazenes, combined with the dominance of nitrogen extrusion products expected from **xxxi**, suggests that the rate determining step for the major decomposition pathway in this case is nitrogen extrusion. The spectral data and kinetic and product analyses suggest that 1,1-diazenes and azomethinimines are in equilibrium in 2MTHF (with the azomethinimine the major species), but that the 1,1-diazene tautomer is more reactive and all observed products (2-tetrazenes, hydrocarbons) are the result of 1,1-diazene reactions. No products expected from azomethinimines (s-tetrazines, hydrazones)[14] were observed.

4. Other Experimental Studies.

A few other experimental studies exist which report direct observation of 1,1-diazenes. Bock and Dammel pyrolyzed dimethylaminoazide at 720 K in the gas phase and recorded the photoelectron (PE) spectrum of the products.[47] Digital subtraction of the known PE spectra of observed contaminants methylamine, hydrogen cyanide, and molecular nitrogen left a PE spectrum they interpreted as belonging to 1,1-dimethyldiazene, as shown in Figure 11. There is a sharp band at 8.22 eV corresponding to ionization out of the terminal nitrogen lone pairs, and the other bands were assigned on the basis of MNDO calculations. The results on 1,1-dimethyldiazene generated in an organic glass suggest that this assignment should be taken with caution, since the authors apparently did not consider the possibility that the PE spectrum may be that of azomethinimine **xxxiii**, although they proposed that the hydrogen cyanide and dimethylamine products arise from decomposition *via* rearrangement to the hydrazone. Recall that Davis and Goddard calculated an ionization potential of 9.4 eV for 1,1-diimide,[23] while Caramella et al. calculated an ionization potential of 7.9-8.5 eV for azomethinimine.[20a] The relative stabilities of the 1,1-diazene-azomethinimine tautomer pair may be sensitive to the change from solution to gas phase, and the high temperature suggests that an equilibrium mixture of the two forms may be present in any case. Miller reported the preparation of acyl 1,1-diazenes **xxxvi-xxxviii** by oxidation of the corresponding hydrazines.[48] The purple solutions (λ_{max}=520 nm) were quite stable thermally (except for the compound **xxxviii** with α-hydrogens); solutions of **xxxvii** remained colored for over a month at room temperature. The products from thermal decomposition of **xxxvi** and **xxxvii** were cyclobutanones; the activation energies were 24.5 and 29.1 kcal/mol respectively. Hydrazone rearrangement products were obtained from **xxxviii**. The compounds were quite sensitive to nucleophiles; cleavage of the C-N bond in the tetrahedral intermediate is undoubtedly quite rapid. There is some doubt, however, as to whether the colored species observed by Miller actually

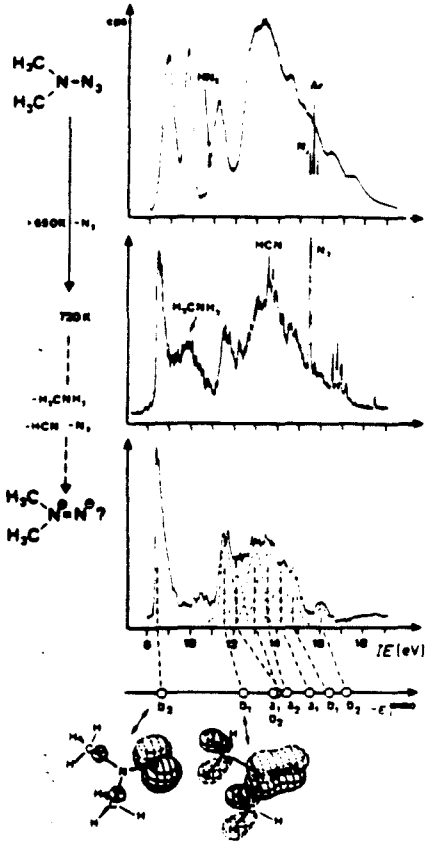

Figure 11. He(I) photoelectron spectra of dimethylaminoazide and its pyrolysis mixture at 720 K. The ionization pattern resulting from subtraction of known contaminants was tentatively assigned by the authors to 1,1-dimethyldiazene **xxx**.[47]

correspond to 1,1-diazenes **xxxvi-xxxviii**. No strong infrared absorptions were observed in the 1550-1800 cm^{-1} region other than the carbonyl at 1755 cm^{-1}. Also, the observed activation energies seem incorrect for compounds that would result in acyl and benzyl radicals on loss of nitrogen. From the measured C-H bond dissociation energies[49] the activation energies should be ~7 kcal/mol lower than those observed for the tetramethyl

substituted 1,1-diazenes (E_a ~20 kcal/mol). A possible explanation for these discrepancies is that the colored species observed by Miller are actually the 1,2-diazenes, which would be consistent with the observed products, kinetics, and spectral data.

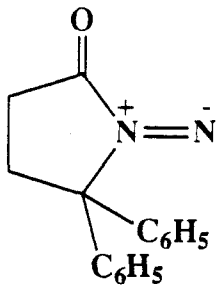

xxxvi

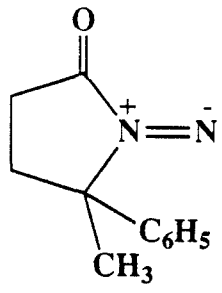

xxxvii

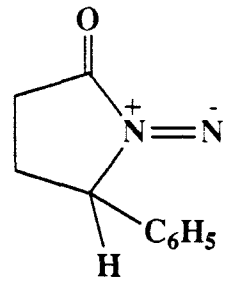

xxxviii

The studies of 1,1-diimide and the simple dialkyl 1,1-diazenes demonstrated the power of the carbamoyl azide route to 1,1-diazenes. The next chapters describe the results of studies intended to further investigate 1,1-diazenes and especially to probe the limitations of the carbamoyl azide route. The species under investigation are several cyclic dialkyl 1,1-diazenes and the first diaryl 1,1-diazene, 1,1-diphenyldiazene. The study of cyclic 1,1-diazenes addresses the effect of lowering the barrier to nitrogen extrusion (destabilizing the 1,1-diazene) while the study of 1,1-diphenyldiazene reveals some effects of substituents on the carbamoyl azide and aminoisocyanate photochemistry. 1,1-Diazenes derived from carbamoyl azides should be useful as precursors to other highly unstable species such as strained hydrocarbons and biradicals. Before such uses can begin, however, the response of the photochemistry to various molecular perturbations caused by substitution should be better understood.

Chapter 2

Cyclic Dialkyl 1,1-Diazenes

To understand the effects of structural modifications on the stability of 1,1-diazenes, a structural parameter which can be varied systematically and quantifiably is ideal. For example, among the known 1,1-diazenes, the series dimethyl to di-*iso*-propyl to di-*tert*-butyl can be understood in terms of stabilization of the radical centers formed on nitrogen extrusion by added methyl groups. 1,1-Dimethyldiazene decomposes chiefly by dimerization to the 2-tetrazene, but 1,1-di-*iso*-propyldiazene decomposes by loss of nitrogen, with a $\Delta G^{\ddagger}$ of 16.8 kcal/mol.[42] Addition of another methyl group to give 1,1-di-*t*-butyldiazene lowers $\Delta G^{\ddagger}$ to 12.5 kcal/mol.[34] The C-H bond dissociation energies suggest that there should be a difference of ~3 kcal/mol in ΔH_f^{o} between *tert*-butyl and *iso*-propyl radicals.[49] This accounts for most of the difference in $\Delta G^{\ddagger}$ between the two 1,1-diazenes. The 1,1-di-*t*-butyldiazene may also be slightly destabilized by steric effects. Other radical stabilizing groups (i.e., phenyl, cyano) attached to the α-carbon of 1,1-diazenes should lead to even lower values of $\Delta G^{\ddagger}$ for fragmentation, as reflected in the studies discussed in section A of Chapter 1.

Another parameter which should have an effect on 1,1-diazene stability is ring size. Table II lists heat of formation (ΔH_f^{o}), strain energy (SE), and olefin strain (OS) for the four smallest methylenecycloalkanes.[50] The strain energy and olefin strain for both methylenecyclohexane and methylenecyclopentane are fairly small, with only the strain energy of the latter (6.1 kcal/mol) larger than 1 kcal/mol. Methylenecyclobutane, however, is quite strained, with a strain energy of 26.9 kcal/mol, although the olefin strain is only 0.4 kcal mol. Methylenecyclopropane is highly strained, with a strain energy of 40.9 kcal/mol and an olefin strain of 13.4 kcal/mol. The 1,1-diazenes analogous to methylene-

Table II. Strain Energies of Methylenecycloalkanes[50]

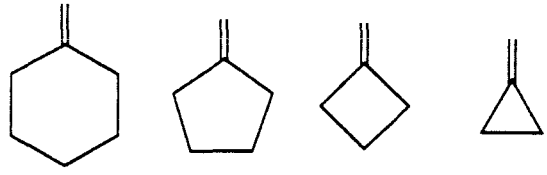

ΔH_f° (kcal/mol)	-8.80	3.29	29.05	47.9
SE (kcal/mol)	-1.1	6.1	26.9	40.9
OS (kcal/mol)	-1.1	-0.1	0.4	13.4

cyclopentane and methylenecyclobutane seemed therefore to be good choices to observe the effect of ring strain on a 1,1-diazene. Since loss of nitrogen involves ring opening and relief of strain, this reaction is expected to be accelerated for smaller ring 1,1-diazenes. Previous studies on products derived from 1,1-diazenes **1** and **2**,[6,10,11] as described in Chapter 1, lend support to this idea. Since the 2,2,5,5-tetramethyl derivative of **1** had already been studied as a kinetically persistent 1,1-diazene,[33,36,38] the unsubstituted 1,1-diazene **1** was not expected to present any special difficulties. With the weakness of the C-N bonds (recall that an activation energy of 24.3 kcal/mol was calculated for cleavage of this bond[29]) in 1,1-diazenes, the 27 kcal/mol of strain energy expected for **2** might lead to some serious problems, perhaps preventing its observation even under matrix isolation conditions.

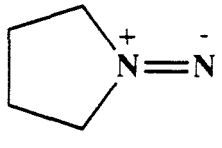

1

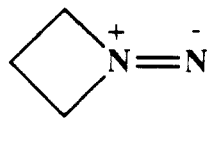

2

A. Synthesis.

The carbamoyl azide precursors for **1** and **2** were prepared from the commercially available amines **3** and **4**, as shown in scheme 5. Reaction with phosgene at -10° C in the presence of triethylamine gives the carbamoyl chlorides **5** and **6**. Treatment of the carbamoyl chlorides with excess sodium azide in acetonitrile results in the carbamoyl azides **7** and **8**. Use of sodium 1-^{15}N-azide allows the introduction of an isotopic label statistically distributed between the two termini of the azide moiety, as shown in scheme 6. Pure carbamoyl azides were obtained by preparative VPC.

Scheme 5. Synthesis of carbamoyl azides.

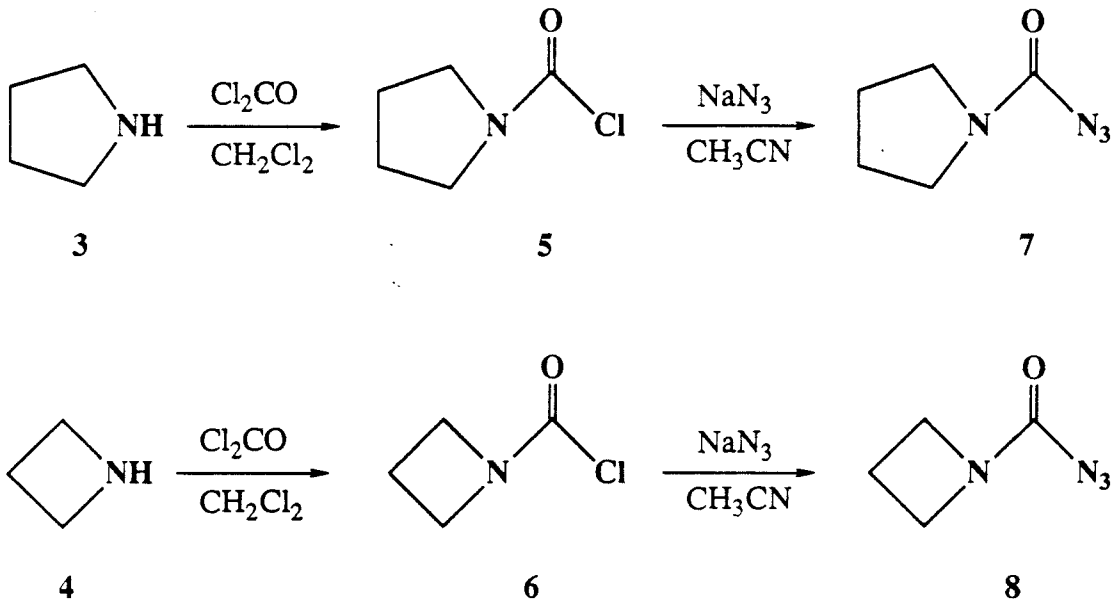

Scheme 6. Synthesis of isotopically labelled carbamoyl azides.

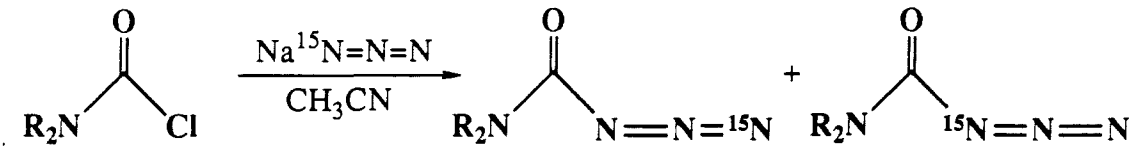

B. 1,1-Tetramethylenediazene.

1. FTIR Studies.

Matrix isolated carbamoyl azide **7** was prepared by codeposition with UHP argon onto a CsI substrate at 20 K. The FTIR spectrum of matrix isolated **7** is shown in Figure 12, and the positions and assignments of the bands are given in Table III. Matrix isolated 1,1-diazene **1** was generated by broad band UV photolysis of **7** (λ=200-400 nm, 140 minutes), resulting in photo-Curtius rearrangement to aminoisocyanate **9** and subsequent photodecarbonylation to 1,1-diazene **1** (scheme 7). The FTIR spectrum of the argon matrix after photolysis is shown in Figure 13. The spectral changes that occur upon irradiation can be seen more clearly in an FTIR difference spectrum, as shown in Figure 14. In this spectrum, the result of subtraction of Figure 12 from Figure 13, the positive bands have grown in with UV photolysis, and the negative bands have decreased. The new bands are due to a several different species: 1,1-diazene **1**, intermediate aminoisocyanate **9**, carbon monoxide (CO) from photodecarbonylation of **9**, ethene from decomposition of **1**, and possibly a minor product resulting from intramolecular C-H bond insertion in pyrrolidine carbonyl nitrene.[51] Assignments of bands due to **1** and its decomposition products can be assigned by observing changes on subsequent visible photolysis (λ=470-610 nm, 60 minutes) which efficiently photodecomposes 1,1-diazene **1** but does not affect **9**. Figure 15 shows a difference FTIR spectrum in which the positive bands are due to 1,1-tetramethylenediazene **1** and the negative bands are due to decomposition products. Note that there are spectral changes in the CO region on visible irradiation of **1**. This effect was seen in the earlier work on matrix isolated 1,1-diazenes[42] and is apparently due to a perturbation of some carbon monoxide molecules by nearby, highly polar 1,1-diazenes. The major unchanged bands (assigned to **9** and to nitrene insertion products) are the isocyanate stretch of **9** at 2221.1 cm^{-1} and a band at 1799.1 cm^{-1} tentatively assigned to the carbonyl stretch of the nitrene insertion product. The product

bands from photolysis of carbamoyl azide **7** (positive in Figure 14) are listed in Table IV along with their assignments.

Scheme 7. Generation of 1,1-diazene **1**.

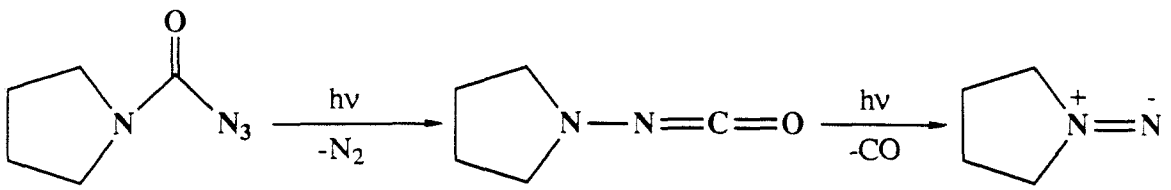

7 **9** **1**

The characteristic N=N stretch of 1,1-diazenes has been observed to occur between 1640 and 1570 cm^{-1}. Of the bands assigned to 1,1-tetramethylenediazene **1**, two are found in this region: one at 1629.6 cm^{-1} and the other at 1622.8 cm^{-1} (partially obscured by a peak due to matrix isolated water at 1623.7 cm^{-1}). Annealing the matrix by repeatedly warming it briefly to 30-35 K results in the decrease of the band at 1622.8 cm^{-1} and increase of the band at 1629.6 cm^{-1}. This behavior could be explained by assignment of these two bands to $\nu_{N=N}$ of **1** in two different matrix sites. The band at 1629.6 cm^{-1} must be in the lower energy site, since allowing the matrix to relax by annealing increases the occupancy of this site.[52] The isoelectronic carbonyl compound, cyclopentanone, exists in a half-chair conformation with C_2 symmetry in the gas phase.[53] The barrier to pseudorotation is found to be 2.1 kcal/mol from the far IR spectra.[54] An envelope form with C_s symmetry was calculated to lie 3.22 kcal/mol above the half-chair,[55] but has not been observed experimentally. Annealing at 35 K may allow envelope conformers of **1** to relax to the half-chair form. It is unclear which conformations carbamoyl azide **7** and the aminoisocyanate **9** will prefer. The N=N stretch region of the FTIR spectrum of **1** before

and after annealing are shown in Figure 16. A discussion of the observed $\nu_{N=N}$ for **1** in relation to the known $\nu_{N=N}$ values for other 1,1-diazenes can be found in Chapter 4.

Isotopic substitution of 1,1-diazenes with a terminal ^{15}N label has proven to be useful for the identification of $\nu_{N=N}$. A simple Hooke's Law treatment predicts this relationship between $\nu_{N=N}$ and $\nu_{N=^{15}N}$:

$$\nu_{N=^{15}N} = \frac{\sqrt{\frac{15+14}{15\cdot14}}}{\sqrt{\frac{14+14}{14\cdot14}}}\ \nu_{N=N} = 0.9832\ \nu_{N=N}$$

For 1,1-diazene **1**, $\nu_{N=N}$ of 1629.6 cm^{-1} results in a calculated $\nu_{N=^{15}N}$ of 1602.2 cm^{-1}. Matrix isolation of carbamoyl azide **7** with ^{15}N incorporated equally at the two terminal azide positions should allow preparation of a 1:1 mixture of labelled and unlabelled 1,1-diazene **1**. The sodium 1-^{15}N azide used in the synthesis of **7**-^{15}N was of low isotopic purity (~40% by mass spectrometry), however, so that the observed mixture is expected to be approximately 5:1. An FTIR spectrum of matrix isolated **7**-^{15}N is shown in Figure 17. Isotopic multiples are observed for the vibrations assigned to the azide moiety at 2126.1 and 1205.8 cm^{-1}. Broad band UV photolysis (λ=200-400 nm, 120 minutes) results in photo-Curtius rearrangement and photodecarbonylation to give 1,1-diazene **1** and labelled **1**-^{15}N. The N=N stretch region before and after annealing is shown in Figure 18. Bands due to matrix isolated water at 1607.8 and 1602.1 cm^{-1} interfere in the region where $\nu_{N=^{15}N}$ is expected, but bands at 1608.1 and 1601.4 cm^{-1} show similar behavior on annealing as the two N=N bands of unlabelled **1**. This allows tentative assignment of these two bands as due to $\nu_{N=^{15}N}$ of **1**-^{15}N in two different matrix sites or in two different conformations. The only other product band to show an isotopic shift on incorporation of ^{15}N into the precursor carbamoyl azide is the aminoisocyanate stretch at 2221.1 cm^{-1}, which shifts to 2207.7 cm^{-1}. The band at 1799.1 cm^{-1}, possibly due to nitrene insertion product, shows no isotopic shifts.

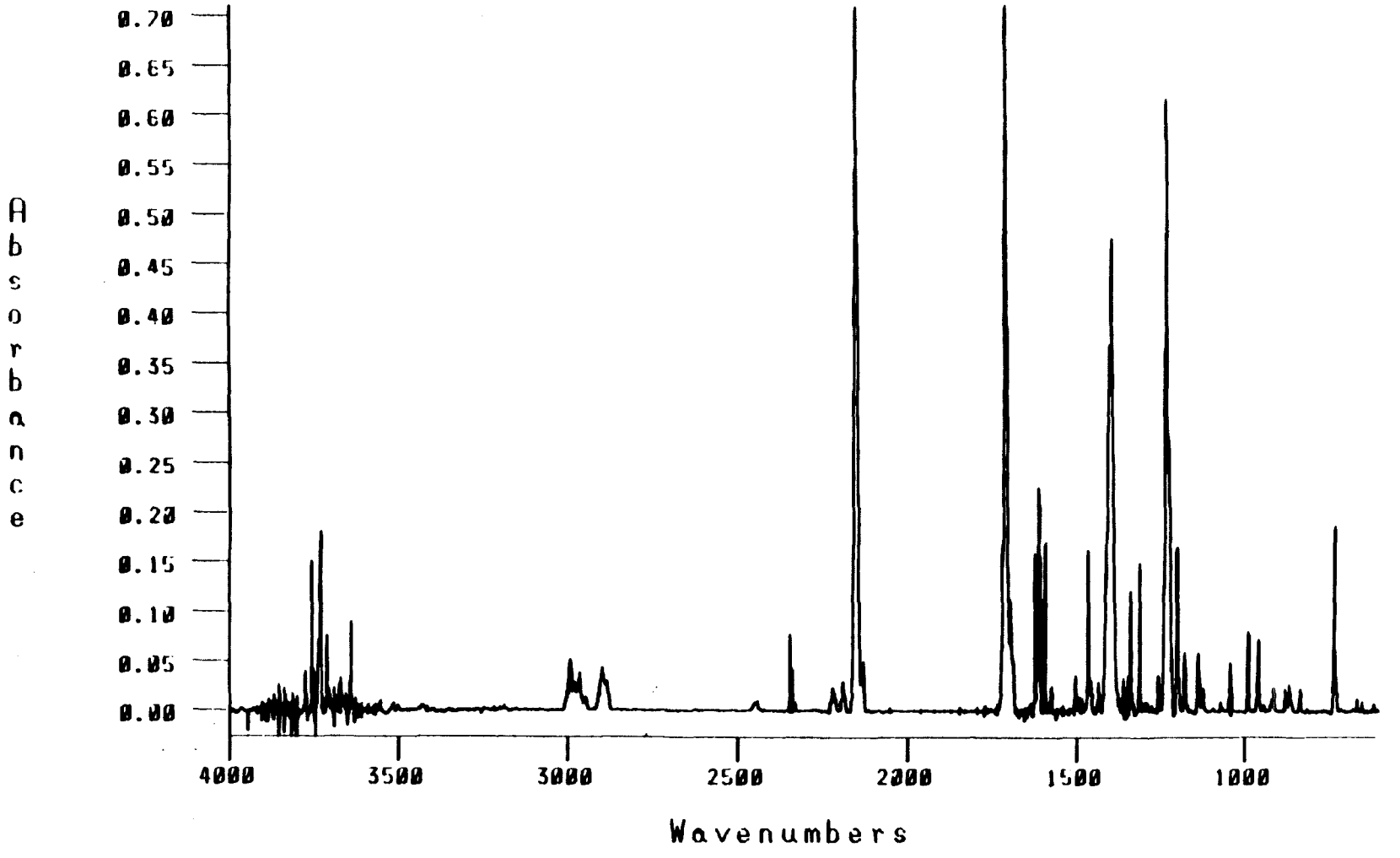

Figure 12. FTIR spectrum of pyrrolidine carbamoyl azide 7 (Ar, 10 K).

Table III. Bands from the FTIR spectrum of pyrrolidine carbamoyl azide **7** (Figure 12) and isotopic multiples (in parentheses) from the FTIR spectrum of labelled carbamoyl azide **7**-^{15}N (Figure 17).

Peak Location (cm^{-1})	Intensity (A)	Assignment
3000.3	0.020	ν C-H
2991.8	0.052	
2991.1	0.052	
2978.5	0.029	
2963.5	0.038	
2897.9	0.043	
2151.8	0.708	ν N_3 (asym)
(2126.1)	(0.452)	ν $^{15}N_3$ (asym)
1709.2	0.710	ν C=O (asym)
1696.8	0.112	
1502.9	0.036	
1465.8	0.163	
1396.4	0.477	ν C=O (sym)
1339.2	0.121	
1311.7	0.149	
1257.5	0.037	
1231.9	0.620	ν N_3 (sym)
(1205.8)	(0.197)	ν $^{15}N_3$ (sym)
1200.4	0.166	
1177.6	0.059	
1136.9	0.058	
1041.7	0.049	
1037.6	0.036	
989.6	0.080	
986.1	0.078	
957.4	0.072	
732.1	0.187	δ N_3
727.0	0.062	

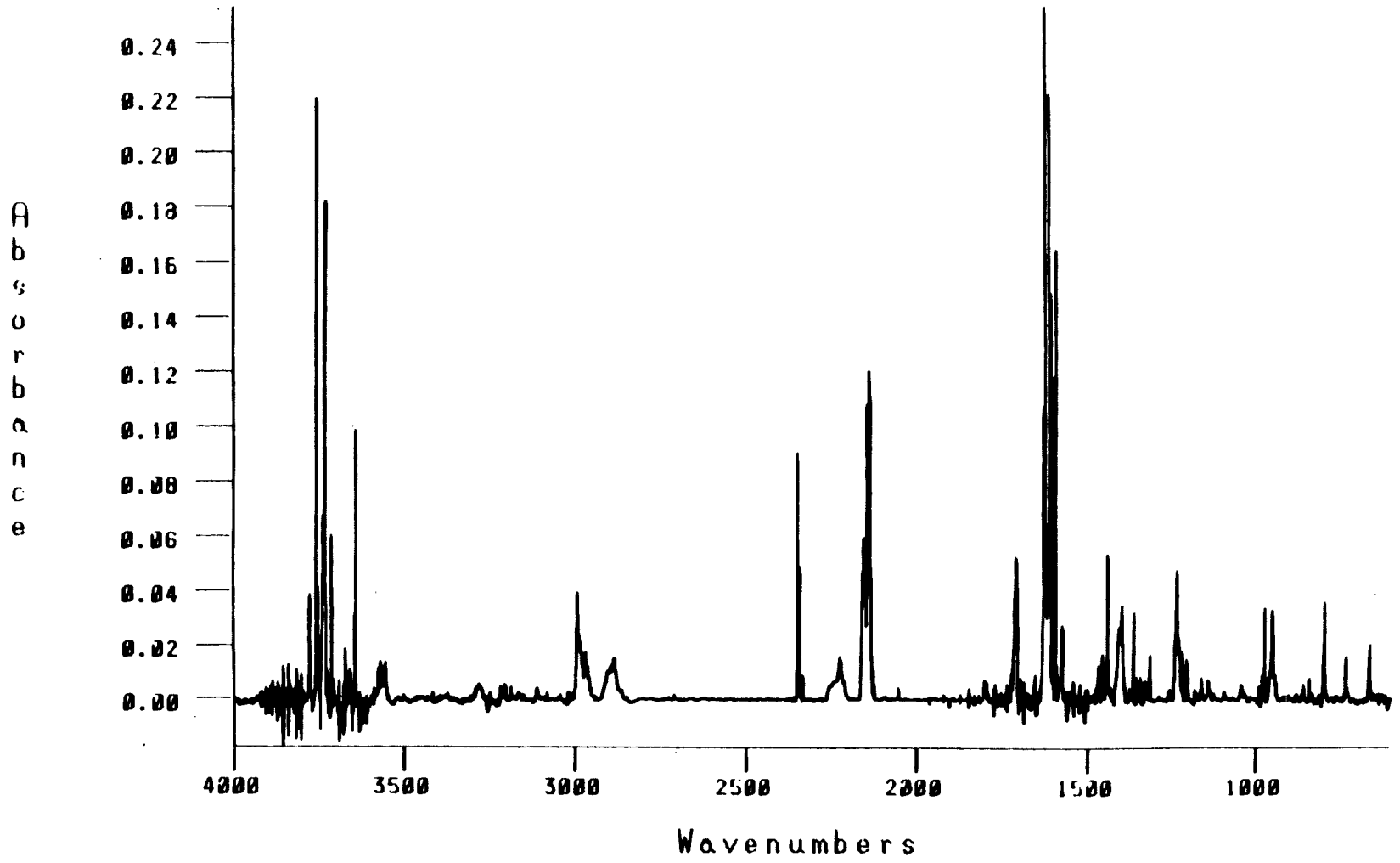

Figure 13. FTIR spectrum of UV photolysis products (λ=200-400 nm, 140 min.) from carbamoyl azide 7 (Ar, 10 K).

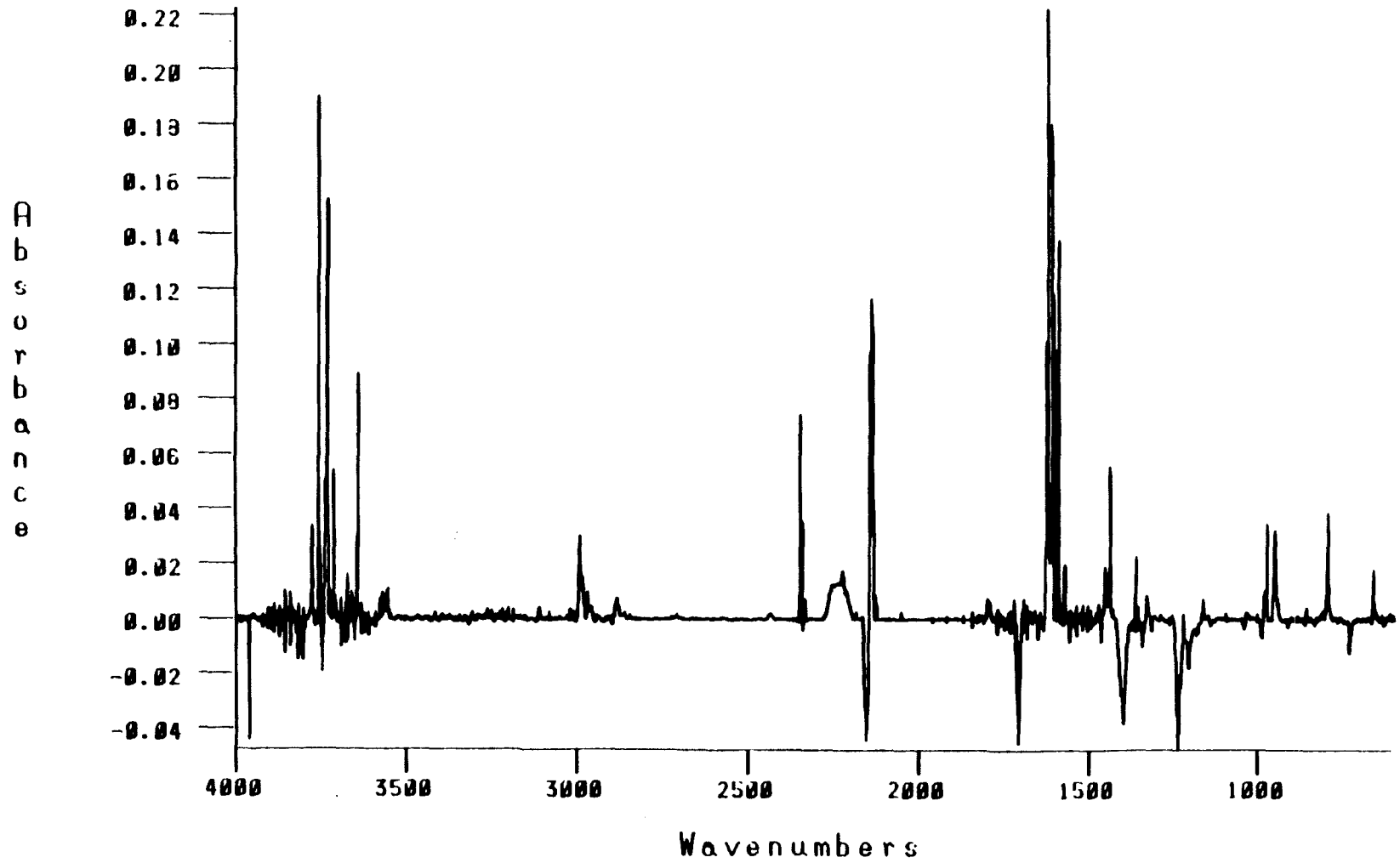

Figure 14. Difference FTIR spectrum of 1,1-diazene **1**, aminoisocyanate **9**, and ethene (Ar, 10 K) resulting from UV photolysis (λ=200-400 nm, 140 min.) of carbamoyl azide **7** minus spectrum of **7** before photolysis (subtraction factor α=1.0).

Table IV. Bands from the FTIR spectrum of UV photolysis products from carbamoyl azide **7** (positive in Figure 14) and isotopic multiples (in parentheses) from UV photolysis of carbamoyl azide **7**-^{15}N (Figure 18).

Peak Location (cm^{-1})	Intensity (A)	Assignment
2992.7	0.030	ethene ν C-H
2984.0	0.016	**1** ν C-H
2968.3	0.010	
2888.0	0.005	
2883.1	0.008	
2221.1	0.018	**9** ν NCO
(2207.7)	(0.004)	**9** ν ^{15}NCO
2141.7	0.098	CO
2135.9	0.118	
1799.1	0.008	insertion product
1629.6	0.102	**1** ν N=N
1623.7	0.227	**1** ν N=N / H_2O
(1608.1)	(0.022)	**1** ν N=^{15}N / H2O
(1601.4)	(0.006)	**1** ν N=^{15}N / H2O
1454.9	0.020	**1**
1439.4	0.055	ethene
1361.4	0.024	?
1326.2	0.009	**1**
1158.4	0.008	
978.7	0.011	
972.3	0.035	
949.6	0.033	ethene
795.83	0.039	**1**
661.9	0.019	

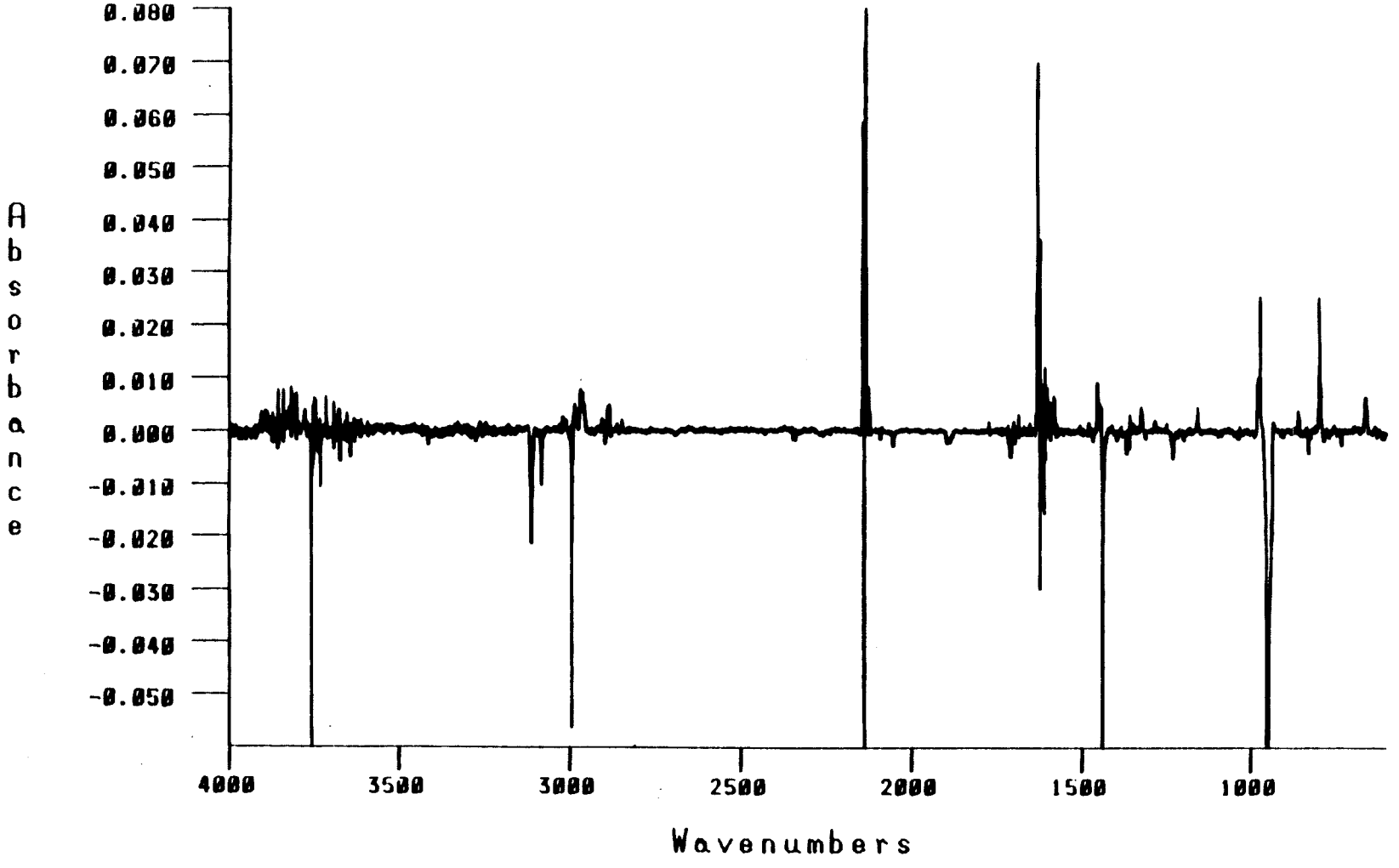

Figure 15. Difference FTIR spectrum of 1,1-diazene **1** (Ar, 10 K) from UV photolysis (λ=200-400 nm, 140 min.) of carbamoyl azide **7** minus spectrum after subsequent visible photolysis (λ=470-610 nm, 60 min.) of **1** (subtraction factor α=1.0).

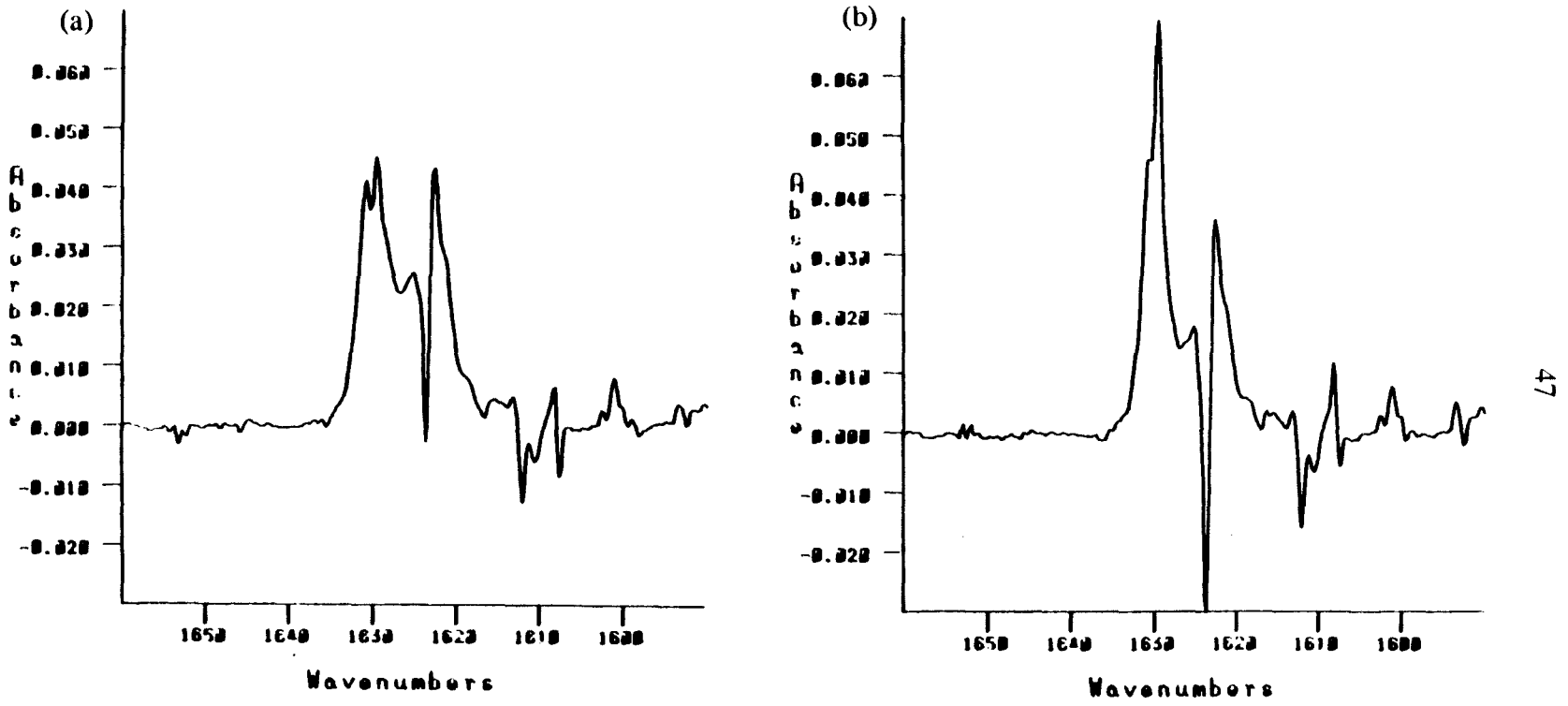

Figure 16. Difference FTIR spectra of N=N stretches of 1,1-diazene **1** (Ar, 10 K) from UV photolysis (λ=200-400 nm, 140 min.) of carbamoyl azide **7** minus spectrum after visible photolysis (λ=470-610 nm, 60 min.) of **1**: (a) unannealed **1** (b) annealed **1** (subtraction factors α=1.0).

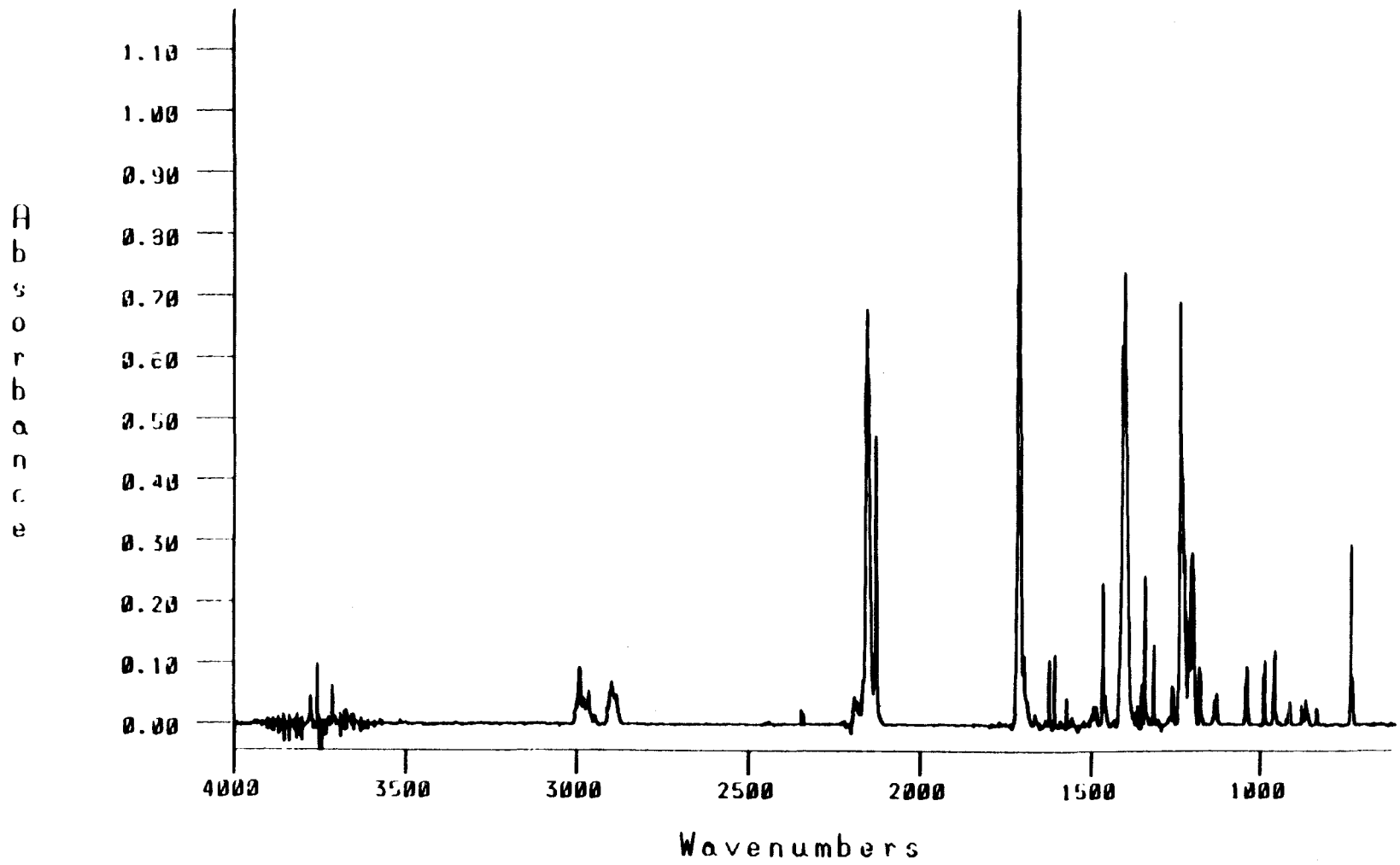

Figure 17. FTIR spectrum of pyrrolidine carbamoyl azide **7** and labelled **7**-^{15}N (Ar, 10 K).

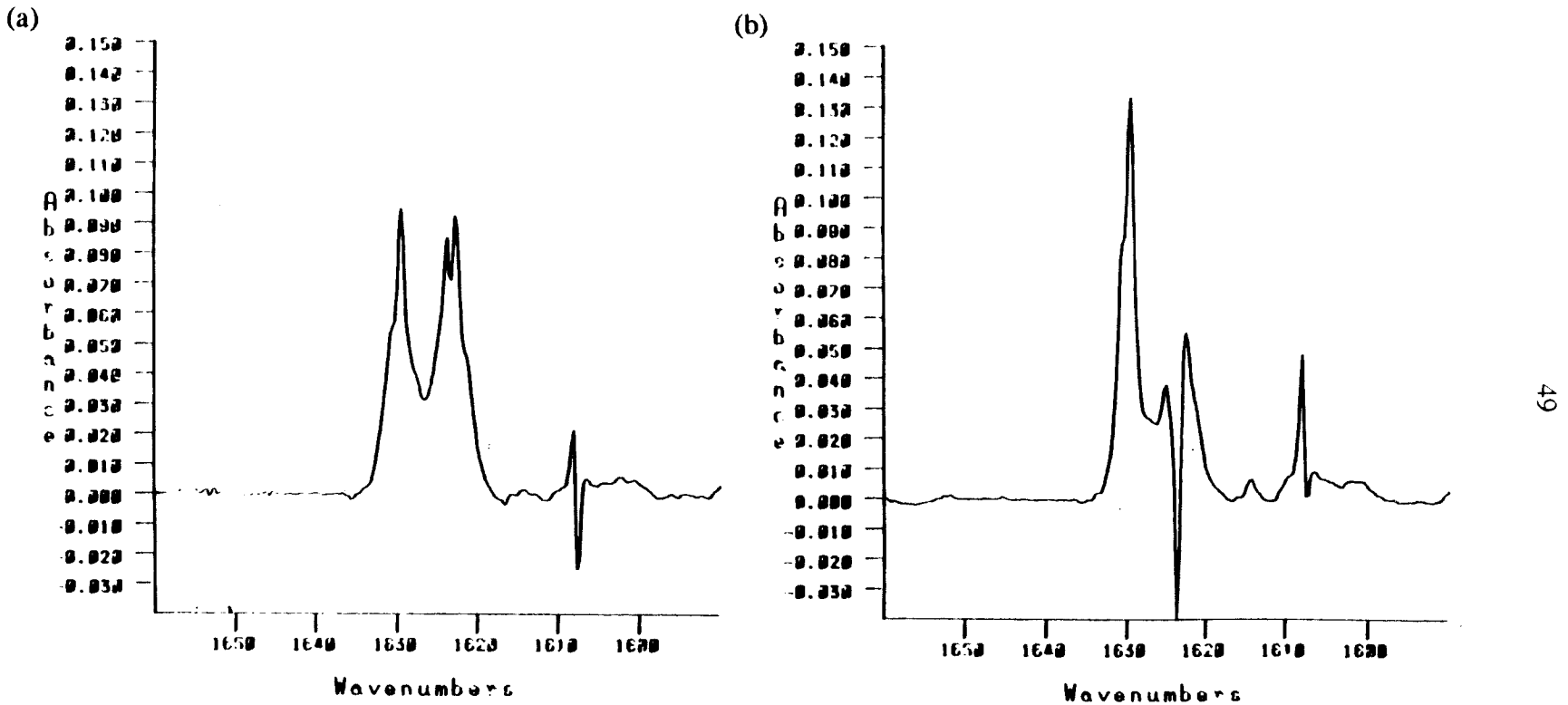

Figure 18. Difference FTIR spectra of N=N stretches of 1,1-diazene **1** and labelled **1**-^{15}N (Ar, 10 K) from UV photolysis (λ=200-400 nm, 120 min.) of carbamoyl azide **7** and **7**-^{15}N minus spectrum after visible photolysis (λ=470-610 nm, 60 min.) of **1**: (a) unannealed **1** and **1**-^{15}N (b) annealed **1** and **1**-^{15}N (subtraction factors α=1.0).

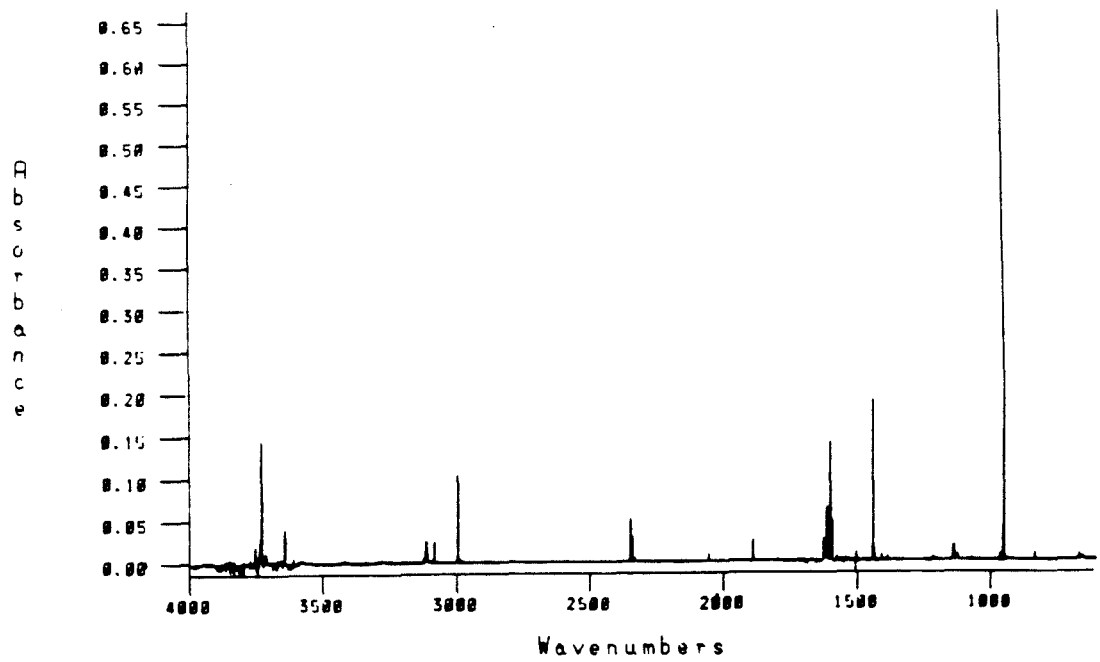

Figure 19. FTIR spectrum of ethene (Ar, 10 K).

Table V. Bands from the FTIR spectrum of matrix isolated ethene (Figure 19).

Peak Location (cm^{-1})	Intensity (A)	Assignment
3112.1	0.025	ν C-H
3082.7	0.024	
2995.7	0.106	
1889.0	0.025	combination
1440.4	0.193	C-H wag
947.6	0.668	C-H oop bend

Visible photolysis of matrix isolated 1,1-tetramethylenediazene **1** results in photodecomposition as described above. The FTIR spectrum of the decomposition products can be seen as negative peaks in the difference FTIR spectrum in Figure 15. These product bands correspond to the spectrum of ethene in an argon matrix, shown in Figure 19 for comparison with band assignments listed in Table V. No cyclobutane is observed. Lack of cyclobutane as a product was also seen in high temperature (~160° C) thermolysis studies of **1** derived from thermal decomposition of the benzenesulfonamide salt.[6] The kinetically persistent tetramethyl derivative of **1** gave some cyclobutane products from both thermolysis and photolysis.[33, 36, 38] A mechanistic interpretation of these earlier results in light of the present study will be given in a later section.

2. Electronic Spectroscopy.

An organic glass containing carbamoyl azide **7** was prepared by cooling a dilute solution (~5 x 10^{-3} M) of **7** in 2MTHF to 80 K in a low temperature spectroscopy cell.[56] Broad band UV photolysis (λ=200-400, 90 min) of **7** under these conditions results in the generation of **1**. The electronic absorption spectrum of **1** is shown in Figure 20. The 0,0 band is at 616 nm (2.01 eV)[57] and λ_{max} is the 0,2 band at 527 nm (2.35 eV). This excitation energy lies in the middle of the range spanned by the other known dialkyl 1,1-diazenes (497 to 556 nm). The vibrational structure in the spectrum is particularly well resolved, with an average spacing of 1353 cm^{-1}. This is a larger vibrational spacing than is observed in the other known 1,1-diazenes. The implications of this data as regards structural effects on the 1,1-diazene functionality will be discussed in Chapter 4.

Warming a 2MTHF glass of **1** to softening at 90 K results in loss of the electronic absorption spectrum of **1** and growth of a strong, structureless absorption with λ_{max} at 495 nm as shown in Figure 21. This same behavior has been seen in the other 1,1-diazenes with α-hydrogens, and was attributed to formation of the tautomeric azomethinimines (see section C.3 of Chapter 1). The λ_{max}=495 nm absorption is similarly assigned to the

tautomer of **1**, azomethinimine **10**. This species is thermochromic in 2MTHF solution.[58] Warming the softened glass shifts the position of λ_{max}, first to shorter wavelengths (482 nm at 110 K), then to longer wavelengths (491 nm at 150 K, 494 nm at 190 K). Recooling to 85 K shifts λ_{max} to 480 nm. Table VI lists values of λ_{max} for **10** at various temperatures. This thermochromism is strong enough to be apparent to the eye in 2MTHF, but does not appear to occur in hydrocarbon solvents. This suggests that changes in solvent polarity (dielectric) with temperature may be responsible for the thermochromism. The red shift with higher temperature (lower dielectric) is consistent with a $\pi \rightarrow \pi^*$ transition. Warming the softened glass above 200 K results in the loss of the absorption due to azomethinimine **10**.

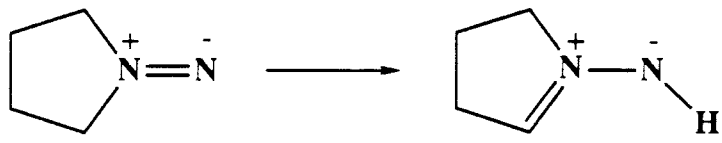

1 **10**

Table VI. Thermochromism of azomethinimine **10**.

T (K)	λ_{max} (nm)
90	480.0
109	482.0
130	477.5
150	491.5
170	493.5
190	494.0

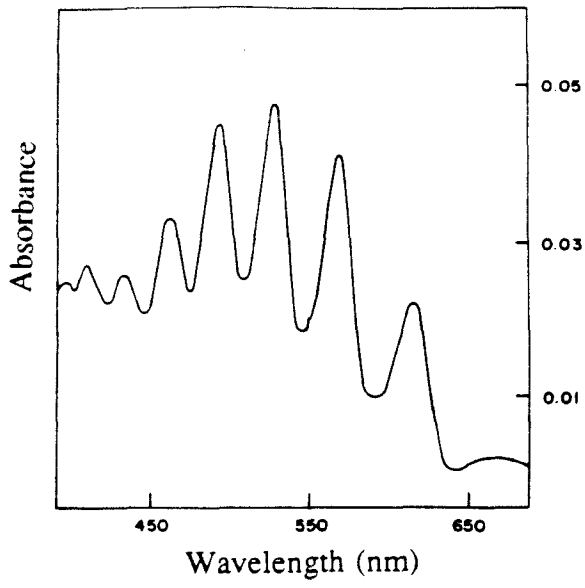

Figure 20. Electronic absorption spectrum of 1,1-diazene **1** (2-MTHF, 80 K).

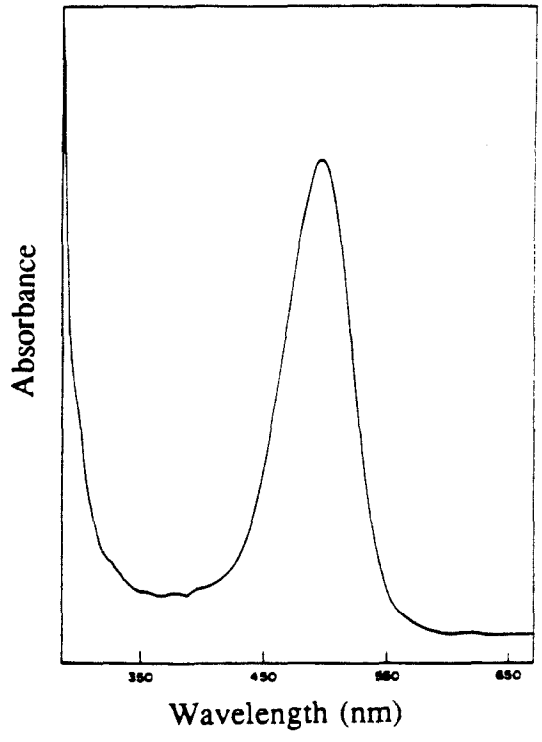

Figure 21. Electronic absorption spectrum of azomethinimine **10** (2-MTHF, 190K).

3. Product Analysis.

Analysis of the products from thermolysis or visible photolysis (λ=470-610 nm) of 1,1-diazene **1** generated in an organic glass at 77 K was accomplished by analytical VPC and NMR spectroscopy as described in the experimental section. The only products observed were ethene and bis(tetramethylene)-2-tetrazene **11**. As in the FTIR experiments, no cyclobutane was observed. The ratios of ethene to **11** for thermolysis and photolysis of **1** are given in Table VII. It appears surprising that the major product from photolysis in a rigid glass is the dimer, but this may be somewhat misleading. It is observed that the purple glass containing **1** becomes an orange glass of azomethinimine **10** after a few minutes of visible photolysis. This is probably due to some softening of the organic glass in the intense beam of the 1000 W xenon arc lamp, although it may be a photochemical isomerization.[59] Since the azomethinimine appears to be stable to visible photolysis, the

Table VII. Decomposition products from 1,1-diazene **1**.

conditions[a]	ethene	2-tetrazene **11**
Δ	2.5	97.5
hν	4.9	95.1

a. Product ratios from NMR analysis, -80° C. Starting carbamoyl azide concentration ~1 x 10^{-1} M. For other conditions see experimental section (Chapter 5).

tetrazene product is largely the result of thermal chemistry of **10** subsequent to photolysis. The yield of ethene is approximately doubled by visible photolysis, which together with the FTIR results suggests that ethene is the sole photoproduct of isolated **1**. The dominance of the dimerization pathway suggests that dimerization occurs quite readily at temperatures where the barrier to nitrogen extrusion is much greater than the thermal energy available. Most of the ethene observed from thermolysis is probably due to decomposition during generation of **1** by UV photolysis.

4. Kinetics and Mechanism.

The kinetic behavior of the transformation of 1,1-diazenes into azomethinimines in softened 2MTHF has proven to be difficult to understand.[42] The reaction is almost certainly unimolecular (it shows a kinetic isotope effect in the case of 1,1-dimethyldiazene-d_6), but the growth of the azomethinimine transition is non-exponential. Presumably this is due to the inhomogeneity of the softened 2MTHF medium. The kinetics of the tautomerization of 1,1-diazene **1** into azomethinimine **10** were likewise uninterpretable.

The decomposition of **10**, however, gives good kinetic data. The disappearance of **10** was monitored by following the decay of the λ_{max}=495 nm transition at 205, 215, and 230 K. The decays fit to unimolecular kinetics as shown in Figure 22, which is surprising given the predominance of 2-tetrazene in the product analysis. The Arrhenius activation parameters are E_a=9.9±0.4 kcal/mol and log A=6.2±0.3 ($\Delta H^{\ddagger}$=9.6 kcal/mol, $\Delta S^{\ddagger}$=-31 e.u.). These values are quite different from the activation parameters for other 1,1-diazenes which show unimolecular kinetics (e.g., 1,1-di-*iso*-propyldiazene gave E_a=16.85±0.5 kcal/mol, log A= 11.8±0.3).

There are two reasonable explanations for the unusual kinetic behavior and activation parameters for the decomposition of **10**. The first is that the rate limiting step for

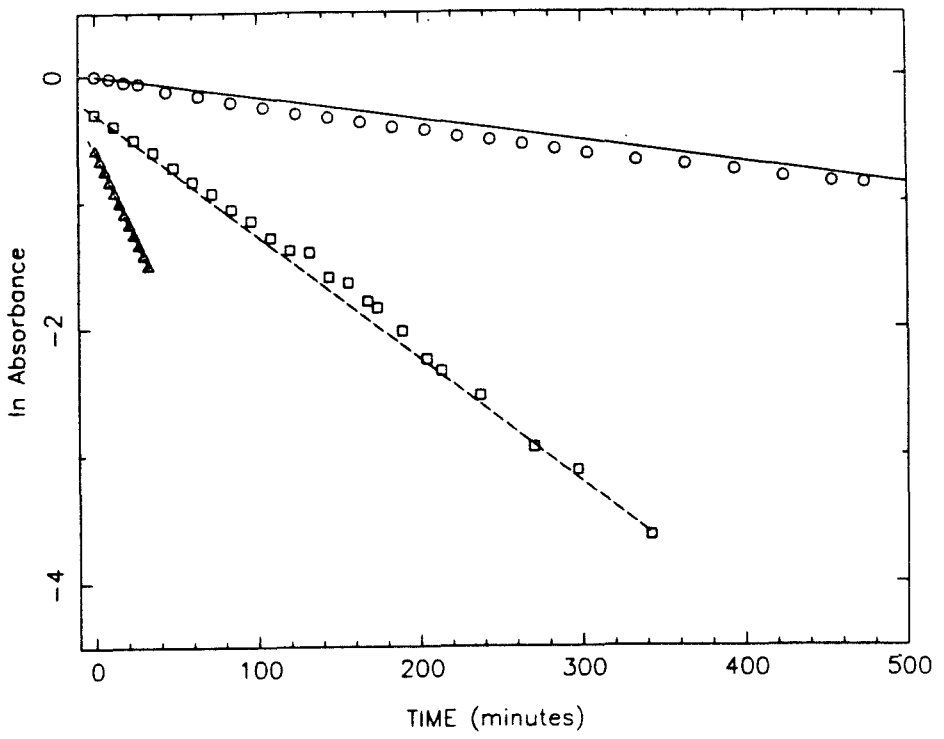

Figure 22. Unimolecular decay kinetics for azomethinimine **10** from thermolysis of **1** (2-MTHF). Fitted rate constants are: 2.869 x 10^{-5} sec^{-1} at 205 K, 1.617 x 10^{-4} sec^{-1} at 215 K, and 4.560 x 10^{-4} sec^{-1} at 230 K.

decomposition of **10** is different than for the other 1,1-diazenes. If this is so, the rate being measured is probably the rate of isomerization from **10** to 1,1-diazene **1** (k_1 in scheme 8). If this step is rate limiting, the kinetics should be first order in **10**. This possibility can be loosely checked by comparing the predicted rate of isomerization with the known rate of decomposition of 1,1-dimethyldiazene[42] (which gives bimolecular kinetics) at 200 K. The bimolecular kinetics of 1,1-dimethyldiazene require rapid equilibration

Scheme 8. Kinetics of decomposition of **10**.

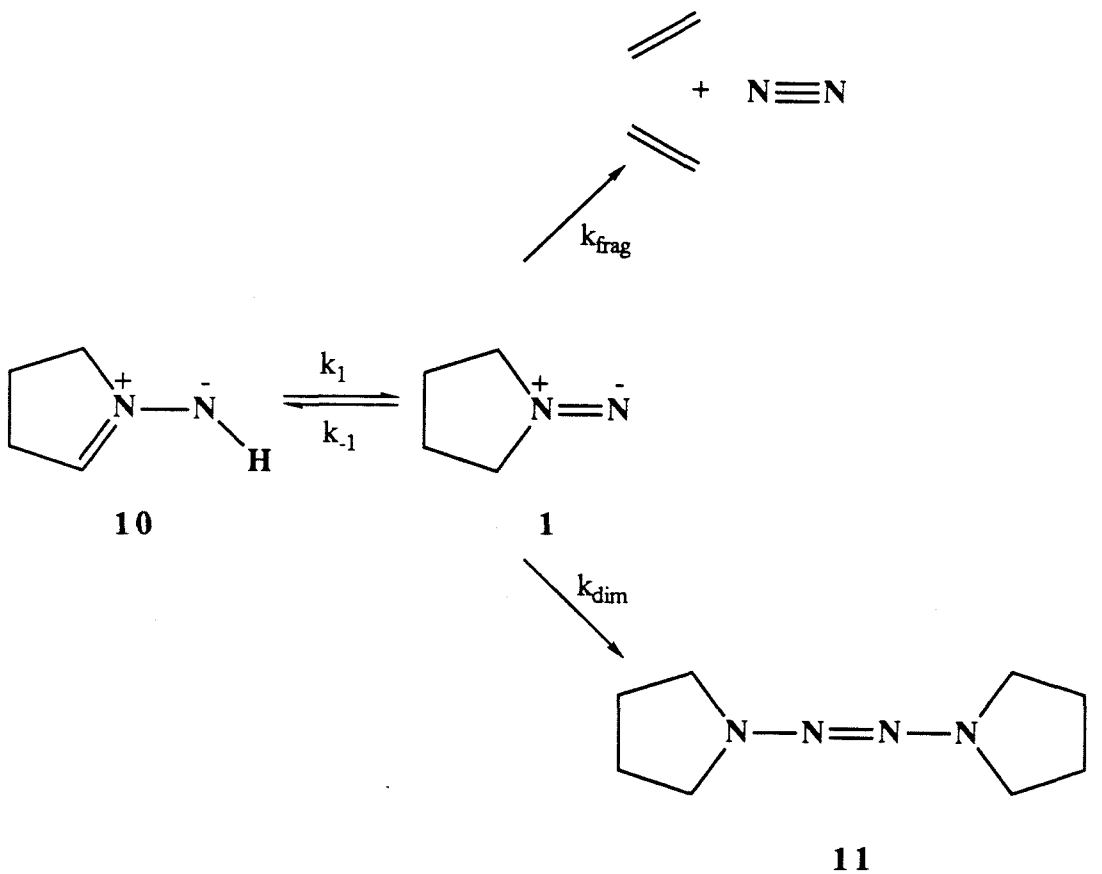

between the 1,1-diazene and azomethinimine tautomers. At 200 K, the measured second order rate constant for 1,1-dimethyldiazene is 4.02 x 10^{-4} A^{-1} sec^{-1}.[42] Assuming an ε of 3000 M^{-1} cm^{-1} and an initial azomethinimine concentration of 3 x 10^{-4} M[42] gives a dimerization rate of 3.6 x 10^{-4} sec^{-1}. The activation parameters of **10** can be used to calculate a rate of 1.8 x 10^{-5} sec^{-1} at 200 K. This is slower than the dimerization rate, so this simple calculation would suggest the rate limiting step for **10** is not isomerization. However, the strain energy of methylenecyclopentane is 2 kcal/mol greater than the strain energy of cyclopentene.[50] If this is applied as a correction factor to the activation energy

for decay of **10**, the calculated isomerization rate is 4 x 10^{-3} sec^{-1}, an order of magnitude faster than the dimerization rate. The observed rate in the decomposition of **10** may indeed correspond to the isomerization of an azomethinimine to a 1,1-diazene, slowed in this special case by the preference of five membered rings for endocyclic over exocyclic double bonds. The large negative value of $\Delta S^{\ddagger}$ implies an ordered transition state, which is not unlikely for what is effectively a 1,3 hydrogen shift. It is also possible to make a rough estimate of the barrier for the reverse reaction, isomerization of **1** to **10**. This reaction occurs at 90 K, so estimating the rate constant at 90 K be 10^{-3} sec^{-1} and assuming the A factor to be the same in both directions gives an E_a of 3.8 kcal/mol. Assuming a rate constant of 10^{-5} sec^{-1} gives an E_a of 4.6 kcal/mol. If E_a for isomerization from 1,1-diazene to azomethinimine is 3-5 kcal/mol and E_a for isomerization from azomethinimine to 1,1-diazene is 7-10 kcal/mol, then by microscopic reversibility the 1,1-diazene isomer must lie at least 4-5 kcal/mol higher in energy than the azomethinimine. (Calculations of the relative energies of a 1,1-diazene/azomethinimine pair can be found in the appendix.) If this is the case, then the equilibrium constant is ~5 x 10^{10} in favor of the azomethinimine form at 90 K, and ~5 x 10^{4} at 200 K. This is consistent with the failure to observe 1,1-diazenes in equilibrium with their azomethinimine tautomers.

A second explanation for the observed kinetic parameters for decomposition of **10** is that the rate being measured is the unimolecular decomposition of **1** by nitrogen extrusion (k_{frag} in scheme 8), and the dissimilarity with the other 1,1-diazene unimolecular kinetics is due to a difference in mechanism. The activation energy for unimolecular decomposition of 1,1-diazenes is assumed to correspond to homolysis of a C-N bond to give two radical centers. 1,1-Tetramethylenediazene **1**, however, can undergo an allowed, concerted reaction to give nitrogen and ethene directly, as suggested by Lemal.[6] This is a 2+2+2 cheletropic reaction, and a qualitative correlation diagram is shown in Figure 23. This concerted reaction requires a C_2 axis of symmetry for 1,1-diazene **1**, which is

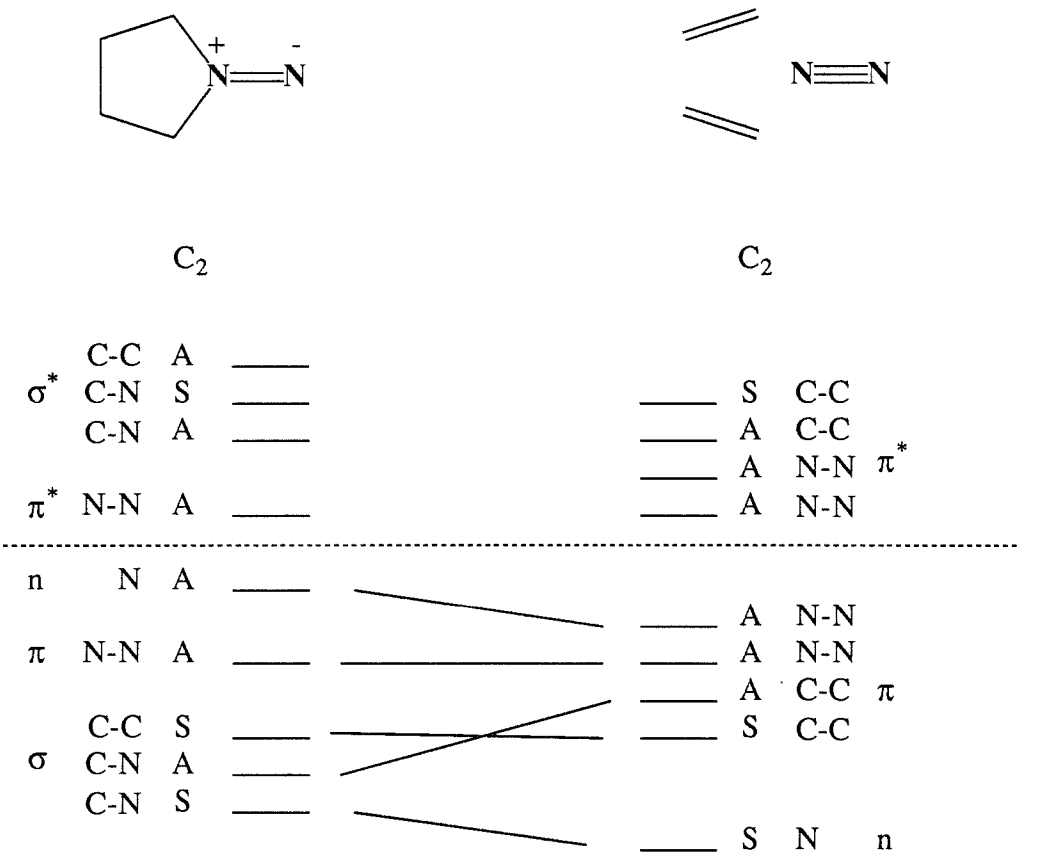

Figure 23. Correlation diagram for concerted fragmentation of 1,1-diazene 1. Orbital energies have been ordered qualitatively but have not been calculated.

observed for cyclopentanone.[53] The transition state is highly ordered, in accord with the observed large negative value of $\Delta S^{\ddagger}$. This reaction should also be allowed photochemically, but with the opposite stereochemistry. Use of all *cis* pyrrolidine carbamoyl azide-d_4 should then produce all *cis* ethene-d_2 thermally and a 1:1 mixture of *cis* and *trans* ethene-d_2 photochemically. For the unusual kinetic parameters from decomposition of **10** to correspond to concerted fragmentation of **1**, the difference in concentration between the product analysis (~1 x 10^{-1} M) and the kinetic studies (~1 x 10^{-3} M) must lead to a change in the product distribution from primarily 2-tetrazene to primarily ethene. This is certainly a possibility, but the results from other 1,1-diazenes show that it is more likely that the measured activation parameters for **10** correspond to the isomerization reaction (k_1).

C. 1,1-Trimethylenediazene.

1. FTIR Studies.

Matrix isolated azetidine carbamoyl azide **8** was prepared by codeposition with UHP argon onto a CsI substrate at 20 K. The FTIR spectrum of matrix isolated **8** is shown in Figure 24, and the positions and assignments of the bands are listed in Table VIII. Broad band UV photolysis (λ=200-400 nm) of matrix isolated **8** resulted in decrease of the spectrum of **8** and the appearance of new bands. None of the new bands could be assigned to 1,1-diazene **2**, however. The photo-Curtius rearrangement of **8** to aminoisocyanate **12** did take place, since the isocyanate stretch of **12** could be observed at 2220.7 cm^{-1}. The other new bands could be assigned to cyclopropane and propene, the expected hydrocarbon products from decomposition of **2**. An attempt was then made to prepare 1,1-diazene **2** in a stepwise fashion, using a monochromator (Oriel, 20 nm

bandpass) to select for narrow wavelength regions. The photo-Curtius rearrangement of **8** to **12** was accomplished by irradiation with 225-245 nm light for 36.5 hours, apparently in nearly quantitative yield. A difference FTIR spectrum demonstrating the results of this photolysis is shown in Figure 25. Aminoisocyanate **12** was then photolyzed with 340-360 nm light to effect photodecarbonylation to 1,1-diazene **2**. The isocyanate stretch at 2220.7 cm^{-1} decreased with photolysis, but no bands that could be assigned to **2** were observed, only the hydrocarbon decomposition products.

It was then found that matrix isolated **2** could be generated by photolysis of **8** with 290-310 nm radiation (Figure 26). The yield of **2** was quite poor, perhaps a tenth of that observed from other carbamoyl azides. A difference FTIR spectrum showing the products from 290-310 nm photolysis can be found in Figure 27, and the new bands and their assignments are listed in Table IX. Visible photolysis (λ=440-580 nm) easily destroyed 1,1-diazene **2**. A difference FTIR spectrum of the results of visible photolysis is shown in Figure 28. The N=N stretch of 1,1-diazene **2** is found at 1674.0 cm^{-1}, the highest energy N=N stretch observed in a 1,1-diazene. There are a number of factors that probably contribute to the difficulty and poor yield in preparing **2**. As discussed earlier, the strain energy of isoelectronic methylenecyclobutane[50] is comparable to the calculated strength of the C-N bonds in 1,1-diazenes.[29] This results in destabilization of 1,1-diazene **2**. Since some **2** is observed by FTIR, the molecule must lie in a potential well, and according to the kinetic analysis given below, the well is of reasonable depth (~15 kcal/mol). This suggests that 1,1-diazene **2** is formed from photodecarbonylation of **12** in a vibrationally excited state, and this excess vibrational energy is sufficient to cause bond scission in this strained 1,1-diazene. (The excitation energy of aminoisocyanates is near 80 kcal/mol; this is more than sufficient energy to decompose any 1,1-diazene.) It is also observed below that the electronic absorption spectrum of **2** is shifted to higher energy (shorter wavelengths) compared to the other 1,1-diazenes, so broad band UV photolysis probably

photodecomposes **2** as fast as it is formed. Even the 360 nm radiation used in the stepwise experiment may lie in the short wavelength tail of the absorption of **2**. It seems unlikely that 310 nm light could be photolysing **2**, so the low yields cannot be due solely to photodecomposition.

Scheme 9. Generation of 1,1-Diazene **2**.

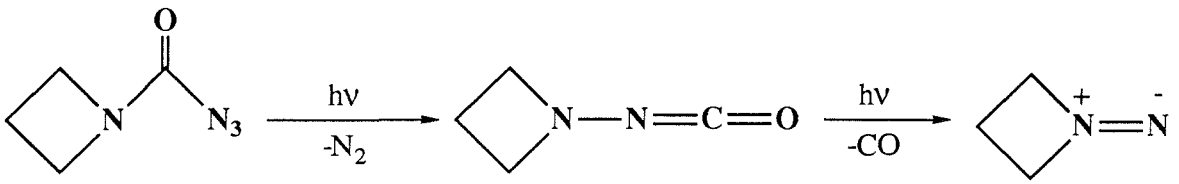

8 **12** **2**

A Hooke's law treatment predicts that the N=N stretch of **2** should shift to 1645.9 cm^{-1} with incorporation of a terminal ^{15}N label. The FTIR spectrum of isotopically labelled carbamoyl azide **8**-^{15}N is shown in Figure 29. Photolysis with 290-310 nm radiation results in the generation of 1,1-diazene **2** and isotopically labelled **2**-^{15}N. A difference spectrum is shown in Figure 30. The ^{15}N multiple of $\nu_{N=N}$ is observed at 1651.8 cm^{-1} as shown in Figure 31. The isocyanate stretch of **12** at 2220.7 cm^{-1} is also observed to shift to 2210.1 cm^{-1}. No minor bands in the 1750-1850 cm^{-1} region were observed from photolysis of **8**. Bands in this region have been found for the other dialkyl 1,1-diazenes and were assigned to the cyclic ureas produced by intramolecular insertion of the carbamoyl nitrene into a C-H bond. Perhaps the small ring size leads to a conformation of the carbamoyl azide precursor that is poor for this insertion process.

Visible photolysis of 1,1-diazene **2** results in photodecomposition. Cyclopropane and propene are the observed decomposition products, with cyclopropane apparently more

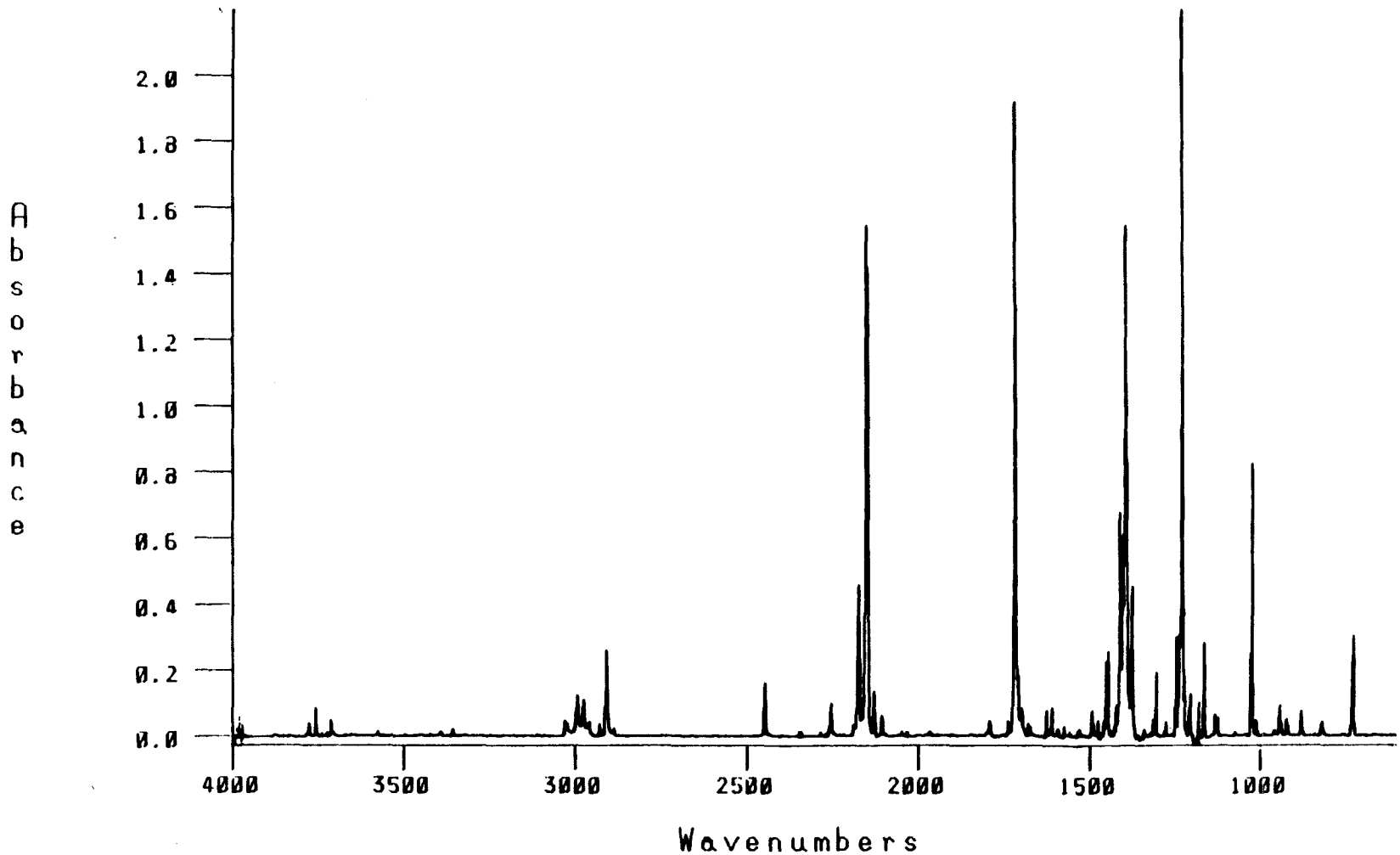

Figure 24. FTIR spectrum of azetidine carbamoyl azide **8** (Ar, 10 K).

Table VIII. Bands from the FTIR spectrum of azetidine carbamoyl azide **8** (Figure 24) and isotopic multiples (in parentheses) from the FTIR spectrum of labelled carbamoyl azide **8**-^{15}N (Figure 29).

Peak Location (cm^{-1})	Intensity (A)	Assignment
3027.1	0.047	ν C-H
2991.9	0.121	
2973.6	0.109	
2956.8	0.043	
2906.9	0.258	
2151.9	1.556	ν N_3 (asym)
2149.9	1.316	
2147.1	1.420	
(2129.1)	(0.306)	
1718.1	1.920	ν C=O (asym)
1710.4	0.182	
1451.1	0.255	
1445.6	0.226	
1412.6	0.679	ν C=O (sym)
1396.4	1.546	
1376.6	0.454	
1304.4	0.190	
1245.9	0.306	
1230.8	2.233	ν N_3 (sym)
(1203.8)	(0.265)	
1164.0	0.284	
1023.7	0.853	
941.3	0.092	
877.0	0.075	
725.0	0.308	δ N_3

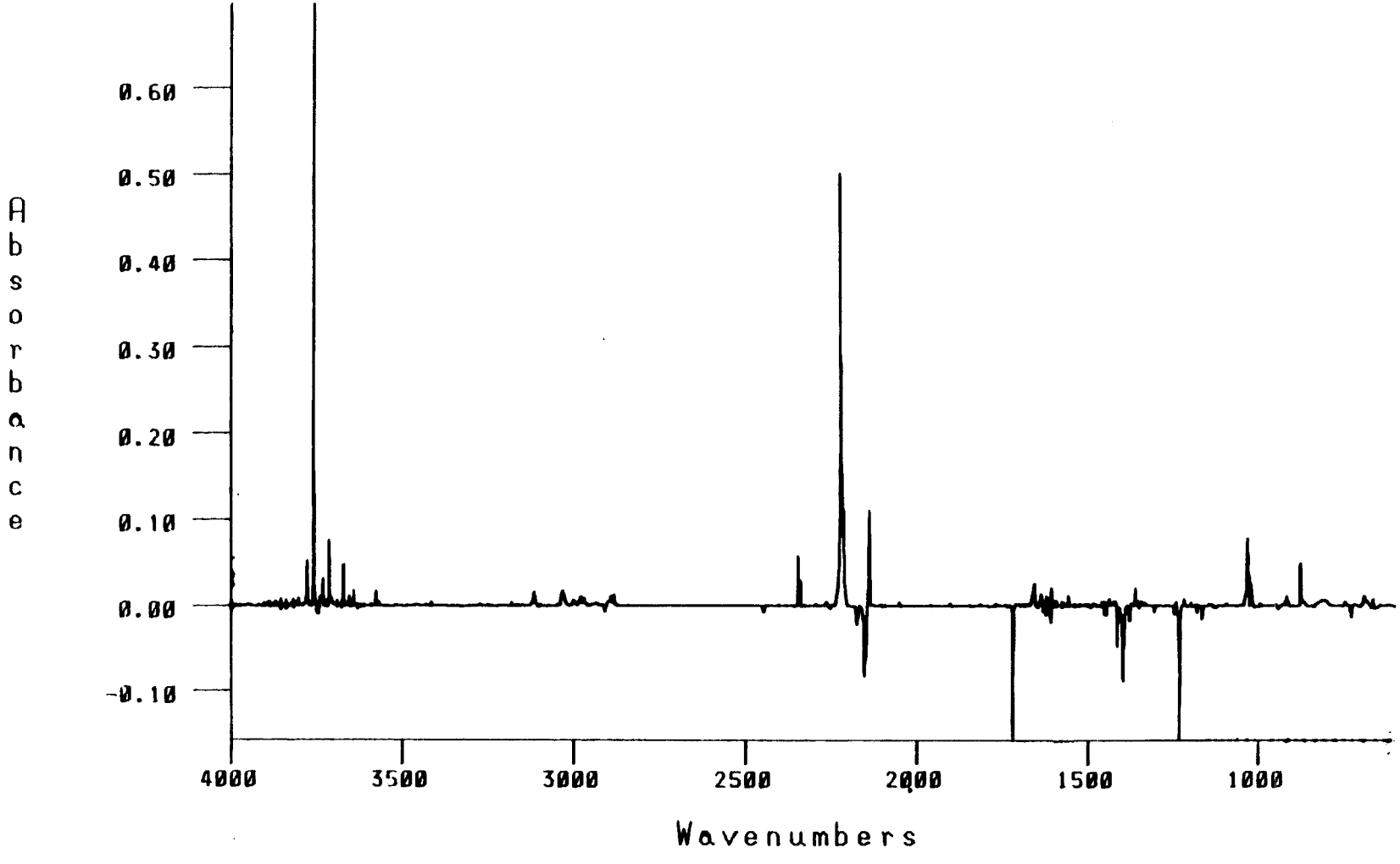

Figure 25. Difference FTIR spectrum of azetidine aminoisocyanate **12** (Ar, 10 K) from UV photolysis (λ=225-245 nm, 2200 min.) of carbamoyl azide **8** minus spectrum of **8** before photolysis (subtraction factor α=1.00).

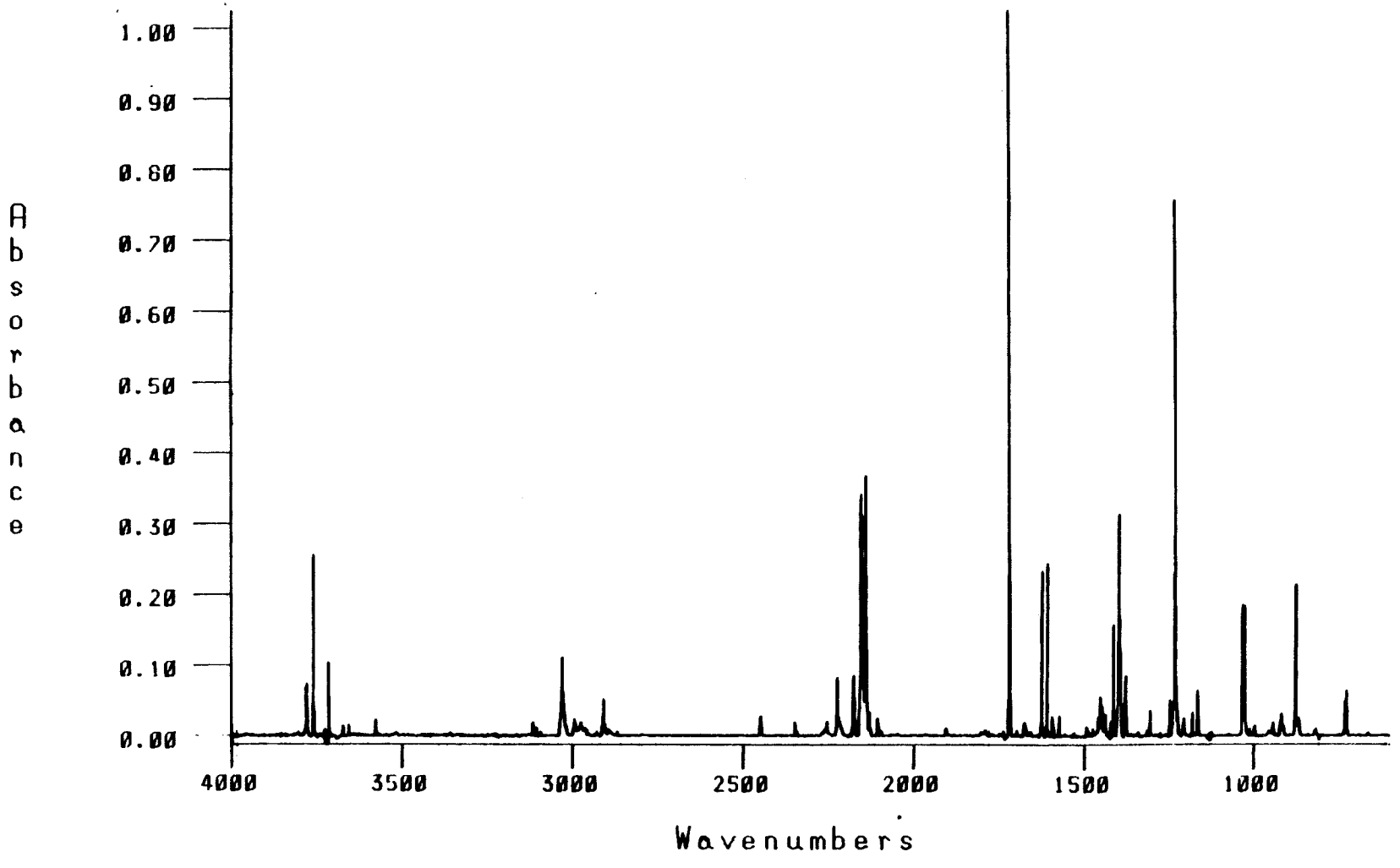

Figure 26. FTIR spectrum of UV photolysis products (λ= 285-305 nm, 1000 min.) from carbamoyl azide 8 (Ar, 10K).

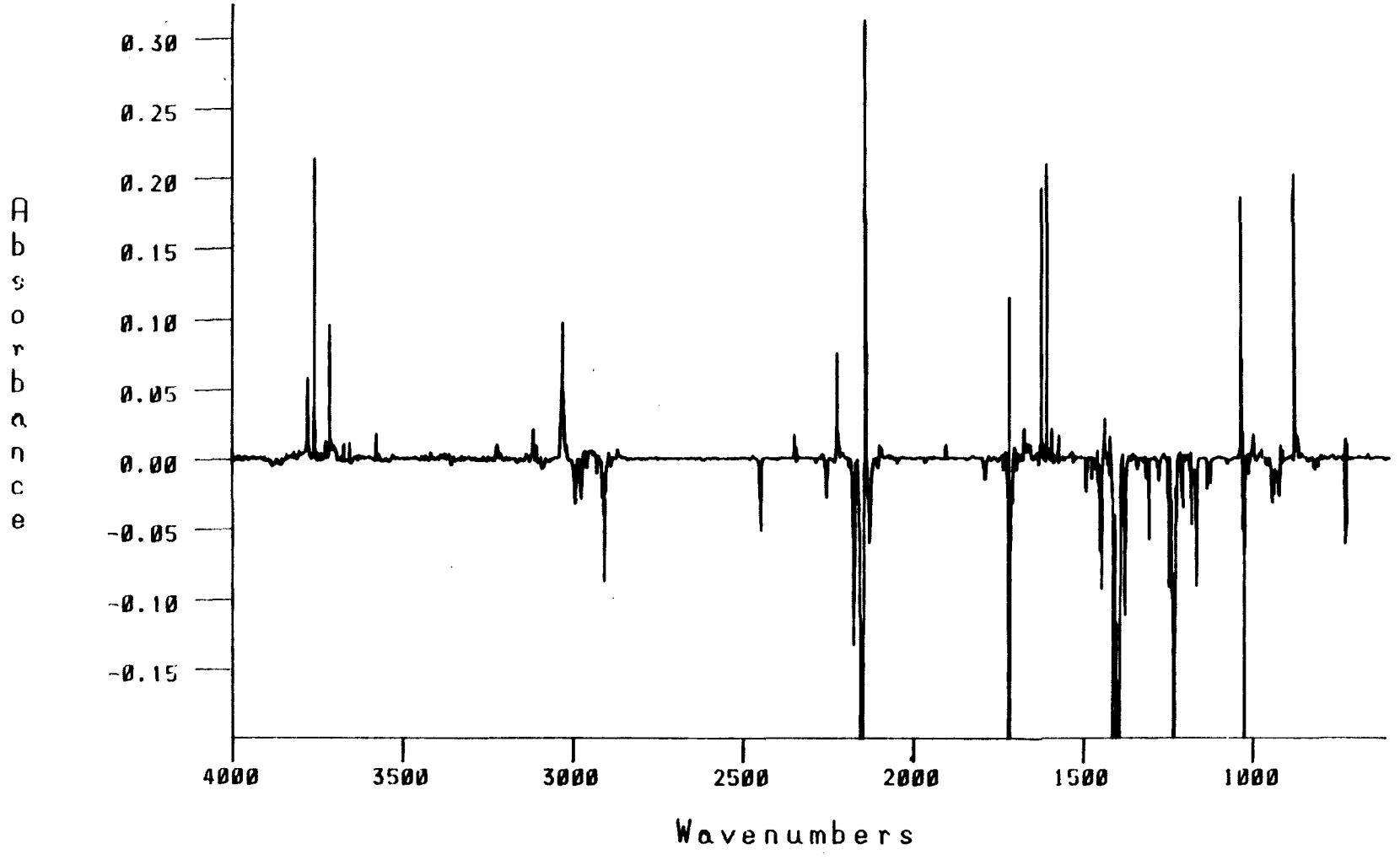

Figure 27. Difference FTIR spectrum of 1,1-diazene **2**, aminoisocyanate **12**, cyclopropane, and propene (Ar, 10 K) resulting from UV photolysis (λ=285-305 nm, 1000 min.) of carbamoyl azide **8** minus spectrum of **8** before photolysis (subtraction factor α=1.00)

Table IX. Bands from the FTIR spectrum of UV photolysis products from carbamoyl azide **8** (positive in Figure 27) and isotopic multiples (in parentheses) from UV photolysis of carbamoyl azide **8**-^{15}N (Figure 30).

Peak Location (cm^{-1})	Intensity (A)	Assignment	
3113.7	0.022	?	
3028.2	0.099	cyclopropane	ν C-H
2967.5	0.005	**2**	ν C-H
2957.3	0.003	**2**	ν C-H
2866.2	0.007	propene	ν C-H
2221.1	0.075	**12**	ν NCO
(2210.5)	(0.028)	**12**	ν ^{15}NCO
2137.9	0.318	CO	
1674.0	0.022	**2**	ν N=N
(1651.7)	(0.009)	**2**	ν N=^{15}N
1661.8	0.010	propene	
1457.6	0.006	propene	
1436.5	0.028	cyclopropane	
1420.4	0.016	**2**	
1031.3	0.189	cyclopropane	
996.1	0.017	propene	
873.7	0.207	cyclopropane	
726.2	0.014	**2**	

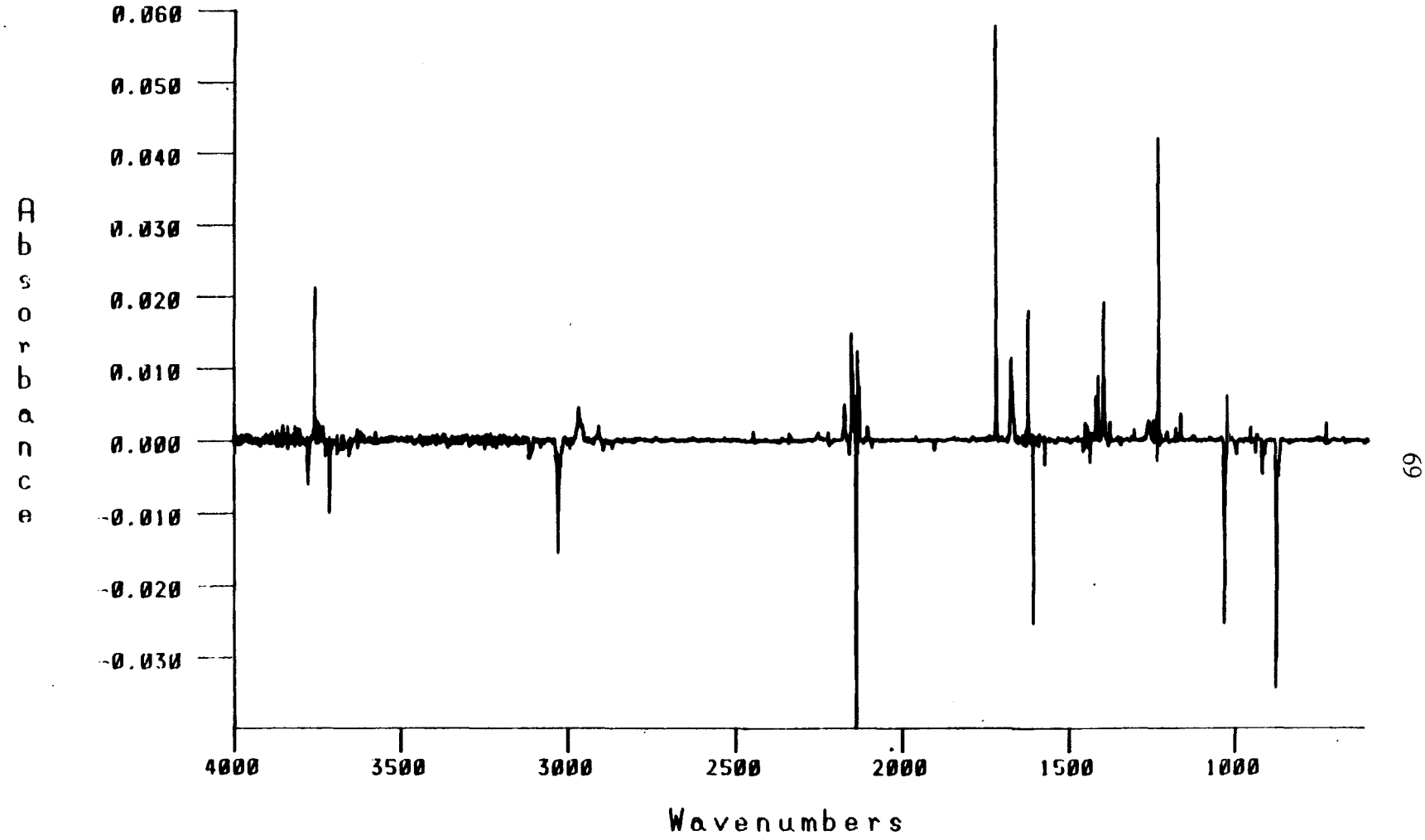

Figure 28. Difference FTIR spectrum of 1,1-diazene **2** (Ar, 10 K) from UV photolysis (λ=285-305 nm, 1000 min.) of carbamoyl azide **8** minus spectrum after subsequent visible photolysis (λ=440-580 nm, 90 min.) of **2** (subtraction factor α=1.00)

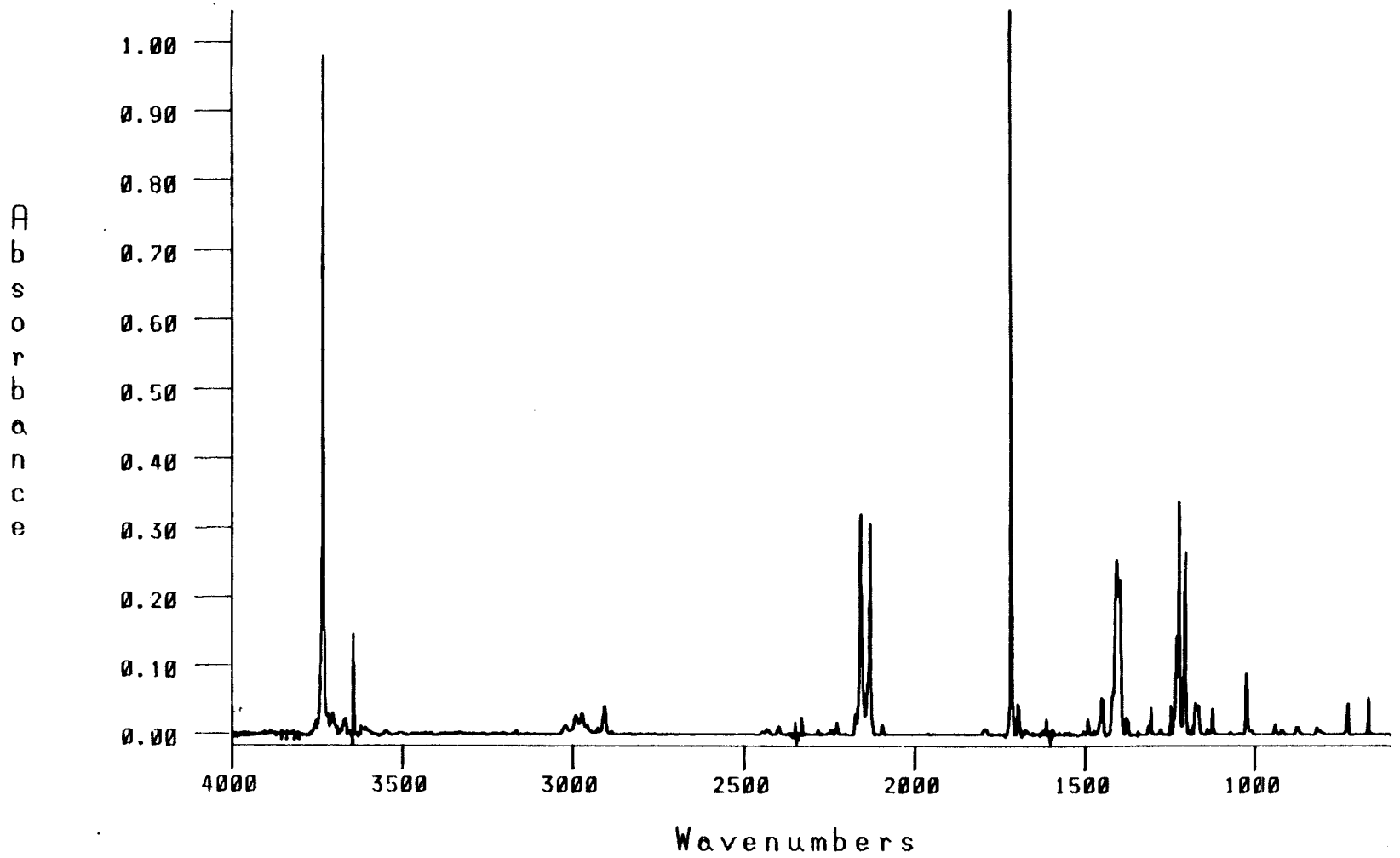

Figure 29. FTIR spectrum of labelled azetidine carbamoyl azide 8-^{15}N (Ar, 10 K).

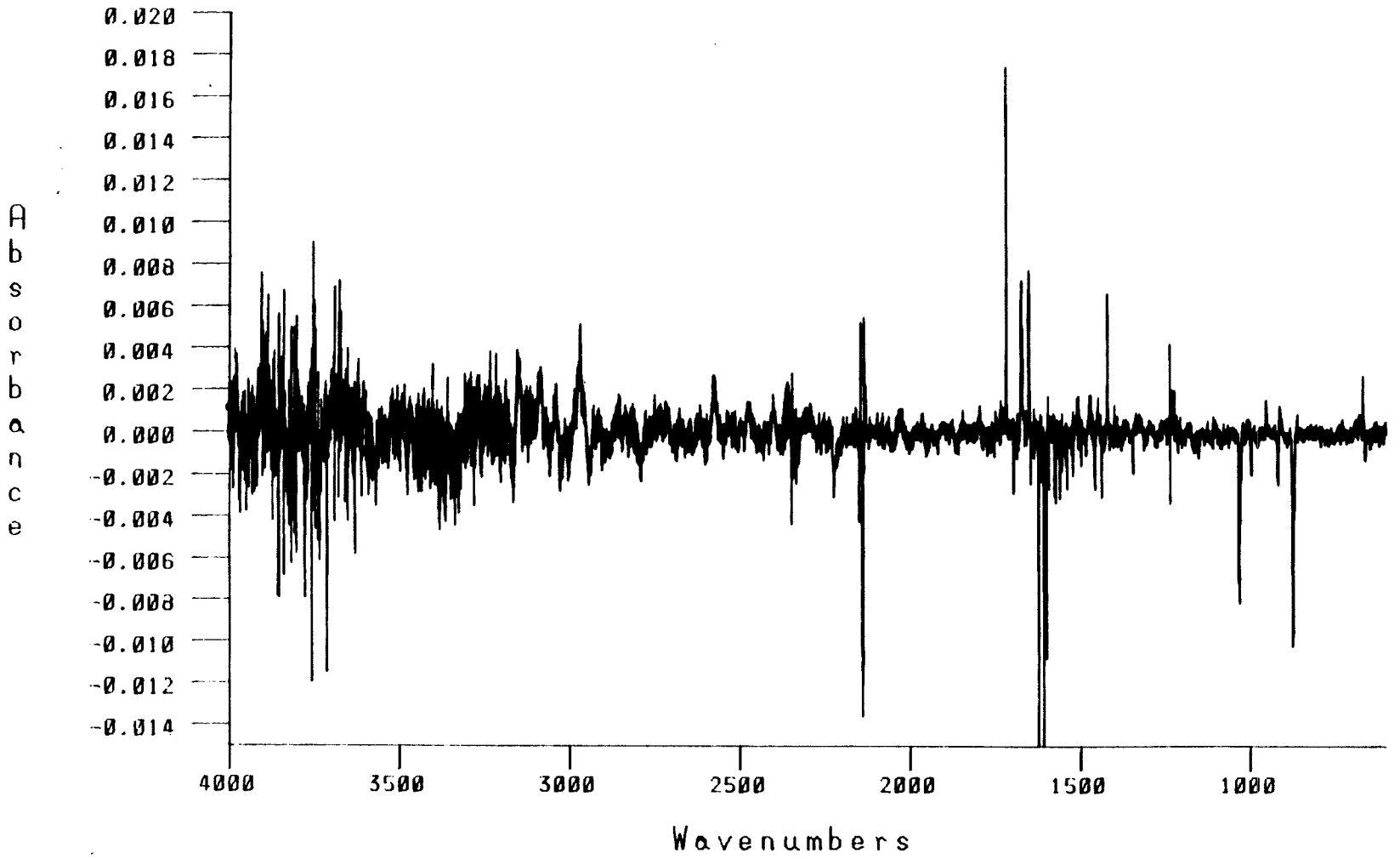

Figure 30. Difference FTIR spectrum of labelled 1,1-diazene **2**-^{15}N (Ar, 10 K) from UV photolysis (λ=285-305 nm, 795 min.) of carbamoyl azide **8**-^{15}N minus spectrum after subsequent visible photolysis (λ=440-580 nm, 160 min.) of **2** (subtraction factor α=1.0)

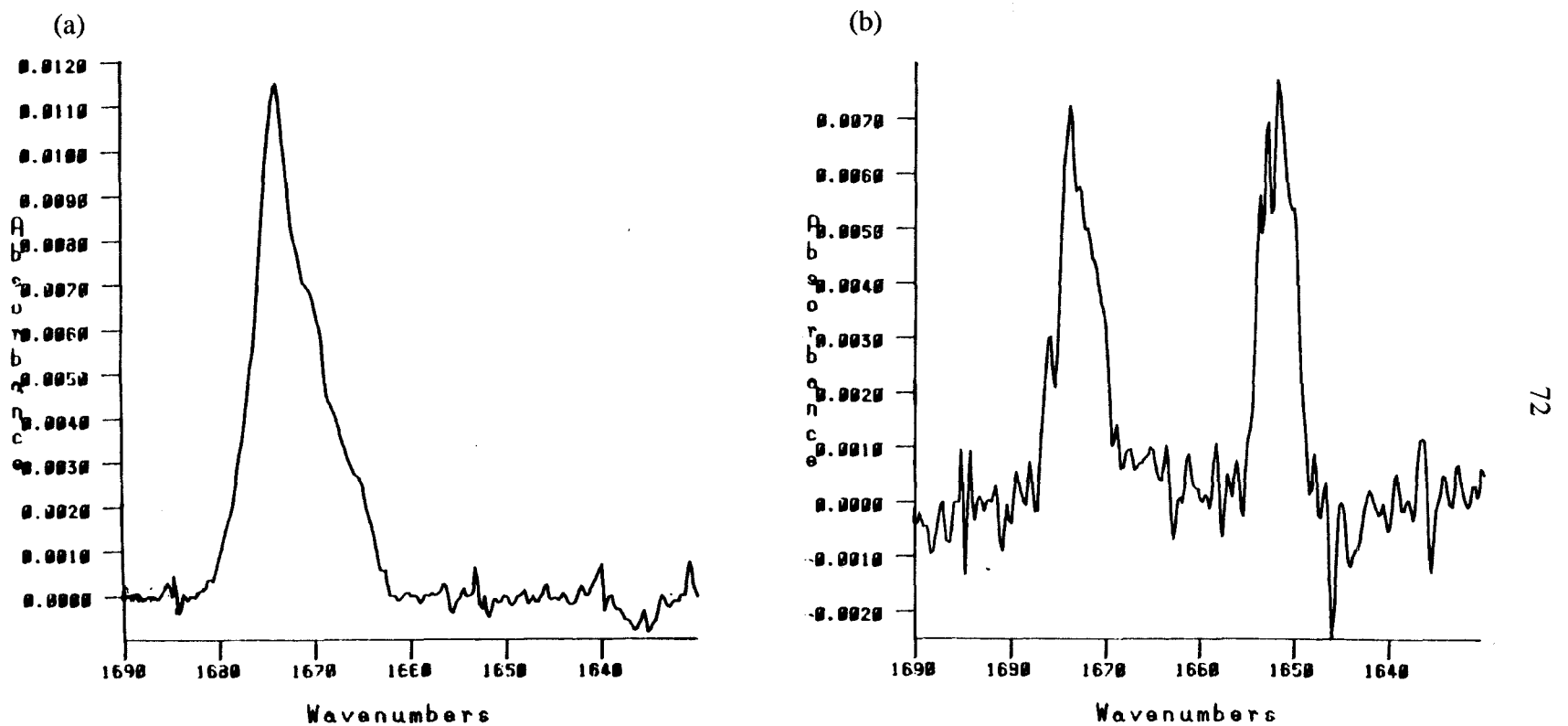

Figure 31. Difference FTIR spectra of N=N stretches of: (a) 1,1-diazene **2** (Ar, 10 K) and (b) 1,1-diazene **2** with labelled **2**-^{15}N (Ar, 10 K) from UV photolysis (λ=285-305 nm) of carbamoyl azides **8** and **8**-^{15}N respectively minus spectra taken after subsequent visible photolysis (λ=440-580 nm) of the 1,1-diazenes (subtraction factors α=1.0).

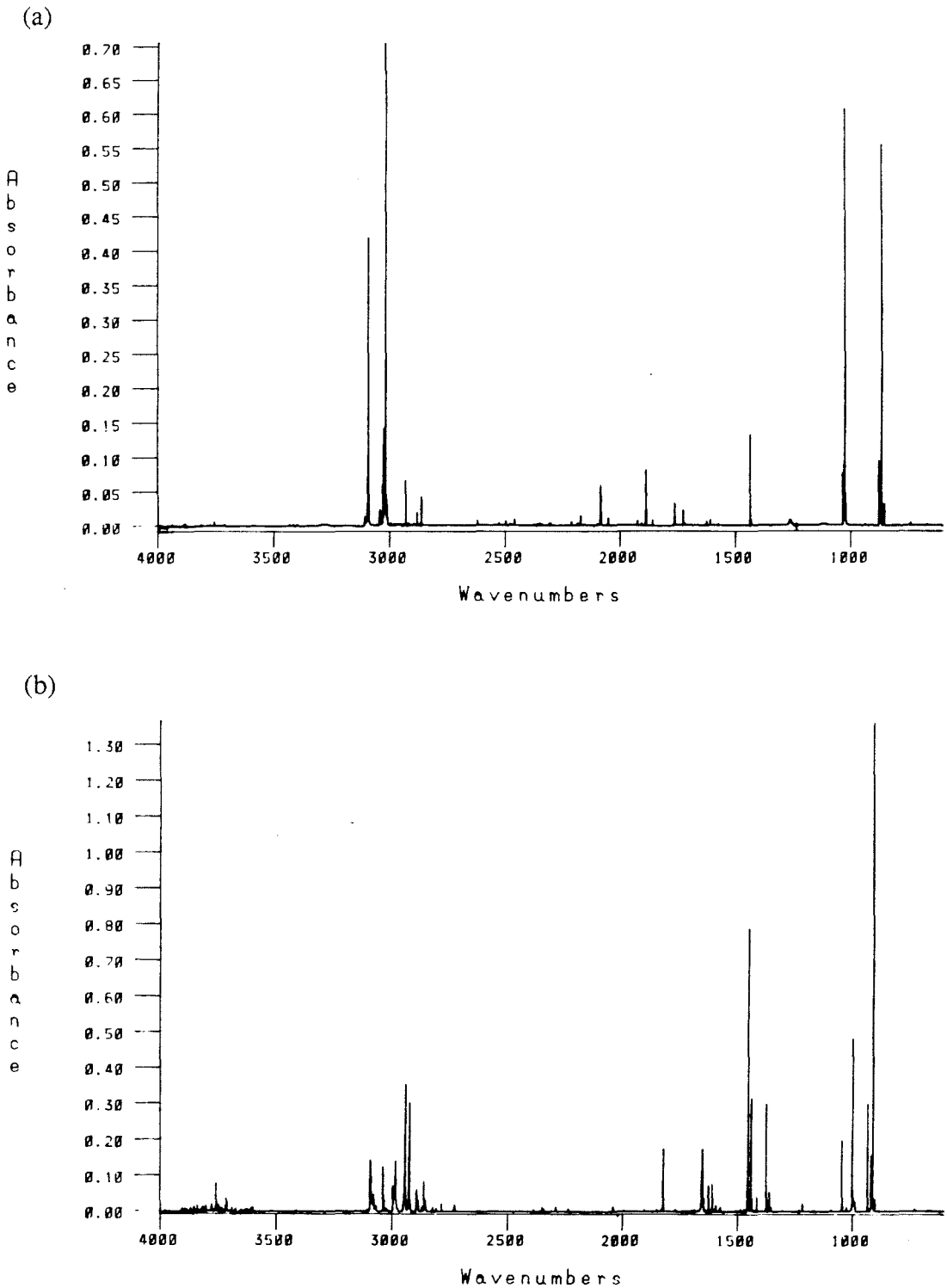

Figure 32. FTIR spectra of: (a) matrix isolated cyclopropane (Ar, 10K); (b) matrix isolated propene (Ar, 10 K).

Table X. Bands from the FTIR spectra of matrix isolated cyclopropane (Figure 32a) and propene (Figure 32b).

Location (cm^{-1})	Intensity (A)		Location (cm^{-1})	Intensity (A)	
cyclopropane			propene		
3091.7	0.426	ν C-H	3091.3	0.144	ν C-H
3024.5	0.145		3036.6	0.127	
3016.3	0.740		2982.9	0.143	
2928.3	0.066		2940.5	0.355	
2861.6	0.042		2922.1	0.313	
			2890.1	0.062	
			2858.8	0.085	
2082.3	0.059	combination			
1885.8	0.081				
			1819.8	0.175	combination
			1650.2	0.178	C=C stretch
1434.3	0.133	CH_2 def.	1452.8	0.821	CH_3 def.
			1439.1	0.317	
			1373.6	0.301	CH_3 def.
1024.8	0.611	CH_2 bend	1043.6	0.200	CH_2 rock
			997.7	0.497	CH_3 rock
			932.4	0.303	C-H bend
			916.2	0.158	C-C stretch
			908.6	1.367	
864.7	0.563	ring def.			

abundant. The assignment of the product bands to these hydrocarbons was checked by matrix isolation of commercially obtained samples as shown in Figure 32. The major peaks are listed in Table X. Previous product studies on 1,1-trimethylenediazene systems have not resulted in the formation of olefins.[10,11] However, olefins were observed from the pyrolysis of pyrazolines by Crawford and Mishra.[12] A more detailed mechanistic interpretation of these results will be given in a later section.

2. Electronic Spectroscopy.

An organic glass containing carbamoyl azide **8** was prepared by cooling a dilute solution (~5 x 10^{-3} M) of **8** in 2MTHF to 80 K in the low temperature spectroscopy cell.[56] Broad band UV photolysis (λ=200-400 nm)[60] of **8** under these conditions results in generation of 1,1-diazene **2**, although in low yield. The electronic absorption spectrum of **2** is shown in Figure 33. The 0,0 band[61] is at 556 nm (2.23 eV) and λ_{max} is the 0,2 band at 486 nm (2.55 eV). This is the largest excitation energy observed in a 1,1-diazene. The average vibrational spacing is also larger than any other known 1,1-diazene at 1389 cm^{-1}. The structural implications of this data are discussed in Chapter 4.

Warming a 2MTHF glass of **2** to softening at 90 K results in the loss of the structured absorption of **2** and growth of the structureless transition (λ_{max}=480 nm) apparently due to azomethinimine **13**. Like azomethinimine **10**, **13** is reversibly thermochromic in 2MTHF solution. Warming the softened glass results in a shift of the

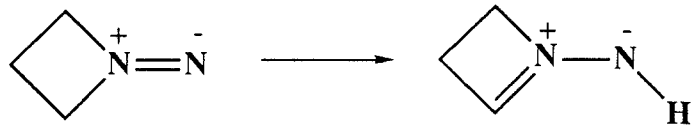

2 **13**

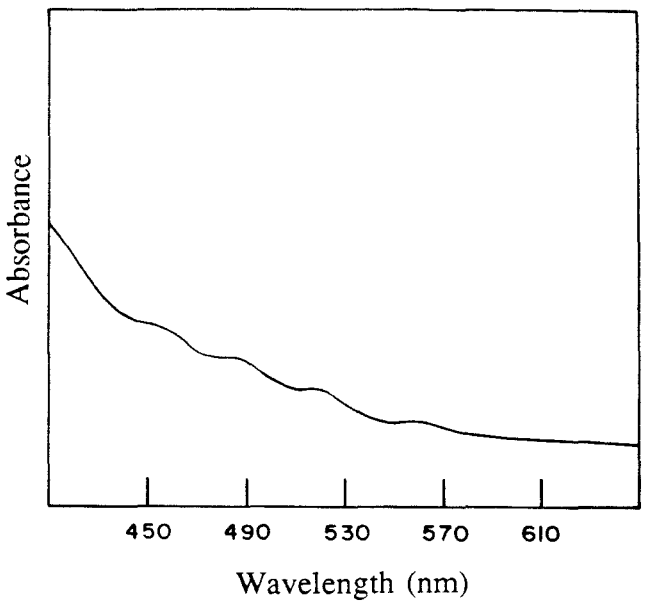

Figure 33. Electronic absorption spectrum of 1,1-diazene **2** (2-MTHF, 80 K).

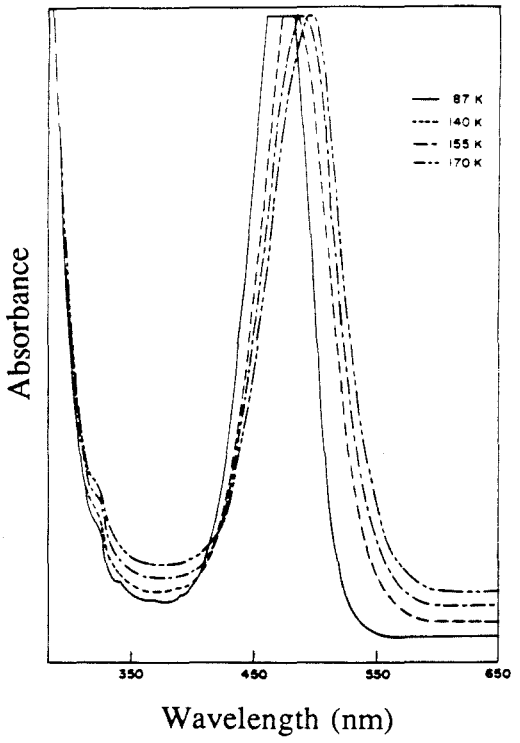

Figure 34. Electronic absorption spectrum of azomethinimine **13** showing thermochromism.

absorption maximum to longer wavelengths (λ_{max}=487 at 150 K, λ_{max}=494 at 170 K and above. Table XI lists λ_{max} for **13** as a function of temperature. Cooling back to 85 K shifts λ_{max} back to shorter wavelengths (470 nm) (Figure 34). Warming the softened glass above 210 K results in the loss of the absorption due to azomethinimine **13**.

Table XI. Thermochromism of azomethinimine **13**.

T (K)	λ_{max} (nm)
90	470.0
140	479.0
150	487.0
170	494.0
190	494.0

3. Product Analysis.

Analysis of product compositions from thermolysis or visible photolysis of 1,1-diazene **2** generated in an organic glass at 77 K was accomplished by analytical VPC and NMR spectroscopy as described in the experimental section. The main products observed from **2** were cyclopropane and propene, with small amounts of ethene, 1-pyrazoline, and propane. The product ratios from thermolysis and photolysis are given in Table XII. It is not too surprising that the ratios are identical within experimental error, since the FTIR and electronic absorption studies indicated that the yield of photogenerated **2** was poor. A large part of the product yield is therefore due to **2** that is generated only transiently and is not

subjected to the thermolysis or photolysis conditions. No 2-tetrazene dimer is observed as a product from **2**, which is not unexpected. The concentrations of **2** must be quite low, and extrusion of nitrogen is quite facile. The bis(trimethylene)-2-tetrazene which would be obtained by dimerization of **2** is a known compound,[13] although the reaction conditions used to synthesize it were quite unusual. The major hydrocarbon products and their ratios are consistent with known trimethylene chemistry.[10-12] The minor products are somewhat unexpected, however. 1-Pyrazoline is apparently derived from closure of the 1,5-trimethylenediazenyl diradical derived from ring opening of **2** (Scheme 10). This suggests that nitrogen extrusion from **2** occurs by a one bond cleavage mechanism, with most of the diradical products losing molecular nitrogen to give trimethylene but that a small portion closes to give the 1,2-diazene. Calculations have predicted that one bond cleavage should generally be favored over concerted two bond cleavage,[29] and observation of the ring closed product is strong evidence that this is in fact the case. These same calculations also predicted that closure to the 1,2-diazene is enthalpically favored over a second cleavage

Table XII. Decomposition products from 1,1-diazene **2**.

conditions[a]	cyclopropane	propene	pyrazoline	ethene	propane
Δ	71.5	20.9	5.6	2.0	trace
hν	71.9	20.5	5.7	1.9	trace

a. Product ratios from NMR analysis, -80° C. Starting carbamoyl azide concentration ~1 x 10^{-1} M. For other conditions see experimental section (Chapter 5).

event. The formation of five membered rings by radical recombination is particularly favorable,[62] and can compete with C-N cleavage in this special diazenyl diradical. Photochemical decomposition of 1-pyrazolines has been observed to lead to alkenes and diazomethane in previous studies.[63] The trace amounts of propane observed are probably the result of hydrogen abstraction from the solvent by trimethylene diradicals.

Photochemical decomposition of **2** in an organic glass leads to some unusual observations which should be noted here. If a glass of **2** is allowed to warm and isomerize to **13**, then is cooled to again form a glass and irradiated (440-580 nm, 30 minutes), the orange color of **13** is observed to change. Electronic spectroscopy reveals maxima at 486 and 522 nm, which appear to correspond to the electronic transition of **2**. Photolysis of a purple glass of **2** (440-580 nm) also appears to give a mixture of **13** and **2**. Apparently photoisomerization from **2** to **13** and from **13** to **2** is possible, and since the absorptions overlap, a photostationary state is produced. This type of photoisomerization is precedented,[59,64] and four membered rings prefer exocyclic double bonds to endocyclic by ~1.5 kcal/mol.[50] The conformational rigidity enforced by incorporation of the 1,1-diazene and azomethinimine functionalities in a ring may also play a part in making these photoisomerizations possible.

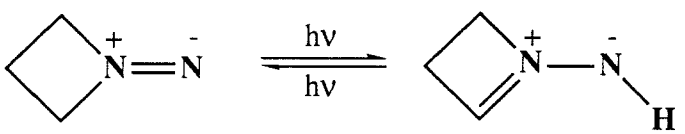

2 **13**

4. Kinetics and Mechanism.

As in the isomerization of **1** to **10**, isomerization of **2** to **13** in a softened 2MTHF glass at 92 K did not give interpretable kinetics. The decomposition of **13** could be fit to unimolecular kinetics. The disappearance of **13** was monitored by following the decay of the λ_{max}=494 transition at 220, 230, 245, and 255 K. The decays and unimolecular fits are shown in Figure 35. The Arrhenius activation parameters are E_a=15.1±0.3 kcal/mol with log A=9.8±0.3 ($\Delta H^{\ddagger}$=15.3 kcal/mol, $\Delta S^{\ddagger}$=-12.3 e.u.). These parameters are quite similar to those found for other 1,1-diazenes which give unimolecular kinetics and can be interpreted as reflecting the strength of the C-N bond and its rate of cleavage (k_{frag} in scheme 10). The value of E_a is lower than any other 1,1-diazene except 1,1-di-*t*-butyldiazene,[34,65] but not as low as might have been expected from the ring strain of **2**. For comparison, the studies of Crawford and Mishra on the thermal decomposition of 1-pyrazoline (the 1,2-diazene isomer of **2**) revealed an E_a of 42.4 kcal/mol with log A of 15.93.[12]

If the difficulty in generating 1,1-diazene **2** is due to its generation in a vibrationally excited state, the modest difference between the activation energies for **2** and 1,1-di-*iso*-propyldiazene raises the question of why these "hot molecule" effects were not seen in this case. Could it be that other 1,1-diazenes are also generated as vibrationally excited species and undergo one bond cleavage, but because of the strong cage effects in the matrix are reformed by radical recombination? If this were so, one might expect to see some percentage of the 1,2-diazene isomers in the other dialkyl 1,1-diazenes, and these species have not been seen. There might also be some particular problem with **2** arising from slower redistribution of the excess vibrational energy, therefore allowing more time for decomposition.[66] Perhaps the 1.7 kcal/mol difference in the activation energies of 1,1-diazene **2** and 1,1-di-*iso*-propyldiazene is sufficient to lead to the radically different stabilities of the two species under the cryogenic photogeneration conditions. If the 15.1

Scheme 10. Decomposition of **13** with kinetics and observed products.

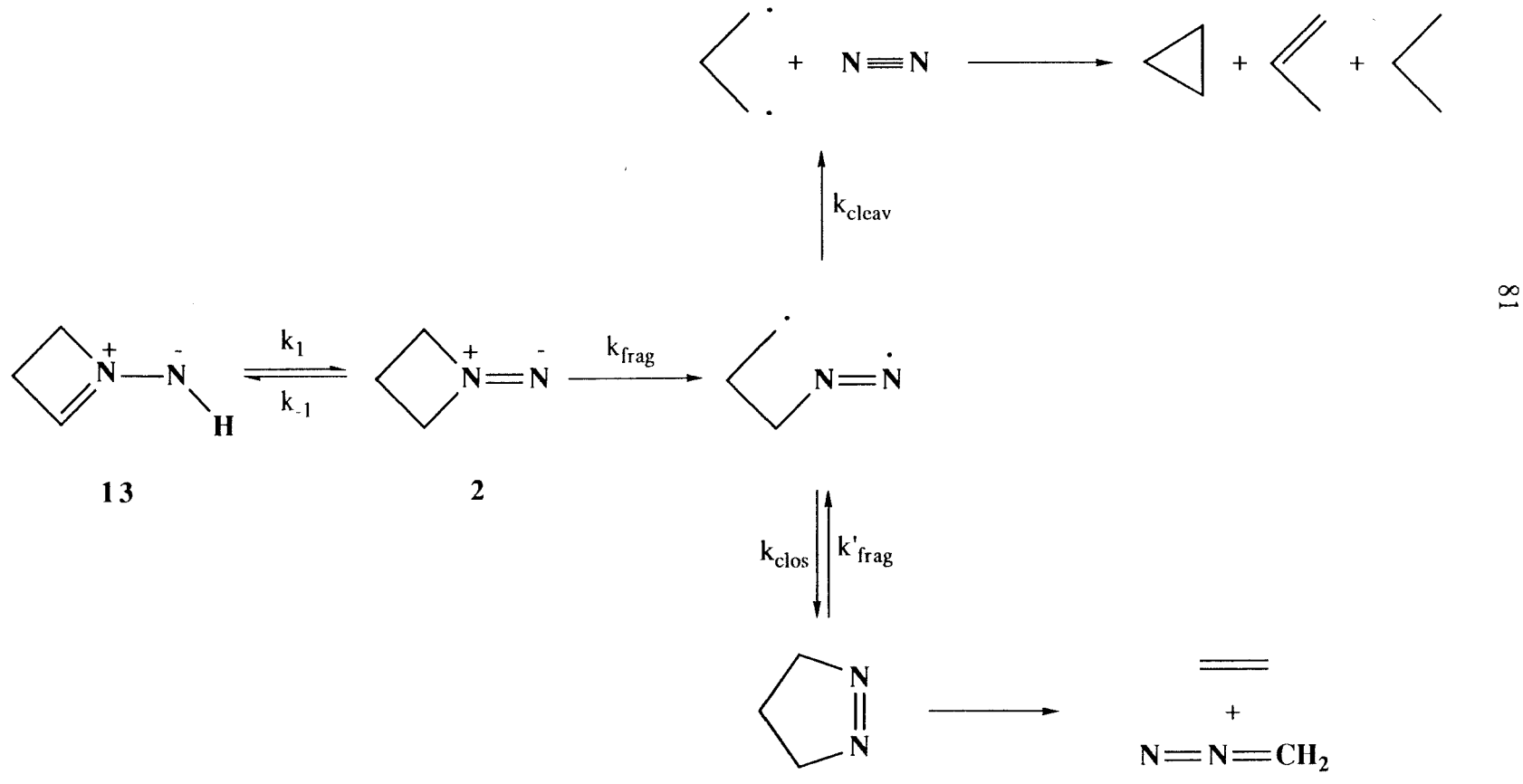

kcal/mol activation energy of **2** is low enough so that the excess vibrational energy available on photogeneration leads to decomposition, then it is unlikely that the 9.9 kcal/mol activation energy observed in decomposition of azomethinimine **10** is due to concerted loss of nitrogen, especially since 1,1-diazene **1** is produced in reasonable yields.

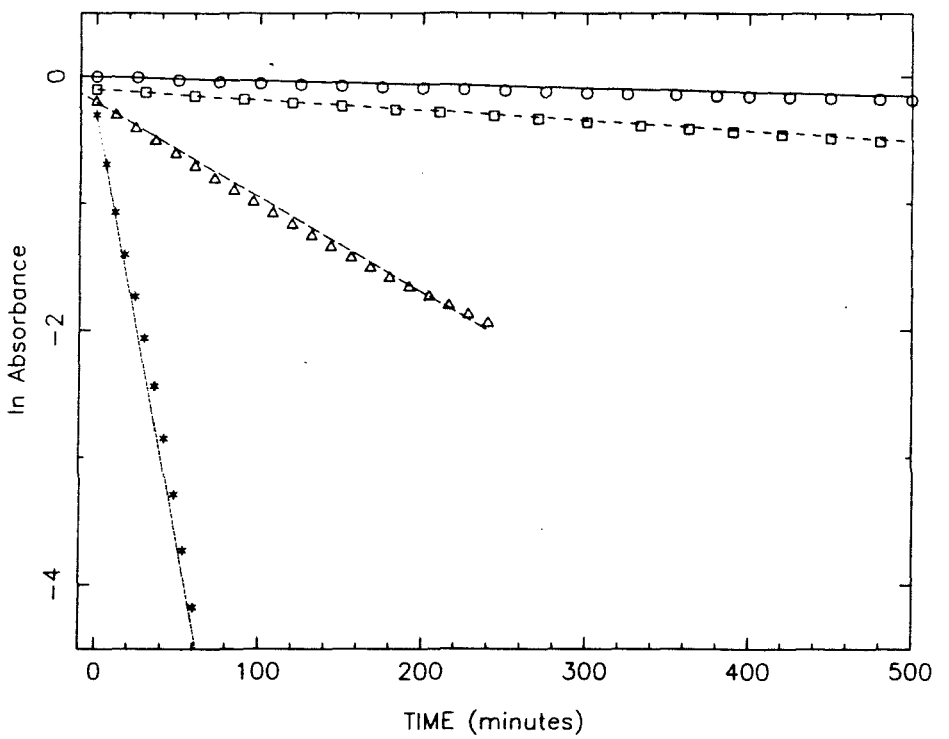

Figure 35. Unimolecular decay kinetics for azomethinimine **13** from thermolysis of **2** (2-MTHF). Fitted rate constants are: 5.014×10^{-6} sec^{-1} at 220 K, 1.345×10^{-5} sec^{-1} at 230 K, 1.250×10^{-4} sec^{-1} at 245 K, and 1.086×10^{-3} sec^{-1} at 255 K.

D. 3,4-Dehydro-1,1-tetramethylenediazene.

The low yields experienced in the studies of 1,1-trimethylenediazene **2** indicated that attempts to make the next smaller cyclic dialkyl 1,1-diazene, three membered 1,1-dimethylenediazene **14**, would meet with failure. This molecule is expected to be 14 kcal/mol more strained than **2**.[67] Synthesis of the carbamoyl azide precursor would require some new approaches as well, since previous reports of reactions of phosgene with aziridine led to ring opening.[68] Destabilization of the 1,1-diazene ground state is not the only approach to studying the limits of 1,1-diazene stability, as the possibility of a concerted loss of nitrogen from 1,1-diazene **1** indicated. Another 1,1-diazene which should have a concerted pathway for nitrogen extrusion is 3,4-dehydro-1,1-tetramethylenediazene **15**. Earlier work on this system by Lemal revealed only 1,3-butadiene and nitrogen as products from deamination of 3-pyrroline.[7] The lack of 2-tetrazene dimerization products from this reaction points to relatively easy loss of nitrogen from the 1,1-diazene. This leads to an additional point of interest in 1,1-diazene **15**, the potential for use as a precursor for the *s-cis* form of 1,3-butadiene, a species which has itself been the subject of several studies.[69] Orbital symmetry considerations suggest that photochemical decomposition (as is usually accomplished in the matrix) should lead to the *s-trans* form while thermal decomposition should lead to the *s-cis* form.[7]

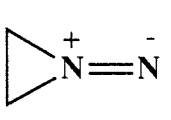

14

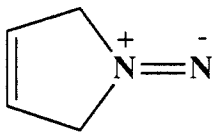

15

1. Synthesis.

A slightly different synthetic route was used to make the carbamoyl azide precursor for **15**. This route, based on the work of Birkofer and Krebs,[70] avoids the use of phosgene at the expense of two synthetic steps. Another source of concern in the synthesis was the commercial unavailability of pure 3-pyrroline **16**. Commercially obtained material is 75% 3-pyrroline and 25% pyrrolidine. It was decided to carry the mixture through the synthesis and effect separation at the carbamoyl azide stage. In most cases, this would probably be a poor decision, but by chance it was the correct choice in this situation.

The synthesis is shown in scheme 11. Only the 3-pyrroline component of the mixture is shown, but it should be kept in mind that the mixture was carried through the entire synthesis. Treatment of the 3-pyrroline/pyrrolidine mixture with chloro-trimethylsilane results in the formation of aminosilane **17**. Bubbling dry carbon dioxide

Scheme 11. Synthesis of carbamoyl azide **20**.

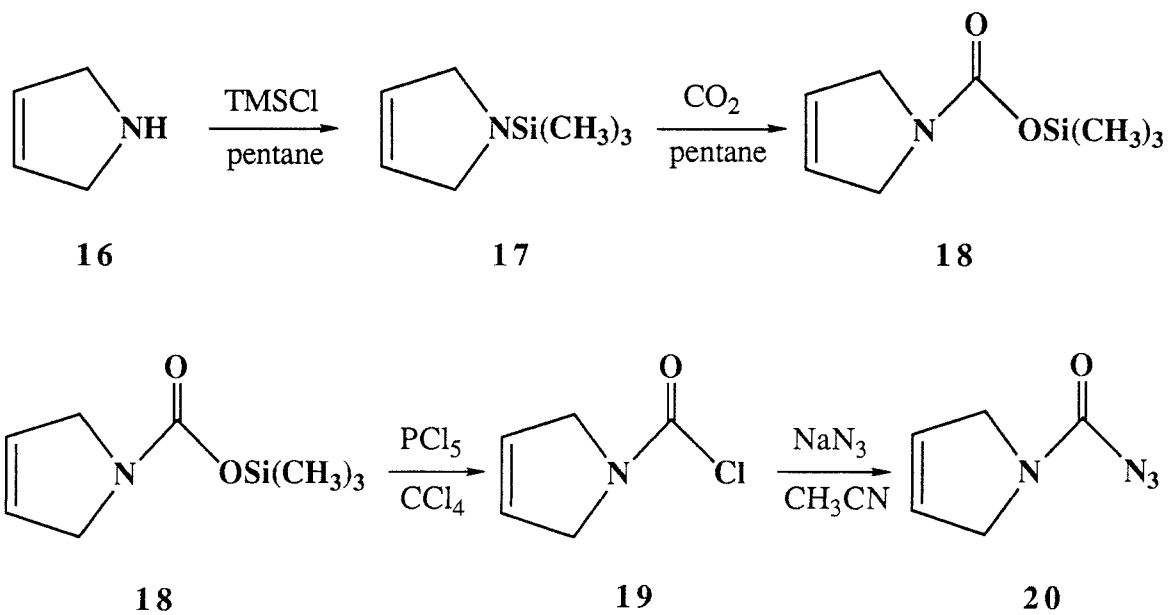

through a solution of **17** in pentane leads to formal insertion of carbon dioxide into the silicon-nitrogen bond to give silyl carbamate **18**. Reaction of **18** with phosphorus pentachloride yields carbamoyl chloride **19**. Substitution of azide for chloride is effected in the usual way to give a mixture of 3-pyrroline carbamoyl azide **20** and pyrrolidine carbamoyl azide **7**. Attempts to separate **20** and **8** by preparative VPC were unsuccessful. However, it was found that carbamoyl azide is a crystalline solid (m.p. 64-66^{o} C) at room temperature while carbamoyl azide **7** is a viscous liquid. Two recrystallizations of the mixture of **20** and **7** from hexane gave pure carbamoyl azide **20**. The crystallinity of **20** is probably due to a nearly planar geometry of the molecule.

2. FTIR Studies.

Matrix isolated carbamoyl azide **20** was prepared by codeposition with UHP argon onto a CsI substrate at 20 K. The FTIR spectrum of matrix isolated **20** is shown in Figure 36, and the positions and assignments of the bands are given in Table XIII. Photolysis with 295-305 nm radiation (using a 10 nm bandpass interference filter centered at 300 nm) results in loss of the bands of **20** and the growth of new bands. The FTIR spectrum resulting from UV photolysis is shown in Figure 37. A difference spectrum showing the results of UV photolysis is shown in Figure 38. Table XIV lists the new bands that appear on photolysis with their assignments. Visible photolysis (λ=470-610 nm) led to no spectral changes, and no new bands in the region where $\nu_{N=N}$ of **15** is expected were observed. This was quite unexpected, since narrow band UV photolysis around 300 nm had been successful in generating 1,1-diazene **2** when broad-band UV photolysis had failed. As in the case of carbamoyl azide **8**, photo-Curtius rearrangement to aminoisocyanate **21** is occurring, as demonstrated by the observation of the isocyanate stretch of **21** at 2240.7 cm^{-1}. Photodecarbonylation of **21** is also occurring, since the

isocyanate band of **21** is of low intensity and the carbon monoxide band at 2138.5 cm^{-1} is observed, but 1,1-diazene **15** is not found as a stable species. It is unlikely that the 300 nm light used for photolysis is photodecomposing **15**, so the inability to observe 1,1-diazene **15** in an argon matrix at 10 K must be due to facile nitrogen extrusion. Although the activation energy for nitrogen extrusion from **15** should be less than the usual value for 1,1-diazenes whether the reaction occurs by a concerted or by a stepwise radical mechanism, it is also unlikely that the activation energy is so low that the reaction proceeds thermally at 10 K. This points to the formation of **15** in an excited vibrational state from photodecarbonylation of **21**. 1,1-Diazene **2** could be observed under these same conditions (although in low yield) and was found to have an activation energy of 15.1 kcal/mol, so the activation energy for nitrogen extrusion from **15** must be less than 15 kcal/mol.

Scheme 12. Photolysis of carbamoyl azide **20**.

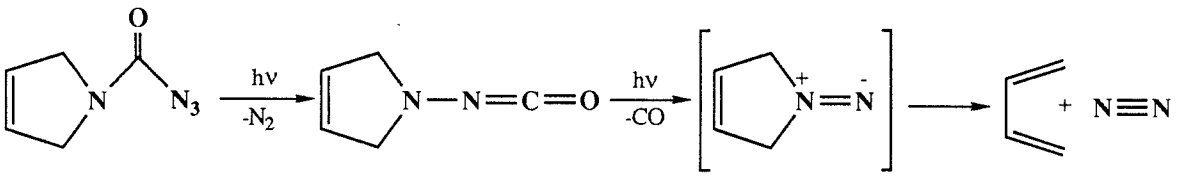

20 **21** **15**

The studies by Lemal on the deamination of 3-pyrroline and its 2,5-dimethyl derivatives indicated that nitrogen extrusion from **15** is concerted, giving products expected from a disrotatory mechanism, as predicted by orbital symmetry.[7] In the matrix, the disrotatory process should result in the higher energy *s-cis* form of 1,3-butadiene. The thermally forbidden, photochemically allowed conrotatory process should give the more stable *s-trans* conformer. Fragmentation by a radical mechanism would probably give both conformers. Radical centers formed on loss of nitrogen from **15** are allyl radicals, and by

consideration of the C-H bond dissociation energies should be stabilized by ~9 kcal/mol relative to primary alkyl radicals and by ~6 kcal/mol relative to *iso*-propyl radicals.[49] As a first approximation, this difference can be correlated to the activation energy of the radical mechanism using the known value for 1,1-di-*iso*-propyldiazene, giving an E_a of ~11 kcal/mol for loss of nitrogen from **15**. The experiments of Lemal suggest that reaction by the concerted mechanism dominates at higher temperatures, which may mean that the activation energy of the concerted pathway is lower.

Matrix isolation experiments on the conformers of 1,3-butadiene have been reported previously by Squillacote and by Michl.[69] Table XV contains the bands assigned by Michl and by Squillacote to the *s-cis* and *s-trans* conformers (Scheme 13). Comparison with the product bands in Table XIV reveals that both conformers are formed on photolysis of **20**, presumably via **15**. This apparent contradiction of the 3-pyrroline deamination results may be explained by photochemical formation of **15** with sufficient energy to fragment by either the radical or concerted mechanism. Recall that the yields of 1,1-trimethylenediazene **2**, with an experimentally determined activation energy for fragmentation of 15.1 kcal/mol, were approximately 10% of the expected yields. This suggests that the excess vibrational energy in photochemically formed 1,1-diazenes is 14-15 kcal/mol. If the barrier for radical decomposition of **15** is 11 kcal/mol, then sufficient energy is available for this process,

Scheme 13. Conformers of 1,3-butadiene.

s-trans *s-cis*

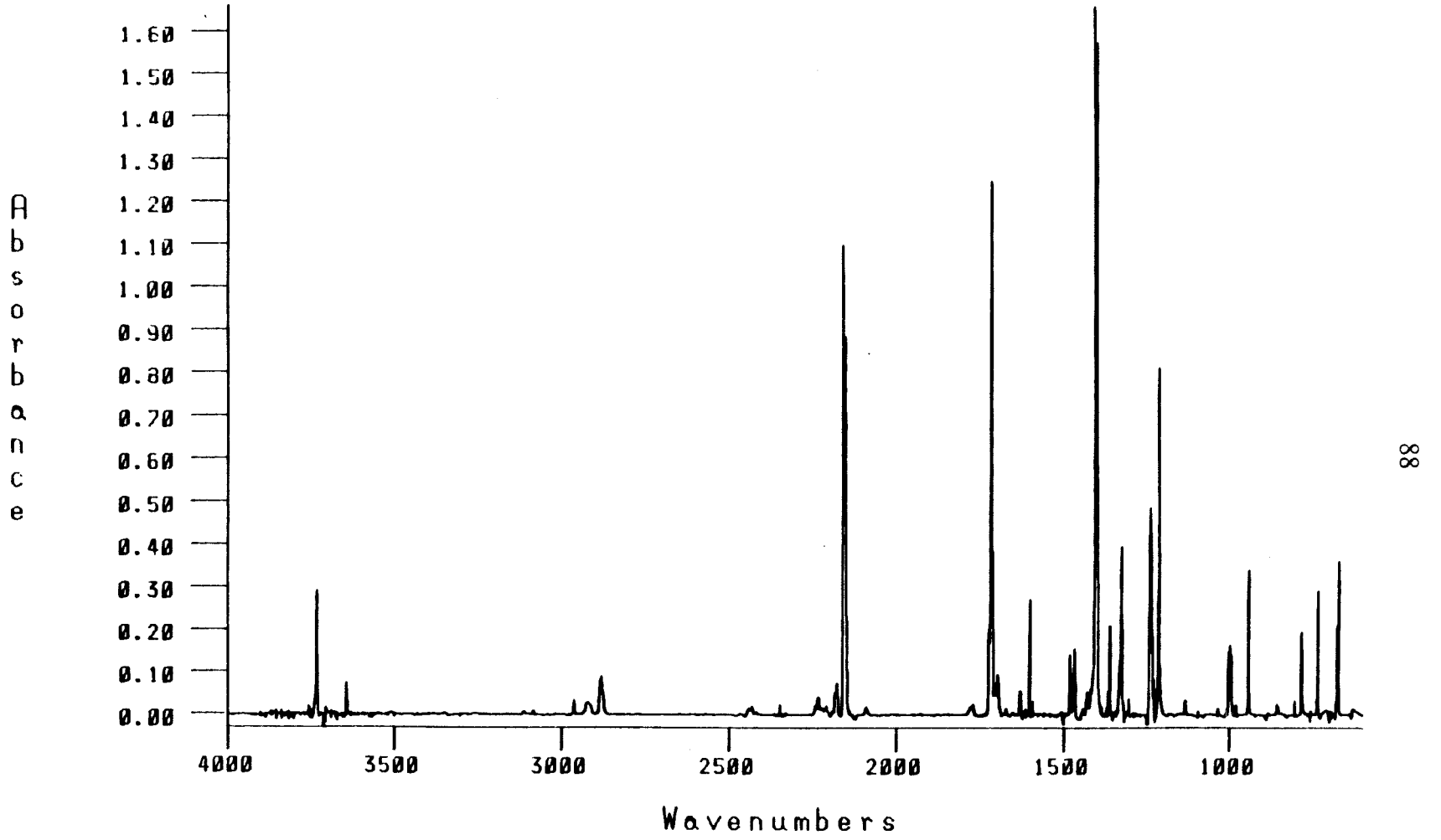

Figure 36. FTIR spectrum of 3-pyrroline carbamoyl azide 20 (Ar, 10 K).

Table XIII. Bands from the FTIR spectrum of 3-pyrroline carbamoyl azide **20** (Figure 36)

Peak Location (cm^{-1})	Intensity (A)	Assignment
3081.1	0.010	ν C-H
2961.3	0.034	
2919.7	0.030	
2879.6	0.092	
2156.6	1.098	ν N_3 (asym)
2148.9	0.892	
1722.6	0.196	ν C=O (asym)
1713.9	1.251	
1696.2	0.095	
1481.1	0.142	
1467.5	0.158	
1404.4	1.672	ν C=O (sym)
1398.3	1.587	
1361.7	0.216	
1325.8	0.398	
1238.9	0.491	ν N_3 (sym)
1211.6	0.812	
1000.8	0.149	
997.2	0.166	
992.7	0.142	
941.8	0.340	
782.5	0.196	
732.6	0.293	δ N_3
675.0	0.208	
670.1	0.364	

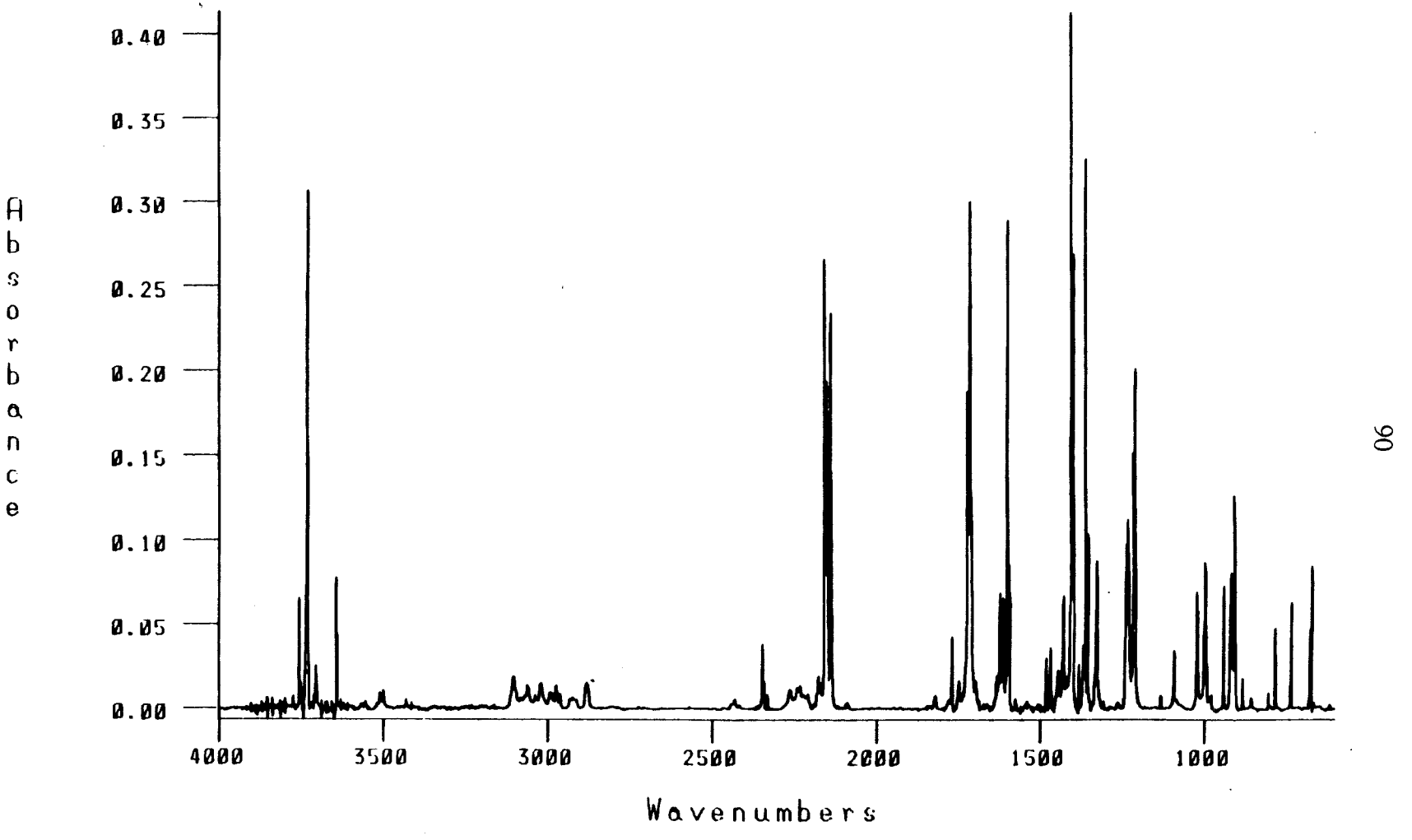

Figure 37. FTIR spectrum of UV photolysis products (λ=295-305 nm, 400 min.) from carbamoyl azide 20 (Ar, 10K).

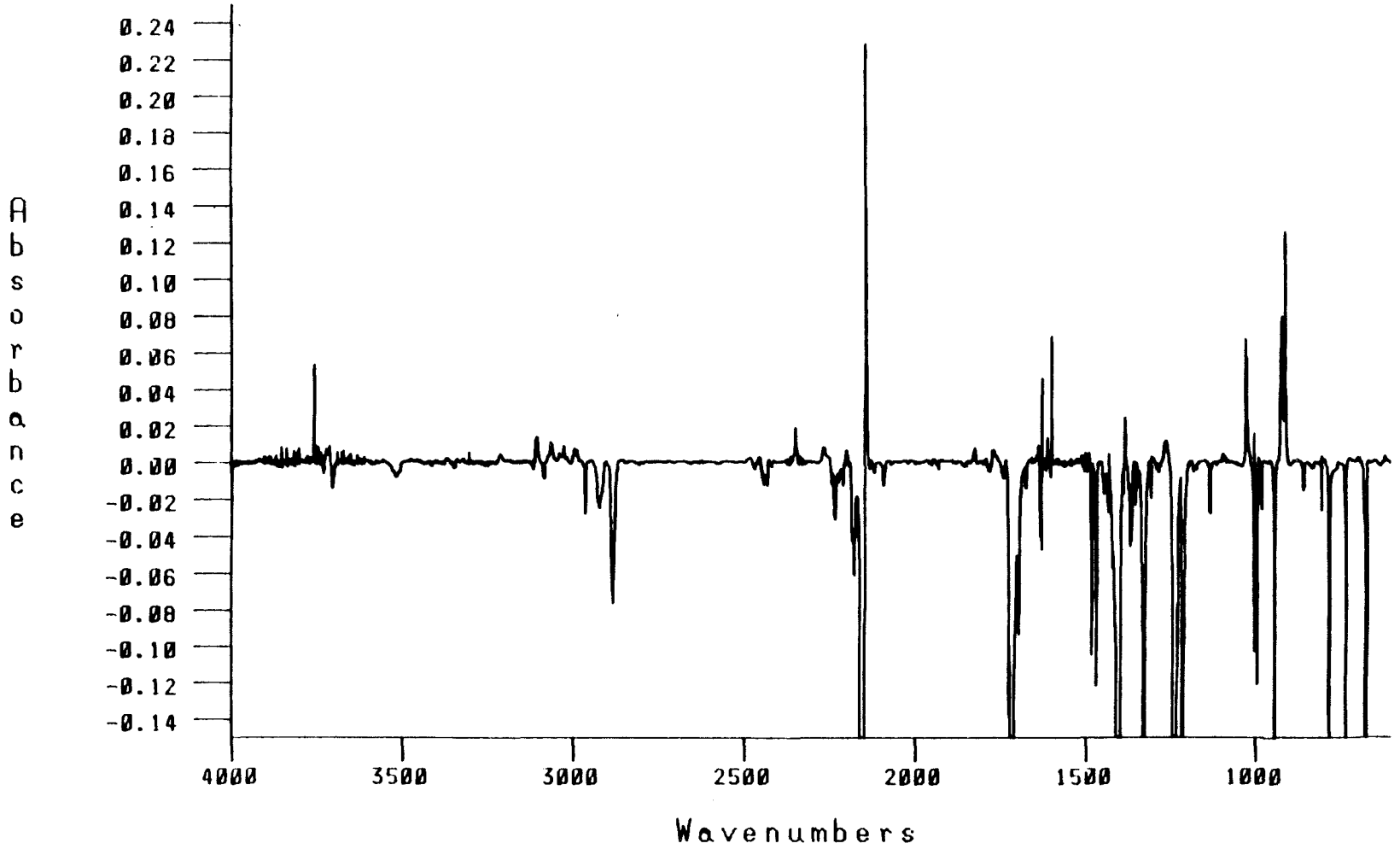

Figure 38. Difference FTIR spectrum of aminoisocyanate **21** and 1,3-butadiene (Ar, 10K) from UV photolysis (λ=295-305 nm, 400 min.) of carbamoyl azide **20** minus spectrum of **20** before photolysis (subtraction factor α=1.00).

Table XIV. Bands from the FTIR spectrum of the products from photolysis of 3-pyrroline carbamoyl azide **20** (positive in Figure 38).

Peak Location (cm^{-1})	Intensity (A)	Assignment
3102.6	0.013	*s-trans*
3061.9	0.011	*s-trans*
3037.8	0.005	*s-trans*
3023.5	0.009	*s-trans*
2992.1	0.007	*s-cis*
2985.4	0.008	*s-trans*
2240.7	0.008	**21**
2138.4	0.228	CO
1820.2	0.007	*s-trans*
1767.9	0.007	?
1634.3	0.009	*s-cis*
1426.7	0.004	*s-cis*
1379.8	0.025	*s-trans*
1259.4	0.012	?
1091.7	0.004	*s-cis*
1024.1	0.067	*s-trans*
1021.3	0.057	*s-trans*
999.0	0.016	*s-cis*
918.2	0.080	*s-cis*
907.2	0.127	*s-trans*

Table XV. Infrared bands assigned to the *s-cis* and *s-trans* conformers of 1,3-butadiene by Squillacote [S] and Michl [M].[69]

Location (cm^{-1})	Location (cm^{-1})
s-cis	*s-trans*
3000 [S]	3100 [S]
	3050 [S]
	2980 [S]
1828 [M]	1820 [S]
1632 [M]	
1612 [M]	
1425 [M]	1380 [S]
1402 [M]	
1089 [M]	
995 [M]	1020 [S]
914 [M]	901 [S]
740 [M]	
601 [M]	

which would result in a mixture of conformers. The concerted process may also be available, which would lead to an excess of the *s-cis* form. The ratios of the *s-cis* and *s-trans* forms from Figure 38 reveal a slight excess of the *s-trans* form (approximately 2:1). Since this is the lower energy form, it may be favored in the radical pathway. Alternatively, sufficient softening of the matrix in the vicinity of the products to allow isomerization would lead to an excess of this form. The excess of *s-trans* 1,3-butadiene could also be explained by some decomposition out of the S_1 manifold of 1,1-diazene **20**.

3. Product Analysis.

Preliminary experiments aimed at generating **15** from **20** in a 2MTHF glass at 77 K were unsuccessful, as the characteristic color and absorption spectrum of a 1,1-diazene were not observed. It had been hoped that the organic glass might be more efficient at vibrational deactivation of photogenerated **15** than solid argon.[66] Although a very faint orange color was observed on warming the glass, this was attributed to slight contamination of the carbamoyl azide precursor **20** with pyrrolidine derivative **7**. The azomethinimine derived from **15** should show a red shift in its electronic absorption spectrum since the azomethinimine chromophore is in conjugation with the double bond. Photochemical transformation of **20** with UV radiation at 77 K in a glass of 1:1 toluene-d_8 and tetrahydrofuran-d_8 also did not show the expected spectral changes indicating formation of 1,1-diazene **15**. After allowing the glass to soften and liquefy, NMR spectroscopy revealed the presence of 1,3-butadiene, corroborating the FTIR experiments. No other products were observed.

Chapter 3

1,1-Diphenyldiazene

Aryl substituted 1,1-diazenes should show some significant differences from the dialkyl derivatives that have been characterized by direct observation. Since the properties of 1,1-diazenes tend to reflect the trends shown in the isoelectronic carbonyl compounds,[42] projections can be made for the properties of 1,1-diphenyldiazene 22 using known properties of 1,1-dimethyldiazene as reference points and the known differences between acetone (dimethylketone) and benzophenone(diphenylketone) as guides. Aryl susbstitution weakens the C=O bond, as evidenced by the change in $\nu_{C=O}$ from 1715 cm^{-1} for acetone to 1660 cm^{-1} for benzophenone.[71] The $n\rightarrow\pi^*$ electronic transition also shifts to lower energy, with λ_{max} at 270 nm (4.59 eV) for acetone and 331 nm (3.75 eV) for benzophenone.[72] There are also differences in the photochemistry of dialkyl and diaryl ketones. Irradiation of acetone results in loss of carbon monoxide, while photolysis of benzophenone results in abstraction of hydrogen from the solvent and subsequent dimerization to benzopinacol.[73] The spectral differences between acetone and benzophenone

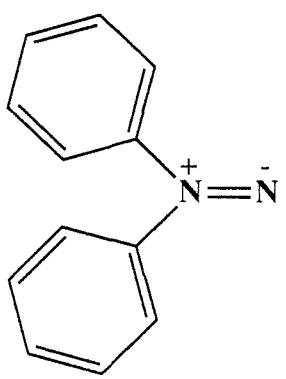

22

are a result of conjugation between the phenyl and carbonyl π systems of benzophenone. Contributions from resonance structures such as B and C in scheme 14 reduce the double bond character of the C=O bond. These interactions of the phenyl rings with the carbonyl π system also lower the $S_0 \rightarrow S_1$ gap and contribute to the observed photochemistry. The lower stability of aryl σ radicals compared to alkyl radicals (the C-H bond dissociation energy for benzene is 8 kcal/mol greater than for methane[49]) is also a factor in the photochemistry. These effects should be mirrored in 1,1-diphenyldiazene **22**. Given that 1,1-dimethyldiazene has $\nu_{N=N}$ of 1601 cm^{-1} and λ_{max} of 556 nm, reasonable projections for the spectroscopic properties of **22** are 1550 cm^{-1} for $\nu_{N=N}$ and 680 nm for λ_{max}(Table XVI). Fragmentation of **22** is not expected to be facile, and tautomerization to an azomethinimine is prevented by the lack of α-hydrogens. The results of oxidation of 1,1-diphenylhydrazine suggest that tetraphenyl-2-tetrazene will be the major product.[74]

Scheme 14. A few of the resonance structures of benzophenone.

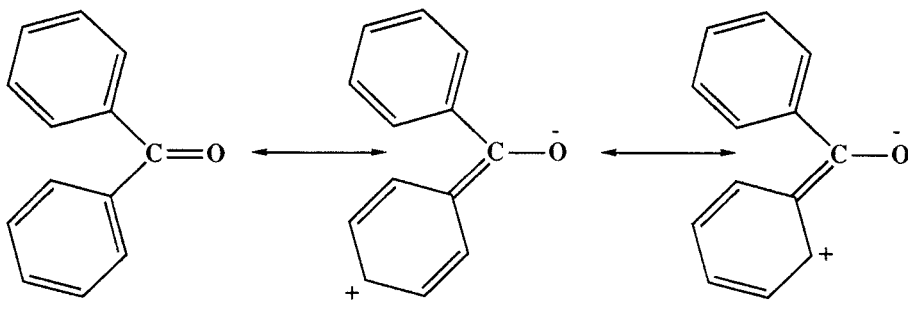

A B C etc.

Table XVI. Projected spectroscopic properties of 1,1-diphenyldiazene **22**.

	$\nu_{C=O}$ (cm^{-1})	λ_{max} (eV)		$\nu_{N=N}$ (cm^{-1})	λ_{max} (eV)
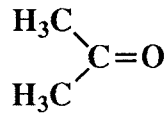	1715	4.59	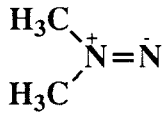	1601	2.23
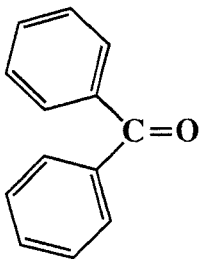	1660	3.75	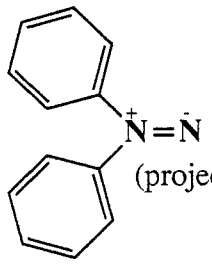 (projected)	1550	1.82

A. FTIR Studies.

Diphenyl carbamoyl azide **24** and labelled diphenyl carbamoyl azide-^{15}N **24**-^{15}N were synthesized by reaction of diphenyl carbamoyl chloride **23** with sodium azide (or sodium 1-^{15}N-azide) in acetonitrile as shown in scheme 15. Recrystallization from methanol gave analytically pure material. Matrix isolated diphenyl carbamoyl azide **24** was prepared by codeposition with UHP argon onto a CsI substrate at 20 K. The FTIR spectrum of matrix isolated **24** is shown in Figure 39, and the positions and assignments of the bands are given in Table XVII. Some differences can be observed between the FTIR spectrum of matrix isolated **24** and the spectra of the dialkyl carbamoyl azides under matrix isolation conditions (see Figure 12 and Figure 24). These differences seem to reflect the conformational flexibility of **24**. The most striking difference is the presence of four bands

Scheme 15. Synthesis of diphenyl carbamoyl azide **24.**

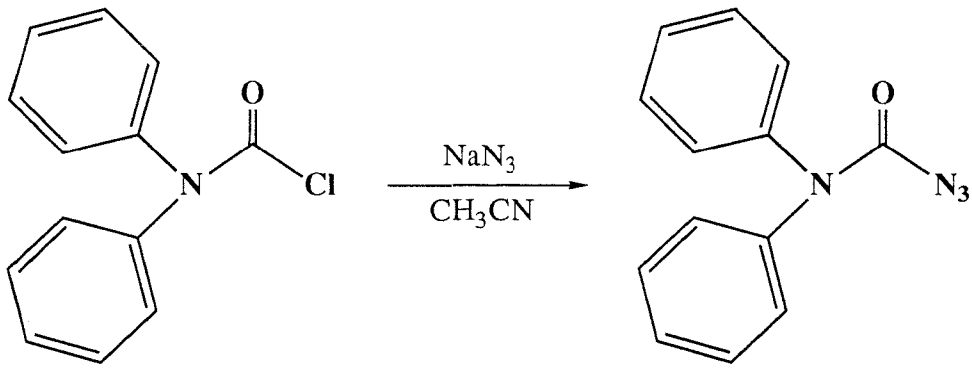

23 **24**

in the carbonyl region of the spectrum, where the dialkyl carbamoyl azides have one strong carbonyl stretch with a weaker side band. This appears to be another demonstration of the interaction of phenyl rings with a neighboring π system, in this case the lone pair of the carbamoyl nitrogen. The two lower energy carbonyl stretches are tentatively assigned to conformations where neither of the phenyl rings is conjugated with the lone pair, since they are quite similar to the carbonyl stretches of the dialkyl carbamoyl azides. The two higher energy bands are then assigned to conformations where one of the phenyl rings is conjugated with the lone pair, reducing the amide resonance and strengthening the carbonyl bond. For steric reasons, it seems unlikely that *both* phenyl rings could be conjugated with the lone pair, so the appearance of two strong bands suggests that the magnitude of this effect is different depending on the orientation of the conjugated phenyl ring with respect to the amide system. The proposed conformations of diphenyl carbamoyl azide **24** are shown in scheme 16. Another result of the conformational flexibility of **24** is that many of the bands are broader than is usual for matrix isolated species.

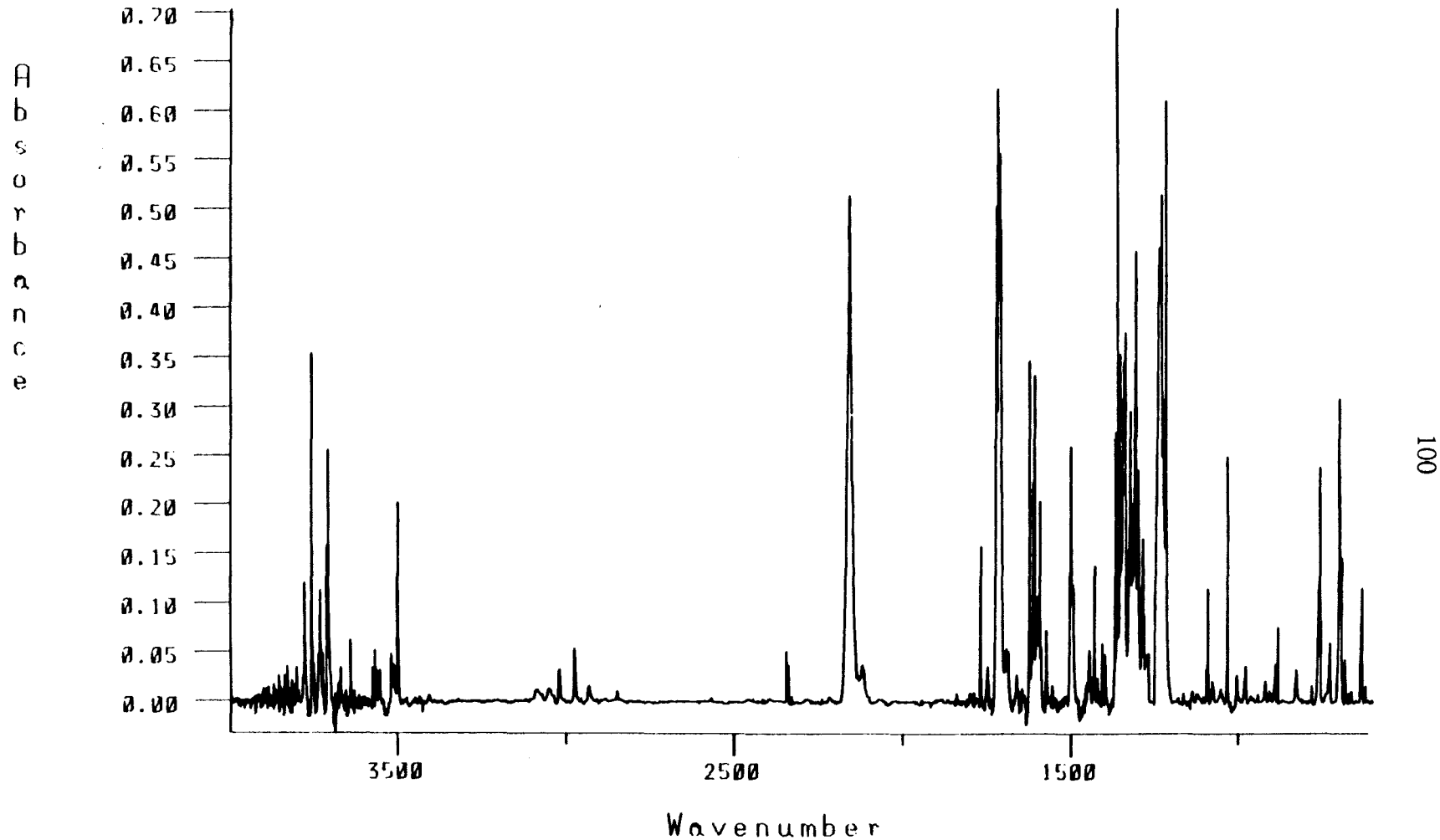

Figure 39. FTIR spectrum of diphenyl carbamoyl azide **24** (Ar, 10 K).

Table XVII. Bands from the FTIR spectrum of diphenyl carbamoyl azide **24** (Figure 39) and isotopic multiples from the FTIR spectrum of labelled carbamoyl azide **24**-^{15}N (Figure 42) (in parentheses).

Peak Location (cm^{-1})	Intensity (A)	Assignment
3019.5	0.033	ν C-H
2973.6	0.054	
2156.5	0.513	ν N_3 (asym)
(2134.1)	(0.143)	ν $^{15}N_3$ (asym)
1768.2	0.159	
1716.5	0.623	ν C=O (asym)
1713.9	0.416	
1710.4	0.556	
1707.8	0.480	
1500.3	0.262	
1494.1	0.120	
1429.3	0.138	
1368.1	0.275	ν C=O (sym)
1361.4	0.731	
1353.9	0.363	
1339.0	0.378	
1323.1	0.296	
1310.0	0.347	
1306.3	0.459	
1300.0	0.236	
1286.8	0.166	
1230.0	0.517	ν N_3 (sym)
1216.3	0.616	
1091.6	0.119	
1033.7	0.251	
756.0	0.240	δ N_3
696.7	0.308	
691.8	0.146	
631.9	0.116	

Scheme 16. Conformers of diphenyl carbamoyl azide **24**.

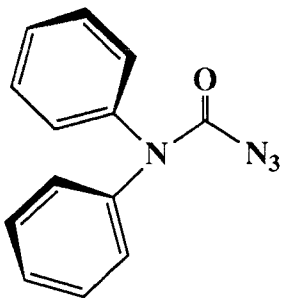

unconjugated

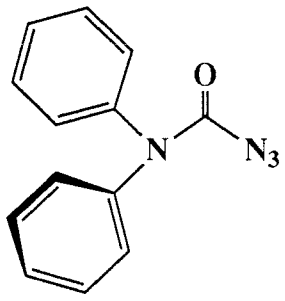

syn-conjugated

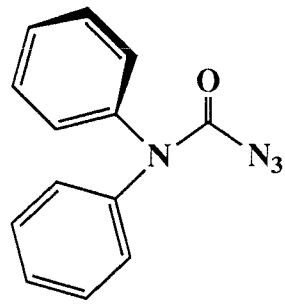

anti-conjugated

Broad band UV photolysis (λ=200-400 nm) of **24** does not produce any bands that can be assigned to 1,1-diazene **22**, although spectral changes do occur. Observation of the isocyanate stretch of diphenylaminoisocyanate **25** at 2253.1 cm^{-1} and the carbon monoxide band at 2136.3 cm^{-1} demonstrates that the photo-Curtius rearrangement and subsequent photodecarbonylation are taking place as expected. Although the $n\rightarrow\pi^*$ absorption of **22** should be well removed spectrally from the UV radiation used for photolysis, the $\pi\rightarrow\pi^*$ absorption of the phenyl rings is in this region. It seemed reasonable that excitation of these chromophores followed by energy transfer could photodecompose the 1,1-diazene. This suggested that the narrow band UV irradiation which successfully generated 1,1-diazene **2** could be successful in this case as well. Photolysis of matrix isolated carbamoyl azide **24** with narrow band UV radiation (λ=295-305 nm) resulted in the FTIR spectrum shown in Figure 40. Spectral subtraction to remove bands due to starting material gave the difference FTIR spectrum shown in Figure 41. The new bands and their assignments are listed in Table XVIII. A band at 1533.7 cm^{-1}, not observed after broad band photolysis, was near the projected position of the N=N stretch of **22**. Broad band visible photolysis

Scheme 17. Generation of 1,1-diazene **22**.

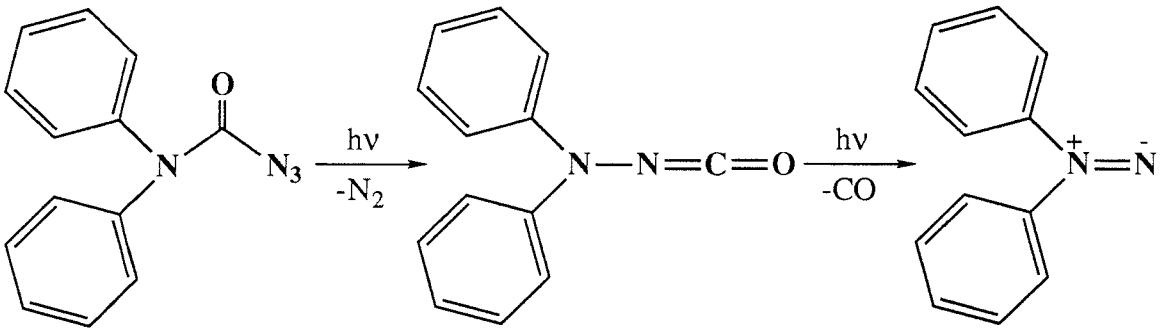

24 **25** **22**

($\lambda > 500$ nm) gave no spectral changes, however. This is not entirely unexpected from the known photochemistry of benzophenone.[73] Identification of the 1533.7 cm^{-1} band as $\nu_{N=N}$ was made by generation of the isotopically labelled compound. The spectrum of matrix isolated labelled carbamoyl azide **24**-^{15}N is shown in Figure 42, and Figure 43 is a difference spectrum showing the results of narrow band UV photolysis. The isotopic multiple of the 1533.7 cm^{-1} band is predicted by Hooke's law to occur at 1507.9 cm^{-1}. A second band is observed at 1516.6 cm^{-1}. Figure 44 shows the N=N stretch regions of the labelled and unlabelled compounds. The bands at 1533.7 cm^{-1} and 1516.6 cm^{-1} are assigned to $\nu_{N=N}$ and $\nu_{N=^{15}N}$ of 1,1-diazene **22** and labelled **22**-^{15}N.

It was noted above that the carbonyl region of matrix isolated **24** is different from the dialkyl carbamoyl azides. This difference is shown even more dramatically on photolysis. Figure 45 shows the carbonyl region of spectrum before and after photolysis. The higher energy carbonyl stretched, tentatively assigned to conformers of **24** with the nitrogen lone pair in conjugation with one of the phenyl rings, appear to be unchanged by UV photolysis. The lower energy stretches are decreased on photolysis as expected. This

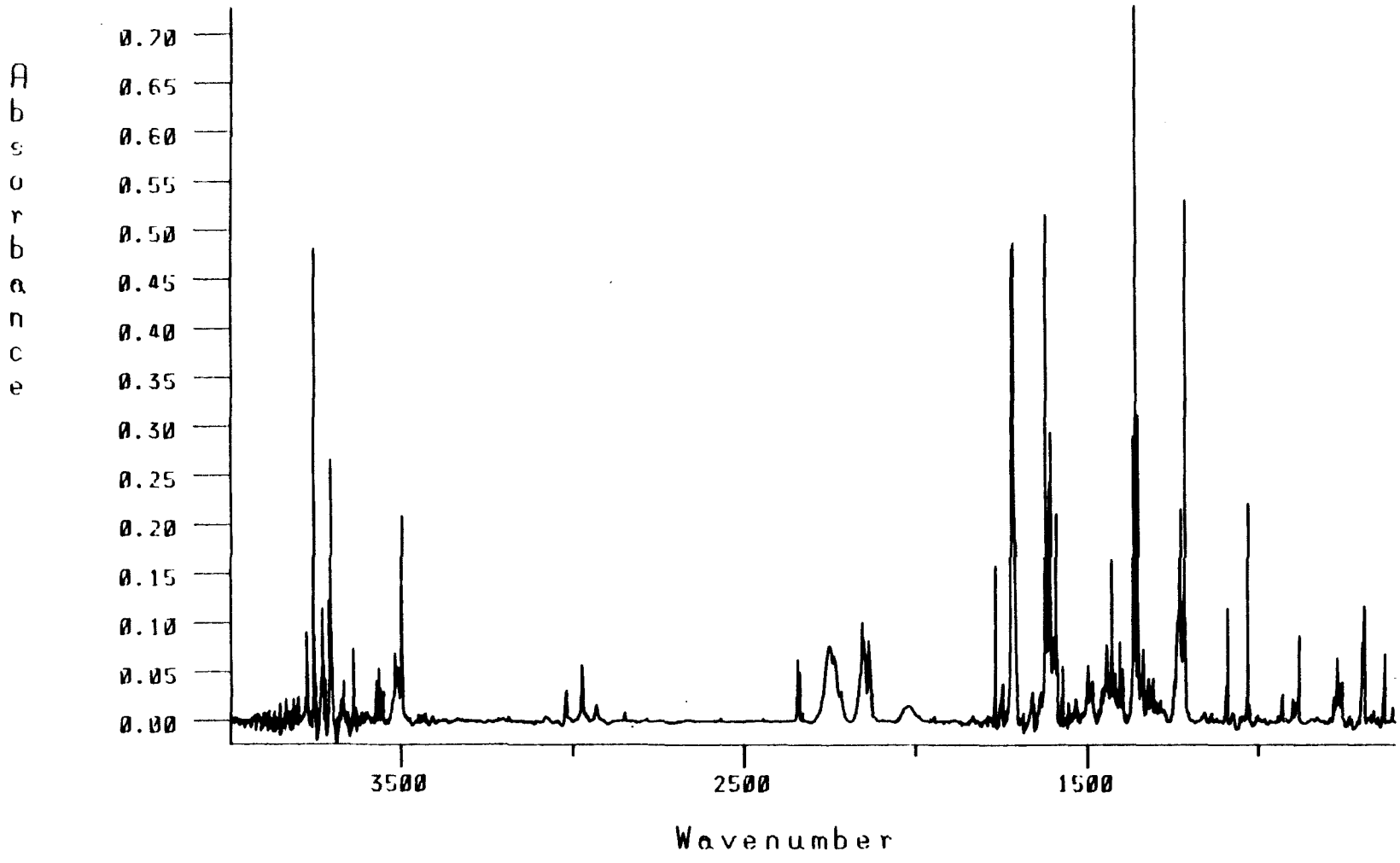

Figure 40. FTIR spectrum of UV photolysis products (λ=295-305 nm, 360 min) from carbamoyl azide **24** (Ar, 10 K)

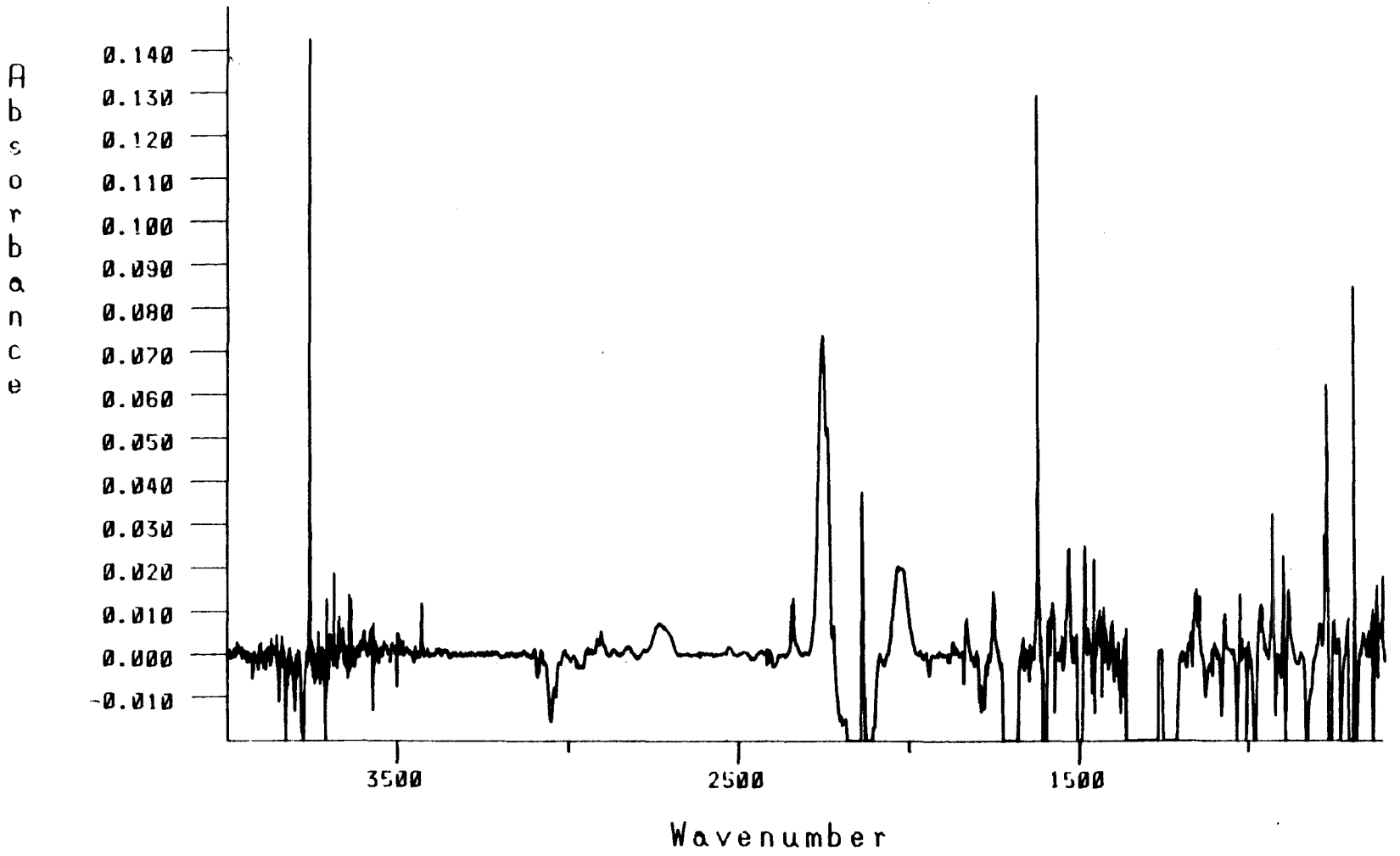

Figure 41. Difference FTIR spectrum of 1,1-diazene **22**, aminoisocyanate **25**, and azobenzene (Ar, 10 K) resulting from UV photolysis (λ=295-305 nm, 360 min.) of carbamoyl azide **24** minus spectrum of **24** before photolysis (subtraction factor α=1.0).

Table XVIII. Bands from the FTIR spectrum of UV photolysis products from carbamoyl azide **24** (positive in Figure 41) and isotopic multiples (in parentheses) from UV photolysis of carbamoyl azide **7**-^{15}N (Figure 43).

Peak Location (cm^{-1})	Intensity (A)	Assignment
2962.5	0.010	? ν C-H
2253.1	0.074	**25** ν NCO
2238.3	0.052	
(2247.0)	(0.032)	**25** ν ^{15}NCO
(2221.7)	(0.016)	
2136.3	0.038	CO
2025.4	0.020	?
1831.7	0.009	?
1753.4	0.015	?
1533.7	0.025	**22** ν N=N
(1516.6)	(0.011)	**22** ν N=^{15}N
1485.8	0.025	azobenzene
1458.4	0.022	azobenzene
1440.6	0.010	**22** or **25**
1428.8	0.011	**22** or **25**
1403.1	0.008	**22** or **25**
1153.6	0.15	azobenzene
1144.8	0.013	azobenzene
1071.6	0.009	azobenzene
1027.0	0.014	**22** or **25**
965.7	0.012	**22** or **25**
930.6	0.033	**22** or **25**
899.6	0.023	**22** or **25**
883.8	0.015	**22** or **25**
778.1	0.028	**22** or **25**
770.6	0.063	azobenzene
690.0	0.086	azobenzene
637.7	0.011	**22** or **25**
625.0	0.016	**22** or **25**
607.8	0.018	**22** or **25**

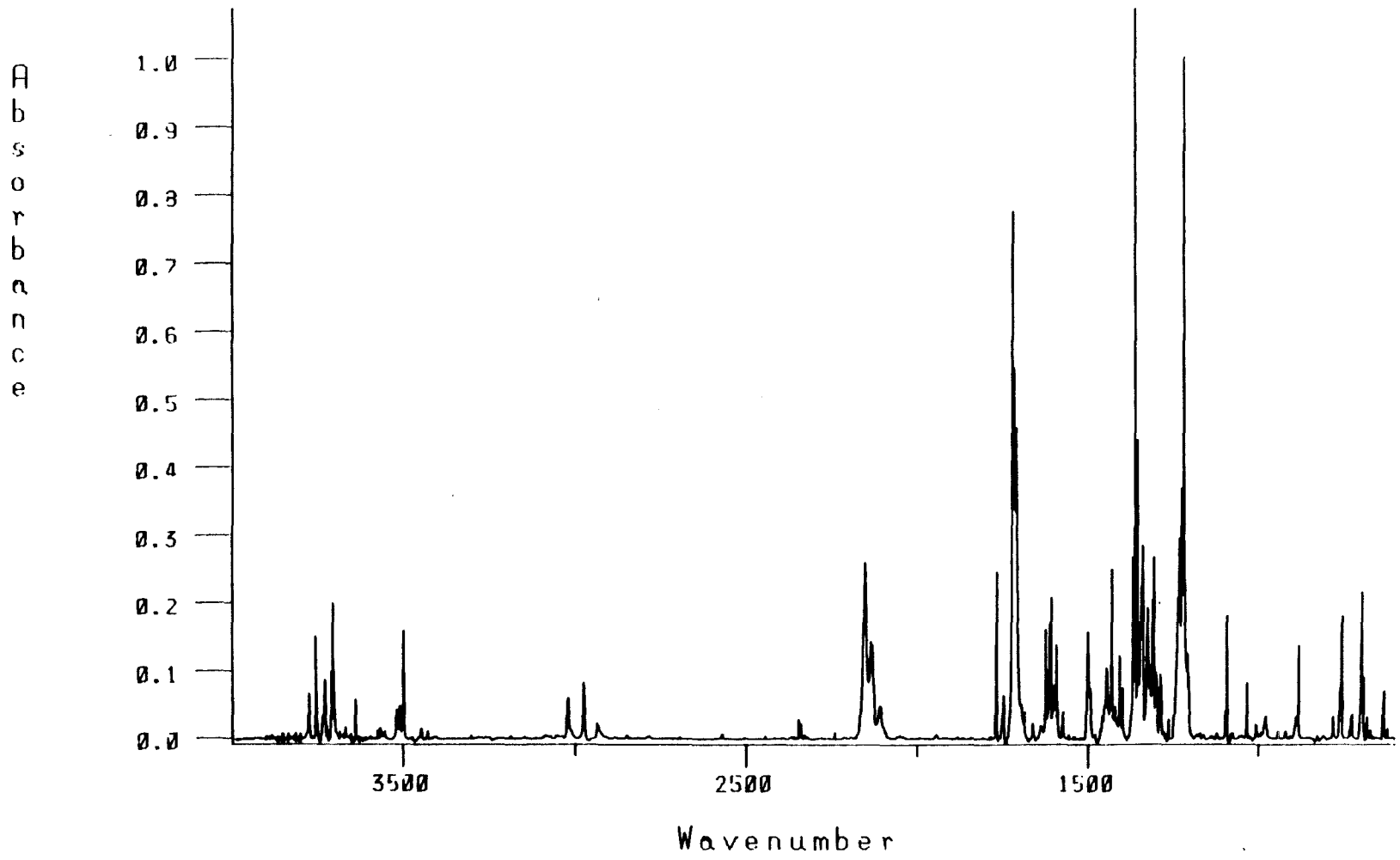

Figure 42. FTIR spectrum of labelled carbamoyl azide **24**-^{15}N (Ar, 10 K).

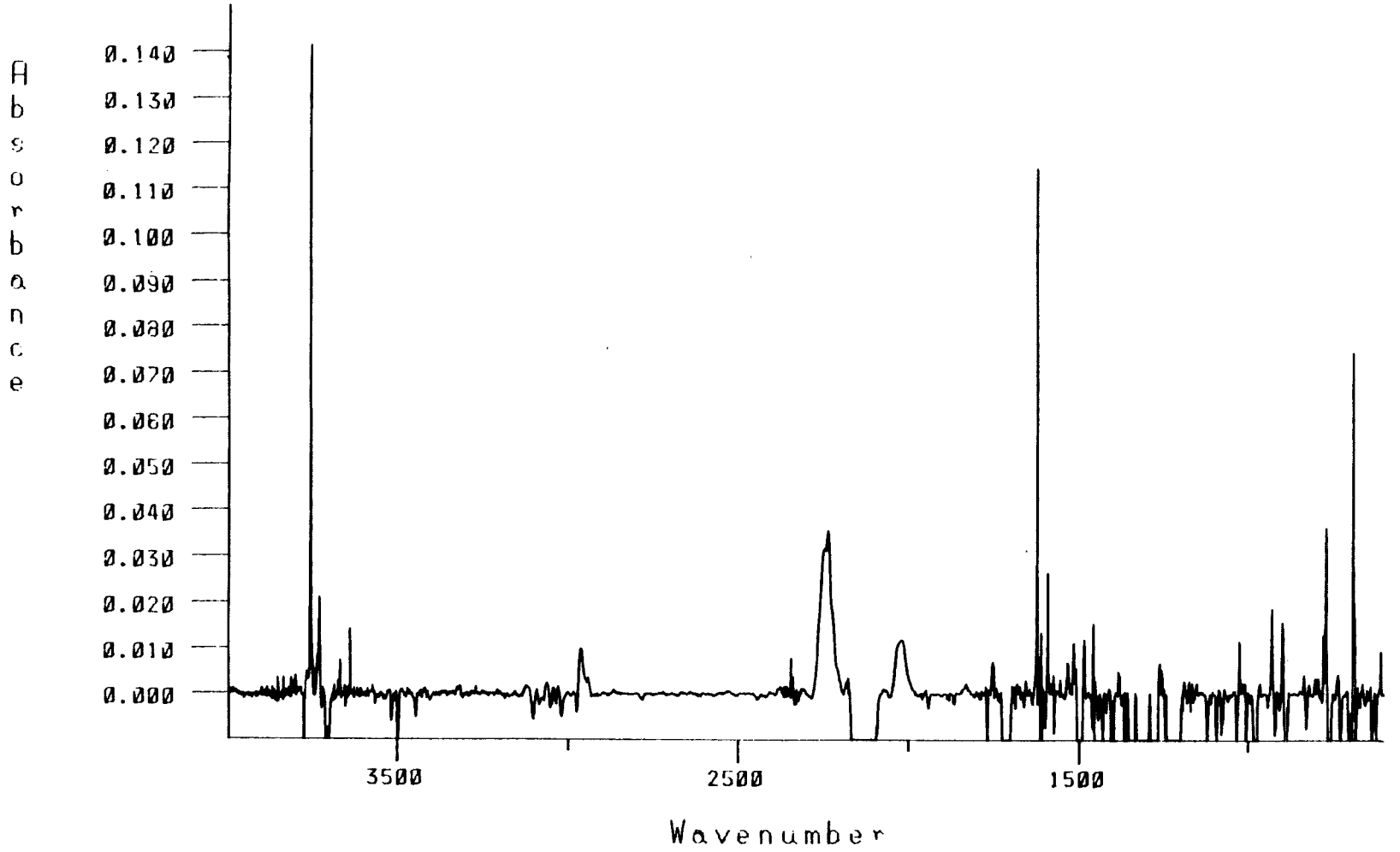

Figure 43. Difference FTIR spectrum of 1,1-diazene **22**, aminoisocyanate **25**, and azobenzene (Ar, 10 K) with isotopic multiples from UV photolysis (λ=295-305 nm, 300 min.) of labelled carbamoyl azide **24**-^{15}N minus spectrum of **24**-^{15}N before photolysis (subtraction factor α=1.0).

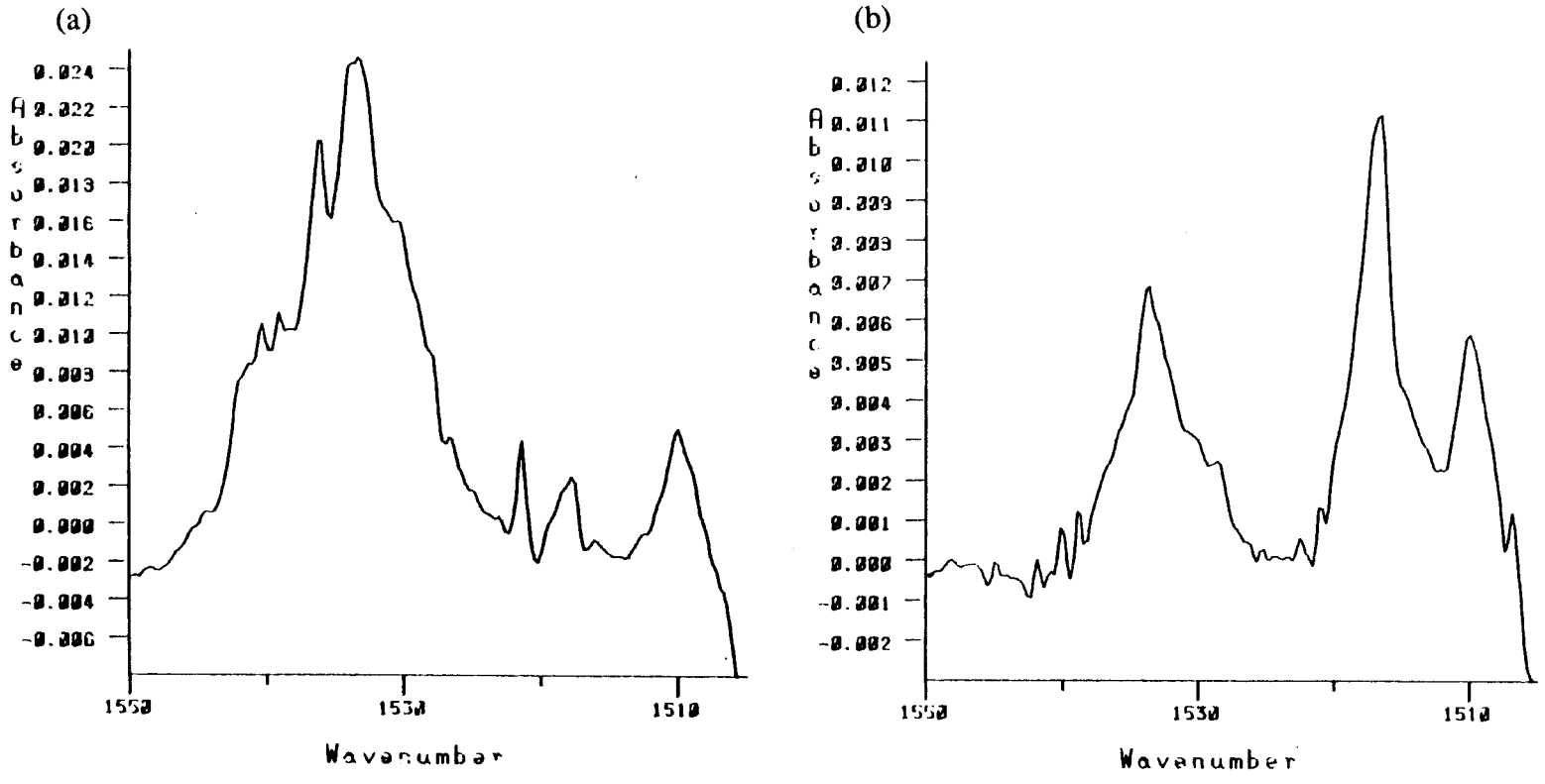

Figure 44. Difference FTIR spectra of N=N stretches of (a) 1,1-diazene **22** (Ar, 10 K) and (b) 1,1-diazenes **22** and labelled **22**-^{15}N (Ar, 10 K) from Figures 41 and 43.

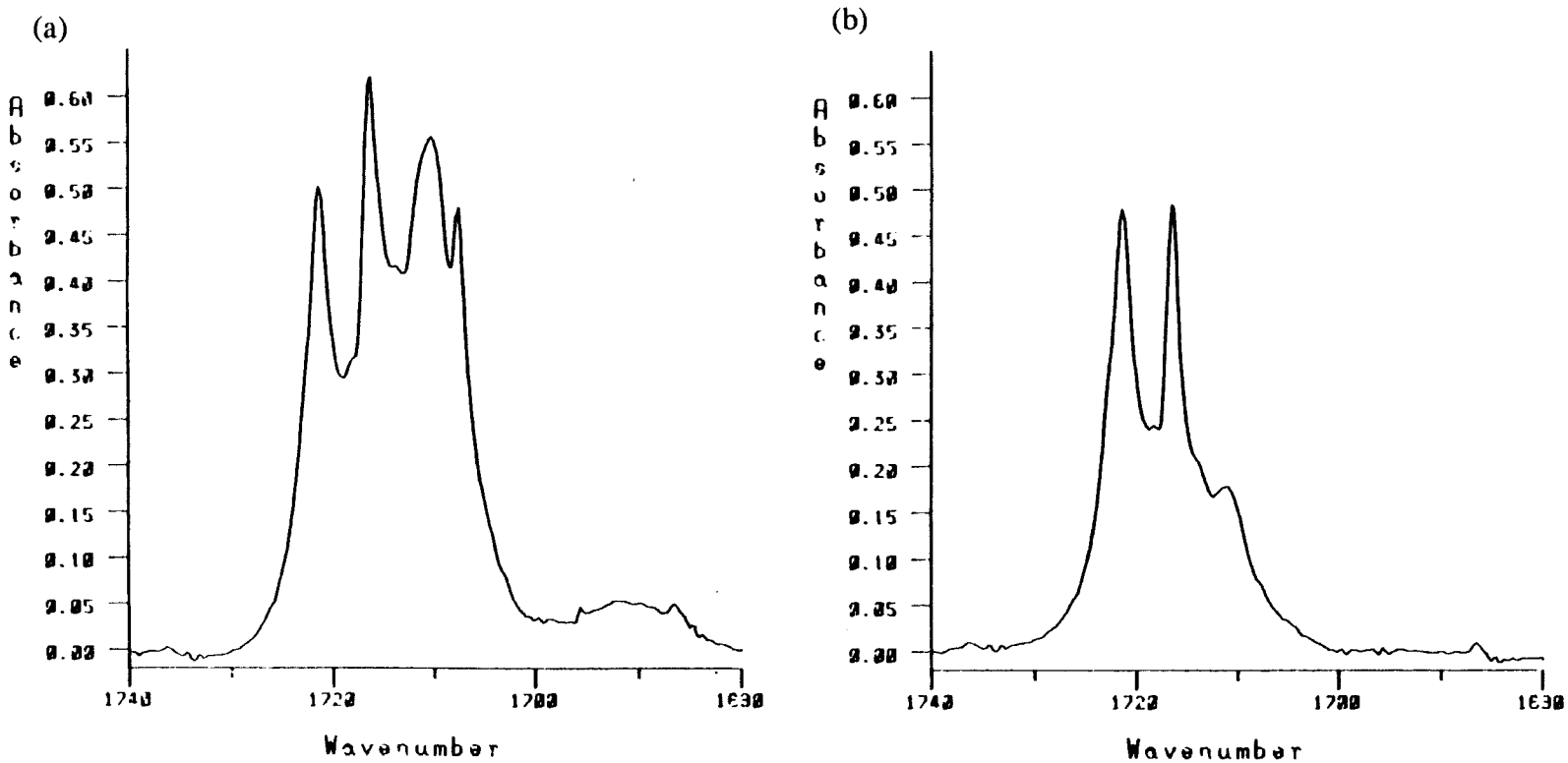

Figure 45. FTIR spectra of the carbonyl bands of carbamoyl azide **24** (Ar, 10 K): (a) before UV photolysis (b) after UV photolysis (λ=295-305 nm, 360 min.).

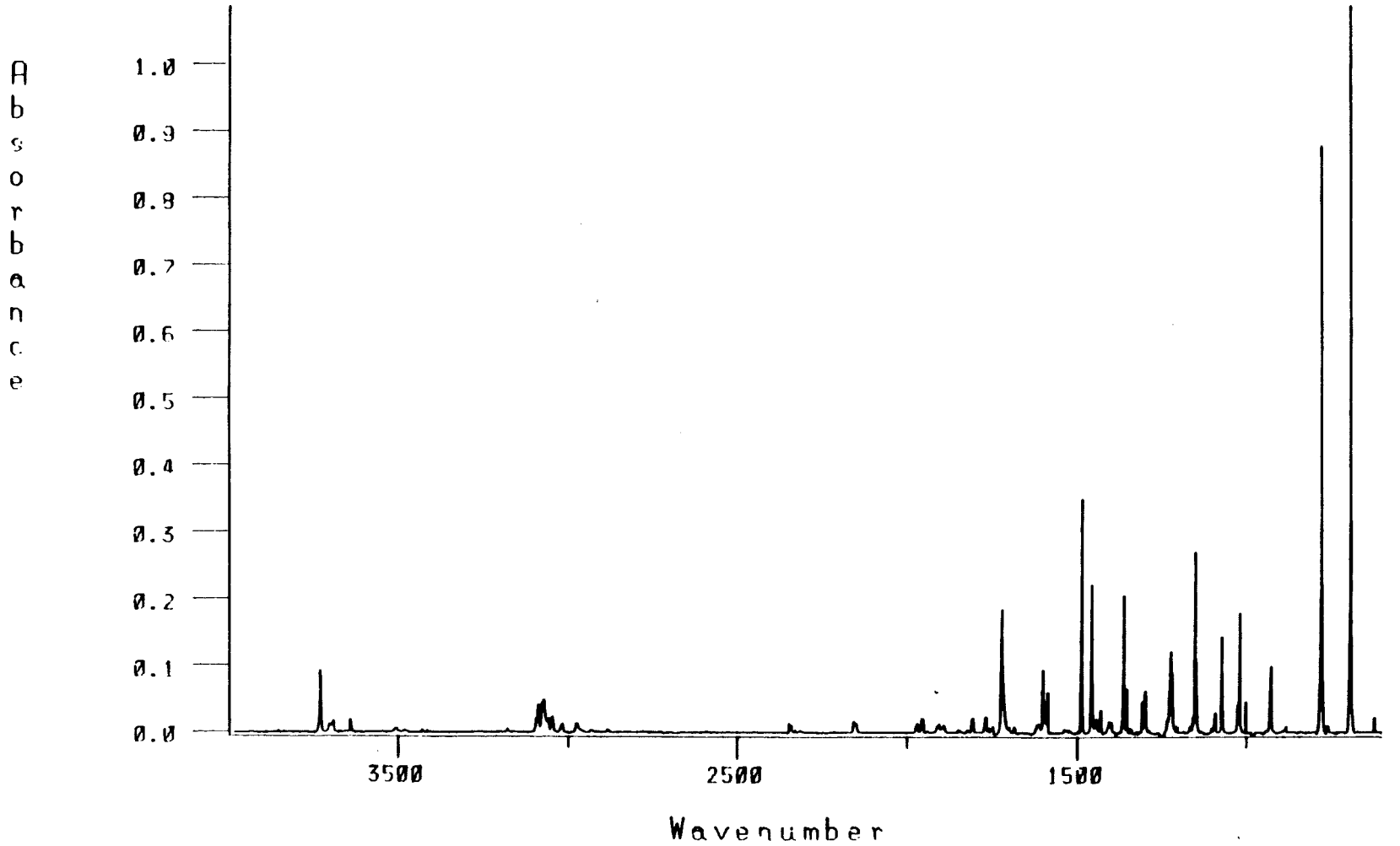

Figure 46. FTIR spectrum of azobenzene (Ar, 10 K).

Table XIX. Bands from the FTIR spectrum of matrix isolated azobenzene (Figure 46).

Peak Location (cm^{-1})	Intensity (A)	Assignment
3086.8	0.041	ν C-H
3070.4	0.049	
3057.1	0.021	
1954.0	0.021	
1806.4	0.021	
1486.6	0.347	
1456.8	0.220	
1361.6	0.208	
1354.1	0.066	
1298.4	0.062	
1221.5	0.119	
1151.7	0.274	
1148.5	0.105	
927.2	0.099	
778.5	0.884	
689.7	1.089	

indicates that the conjugated conformers do not undergo the photo-Curtius rearrangement. The mechanism of this reaction is poorly understood,[41,75] so this observation should provide some new insights. One explanation, based partly on the calculations of Frenking and Schmidt,[76] is that a certain geometry of the carbamoyl azide moiety is required for rearrangement (such as coplanarity of the amide and azide systems), and the conformations

with the higher energy carbonyl stretches are not in this geometry. Frenking and Schmidt looked at nitrene rearrangements, and much of the evidence suggests that the photo-Curtius rearrangement does not involve the nitrene.[75,77] It is also possible that the nitrogen lone pair is actively involved in the reaction, or that the transition state suffers from steric crowding in these conformations. However, alkyl carbonyl azides readily undergo the Curtius rearrangement both thermally and photochemically with no adjacent lone pair.[41,75] Another possibility is that the carbonyl azide excited state is quenched by energy transfer before it can rearrange. N,N-Dimethylaniline absorbs at 298 nm,[72] so this is energetically feasible. This observation of what appears to be a conformational dependence of the photo-Curtus rearrangement could be a point of departure for further studies of the mechanism of this reaction. For example, would the fused ring compounds carbazole carbamoyl azide **26** and indole carbamoyl azide **27** rearrange in a matrix?

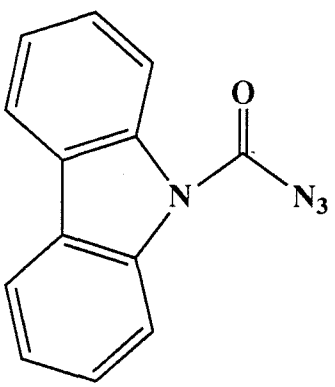

26

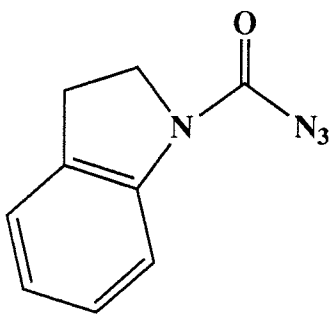

27

There are a number of new bands produced by photolysis of **24** that appear to be too intense to belong to 1,1-diazene **22** based on the intensity of the N=N stretch at 1533.7 cm^{-1}. These bands did not match the spectrum of matrix isolated biphenyl, the expected product of nitrogen extrusion from **22**, but they are quite similar to the spectrum of azobenzene **28** (1,2-diphenyldiazene). The FTIR spectrum of matrix isolated azobenzene is shown in Figure 46, and the bands are listed in Table XIX. Since

is shown in Figure 46, and the bands are listed in Table XIX. Since visible photolysis of **22** did not lead to formation of azobenzene, the observed azobenzene is not necessarily derived from **24** via **22**, although this does seem the most likely explanation.

The isocyanate stretch of diphenylaminoisocyanate **25** is also shifted by interaction with the phenyl rings. For the dialkylaminoisocyantes, this band is found near 2220 cm^{-1}, but it is shifted to higher energy (2253.1 cm^{-1}) and broadened for **25**. This is similar to the effect of the phenyl rings on the carbonyl stretch of **24** and opposite to the effect on the N=N stretch of **22**. Apparently, interaction of the nitrogen lone pair with the isocyanate π system results in a decreased bond order in the isocyanate group. When the nitrogen lone pair is conjugated with one of the phenyl rings, this interaction is weakened or lost, and the isocyanate stretch shifts toward its position in unperturbed isocyanates. The isocyanate band of methyl isocyanate is at 2280 cm^{-1}.[71] Note also in Figure 40 that the isocyanate band is more intense than for the dialkyl derivatives, suggesting that the photodecarbonylation reaction is also disfavored by aryl substitution. This is not surprising, since the stronger NCO stretch corresponds to a stronger N=C bond with more double bond character.

B. Electronic Spectroscopy and Product Analysis.

Broad band UV photolysis of diphenyl carbamoyl azide **24** at 77 K in a 2MTHF glass gives a yellowish glass. Electronic absorption spectroscopy reveals a new absorption with λ_{max} of 330 nm. This is inconsistent with the projected transition for 1,1-diazene **22**. The spectral region is appropriate for the transition of an aminoisocyanate such as **25**, however. Upon warming, the softened glass becomes a brilliant blue color, and a new absorption with λ_{max} of 630 nm is observed. With further warming, this blue color fades and is replaced by a faint orange color. Electronic absorption spectroscopy reveals the presence of tetraphenyl-2-tetrazene **29** and azobenzene **28**. The electronic transition at 630

Scheme 18. Products from 1,1-diphenyldiazene **22**

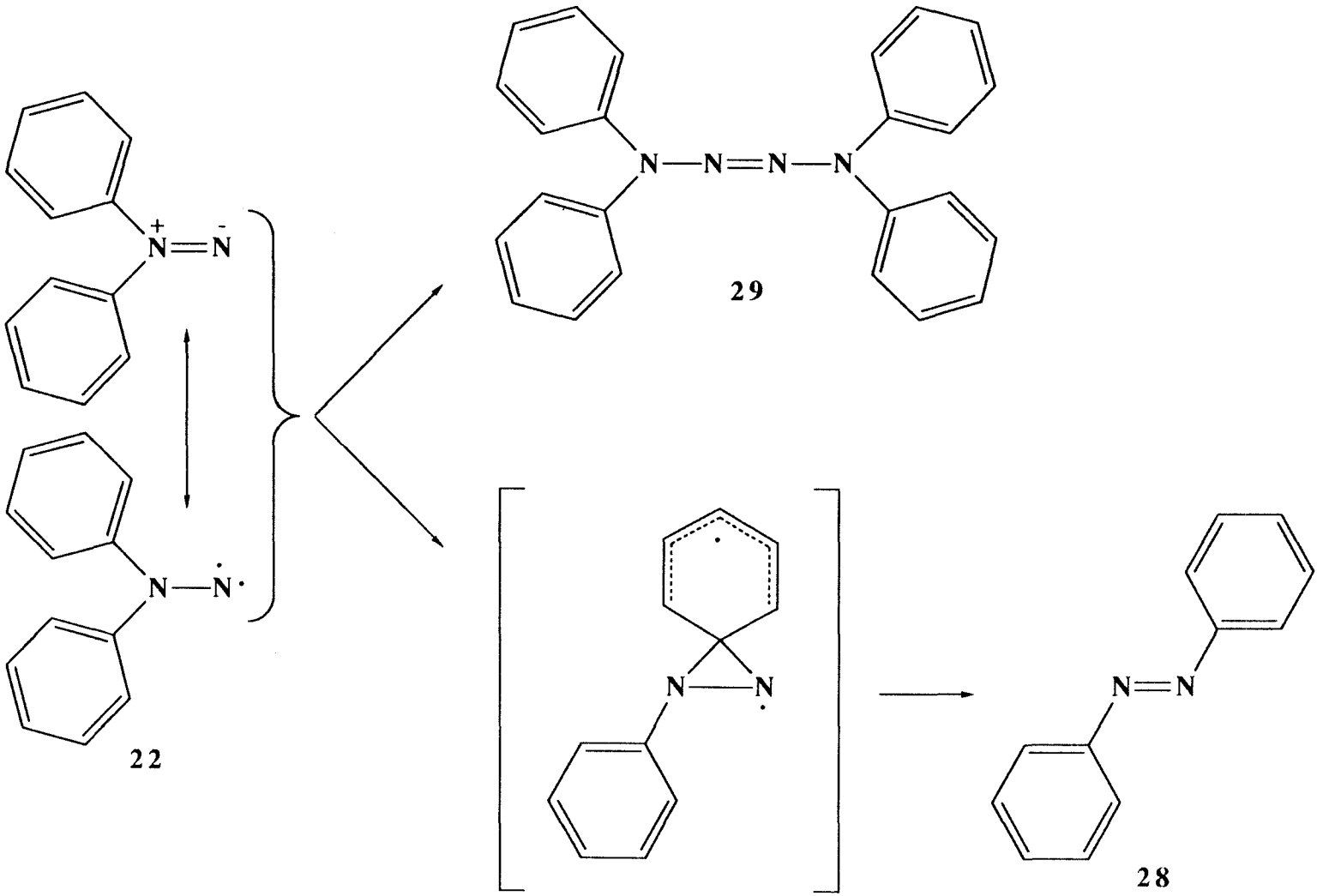

nm is near the projected transition of 1,1-diazene **22**. The requirement for softening the glass to observe this transition is unusual, and the spectrum does not show the typical 1,1-diazene vibronic structure. The lack of vibronic structure may be another result of the conformational flexibility of **22**, in this instance broadening the vibronic transitions. The requirement for softening the glass is not so easily explained, however. Aminoisocyanates are known to dimerize to the 1,2,4-triazolidin-3,5-dion-1,2-ylids in non-nucleophilic solvents,[41] but these compounds are typically colorless and this reaction fails to explain the observed products, which point to the 1,1-diazene. On this evidence, the $n\rightarrow\pi^*$ transition of 1,1-diazene **22** is tentatively identified as the band with λ_{max}=630 nm .

NMR spectroscopy of the products resulting from **22** generated by photolysis in a glass of 1:1 toluene-d_8 and tetrahydrofuran-d_8 followed by warming confirms the presence of azobenzene. Tetraphenyl-2-tetrazene could not be positively identified since its resonances overlap with those of the starting material. Analytical VPC also identified azobenzene as a product, but the tetrazene was unstable even at injector conditions of 200° C and again could not be positively identified. The formation of azobenzene from **22** is unlikely to proceed by cleavage to diazenyl and phenyl radicals followed by recombination. 1,1-Diazene **22** should be more nitrene-like than the dialkyl derivatives, and attack of a singly occupied nitrene-like orbital at the *ipso* carbon of one of the phenyl rings would lead to a phenyl bridged diradical intermediate which could further rearrange to azobenzene **28**, as shown in scheme 18.

Chapter 4

Conclusions

The experiments reported in the preceding chapters had a twofold purpose. First, to help define the influence of structure and substitution on the chemical and spectroscopic properties of 1,1-diazenes; and second, to explore some of the limitations of the photochemical generation of 1,1-diazenes from carbamoyl azides. Both of these issues have been addressed to some extent, and this chapter will be a summary of the results that have been obtained and also an attempt to put those results into perspective.

The spectroscopic data emphasizes the similarity between 1,1-diazenes and the isoelectronic carbonyl compounds. Table XX compiles the data on the $n\rightarrow\pi^*$ electronic transitions of known 1,1-diazenes and compares them to the $n\rightarrow\pi^*$ transitions of the analogous carbonyl compounds. Many of the trends found in the carbonyls are reproduced in the 1,1-diazenes. Decreasing the size of the ring into which the chromophore is incorporated tends to increase the $S_0\rightarrow S_1$ gap, for instance. Delocalization into neighboring π systems in 1,1-diphenyldiazene **22** has a similar effect as in benzophenone. The 1,1-diazene chromophore appears to be more sensitive to inductive effects. The $n\rightarrow\pi^*$ transition can be thought of as a charge transfer from the terminal nitrogen to the central nitrogen. 1,1-Diazenes are highly polar, with a formal positive charge on the central nitrogen. When this inherent polarity is mitigated by σ donating substituents, the $S_0\rightarrow S_1$ gap increases. This accounts for the much larger changes in the series 1,1-diimide to 1,1-dimethyldiazene to 1,1-di-*iso*-propyldiazene than in the series formaldehyde to acetone to 2,4-dimethyl-3-pentanone. The 1,1-diazene analogs of carbonyl chloride (phosgene) and carbonyl fluoride, with σ withdrawing susbstituents, might have extremely low energy electronic transitions. The vibrational spacing in the excited state reflects the balance between pyramidalization and two center three electron bonding in the excited state.

Table XX. Electronic transitions of 1,1-diazenes.

1,1-Diazene	λ_{max} (nm)	$\lambda_{0,0}$ (nm)	ν (cm^{-1})	S_0-S_1 (eV)	carbonyl S_0-S_1 (eV)
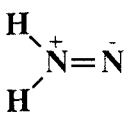 [42]	636	695	1315	1.95	4.00
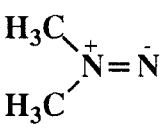 [42]	556	653	1315	2.23	4.46
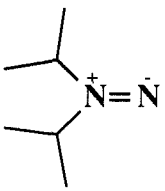 [42]	504	580	1306	2.46	4.30
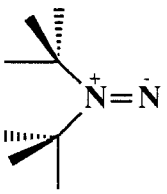 [34]	506	620	1200	2.45	4.17
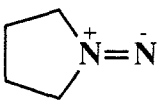	527	616	1353	2.35	4.13
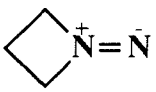	486	556	1389	2.55	4.46
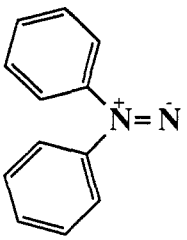	630	670	—	1.97	3.75
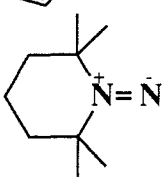 [31,38]	543	610	1040	2.28	4.06
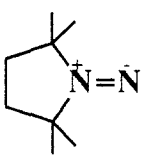 [33,38]	497	572	1238	2.49	4.19

Pyramidalization relieves unfavorable steric interactions in the persistent 1,1-diazenes, leading to lower vibrational frequencies. Pyramidalization is unfavorable in the smaller cyclic 1,1-diazenes, and the inherently greater s character of the NN σ bond results in better overlap for two center three electron bonding. Both of these effects combine to increase the excited state vibrational frequency.

Similar effects are seen in the ground state vibrational spectra. Table XXI is a compilation of the vibrational frequencies of $\nu_{N=N}$ for the known 1,1-diazenes with the analogous carbonyl bands for comparison. Again many of the trends are the same, with certain exceptions. 1,1-Diimide is one of these exceptions: it has a much lower vibrational frequency than expected from the carbonyl data. The cyclic 1,1-diazenes and 1,1-diphenyldiazene **22** follow the same trends as the carbonyls. The greater s character of the NN σ bond with decreasing ring size leads to stronger bonds and higher frequencies, while interaction of the nitrogen lone pair with neighboring phenyl rings lessens the NN double bond character and lowers $\nu_{N=N}$.

The chemical behavior of each of the 1,1-diazenes studied has its own peculiarities. 1,1-Diazenes **1** and **2** tautomerize to the azomethinimines **10** and **13** at 90 K in 2MTHF. This behavior is consistent with the other known 1,1-diazenes with α-hydrogens.[42] 1,1-Diazene **1** ultimately gives dimerization products, consistent with the work of Lemal,[6] yet the kinetics of thermolysis of **10** are unimolecular. These kinetic parameters are attributed to rate limiting tautomerization of **10** to **1** prior to dimerization. The decay of azomethinimine **13** derived from **2** is also unimolecular; this is not surprising since no dimer product is observed. The measured activation energy of 15.1 kcal/mol for decomposition of **2** is used to estimate the amount of excess vibrational energy in photogenerated 1,1-diazenes, since **2** is formed in low yield. Another unusual aspect of the chemistry of **2** is the presence of 1-pyrazoline, the 1,2-diazene isomer, among the observed products. 1,1-Diazene **15** cannot be observed at all, even under matrix isolation conditions. A simple

Table XXI. Frequencies of 1,1-diazene N=N stretches.

1,1-Diazene	$\nu_{N=N}$ (cm^{-1})	$\nu_{N=^{15}N}$ (cm^{-1})	carbonyl $\nu_{C=O}$ (cm^{-1})
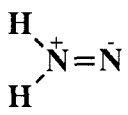 [42]	1574	1548	1742
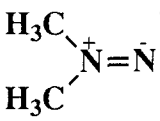 [42]	1601	1582	1719
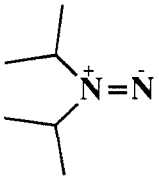 [42]	1601	1579	1713
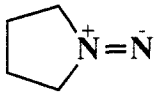	1630	1608	1733
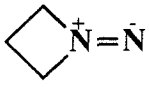	1674	1652	1785
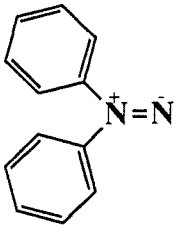	1534	1517	1660
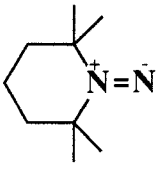 [31,38]	1595	1568	1690
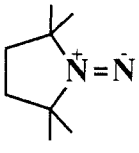 [33,38]	1638	1612	1725

analysis shows that the activation energy for nitrogen extrusion should be less than 11 kcal/mol. Both conformers of 1,3-butadiene are observed in the matrix isolated products, with a slight excess of the lower energy *s-trans* conformer. The *s-cis* conformer would have been expected to dominate if the thermally allowed concerted pathway were followed with no subsequent isomerization. The excess of *s-trans* is therefore ambiguous, since it could indicate isomerization, stepwise decomposition, or concerted decomposition out of the S_1 state. 1,1-Diphenyldiazene **22** resists nitrogen extrusion. Isomerization to azobenzene and dimerization to tetrazene are the apparent reactive pathways.

The difficulty in preparing 1,1-diazenes **2**, **15**, and **22** demonstrates some of the weaknesses of the photochemical route to 1,1-diazenes from carbamoyl azides. This method should be successful for most 1,1-diazenes with an activation energy for nitrogen extrusion greater than 15 kcal/mol.[78] If the activation energy is smaller than 15 kcal/mol, this route may fail. If the 1,1-diazene is desired only as a precursor for some other strained molecule, then inability to isolate the 1,1-diazene may not be a major drawback. In this case the ease of synthesis and handling of carbamoyl azides is a significant advantage. The difficulty in preparing 1,1-diazene **22** appears to be a result of energy transfer from the excited aryl rings rather than due to "hot molecule" decomposition from excess vibrational energy on photogeneration. The activation energy for nitrogen extrusion from **22** is probably quite high. The observed decomposition product is azobenzene, not biphenyl. It is possible that this isomerization in the matrix is a result of hot molecule effects on photogeneration or triplet energy transfer rather than singlet energy transfer, since direct irradiation of **22** did not result in isomerization. Certain conformations of diphenyl carbamoyl azide **24** and diphenylaminoisocyanate **25** resist photochemical transformation. It is inferred that this is a result of delocalization of the amino lone pair into a phenyl ring. These effects--energy transfer and delocalization--are also potential pitfalls in the use of carbamoyl azides to generate 1,1-diazenes. In conclusion, it seems that most dialkyl

carbamoyl azides should be excellent 1,1-diazene precursors. High strain energy or radical stabilizing substituents on the α-carbons will make for poor precursors. Diaryl carbamoyl azides will generally be less attractive precursors since the yields will be poorer. Diaryl carbamoyl azides have potential for investigations of the mechanism of the photo-Curtius rearrangement, however, and substituent effects on the N=N stretch and chemistry of diaryl 1,1-diazenes are also of interest. Some of the 1,1-diazenes most attractive for study, such as acyl 1,1-diazenes and 1,1-diazenes incorporated into aromatic systems, may be inaccessible from the carbamoyl azides due to delocalization effects.

Chapter 5

Experimental Section

General

Melting points were determined using a Thomas-Hoover melting point apparatus and are uncorrected. Infrared spectra were recorded on a Shimadzu IR-435 spectrophotometer. Fourier transform infrared (FTIR) spectra were recorded on a Mattson Instruments Sirius 100 spectrometer equipped with Starlab minicomputer data station and high resolution graphics terminals under positive nitrogen purge at 0.25 cm^{-1} resolution using a HgCdTe detector cooled to 77 K unless otherwise noted. Proton NMR spectra were recorded on a Varian Associates EM-390, a JEOL FX-90Q, or a JEOL GX-400 spectrometer. Chemical shifts are recorded in parts per million (ppm) downfield from tetramethylsilane (TMS) in δ units and coupling constants are in Hertz. NMR data are reported in this order: chemical shift, multiplicity (s=singlet, d=doublet, t=triplet, q=quartet, m=multiplet), number of protons, coupling constants. Electronic spectra were recorded on a Varian Associates Cary 219 spectrophotometer. Mass spectra (MS) were recorded on a DuPont 24-49213 Mass Spectrometer. Chemical analyses were performed at the Caltech Microanalytical Laboratory.

All reactions were run under a positive pressure of argon unless otherwise noted. All reagents were used as received from standard suppliers with the following exceptions. Ethane, ethene, and propene were passed through a -78° C trap prior to use. Methylcyclohexane (MCH) and 2-methyltetrahydrofuran (MTHF) were distilled from calcium hydride and stored over sodium/benzophenone ketyl using excess sodium in sealed, evacuated flasks, then vacuum transferred immediately prior to use. Toluene, pentane, dichloromethane, and acetonitrile were dried over activated Linde 4A molecular sieves. Pyrrolidine was distilled from barium oxide. Azobenzene was recrystallized from ethanol. Many of the reagents used in synthesis are toxic, and proper caution should be used in repeating any of the reported reactions. Special caution is urged in the handling of

azides, as these compounds have a history of explosions. No explosions have occurred in this laboratory while handling carbamoyl azides, but analytical samples were reported to have exploded when subjected to combustion analysis. (This may explain the somewhat low carbon analyses reported for the carbamoyl azides.)

For analytical vapor phase chromatography (VPC) with capillary columns, a Hewlett-Packard 5700A gas chromatograph equipped with a Hewlett Packard 18704A inlet splitter and flame ionization detector was used, employing chromatographic grade hydrogen as the carrier gas and nitrogen as the make-up gas. In all cases a 15 meter SE-54 fused silica capillary (0.2 mm ID) column was used. Analytical VPC with packed columns was performed using a Hewlett-Packard 5720A gas chromatograph equipped with a flame ionization detector and nitrogen carrier gas. This instrument used 0.125 inch steel columns, and was used for volatile hydrocarbon analysis with a 10 foot column packed with VZ-10 (Alltech). All quantitative VPC was accomplished with a Hewlett-Packard 3390A electronic integrator. VPC response factors for hydrocarbons were assumed to be 1.00 relative to *n*-alkanes. Quantitative analyses of other products were corrected for detector response. For preparative VPC, a Varian 920 gas chromatograph with a thermal conductivity detector and helium carrier gas was used. This instrument used 0.375 inch aluminum packed columns, and for carbamoyl azides a 10 foot column packed with Carbowax 20M on 60/80 Chromosorb W (acid washed, dimethyldichlorosilane treated) was used. Identities of products were established by coinjection techniques with authentic samples.

Synthesis

Pyrrolidine Carbamoyl Chloride (5).[79] To a stirred solution of 9.0 ml (127 mmol) phosgene (CAUTION! extreme poison) in 150 ml dry dichloromethane at -10° C, a solution of 3.02 g (42 mmol) pyrrolidine and 4.3 g (42 mmol) dry triethylamine in 40 ml

dry dichloromethane was added dropwise over 90 minutes. The mixture was stirred at -10° C for another 120 minutes and allowed to warm to room temperature. After stirring an additional 120 minutes, the solvent and excess phosgene were removed *in vacuo* to a -78° C trap containing moist potassium hydroxide. The remaining oil was dissolved in 30 ml dry diethyl ether and the triethylamine hydrochloride removed by filtration. The filtered solids were washed with dry ether, the ether portions combined and the ether removed *in vacuo*. Distillation under reduced pressure of the remaining yellow oil afforded 3.74 g (28 mmol, 67% yield) of pyrrolidine carbamoyl chloride, bp 117-119° C (18 mm).

NMR ($CDCl_3$): δ3.50 (m, 4H), 1.93 (m, 4H)

IR (CCl_4): 2990, 2890, 1745, 1365, 1320, 1160 cm^{-1}

Pyrrolidine Carbamoyl Azide (7).[41] To a suspension of 5.0 g (77 mmol) sodium azide in 10.0 ml dry acetonitrile was added 1.5 g (11.2 mmol) pyrrolidine carbamoyl chloride in 10.0 ml dry acetonitrile. The mixture was stirred for 3 days in the dark at room temperature. The reaction was checked by IR ($\nu_{C=O}$ is ~1690 cm^{-1} for carbamoyl azide, ~1750 cm^{-1} for carbamoyl chloride) and analytical VPC. When no carbamoyl chloride remained, the solids were filtered and washed with dry acetonitrile. The acetonitrile was removed *in vacuo*, leaving a yellow oil. Distillation at reduced pressure afforded 1.4 g (10 mmol, 89% yield) of pyrrolidine carbamoyl azide as a colorless oil, bp 109-110° C (15 mm). Preparative VPC (Carbowax 20M, 170° C, 180° C injector) gave analytically pure material.

NMR ($CDCl_3$): δ3.40 (m, 4H), 1.90 (m, 4H)

IR (CCl_4): 2975, 2890, 2140, 1695, 1340, 1220, 1010 cm^{-1}

MS: m/e=140 (M+).

Pyrrolidine Carbamoyl Azide-^{15}N (7-^{15}N). To a suspension of 0.2 g (3.0 mmol) of a 1:1 mixture of sodium 1-^{15}N-azide and sodium azide in 5.0 ml dry acetonitrile was added 0.4 g (3.0 mmol) pyrrolidine carbamoyl chloride. The mixture was stirred in the

dark for 5 days at room temperature. Progress of the reaction was checked by IR. When reaction was complete, the solids were removed by filtration and washed repeatedly with dry acetonitrile. The acetonitrile portions were combined and the solvent removed *in vacuo*. Preparative VPC (Carbowax 20M, 170° C, 180° C injector) afforded analytically pure material.

IR (CCl_4): 2975, 2890, 2140, 2120, 1695, 1390, 1220, 1010 cm^{-1}

MS: m/e=141(M+, ^{15}N), 140(M+); 141/140=1.57/1.00.

Azetidine Carbamoyl Chloride (6). To a stirred solution of 4.5 ml (63 mmol) phosgene (CAUTION! extreme poison) in 50 ml dry dichloromethane at -10° C, a solution of 1.0 g (17.5 mmol) azetidine and 2.02 g (20 mmol) dry triethylamine in 15 ml dry dichloromethane was added dropwise over 20 minutes. The solution was stirred at -10° C for 1.5 hours and allowed to warm to room temperature. Solvent and excess phosgene were removed *in vacuo* to a -78° C trap containing potassium hydroxide. The remaining oil was dissolved in 20 ml dry pentane and the triethylamine hydrochloride removed by filtration. The filtered solids were washed with pentane, and the pentane portions combined. Removal of pentane *in vacuo* afforded 1.41 g (12 mmol, 68% yield) azetidine carbamoyl chloride as a colorless oil. An analytically pure sample was obtained by preparative VPC (Carbowax 20M, 135° C, 150° C injector).

NMR ($CDCl_3$): δ4.13 (q, 4H, J=8), 2.33 (quintet, 2H, J=8)

IR (CCl_4): 3000, 2960, 2890, 1755, 1365, 1310, 1297, 1240, 1140, 980 cm^{-1}

MS: m/e=119(M+), m/e=121/m/e=119=1/4.

Azetidine Carbamoyl Azide (8). To a suspension of 1.54 g (23.6 mmol) sodium azide in 5.0 ml dry acetonitrile was added 1.41 g (11.8 mmol) azetidine carbamoyl chloride **6**. The mixture was stirred in the dark at room temperature for 4 days. Progress of the reaction was checked by IR and VPC as described above. When no carbamoyl chloride remained, the solids were filtered and washed with dry acetonitrile. The

acetonitrile portions were combined and the solvent removed *in vacuo*, affording 1.30 g (10.3 mmol, 87% yield) azetidine carbamoyl azide as a colorless oil. Preparative VPC (Carbowax 20M, 135° C, 150° C injector) gave analytically pure material.

NMR ($CDCl_3$): δ4.02 (m, 4H), 2.23 (m, 2H)

IR (CCl_4): 3000, 2960, 2895, 2220, 2140, 1695, 1390, 1220, 1150, 1015 cm^{-1}

Analysis ($C_4H_6N_4O$): calculated C 38.09 ; H 4.76 ; N 44.44

found C 37.55 ; H 4.81 ; N 44.43

MS: m/e=126 (M+).

Azetidine Carbamoyl Azide-^{15}N (8-^{15}N). To a suspension of 0.19 g (2.9 mmol) sodium 1-^{15}N-azide in 2.0 ml dry acetonitrile was added 0.30 g (2.5 mmol) azetidine carbamoyl chloride **6**. The mixture was stirred in the dark at room temperature for 5 days. Progress was monitored by IR as above. When reaction was complete, the solids were filtered and repeatedly washed with dry acetonitrile, the acetonitrile portions combined, and the solvent removed *in vacuo*, affording 0.29 g (2.3 mmol, 92% yield) azetidine carbamoyl azide-^{15}N. Preparative VPC (Carbowax 20M, 135° C, 150° C injector) gave analytically pure material.

IR (CCl_4): 3000, 2960, 2895, 2220, 2140, 2120, 1695, 1390, 1220, 1150, 1015 cm^{-1}

MS: m/e=127 (M+).

1-Trimethylsilyl-3-pyrroline (17).[80] A solution of 2.52 g (23 mmol) chlorotrimethylsilane in 5.0 ml pentane was added dropwise to a well-stirred solution of 2.12 g (30.5 mmol) of 75% 3-pyrroline (25% pyrrolidine) and 2.02 g (20 mmol) triethylamine in 60 ml pentane at 0° C. The mixture was stirred at 0° C for 4 hours, then allowed to warm to room temperature. The amine hydrochloride was filtered under N_2 and washed thoroughly with pentane. The pentane portions were combined and the solvent removed *in vacuo* to give 3.04 g (21.5 mmol, 70.5% yield) of the aminosilane as a clear

oil. The product was checked by NMR, then carried through to the next synthetic step without further purification.

NMR ($CDCl_3$): δ5.78 (d, 2H, J=6), 3.72 (d, 4 H, J=8), 0.05 (s, 9H).

Trimethylsilyl-3-pyrroline Carbamate (18).[81] Carbon dioxide (bone dry) was bubbled through a solution of 1.57 g (11 mmol) 75% 1-trimethylsilyl-3-pyrroline (25% 1-trimethylsilylpyrrolidine) in 50 ml pentane for 6 hours. A white solid precipitated from the solution as the reaction progressed and more pentane was added as needed. The solvent was removed *in vacuo* to give 1.146 g (6.1 mmol, 56% yield) trimethylsilyl-3-pyrroline carbamate as a white solid. The product was checked by NMR, then carried through to the next synthetic step without further purification.

NMR ($CDCl_3$): δ5.72 (s, 2H), 4.08 (s, 4H), 0.25 (s, 9H).

3-Pyrroline Carbamoyl Chloride (19).[70] A solution of 1.3 g (7.0 mmol) 75% trimethylsilyl-3-pyrroline carbamate (25% trimethylsilylpyrrolidine carbamate) in 10 ml carbon tetrachloride was added dropwise to a stirred mixture of 1.37 g (6.6 mmol) phosphorus pentachloride in 30 ml carbon tetrachloride at 0^{o} C. The mixture was stirred for 1 hour at 0^{o} C, allowed to warm to room temperature, and then stirred for another 8 hours. The solvent was removed *in vacuo*, and the resulting black viscous oil was distilled under reduced pressure to give 0.84 g (6.4 mmol, 91% yield) 3-pyrroline carbamoyl chloride. NMR ($CDCl_3$): δ5.80 (m, 1H), 5.76 (m, 1H), 4.32 (m , 2H), 4.22 (m, 2H)

IR (CCl_4): 3080, 2980, 2960, 2900, 2875, 1746, 1470, 1375, 1360, 1310, 1185, 885, 660 cm^{-1}.

3-Pyrroline Carbamoyl Azide (20). To a suspension of 1.1 g (16.9 mmol) sodium azide on 20 ml dry acetonitrile was added 0.42 g (3.2 mmol) of a 75:25 mixture of 3-pyrroline carbamoyl chloride and pyrrolidine carbamoyl chloride. The mixture was stirred in the dark at room temperature for 4 days. Progress of the reaction was monitored by IR, as described above. When reaction was complete, the solids were removed by

filtration and washed repeatedly with dry acetonitrile. The acetonitrile portions were combined and the solvent removed *in vacuo*. Two recrystallizations from hexane gave 0.243 g (1.76 mmol, 55% yield) of analytically pure 3-pyrroline carbamoyl azide, mp 64-66° C.

NMR ($CDCl_3$): δ5.73 (m, 2H), 4.18 (m, 4H)

IR (CCl_4): 3080, 2985, 2950, 2870, 2140, 1695, 1392, 1321, 1225, 1197, 670 cm^{-1}

Analysis ($C_5H_6N_4O$): calculated C 43.48 ; H 4.38 ; N 40.56

found C 43.11 ; H 4.32 ; N 40.84

MS: m/e=138 (M+), m/e=140/139/138/137 = 1.00/1.91/22.2/1.7.

3-Pyrroline Carbamoyl Azide-^{15}N (20)-^{15}N. A mixture of 0.012 g (0.18 mmol) sodium 1-^{15}N-azide and 0.030 g (0.21 mmol) 3-pyrroline carbamoyl chloride in 10 ml dry acetonitrile was stirred in the dark at room temperature for seven days. At the end of this period the reaction was checked by IR and found to be complete. The solids were removed by filtration and washed with dry acetonitrile. The solvent was removed *in vacuo* and the remaining oil recrystallized from 2 ml of hexane to give 0.011 g (0.079 mmol, 44% yield) of the ^{15}N-labelled carbamoyl azide as small plates.

NMR (CDCl3): δ5.78 (m, 2H), 4.17 (m, 4H)

IR (CHCl3): 3090, 3070, 3005, 2980,2950, 2860, 2140, 2120, 1690, 1470, 1450, 1400, 1324, 1280, 1190, 1110, 865 cm^{-1}

Bis(tetramethylene)-2-tetrazene (11).[6] A solution of 2.5 g (20 mmol) N-aminopyrrolidine hydrochloride in 15.0 ml 33% aqueous sodium hydroxide was extracted with diethyl ether (3 x 30 ml). The combined ether portions were dried over calcium sulfate, then added dropwise to a suspension of 5.0 g (23.1 mmol) yellow mercuric oxide in 100 ml dry diethyl ether. The mixture was refluxed for 10 hours. The solids were filtered through celite and the solvent removed *in vacuo* to afford a yellow oil.

Recrystallization from ethanol/water gave 1.01 g (6.0 mmol, 60% yield) bis-(tetramethylene)-2-tetrazene. UV/Vis (cyclohexane): 290 nm (log ε = 4.0)

NMR ($CDCl_3$): δ3.28 (m, 4H), 1.83 (m, 4H)

IR (CCl_4): 2950, 1445, 1326, 1257, 1090, 1011 cm^{-1}

MS: m/e=168 (M+).

Diphenyl Carbamoyl Azide (24).[82] A solution of 0.825 g (3.56 mmol) diphenyl carbamoyl chloride in 40 ml dry acetonitrile was added to 3.57 g (54.9 mmol) sodium azide. The mixture was stirred in the dark at room temperature for two days. Progress of the reaction was monitored by IR as described above. When the reaction was complete, the solids were removed by filtration and the solvent removed *in vacuo* to give a viscous oil which solidified on standing. The solid product was recrystallized by making a saturated solution in anhydrous methanol at room temperature and then placing the solution in a -18° C freezer, affording 0.53 g (2.2 mmol, 63% yield) of white crystals, m.p. 80-81° C. The recrystallized material was found to be analytically pure.

NMR (CDCl3): δ7.36 (t, 4H, J=7.32 Hz), 7.26 (m, 6H)

IR (CCl_4): 3070, 3040, 2150, 1696, 1595, 1492, 1450, 1335, 1320, 1300, 1282, 1226, 975, 885, 693, 630 cm^{-1}

Analysis: ($C_{13}H_{10}N_4O$) calculated C 65.54 ; H 4.23 ; N 23.52

found C 65.26 ; H 4.31 ; N 23.44

MS: m/e=238 (M+).

Diphenyl Carbamoyl Azide-15N (24-^{15}N). A solution of 0.1743 g (0.786 mmol) diphenyl carbamoyl chloride in 15 ml dry acetonitrile was added to 0.0504 g (0.764 mmol) sodium 1-^{15}N-azide. The mixture was stirred in the dark at room temperature for five days, and the progress of the reaction was monitored by IR. When reaction was complete, the mixture was filtered and the solids were washed thoroughly with dry

acetonitrile. The solvent was removed *in vacuo*, and the remaining oil was recrystallized from anhydrous methanol.

NMR ($CDCl_3$): d7.35 (m, 4H), 7.26 (m, 6H)

IR (CCl_4): 3070, 3040, 2150, 2130, 1690, 1595, 1495, 1452, 1340, 1307, 1220, 692, 630 cm^{-1}

Spectroscopy

Matrix Isolation Apparatus. The matrix isolation system was designed and assembled by A. P. Sylwester.[42] A closed cycle helium refrigerator with two expansion stages (Air Products Displex CSW-202 DMX-1E) was used to cool the sample. The cold sample was kept within an optical vacuum shroud which can be rotated, allowing access to the sample through two different types of windows. The cold head assembly is mounted so as to provide both horizontal and vertical positioning. Dynamic vacuum was maintained with an oil diffusion pump (Edwards MkII Diffstak) which could pull the system down to an ultimate pressure of $<10^{-7}$ mbar. Temperature was controlled by an Air Products Displex-E heater/controller unit using an iron-doped gold/chromel thermocouple. Matrix gases were contained in a glass manifold with greaseless joints equipped with a Pennwalt 1500 absolute pressure guage. Matrix gas deposition rates were modulated with a Granville-Phillips variable leak. Samples for sublimation and co-deposition were contained in a Pyrex chamber connected to the shroud by a 0.25 inch Pyrex tube through a Cajon Ultra-Torr fitting. The sublimation chamber could be sealed from the vacuum shroud with a Teflon stopcock. For infrared spectroscopy, a CsI inner window was attached to the cold finger; a radiation shroud was provided between the cold sample and the outer shroud, and two outer windows of KBr (for IR) and one of Suprasil (for photolysis) were used. For electronic spectroscopy in organic glasses and low temperature solutions, a specially constructed cell[56] was attached to the cold finger. This cell was made of plated OFHC

copper with Suprasil windows. Solutions could be introduced into the cell through two ports which were connected to the outside by Teflon tubing. This tubing passes through Cajon ultra-torr feed-throughs in the vacuum shroud. The outer shroud windows were of Suprasil for electronic spectroscopy, and the system was kept at rough vacuum (~10^{-3} mbar). Detailed procedures for the different spectroscopic techniques are provided below.

FTIR Spectroscopy. A Mattson Instruments Sirius 100 spectrometer was modified to allow access of the low temperature matrix isolation apparatus,[42] while still maintaining nitrogen purge. An interferogram of the blank CsI inner window was acquired and Fourier transformed for use as a background spectrum prior to each experiment. Deposition conditions and photochemical transformations of the individual carbamoyl azides are described below. All interferograms were processed with triangle apodization and referenced to the previously collected background spectrum to give absorbance spectra. These were carefully corrected for residual atmospheric impurities ($H_2O(g)$ and $CO_2(g)$) with interactive subtraction programs. Baseline inclination or roll was corrected with appropriate software. Difference FTIR spectra are presented to clearly demonstrate the effects of certain transformations. Subtraction factors (α) refer to the formula A-αB=C where A and B are the absorbance spectra to be subtracted and C is the resulting difference spectrum. In most cases α was chosen to be 1.00.

Matrix Isolation Experiments. For matrix isolation experiments, the gas manifold of the matrix isolation apparatus was attached via a flex hose to a tank of UHP argon, and the entire assembly pumped down to $\leq 10^{-6}$ mbar. The gas manifold and flex hose were outgassed by careful heating with a heat gun. The manifold was then closed to the vacuum system and filled with UHP argon to approximately 750 torr. This amount of matrix gas was usually sufficient for five or six experiments. (The volume of the gas manifold is ~5.8 l, so the amount of gas at 750 torr and 295 K is ~0.24 mol.)

The sample (if non-volatile) was then introduced into the sublimation chamber and degassed by opening the chamber to the vacuum system for two or three one minute cycles. (Extremely non-volatile samples such as diphenyl carbamoyl azide could be pumped on more extensively.) The cold head area of the matrix isolation apparatus was then purged of atmospheric contaminants by heating all metal surfaces with a heat gun. When the vacuum was below 10^{-6} mbar, the level of these contaminants was considered to be sufficiently low for matrix isolation work.

To begin an experiment, the closed cycle refrigerator was turned on and the CsI inner window cooled to 20 K. At 77 K, the cold head was closed off from the vacuum system to prevent cryopumping of diffusion pump oil to the cold finger. The cold head was effectively cryopumped by the extremely cold temperatures of the cold finger for the duration of the experiment. When the inner window temperature reaches 20 K, it is allowed to equilibrate for 45-60 minutes while a background interferogram of the CsI inner window is acquired. After this is completed, the sample is cooled or heated to the proper temperature for sublimation. The matrix gas flow is adjusted with the variable leak to give the required flow rate (~0.3 mm/minute from the manifold). The deposition parameters are important for achieving good isolation of the sample molecules in the argon matrix. The sublimation chamber is outgassed one final time by opening to the side of the radiation shroud, then the cold head shroud is rotated and deposition is begun.

The matrix is checked by FTIR to be certain that the deposition rates are correct. With the carbamoyl azides, by analogy to dimethyl carbamoyl azide (which was sufficiently volatile that it could be prepared as a gas mixture[42]), a final matrix of 100-125 torr (30-40 mmol) of argon with an azide stretch with A=1.0-1.1, laid down over five hours, was considered ideal. (This corresponded to a 1400:1 mixture for dimethyl carbamoyl azide.) Matrices with higher argon to sample ratios (down to A=0.40 for the azide stretch) were sometimes used. The deposition conditions were generally checked at 10 and 30 minutes

and at approximately the halfway point. For other non-volatiles (azobenzene, biphenyl) the absorbance of the strongest peak was generally kept below 1.0 with a 100-125 mm matrix. Once deposition was complete, the temperature of the matrix was slowly lowered to 10 K, the ultimate temperature of the cold finger with no electrical heating. An FTIR spectrum of the matrix was recorded, and appropriate transformation were carried out using the 1000W Xenon arc lamp and appropriate colored glass or interference filters or a monochromator. Photolysis was carried out through a Suprasil window and the back of the CsI inner window. To anneal a matrix, the temperature was raised to 30-35 K (the softening point of solid Ar) for several minutes, then lowered to 20 K. This cycle was repeated several times and the matrix cooled to 10 K again.

For volatile samples (ethene, propene, cyclopropane), a gas mixture of UHP argon and the sample gas was made up in the manifold by manometric techniques. The ratio of Ar to sample was approximately 700:1. This gas mixture could then be deposited onto the 20 K CsI inner window as described above, and spectra of the isolated molecules recorded.

Matrix Isolation of 1,1-Tetramethylenediazene 1 and 1-^{15}N. Pyrrolidine carbamoyl azide or pyrrolidine carbamoyl azide-^{15}N were purified by preparative VPC, placed in the sublimation chamber and thoroughly degassed. They were then cryopumped from a -13^{o} C ice/salt bath and codeposited with UHP argon on the CsI inner window at 20 K. The sample was slowly cooled to 10 K and a spectrum of the precursor carbamoyl azide was recorded. Photolysis with defocussed broad band UV radiation (λ=200-400 nm) was carried out for 90-120 minutes and monitored by FTIR. A spectrum of the 1,1-diazene was recorded when photoconversion was essentially complete. Photolysis of the product diazenes was carried out with defocussed visible light (λ=470-610 nm) for 90-120 minutes and followed by FTIR. A spectrum of the 1,1-diazene photocleavage products was recorded following visible photolysis.

Matrix Isolation of 1,1-trimethylenediazene 2 and 2-^{15}N. Azetidine carbamoyl azide or azetidine carbamoyl azide-^{15}N was purified by preparative VPC, placed in the sublimation chamber and thoroughly degassed. They were then cryopumped from a -16^{o} C ice/salt bath and co-deposited with UHP argon onto the CsI inner window at 20 K. The window was slowly lowered to 10 K and a spectrum of starting material was recorded. Photolysis with a monochromator (Oriel) set at 295 nm (20 nm slits) was carried out for 16-20 hours and monitored by FTIR. A spectrum of the 1,1-diazene was recorded when photoconversion was essentially complete. Photolysis of the product diazenes was effected with defocussed visible light (λ=400-580 nm) for 90-120 minutes and monitored by FTIR. A spectrum of the 1,1-diazene photoproducts was recorded following visible photolysis. For preparation of azetidine aminoisocyanate, the monochromator was set at 235 nm and photolysis was carried out for 20 hours. Subsequent photolysis of the aminoisocyanate with the monochromator set at 350 nm did not result in any observed 1,1-diazene, although the aminoisocyanate was transformed into the products expected from the 1,1-diazene. Broad band UV photolysis (λ=200-400 nm) also failed to produce 1,1-trimethylenediazene.

Matrix Isolation and Photolysis of 3-Pyrroline Carbamoyl Azide(7) and (7)-^{15}N. 3-Pyrroline carbamoyl azide or 3-pyrroline carbamoyl azide-15N was placed in the sublimation chamber and thoroughly degassed. The carbamoyl azide was then cryopumped from a -10^{o} C ice/salt bath and codeposited with UHP argon onto the CsI inner window at 20 K. The matrix was slowly cooled to 10 K, and a spectrum of the starting material was recorded. Broad band UV photolysis (λ=200-400 nm) for seven hours resulted in transformation of the starting material. A spectrum was recorded and the matrix photolyzed with visible light (λ=470-610 nm) for two hours. Visible photolysis resulted in {no} spectral changes.

Matrix Isolation of 1,1-Diphenyldiazene (22) and (22)-^{15}N. Diphenyl carbamoyl azide or diphenyl carbamoyl azide-^{15}N (~10 mg, recrystallized) was placed in

the sublimation chamber and thoroughly degassed. The sublimation chamber and the Pyrex tube connecting it to the cold head were wrapped in heat tape and warmed to 35-45 C. The carbamoyl azide was then cryopumped onto the CsI inner window held at 20 K and codeposited with UHP argon. The matrix was slowly cooled to 10 K and a spectrum of the carbamoyl azide starting material was recorded. Photolysis through a 10 nm bandpass interference filter centered at 300 nm (Oriel) for six hours resulted in the generation of the 1,1-diazene. Broad band visible photolysis (λ=500-1000 nm) did not result in any spectral changes.

Low Temperature Electronic Spectroscopy. Dilute solutions (~5 x 10^{-3} M) of carbamoyl azides were prepared in freshly distilled dry solvents (usually 2MTHF) and freeze-pump-thaw degassed through at least three cycles. Sample solutions were introduced into the low temperature spectroscopy cell through teflon tubing under positive argon pressure using syringe suction. As the cell is cooled to form a glass (~80 K for 2MTHF), more of the sample solution is drawn in due to solvent contraction. Photochemical transformations were carried out with defocussed light from an Oriel 1000W ozone-free xenon arc lamp. The light was passed through a 20 cm infrared (water) filter and appropriate colored glass filters. Stray light was excluded from the sample compartment of the Cary 219 by draping with a heavy black cloth. Temperature control was typically ±0.5 K with the tip of the thermocouple mounted just above the cell taken as representative of the cell temperature. In a typical experiment, after formation of an optically clear glass, a spectrum of the precursor carbamoyl azide at 80-82 K was recorded. The 1,1-diazene was generated by broad-band UV irradiation (λ=200-400 nm). Photolysis times ranged from 15 to 120 minutes. A spectrum of the 1,1-diazene was recorded. The glass was then warmed to 90 K, and allowed to equilibrate. Any spectral changes were noted, and a new spectrum recorded. The solution was then warmed further to several other temperatures and spectra recorded. Kinetics were measured as described below.

Kinetics. Glasses of the respective 1,1-diazenes in 2MTHF were prepared in the low-temperature electronic spectroscopy cell as described above. The cell temperature was slowly raised to begin decomposition of the 1,1-diazenes. Decompositions were monitored using either the repetitive scan program of the Cary 219 spectrophotometer or using a time delay single wavelength monitor. All data prior to temperature equilibration (~30 minutes) were discarded if possible. (At higher temperatures where decomposition was very fast, less time could be allowed for equilibration.) Typically, reactions were monitored through several half-lives and reported rate constants are derived from a conventional linear least squares analysis. First order decays were checked at two different starting concentrations and in all cases gave identical rate constants to within experimental error.

Product Analysis. For product analysis by VPC, 1,1-diazenes were prepared by broad-band UV irradiation (λ=200-400 nm) in a 2MTHF glass in 5 mm quartz tubes immersed in a liquid nitrogen filled quartz finger Dewar. For thermal decompositions, samples were removed from the liquid nitrogen and allowed to warm to room temperature. For photochemical decompositions, the 77 K samples were irradiated with light of the appropriate wavelengths for 30-60 minutes. Volatile products were analyzed on a VZ-10 (Alltech) packed column, and non-volatiles were analyzed on a SE-54 capillary column.

For product analysis by NMR, 1,1-diazenes were prepared by broad-band UV irradiation (λ=200-400 nm) in a glassy mixture of 1:1 toluene-d_8 and tetrahydrofuran-d_8 in medium walled 5 mm quartz NMR tubes held at 77 K in a liquid nitrogen filled quartz finger Dewar. Appropriate thermal or photochemical decomposition conditions (as described for VPC analysis) were effected, and NMR spectra were taken at 25° C and -80° C (to solubilize volatiles) on a JEOL GX-400 NMR spectrometer. Each spectrum was taken twice and the integrations were averaged. Thorough vacuum transfer of volatiles from an NMR sample and subsequent VPC analysis agreed to within 2%. NMR analysis allows direct comparison of volatile and non-volatile products.

Appendix

GVB Calculations on 1,1-Diazenes and Azomethinimines

To gain an understanding of the equilibrium between 1,1-diazenes and their azomethinimine tautomers, some GVB[24,83] calculations were performed on the simplest tautomer pair, 1,1-methyl-H-diazene **C** and azomethinimine **B**. Calculations on two 1,1-diazenes which promised to have interesting electronic properties, 1,1-tetramethynediazene **C** and 1,1-diformyldiazene **D**, were also performed.

A **B**

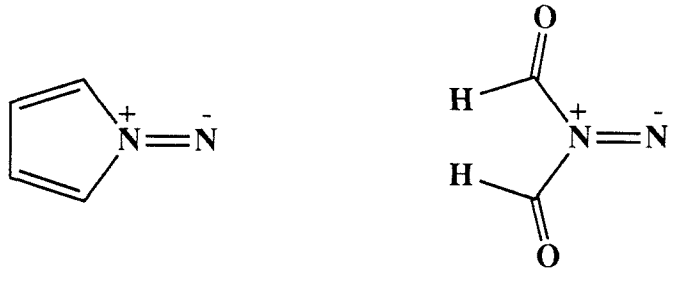

C **D**

A. 1,1-Diazene Tautomerization.

The structure of 1,1-diazene **A** was based on previous studies.[23,84] A minimal optimization was done to arrive at a geometry for **B**, beginning with previous calculations.[20] Only the CN and NN bond lengths were optimized. The geometries used for **A** and **B** are shown in Figure A. The optimal structure of **B** is not too different from the one known azomethinimine geometry, which had R_{CN}=1.32 Å and R_{NN}=1.34 Å.[45c]

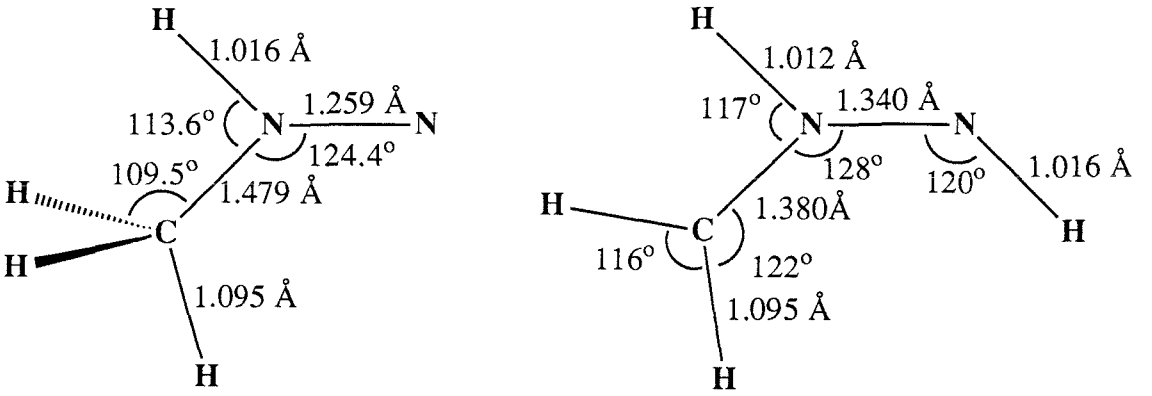

A **B**

Figure A. Geometries employed in GVB calculations on **A** and **B**.

The basis set was GTO valence double zeta. Huzinaga's scaled hydrogen basis[85] and Dunning's basis for the s and p functions on the heavy atoms[86] were used. A single set of d polarization functions was used on the heavy atoms, with d exponents of 0.76 for nitrogen and 0.64 for carbon. The highest level of calculation done for comparison of **A** and **B** was GVBCI 4/3. This involved correlation of the π (A") electrons along with configuration interaction of these electrons over the occupied π (A") orbitals. A higher level CI, with configuration interaction over both occupied and unoccupied π (A") orbitals, was used to estimate the $S_0 \rightarrow S_1$ gap for **B**.

The difference in energy between **A** and **B** was found to be 13.7 kcal/mol, with the 1,1-diazene isomer **A** lower in energy. This was disappointing, since experiments had suggested that the azomethinimine should be lower in energy. This discrepancy may be due to the minimal geometry optimization. An in-depth study of this problem, with complete geometry optimization, might yield an answer in accord with experimental observations. A higher level of electron correlation might also improve the agreement with experiment. The current level of correlation (GVBCI 4/3) may be biased in favor of the 1,1-diazene. An

interesting note is that the calculation shows the ground state of **B** to be similar to isoelectronic ozone.[24] This singlet 1,3-diradical character (rather than 1,3-dipolar) may be important in understanding the intermediacy of azomethinimines in the diazene to hydrazone rearrangement. Finally, the excitation energy of **B** was calculated to be 5.5 eV from the GVBCI 4/12 calculation. This differs from the experimentally observed values of 2.5-2.6 eV. However, a similar discrepancy was found in a GVB study of ozone.[24]

B. Electrophilic 1,1-Diazenes.

1,1-Diazenes with electron withdrawing substituents are known to add to olefins.[5] This is a reaction which is common for simple nitrenes, but unknown for dialkyl 1,1-diazenes. Apparently, electron withdrawing substituents reduce the ability of the central nitrogen to donate electrons to the terminal nitrogen, leaving the terminal nitrogen electrophilic. If the electron withdrawing power of the substituents was strong enough, a triplet ground state might result, and the species might be described more truly as an aminonitrene. Incorporation of the central nitrogen lone pair into an aromatic sextet might be sufficient for this. Experimentally, attempts to prepare 1,1-diazene **C** by oxidation of 1-aminopyrrole or thermolysis of the sodium sulfonylhydrazine salt have failed to show the intermediacy of **C**. Most of the electrophilic 1,1-diazenes that have been studied have had acyl substituents. These experimental observations suggested the calculations on **C** and **D**.

Due to the size of these systems, no geometry optimization was performed for **C** or **D**. The known geometry of pyrrole[87] with a typical 1,1-diazene NN bond length of 1.251 Å was used for **C**. A previous calculation on N-formylformamide provided a basic geometry for **D**,[88] again with an NN bond length of 1.251 Å (Figure B). These geometries are expected to *overestimate* the interaction of the two nitrogens and favor the "1,1-diazene"

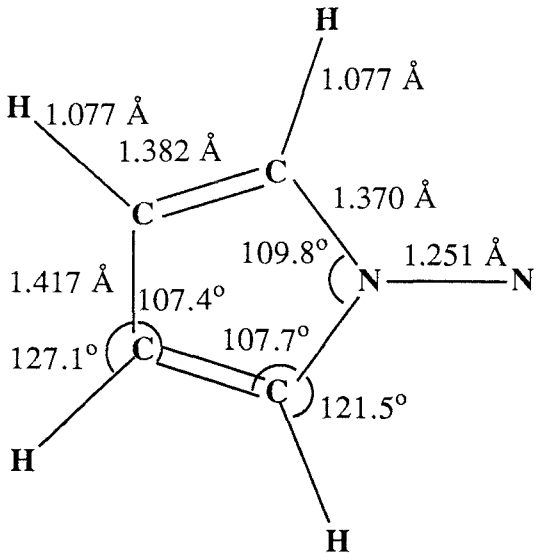

C

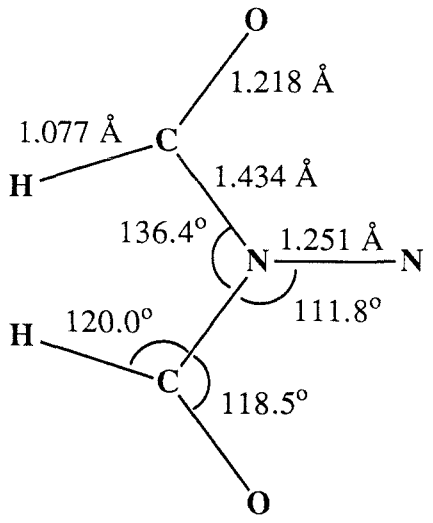

D

Figure B. Geometries employed in GVB calculations on **C** and **D**.

singlet state. Optimization is expected to result in longer NN bonds. The basis set used was the same as for the calculations on **A** and **B**, except that no d polarization functions were employed.

A GVB 1/2 calculation on the singlet "1,1-diazene" state of C was found to lie 15.4 kcal/mol above a triplet "aminonitrene" state calculated with equal correlation (open shell Hartree-Fock). Similarly, a GVB 1/2 calculation on the singlet of D lies 21.3 kcal/mol above the Hartree-Fock triplet. These calcualtions *should not* be taken as proof of a triplet ground state for C or D. The singlet-triplet gap is observed to decrease with increasing correlation, and the level of correlation used here is quite low. Adding d polarization functions has also been known to be necessary for calulating accurate singlet-triplet gaps.[24] Even so, these results indicate that the triplet "aminonitrene" state is lowered relative to the singlet "1,1-diazene" state by decreasing the electron donating capability of the central

nitrogen. The singlet "aminonitrene" state ($^1A_2$), calculated by Davis and Goddard to lie 51 kcal/mol above the ground state,[23] should also be lowered. This state, similar to that of a singlet nitrene, may be the reactive state in the addition of electrophilic 1,1-diazenes to olefins. It is unfortunate that the experimental studies of 1,1-diphenyldiazene **22** suggest that the carbamoyl azide route may meet with failure for these interesting 1,1-diazene derivatives.

References and Notes

1. a) Michaelis, A.; Luxembourg, K. *Ber.* **1893**, *26*, 2174-2181. b) Busch, M.; Weiss, B. *Ber.* **1900**, *33*, 2701-2711.

2. Reviews of 1,1-diazene chemistry: a) Lemal, D.M. in "Nitrenes," Lwowski, W., ed., Interscience, New York: 1970, 345-404. b) Ioffe, B.V.; Kuznetsov, M.A. *Russ. Chem. Rev.* **1972**, *41*, 131-145. c) Atkinson, R.S. in "Azides and Nitrenes," Scriven, E.F.V. ed., Academic Press, Orlando FL: 1984, 258-285. d) Platz, M.S. in "Azides and Nitrenes," Scriven, E.F.V. ed., Academic Press, Orlando FL: 1984, 381-388. e) Lwowski, W. in "Reactive Intermediates," Jones, M. ; Moss, R.A. eds., Wiley, New York: 1985, 325-327.

3. Other names that have been used for 1,1-diazenes are azene, azalene, and azamine.

4. Watson, J.S. *J. Chem. Soc.* **1956**, 3677-3679.

5. Anderson, D.J.; Gilchrist, T.L.; Rees, C.W. *Chem. Commun.* **1971**, 800.

6. Lemal, D.M.; Rave, T.W.; McGregor, S.D. *J. Am. Chem. Soc.* **1963**, *85*, 1944-1948.

7. a) Lemal, D.M.; McGregor, S.D. *J. Am. Chem. Soc.* **1966**, *88*, 1335-1336. b) McGregor, S.D.; Lemal, D.M. *J. Am. Chem. Soc.* **1966**, *88*, 2858-2859.

8. Overberger, C.G.; Valentine, M.; Anselme, J.-P. *J. Am. Chem. Soc.* **1969**, *91*, 687-694.

9. Overberger, C.G.; Herin, L.P. *J. Org. Chem.* **1962**, *27*, 417-422.

10. Bumgardner, C.L.; Martin, K.J.; Freeman, J.P. *J. Am. Chem. Soc.* **1963**, *85*, 97-99.

11. a) Freeman, J.P.; Graham, W.H. *J. Am. Chem. Soc.* **1967**, *89*, 1761-1762. b) Freeman, J.P.; Pucci, D.G.; Binsch, G. *J. Org. Chem.* **1972**, *37*, 1894-1898.

12. a) Crawford, R.J.; Mishra, A. *J. Am. Chem. Soc.* **1965**, *87*, 3768-3769. b) Crawford, R.J.; Mishra, A.; Dummel, R.J. *J. Am. Chem. Soc.* **1966**, *88*,

3959-3963. c) Crawford, R.J.; Mishra, A. *J. Am. Chem. Soc.* **1966**, *88*, 3963-3969.

13. Kirste, K.; Luttke, W.; Rademacher, P. *Angew. Chem. Int. Ed. Engl.* **1978**, *17*, 680-681.
14. Lemal, D.M.; Rave, T.W. *J. Am. Chem. Soc.* **1965**, *87*, 393-394.
15. Viswanathan, N.; Sidhaye, A.R. *Tet. Lett.* **1979**, 5025-5026.
16. Lemal, D.M.; Menger, F.; Coats, E. *J. Am. Chem. Soc.* **1964**, *86*, 2395-2401.
17. Huisgen, R.; Grashey, R.; Krischke, R. *Tet. Lett.* **1962**, 387-391.
18. Lichter, R.L., Doctoral Dissertation, University of Wisconsin, Madison, WI: 1967.
19. Carter, P.; Stevens, T.S. *J. Chem. Soc.* **1961**, 1743-1748.
20. a) Caramella, P.; Gandour, R.W.; Hall, J.A.; Deville, C.G.; Houk, K.N. *J. Am. Chem. Soc.* **1977**, *99*, 385-392. b) Hiberty, P.C.; Leforestier, C. *J. Am. Chem. Soc.* **1978**, *100*, 2012-2017. c) Kahn, S.D.; Hehre, W.J.; Pople, J.A. *J. Am. Chem. Soc.* **1987**, *109*, 1871-1873.
21. a) Atkinson, R.S.; Rees, C.W. *J. Chem. Soc. (C)* **1969**, 772-778. b) Atkinson, R.S.; Malpass, J.R.; Skinner, K.L.; Woodthorpe, K.L. *Chem. Commun.* **1981**, 549-550.
22. Casewit, C.J.; Goddard, W.A. III *J. Am. Chem. Soc.* **1980**, *102*, 4057-4062.
23. Davis, J.H.; Goddard, W.A. III *J. Am. Chem. Soc.* **1977**, *99*, 7111-7121.
24. Goddard, W.A. III; Dunning, T.H. Jr.; Hunt, W.J.; Hay, P.J. *Acc. Chem. Res.* **1973**, *6*, 368-376.
25. a) Collin, R.L.; Lipscomb, W.N. *Acta Cryst.* **1951**, *4*, 10-14. b) Yamaguchi, A.; Ichishima, I.; Shimanouchi, T.; Mizushima, S. *J.Chem. Phys.* **1959**, *31*, 843.
26. Carlotti, M.; Johns, J.W.C.; Trombetti, A. *Can. J. Phys.* **1974**, *52*, 340-344.
27. Jensen, H.J.A.; Jorgensen, P.; Helgaker, T. *J. Am. Chem. Soc.* **1987**, *109*, 2895-2901.

28. Engel, P.S. *Chem. Rev.* **1980**, *80*, 99-150.

29. Dannenberg, J.J.; Rocklin, D. *J. Org. Chem.* **1982**, *47*, 4529-4534.

30. Dewar, M.J.S.; Thiel, W. *J. Am. Chem. Soc.* **1977**, *99*, 4899-4907.

31. a) Hinsberg, W.D. III; Dervan, P.B. *J. Am. Chem. Soc.* **1978**, *100*, 1608-1610. b) Hinsberg, W.D. III; Dervan, P.B. *J. Am. Chem. Soc.* **1979**, *101*, 6142-6144.

32. Griller, D.; Ingold, K.U. *Acc. Chem. Res.* **1976**, **9**, 13-19.

33. Schultz, P.G.; Dervan, P.B. *J. Am. Chem. Soc.* **1980**, *102*, 878-880.

34. McIntyre, D.K.; Dervan, P.B. *J. Am. Chem. Soc.* **1982**, *104*, 6466-6468.

35. Turro, N.J. "Modern Molecular Photochemistry," Benjamin/Cummings, Menlo Park CA: 1978.

36. a) Schultz, P.G.; Dervan, P.B. *J. Am. Chem. Soc.* **1981**, *103*, 1563-1564. b) Schultz, P.G.; Dervan, P.B. *J. Am. Chem. Soc.* **1982**, *104*, 6660-6668.

37. Dervan, P.B.; Squillacote, M.; Lahti, P.; Sylwester, A.P.; Roberts, J.D. *J. Am. Chem. Soc.* **1981**, *103*, 1120-1122.

38. Hinsberg, W.D. III; Schultz, P.G.; Dervan, P.B. *J. Am. Chem. Soc.* **1982**, *104*, 766-773.

39. Sylwester, A.P.; Dervan, P.B. *J. Am. Chem. Soc.* **1984**, *106*, 4648-4650.

40. Thiele, J.; Stange, O. *J. Liebigs Ann. Chem.* **1894**, *283*, 1-46.

41. a) Lwowski, W.; deMauriac, R.; Mattingly, T.W.; Scheiffele, E. *Tet.Lett.* **1964**, 3285-3288. b) Lwowski, W.; deMauriac, R.A.; Murray, R.A.; Lunow, L. *Tet. Lett.* **1971**, 425-428. c) Lwowski, W.; deMauriac, R.A.; Thompson, M.; Wilde, R.E.; Chen, S.-Y. *J. Org. Chem.* **1975**,*40*, 2608-2612. d) Reichen, W. *Helv. Chim. Acta* **1976**, *59*, 2601-2609.

42. Sylwester, A.P., Doctoral Dissertation, California Institute of Technology, Pasadena CA: 1986.

43. Yannoni, C.S.; Reisenauer, H.P.; Maier, G. *J. Am. Chem. Soc.* **1983**, *105*, 6181-6182.

44. a) Yannoni, C.S.; Clarke, T.C. *Phys. Rev. Lett.* **1983**, *51*, 1191-1193. b) Horne, D. ; Kendrick, R.D.; Yannoni, C.S. *J. Magn. Res.* **1983**, *52*, 299-304.

45. Singh, B. *J. Am. Chem. Soc.* **1969**, *91*, 3670-3671. For other azomethinimine data, see: a) Huisgen, R.; Fleischmann, R.; Eckell, A. *Tet. Lett.* **1960**, 1-4. b) De Mayo, P.; Ryan, J.J. *Chem. Commun.* **1967**, 88-89. c.) Brandl, F. ; Hoppe, W. *Z. Kristall.* **1967**, *125*, 80-91.

46. a) Capon, B.; Siddhanta, A.K.; Zucco, C. *J. Org. Chem.* **1985**, *50*, 3580-3584. b) Capon, B.; Guo, B.-Z.; Kwok, F.C.; Siddhanta, A.K.; Zucco, C. *Acc. Chem. Res.* **1988**, *21*, 135-140.

47. Bock, H.; Dammel, R. *Angew. Chem. Int. Ed. Engl.* **1987**, *26*, 504-526.

48. a) Miller, R.D.; Golitz, P.; Janssen, J.; Lemmens, J. *J. Am. Chem. Soc.* **1984**, *106*, 1508-1510. b) Miller, R.D.; Golitz, P.; Janssen, J.; Lemmens, J. *J. Am. Chem. Soc.* **1984**, *106*, 7277-7279.

49. Lowry, T.H.; Richardson, K.S. "Mechanism and Theory in Organic Chemistry," 3rd ed., Harper and Row, New York: 1987.

50. Wiberg, K.B. *Angew. Chem. Int. Ed. Engl.* **1986**, *25*, 312-322.

51. There are two possibilities for this nitrene insertion product. The most likely structure is 1,7-diazabicyclo-[3.2.0]heptan-5-one, the result of insertion into a C-H bond of the α carbon. 1,3-Diazabicyclo[2.2.1]heptan-2-one from β insertion is less likely.

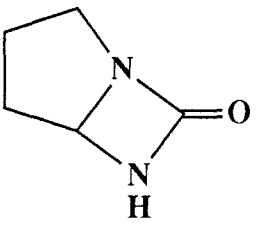

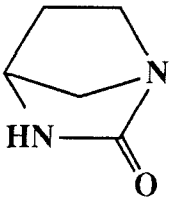

52. Reciprocal to the observation that some of the photogenerated CO is in a site perturbed by nearby 1,1-diazenes, this second band could be due to perturbation of the 1,1-diazene by nearby CO.

53. a) Kim, H.; Gwinn, W.D. *J. Chem. Phys.* **1969**, *51*, 1815-1819. b) Geise, H.J.; Mijlhoff, F.C. *Rec. trav. chim.*. **1971**, *90*, 577-583. c) Tamagawa, K.; Hilderbrandt, R.L.; Shen, Q. *J. Am. Chem. Soc.* **1987**, *109*, 1380-1383.

54. Ikeda, T.; Lord, R.C. *J. Chem. Phys.* **1972**, *56*, 4450-4466.

55. Pitzer, K.S.; Donath, W.E. *J. Am. Chem. Soc.* **1959**, *81*, 3213-3218.

56. The low temperature spectroscopy cell was designed by Hinsberg. Hinsberg, W.D. Doctoral Dissertation, California Institute of Technology, Pasadena CA: 1978.

57. An emission spectrum of **1** has been recorded, and it demonstrates that this is the 0,0 band. The emission maximum is at 691 nm.

58. Thermochromism has been reported previously for some azomethinimines. However, these azomethinimines were incorporated into aromatic systems and the thermochromism was attributed to the temperature dependence of the equilibrium between the azomethinimines and their s-tetrazine dimers. Huisgen, R.; Grashey, R.; Krischke, R. *Tet. Lett.* **1962**, 387-391.

59. Photochemical 1,3-sigmatropic hydrogen shifts are known for alkenes. Kropp, P.J.; Fravel, H.G. Jr.; Fields, T.R. *J. Am. Chem. Soc.* **1976**, *98*, 840-841.

60. These experiments were performed prior to the discovery in the FTIR experiments that an improved yield could be obtained by using narrow band photolysis centered at 300 nm and longer irradiation times.

61. In the absence of a fluorescence spectrum, this band can only be tentatively assigned as the 0,0 band.

62. a) Baldwin, J.E. *J. Chem. Soc. Chem. Commun.* **1976**, 734-736. b) Beckwith, A.L.J. *Tetrahedron* **1981**, *37*, 3073-3100.

63. a) Van Auken, T.V.; Rinehart, K.L. Jr. *J. Am. Chem. Soc.* **1962**, *84*, 3736-3743. b) McGreer, D.E.; Chiu, N.W.K.; Vinje, M.G.; Wong, K.C.K. *Can. J. Chem.* **1965**, *43*, 1407-1416.

64. Sammes, P.G. *Tetrahedron*, **1976**, *32*, 405-422.

65. The activation energy for 1,1-di-*t*-butyldiazene was calculated using an assumed value of 10^{13} for A. A different value for A would give a different activation energy.

66. This would also suggest that preparation of **2** in an organic glass, such as 2MTHF, has advantages over solid argon since organic glasses are more efficient at vibrational deactivation.

67. a) A MNDO caclulation has been performed for 1,1-diazene **14**. The calculated heat of formation was 41.4 kcal/mol, and the NN bond length was only 1.140 Å, just slightly longer than molecular nitrogen at 1.0975 Å. Minyaev, R.M.; Kletskii, M.E.; Minkin, V.I. *Zh. Org. Khim.* **1987**, *23*, 2508-2521. b) Another interesting aspect of 1,1-diazene **14** is the strain energies of the cycloalkenes. Cyclopropene is 14.3 kcal/mol more strained than methylenecyclopropane.[50]

68. Tomalia, D.A.; Paige, J.N. *J. Heterocycl. Chem.* **1967**, *4*, 178-182.

69. a) Squillacote, M.E.; Sheridan, R.S.; Chapman, O.L.; Anet, F.A.L. *J. Am. Chem. Soc.* **1979**, *101*, 3657-3659. b) Fisher, J.J.; Michl, J. *J. Am. Chem. Soc.* **1987**, *109*, 1056-1059.

70. Birkofer, L.; Krebs, K. *Tet. Lett.* **1968**, 885-888.

71. Pouchert, C.J., ed. "The Aldrich Library of FTIR Spectra," 1st ed., Aldrich Chemical Co., Milwaukee WI: 1985.

72. Grasselli, J.G., ed. "The CRC Atlas of Spectral Data and Physical Constants for Organic Compounds," CRC Press, Cleveland OH: 1973.

73. Patai, S., ed. "The Chemistry of the Carbonyl Group," Interscience, New York, NY: 1966.

74. Cauquis, G.; Genies, M. *Tet. Lett.* **1970**, 2903-2905.

75. a) Lieber, E.; Minnis, R.L. Jr.; Rao, C.N.R. *Chem. Rev.* **1965**, *65*, 377-384. b) Lwowski, W. *Angew. Chem. Int. Ed. Engl.* **1967**, *6*, 897-906. c) L'Abbe, G. *Chem. Rev.* **1969**, *69*, 345-363. d) Reichen, W. *Chem. Rev.* **1978**, *78*, 569-588.

76. Frenking, G.; Schmidt, J. *Tetrahedron* **1984**, *40*, 2123-2132.

77. Inagaki, M.; Shingaki, T.; Nagai, T. *Chem. Lett.* **1982**, 9-12.

78. This 15 kcal/mol value is only a guideline, since molecules larger than **2** will have more vibrational modes in which to distribute any excess energy. The use of 1,1-diazene/nitrosobenzene adducts as precursors should also be useful, as described in the introduction for 1,1-dimethyldiazene. Here, since nitrosobenzene can carry off more of the vibrational energy then carbon monoxide, the 1,1-diazene could be generated cleanly from the 1-phenyltriazene-1-oxide precursor but not from the carbamoyl azide.[42] Aminoazides are expected to be worse precursors in this respect, since the excitation energy is higher.

79. English patent 971000, Monsanto Co, 1964. (Chem. Abstr. 62:1633d)

80. a) Birkofer, L.; Richter, P.; Ritter, A. *Ber.* **1960**, *93*, 2804-2809. b) Scherer, O.J.; Schmidt, M. *Ber.* **1965**, *98*, 2243-2247.

81. Breederveld, H. *Rec. trav. chim.* **1962**, *81*, 276-278.

82. Scott, F.L.; Scott, M.T. *J. Am. Chem. Soc.* **1957**, *79*, 6077-6082.

83. Bair, R.A.; Goddard, W.A. III; Voter, A.F.; Rappe, A.K.; Yaffe, L.G.; Bobrowicz, F.W.; Wadt, W.R.; Hay, P.J.; Hunt, W.J. GVB2P5 program, unpublished.

84. Stauffer, D.A. unpublished results.

85. Huzinaga, S. *J. Chem. Phys.* **1965**, *42*, 1293-1302.

86. Dunning, T.H. *J. Chem. Phys.* **1970**, *53*, 2823-2833.

87. Nygaard, L.; Nielson, J.T.; Kirchheiner, J.; Moltesen, G.; Rastrup-Anderson, J.; Sorenson, G.O. *J. Mol. Struct.* **1969**, *3*, 491-506.

88. Radom, L.; Riggs, N.V. *Aust. J. Chem.* **1980**, *33*, 2337-2342.

Part II

Distance, Temperature, and Dynamic Solvent Effects on Electron Transfer Reactions

Chapter 6

Introduction: Electron Transfer

Electron transfer processes are important in a wide variety of fields, from biology to solid state physics. The transfer of an electron is one of the most fundamental chemical reactions, and the conceptual simplicity of the process together with its practical significance have inspired a voluminous literature. Excellent reviews exist which cover the subject from different perspectives.[1] This introductory chapter will summarize some previous theoretical and experimental results which are relevant to the electron transfer studies presented in the next two chapters, particularly the influence of distance, thermodynamic driving force, orientation, temperature, and solvent dynamics.

A. Theory.

The work of Marcus[2] is probably the best place to begin any discussion of electron transfer theory. Beginning in the mid 1950's, he developed a framework which remains fundamental to current theoretical developments. The transfer of an electron is considered to be coupled to changes in the nuclear coordinate of the donor and acceptor as shown in Figure 47. The potential energy surface of the reactant state (here shown schematically as a parabola) is labelled R, and the product surface (after electron transfer) is labelled P. Classically, the system must reach point X (where the curves cross) for electron transfer to occur. If the coupling between the donor and acceptor is strong, electron transfer will occur each time this point is reached, and the reaction is said to be *adiabatic*. If the coupling is weak, the system must move through this point many times before the electron transfers, and the reaction is called *nonadiabatic*. The energy required to reach this point from the bottom of reactant potential well is the activation energy $\Delta G^{\ddagger}$. The electron transfer rate k_{ET} can be calculated from absolute reaction rate theory[3] as

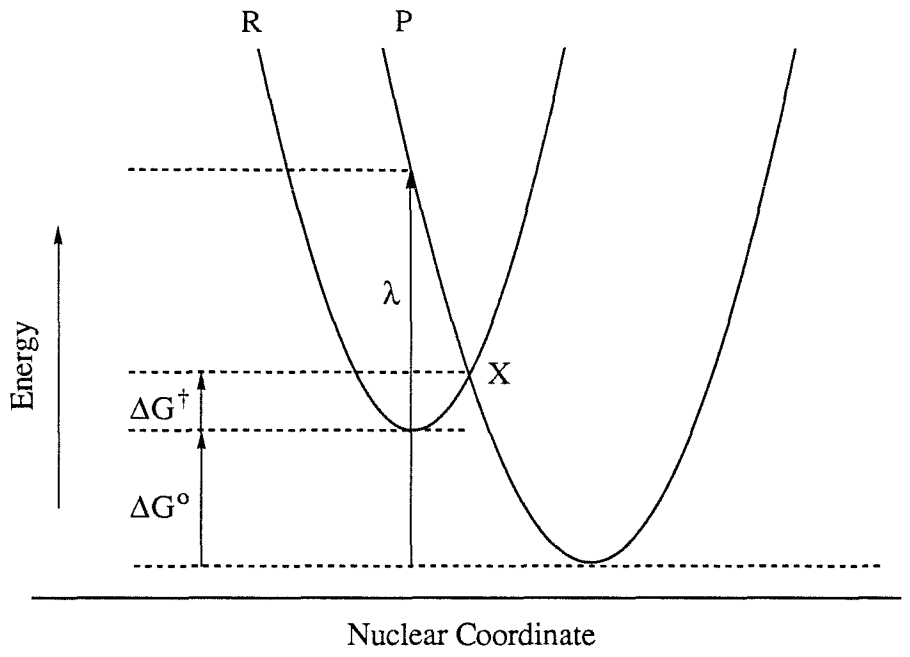

Figure 47. Classical nuclear potential energy surfaces coupled to electron transfer.

$$k_{ET} = \kappa B \exp\left[-\frac{\Delta G^{\ddagger}}{k_B T}\right] \tag{1}$$

The transmission coefficient κ is considered to be unity if the transfer is adiabatic, and <<1 if it is nonadiabatic. The factor B is the collision frequency for bimolecular reactions or a vibrational frequency of the reaction coordinate for intramolecular reactions. The activation free energy $\Delta G^{\ddagger}$ can be related to the thermodynamic driving force of the reaction ΔG^{o}, that is, the difference in energy between the minima of the reactant and product potential wells, as

$$\Delta G^{\ddagger} = \frac{(\lambda + \Delta G^{o})^2}{4\lambda} \tag{2}$$

where λ is the reorganization energy coupled to electron transfer, the energy required to move the atoms to their equilibrium positions on the product potential surface *without*

transferring the electron. Combination of equations (1) and (2) gives the simplest form of the Marcus electron transfer theory,

$$k_{ET} = \kappa B \exp\left[-\frac{(\lambda + \Delta G^{o})^2}{4\lambda k_B T}\right]. \qquad (3)$$

This equation predicts a quadratic dependence on the driving force ΔG^{o}, with a maximum rate when $-\Delta G^{o}$ equals λ.

The factor κB can be treated more explicitly using Landau-Zener theory[4] to give

$$k_{ET} = \frac{2\pi}{h} |H_{RP}|^2 (4\pi\lambda k_B T)^{-1/2} \exp\left[-\frac{(\lambda + \Delta G^{o})^2}{4\lambda k_B T}\right]. \qquad (4)$$

Here H_{RP} is the matrix element for transition from the reactant surface to the product surface. The reorganization energy λ can also be separated into a sum of changes in the normal modes of the reactants and changes in solvent modes. Marcus[2b] gave an expression for the inner shell (reactant) reorganization λ_i using the set of normal modes *j* as

$$\lambda_i = \frac{1}{2} \sum_j k_{Hj} Q_j^2 \qquad (5)$$

where k_{Hj} is the Hooke's law force constant for the *j*th mode and Q_j is the displacement along this mode's coordinate caused by electron transfer. The outer shell reorganization λ_o is then given as

$$\lambda_o = \frac{(\Delta e)^2}{4\pi\varepsilon_o}\left(\frac{1}{2r_1} + \frac{1}{2r_2} - \frac{1}{r_1 + r_2}\right)\left(\frac{1}{n^2} - \frac{1}{\varepsilon}\right) \qquad (6)$$

where Δe is the charge transferred, r_1 and r_2 are the radii of the donor and acceptor, n is the refractive index of the medium, and ε is the static dielectric constant. The factor ε_o is the permittivity of space to give the proper units.

The Marcus theory has been very successful in describing electron transfer between reagents in solution and for electrode reactions. One of the remarkable aspects of the theory (as noted above) is that it predicts a quadratic dependence of the electron transfer rate

on the thermodynamic driving force ΔG^o as shown in Figure 48. The maximum rate is predicted to occur when $-\Delta G^o$ is equal to λ, where the reaction should be activationless. The Marcus theory is considered to be *classical* since activation of the reactants is not quantized. It is strictly valid, therefore, only when the temperature is high and the important vibrational modes are fully excited. Under these conditions, the temperature dependence should obey the Arrhenius rate law with ln k_{ET} linear in T^{-1}, with a slope equal to $\Delta G^{\ddagger} / k_B$. Factors such as donor-acceptor distance and relative orientation affect the matrix element H_{RP}. The magnitude of H_{RP} is generally considered to decay

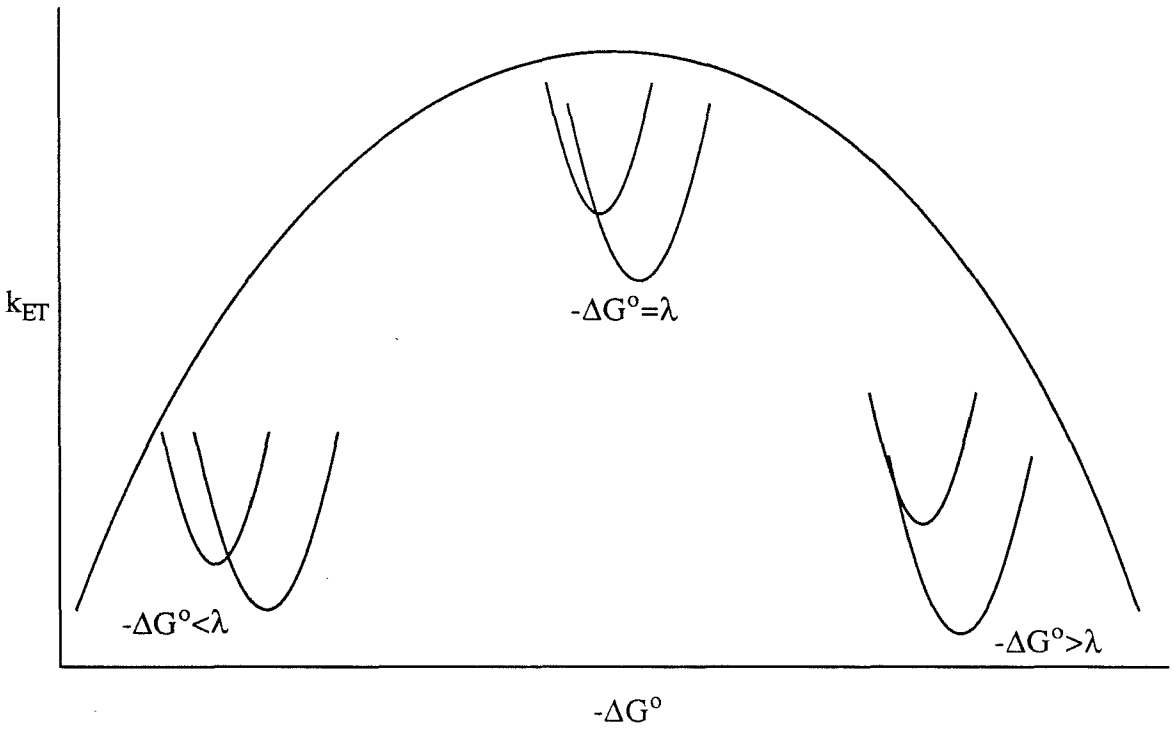

Figure 48. Quadratic dependence of k_{ET} on driving force as predicted by Marcus theory.

exponentially with distance.[5] Beratan has considered the decay of H_{RP} through bonds as a function of the bonding framework and the energy difference between the orbitals directly involved in the electron transfer and the unoccupied orbitals of the bridge.[6] The decay depends on the bridge and also on the position of the donor and acceptor levels relative to the bridge levels. Siders, Cave, and Marcus have treated the orientational dependence of electron transfer.[7] The nodal character of the orbitals involved in the electron transfer was found to be important, and the rates could vary by factors of nearly 1000 for some cases.

Experimental studies of some biological electron transfer reactions at low temperature (see below) revealed some weaknesses in the classical electron transfer theory. These reactions became temperature independent at low temperatures, and some demonstrated apparently negative activation energies, that is, they became faster at lower temperatures. These were considered to be quantum effects, the result of the ability of quantum mechanical systems to pass through a barrier without strictly having sufficient energy to pass over it (tunnelling) and of variable overlap between quantized states of the reactant and product surfaces.

One of the first theoretical approaches to address this issue was the equation derived by Hopfield.[8] This theory was derived by analogy to Forster-Dexter energy transfer, beginning with a "Golden Rule" equation for a transition between two states

$$k_{ET} = \frac{2\pi}{h} |H_{RP}|^2 \text{ (FC)} \tag{7}$$

where (FC) is the Frank-Condon weighted density of states. The expression Hopfield arrived at for an electron transfer reaction coupled to a mode of frequency ω is

$$k_{ET} = \frac{2\pi}{h} |H_{RP}|^2 (2\pi\sigma^2)^{-1/2} \exp\left[- \frac{(\lambda + \Delta G^\circ)^2}{2\sigma^2} \right] \tag{8}$$

where σ has the nature of an effective temperature and is defined as

$$\sigma = \frac{h\omega}{2k_H} \coth\left(\frac{h\omega}{2k_B T}\right) . \qquad (9)$$

This expression is considered to be *semiclassical* since it models the behavior of quantized vibrations without explicitly treating the occupation of the vibrational states. Theories which treat the quantum behavior explicitly have also been derived. Most of these become quite complicated to employ for real systems with many vibrational modes. Jortner,[9] for example, arrived at an equation for a system with only one mode of frequency ω:

$$k_{ET} = \frac{2\pi}{h^2\omega} |H_{RP}|^2 \exp[-S(2\bar{n}+1)] \left(\frac{\bar{n}+1}{\bar{n}}\right)^{\frac{1}{2}p} I_p(2S[\bar{n}(\bar{n}+1)]^{1/2}) . \qquad (10)$$

Here n are quantum numbers and $\bar{n}$ is an averaged quantum number, S is a summation over the overlaps of the donor and acceptor levels, p is associated with the change in quantum numbers going from reactant to product, and $I_p(x)$ is a modified Bessel function. The review by DeVault[1] contains detailed derivations and explanations for the different electron transfer theories and is recommended for those interested in a fuller treatment of the theory.

The classical electron transfer theory of Marcus and its semiclassical and quantum mechanical extensions begin generally from transition state theory.[3,10] In transition state theory, there is an equilibrium condition between reactants and the activated complex, and each activated complex is assumed to proceed on to products. The rate is then redefined in terms of the equilibrium concentration of activated systems. Some recent theoretical work has examined how transition state theory may break down for certain chemical reactions, including electron transfer reactions, due to the dynamics of the solvent. The theory of Kramers is the starting point for most of this work. Kramers proposed in 1940 that chemical reactions could be treated as Brownian motion (diffusion) in phase space.[11] Kramers found three regimes where the solvent viscosity has different effects. In the moderate friction regime, collisions with the solvent are sufficient to maintain an energy equilibrium for barrier crossing, but insufficient to disturb the reacting systems during

passage over the barrier. In this regime, transition state theory is valid. In the "high friction" or "overdamped" regime, collisions with the solvent are able to cause recrossing of the barrier before stable products are formed. Transition state theory breaks down since only a fraction of the systems which reach the top of the barrier (the activated state) go on to products. The rate is reduced below the transition state theory prediction, and is inversely proportional to a solvent property related to viscosity and usually called friction. In the "low friction" or "underdamped" regime, the solvent is so weakly coupled to the reaction that equilibrium between reactants and the activated state cannot be maintained. The rate of reactant activation and/or product deactivation becomes rate limiting, and the rate again falls below the transition state theory prediction. In this case, however, the rate is proportional to the solvent friction. For the normal and overdamped regimes, Kramers proposed an equation of the form:

$$k = k_{TST}\left[\left(1+\left(\frac{\zeta}{2\omega_b}\right)^2\right)^{1/2} - \left(\frac{\zeta}{2\omega_b}\right)\right] \qquad (11)$$

where k_{TST} is the rate according to transition state theory, ω_b is the barrier frequency, and ζ is the solvent friction. The Kramers model therefore predicts an initial increase in rate with increasing friction in the underdamped regime, a maximum near k_{TST} in the "nonadiabatic" regime described by transition state theory, and an ultimate decrease with increasing friction in the overdamped regime. Except for special cases, however, it is not trivial to produce an equation which will cover the entire range. Part of the problem is that the relationship of friction to viscosity and other solvent properties is not necessarily simple and may not be constant over the entire range of frictional values. Only solvent motion on a time scale relevant to barrier crossing should be considered, so that there is a frequency dependence to the friction. The shape of the barrier can become important as well, especially in underdamped cases. Complete treatments of Kramers theory and its modern variants can be found in a number of reviews.[12]

Several theoretical groups have recently derived expressions relating Kramers theory to electron transfer reactions in the overdamped regime. Hynes showed that there should be a strong dependence of electron transfer rates on the longitudinal relaxation time (τ_L) of the solvent in the overdamped regime.[13] In this treatment, the solvent forms a "polarization cage" around the reactants which resists electron transfer. Reorientation of the solvent molecules (which occurs with a relaxation time τ_L) destroys the cage and the electron transfer proceeds. The rate of electron transfer is then given by

$$k_{ET} = k_{TST} \frac{\omega_b}{\omega_c^2 \tau_L} \tag{12}$$

where ω_b is the frequency of the intrinsic barrier to electron transfer and ω_c is the frequency of the solvent cage. A recent calculation by Morillo and Cukier showed that when nuclear tunnelling makes a large contribution to the electron transfer rate, solvent friction should have a larger effect.[14] They dealt specifically with reactions in the inverted region, where tunnelling is usually important, and derived the equation

$$k_{ET} = \frac{k_{NA}\, k_D}{(k_{NA} + k_D)} \quad . \tag{13}$$

Here k_D depends on the solvent dynamics (it scales as τ_L^{-1}) while k_{NA} is the nonadiabatic electron transfer rate. When tunnelling is unimportant, k_{NA} is equal to k_{TST}, but when tunnelling makes a large contribution,

$$k_{NA} = k_{TST} \exp\left[-\chi \frac{(\lambda + \Delta G^o)^2}{4\lambda k_B T} \right] \tag{14}$$

where λ and ΔG^o have their usual meanings, and χ depends on τ_L and the barrier shape as

$$\chi = (\lambda\, \tau_L)^{-1} \left(\frac{F\, \lambda_T}{(\Delta F)\, (\Delta x)_d} \right)^{3/4} \tag{15}$$

where F is an average restoring force across the potential barrier, λ_T is the thermal deBroglie wavelength, ΔF is the difference in slopes between the product and reactant wells, and $(\Delta x)_d$ is the width over which the nonadiabatic surfaces are coupled.

Calef and Wolynes examined the role of solvent in activated, adiabatic electron transfer reactions using a continuum model for the solvent.[15] Their model considered reactant and product wells as in Marcus theory while the dielectric properties of the solvent were described by a Debye law. They found that the electron transfer rate was strongly influenced by the shape of the barrier. They derived a general equation:

$$k_{ET} = \frac{1}{\tau_L}\left[\frac{1}{2} + \frac{1}{2}\left(1 + \frac{2\tau_{rot}^2}{\tau_L^2 \varepsilon_0 C^2 \gamma}\right)^{1/2}\right]^{-1} \frac{1}{2\pi C} \exp\left[-\frac{\Delta G^{\ddagger}}{k_B T}\right] \tag{16}$$

where τ_L is the longitudinal relaxation time of the solvent, ε_0 is the static dielectric constant, τ_{rot} is the gas phase thermal rotation time of the solvent which depends on the moment of inertia I such that

$$\tau_{rot} = \left(\frac{I}{k_B T}\right)^{1/2}, \tag{17}$$

γ is a factor defined by the dipole moment μ and density ρ as

$$\gamma = \frac{4\pi}{3}\frac{\rho\mu}{k_B T}\frac{1}{\varepsilon_0 - 1}, \tag{18}$$

and C is a factor which depends on the shape of the barrier. For broad, parabolic barriers this factor is defined as:

$$C = \left(\frac{\lambda^2 - (\Delta G^{o})^2}{4\lambda H_{RP}} - 1\right)^{1/2}. \tag{19}$$

For sharp, cusplike barriers the definition

$$C = \frac{1}{2}\left[\left(\frac{k_B T}{\Delta G^{\ddagger}}\right)^{1/2} + \left(\frac{k_B T}{\Delta G^{\ddagger} - \Delta G^{o}}\right)^{1/2}\right] \tag{20}$$

is used instead. The factors $\Delta G^{\ddagger}$, ΔG^{o}, and λ are defined as in Marcus theory (equations 2, 5, and 6). This equation predicts that the rate should depend on τ_L in the overdamped regime, but in the underdamped regime (and especially when $I/k_BT >> \tau_L^2$) the rate will depend instead on the rotational time of the solvent. Calef and Wolynes also derived equations with the solvent structure treated explicitly.[16] The results are quite complex, but the essential dependence of the electron transfer rate on τ_L is retained.

Sumi and Marcus also explored the influence of solvent relaxation on electron transfer reactions.[17] They separated the reaction potential surface into an internal vibrational coordinate *q* and a Debye solvent coordinate X. They found four limiting cases. In the "slow reaction" case, electron transfer is slow compared to solvent motion and the usual Marcus theory holds. In the "wide window" case, rearrangement of the internal coordinate is much greater than solvent rearrangement and the Marcus theory again holds. In the "narrow window" case, the solvent rearrangement is much greater than the internal rearrangement, and there is a tendency towards multi-exponentiality with a strong dependence of the rate on τ_L. Finally, in the "non-diffusing" case, the solvent motion is extremely slow resulting in a distribution of initial conditions in the solvent coordinate and multi-exponential behavior is predicted. Equations which allow for interpolation between these limits were derived. Given an initial equilibrium distribution in the X coordinate, two equations were proposed for the narrow window limit (large solvent rearrangement). When τ_L is large (slow solvent relaxation)

$$k_{ET} = \frac{1}{\tau_L}\left(\frac{\Delta G^{\ddagger}}{\pi k_B T}\right)^{1/2} \exp\left[-\frac{\Delta G^{\ddagger}}{k_B T}\right], \tag{21}$$

and when τ_L is small (fast solvent relaxation)

$$k_{ET} = \frac{\pi}{h}\,|H_{RP}|^2\,(\pi\lambda k_B T)^{-1/2} \exp\left[-\frac{\Delta G^{\ddagger}}{k_B T}\right]. \tag{22}$$

In these equations, $\Delta G^{\ddagger}$ is defined as in equation 2. Numerical calculations using these equations and assuming activated behavior for τ_L such that

$$\tau_L(T) = \tau_L^o \exp\left[\frac{E_L}{k_B T}\right] \tag{23}$$

gave a relatively temperature insensitive rate at high temperatures (small τ_L) which tended to τ_L as the temperature decreased and the value of τ_L increased.

Rips and Jortner have published a series of studies on solvent dynamics and electron transfer. They initially described three cases: nonadiabatic electron transfer (described by standard electron transfer theories), solvent controlled electron transfer (Kramers' high friction limit), and uniform adiabatic electron transfer (transition state theory).[18] They derived this expression to describe electron transfer rates in the nonadiabatic and solvent controlled limits and in the transition region between these limits:

$$k_{ET} = \frac{\frac{2\pi}{h}(H_{RP})^2 (4\pi\lambda k_B T)^{-1/2}}{1 + \frac{4\pi\tau_L}{h\lambda}(H_{RP})^2} \exp\left[-\frac{(\lambda + \Delta G^o)^2}{4\lambda k_B T}\right] . \tag{24}$$

This is essentially the Marcus equation (equation 4) with an added factor of $(1 + \kappa_A)^{-1}$, where κ_A is the adiabaticity parameter, in this case given by

$$\kappa_A = \frac{4\pi\tau_L}{h\lambda}(H_{RP})^2 . \tag{25}$$

When $\kappa_A << 1$, the conventional Marcus nonadiabatic limit holds, but when $\kappa_A >> 1$ solvent controlled electron transfer prevails and equation 24 reduces to

$$k_{ET}(solv) = \frac{1}{\tau_L}\left(\frac{\lambda}{16\pi k_B T}\right)^{1/2} \exp\left[-\frac{(\lambda + \Delta G^o)^2}{4\lambda k_B T}\right] . \tag{26}$$

Equation 24 can be reformulated as in equation 13 or in the reciprocal form

$$\frac{1}{k_{ET}} = \frac{1}{k_{ET}(na)} + \frac{1}{k_{ET}(solv)} \tag{27}$$

with $k_{ET}(solv)$ given by equation 26 and $k_{ET}(na)$, the nonadiabatic rate, by equation 4. Later, Rips and Jortner demonstrated that this equation strictly holds only in the normal region where $\lambda > \Delta G^o$, and gave a more general equation

$$k_{ET} = \frac{k_{NA}}{(1 + \kappa_A F)} \tag{28}$$

where F is a factor which depends on λ and ΔG^o.[19] They gave these approximate relations for F in the different regions:

Normal ($\lambda > \Delta G^o$)
$$F = \left(1 - \left(\frac{\Delta G^o}{\lambda}\right)^2\right)^{-1}$$

Inverted ($\lambda < \Delta G^o$)
$$F = \frac{\lambda}{\Delta G^o}\left(1 - \left(\frac{\lambda}{\Delta G^o}\right)^2\right)^{-1}$$

Activationless ($\lambda = \Delta G^o$)
$$F = \frac{1}{4}\left[1 + \left(\frac{\lambda}{\pi k_B T}\right)^{1/2} \ln 2\right] \tag{29}$$

For low barriers in both the normal and inverted regions, the expression

$$F = \frac{1}{2}\left[\frac{\lambda}{\lambda + \Delta G^o} + \left(\frac{\lambda}{4\pi k_B T}\right)\left(\ln 2 + 1.307\,\frac{(\lambda + G^o)^2}{4\lambda k_B T}\right)\right] \tag{30}$$

was found. Further considerations of the initial conditions for activationless electron transfer showed that the population decay could be non-exponential, especially at short times.[20]

There have not been many studies concerned with the underdamped regime for electron transfer reactions. Skinner and Wolynes considered the underdamped to moderately damped cases for general single and double minimum potentials.[21] The double minimum potential is applicable to electron transfer reactions. Using an impulsive collision model and two symmetric rectangular wells of width *l* with a barrier of height Q and width 2*d* they found a rate such that

$$k = gl \frac{\operatorname{erfc}\left[\left(\frac{Q}{k_B T}\right)^{1/2}\right] \operatorname{erf}\left[\left(\frac{Q}{k_B T}\right)^{1/2}\right]}{l + d \exp\left[-\frac{Q}{k_B T}\right]} \tag{31}$$

where g is an average collision frequency related to friction ζ and mass m as

$$g = \frac{\zeta}{m} \ . \tag{32}$$

Using a Pade´ approximant,[22] they derived an expression to connect the underdamped and overdamped regimes:

$$k = k_{TST} \frac{gT}{1 + \frac{gT}{2} + \frac{(gT)^2}{2\pi}} \ . \tag{33}$$

In the underdamped regime, where g is quite small, this reduces to

$$k = k_{TST} (gT) \ , \tag{33A}$$

and for large g, the overdamped limit, the rate is given by

$$k = k_{TST} \left(\frac{2\pi}{gT}\right) \ . \tag{33B}$$

These expressions give the proper dependence of the rate on friction in both limits. This work was extended by Onuchic and Wolynes, who considered quantum effects as well.[23] When quantum effects are important, they found that the rate is given by

$$k = \frac{P_{LZ} (h\Omega_o)^2}{2\pi^2 h} \frac{(h / t_{coh})}{(h / t_{coh})^2 + \delta E^2} \exp\left[-\frac{E^{\ddagger}}{k_B T}\right] \tag{34}$$

where P_{LZ} is the Landau-Zener probability for transition from reactant to product, Ω_o is the frequency of the quantized vibrational mode, t_{coh} is a coherence time, δE is the energy difference between the two quantum levels involved in the transition, and $E^{\ddagger}$ is the height of the barrier between the product and reactant wells. The matching between the levels can introduce some more complex behavior into the dependence of the rate on friction.

B. Experimental Studies.

1. Biological Electron Transfer.

Historically, theoretical and synthetic efforts toward the understanding of electron transfer reactions have been stimulated by the unusual phenomena observed for electron transfer in biological systems.[1] The photosynthetic systems of green plants and bacteria are among the biological electron transfer systems which have been studied extensively. The photosynthetic apparatus found in bacteria is simpler than that found in green plants, and much of the present understanding of the details of photosynthetic electron transfer come from bacterial studies. The recent success in crystallizing the reaction center protein complex from *Rhodopseudomonas viridis*[24] and *Rhodobacter sphaeroides*[25] has spurred further work in this area. Figure 49 shows the arrangement of the cofactors involved in electron transfer from the crystal structure of *Rps. viridis*.[26] These cofactors consist of four bacteriochlorophylls, two bacteriopheophytins, and two quinones.[27] These pigments are arranged in two branches related by a twofold axis of pseudosymmetry, yet only one branch is functional for electron transfer. The initial event in the electron transfer chain in the reaction center is excitation of the primary donor (D), a dimer composed of two bacteriochlorophyll molecules held face-to-face. In a few picoseconds, the excited dimer transfers an electron to a nearby bacteriopheophytin (ϕ_A).[28] The reduced bacteriopheophytin transfers the electron to the primary quinone acceptor Q_A in 200 picoseconds, and this quinone then transfers the electron to the secondary quinone Q_B in 200 microseconds. The primary donor is reduced by a cytochrome,[29] and the cycle is repeated. The doubly reduced quinone Q_B then diffuses into the cytoplasm to be utilized in driving the cellular metabolism. The kinetics of the electron transfer reactions of bacterial reaction centers are summarized in Figure 50. More details concerning the bacterial photosynthetic reaction center can be found in a number of reviews and compilations.[30]

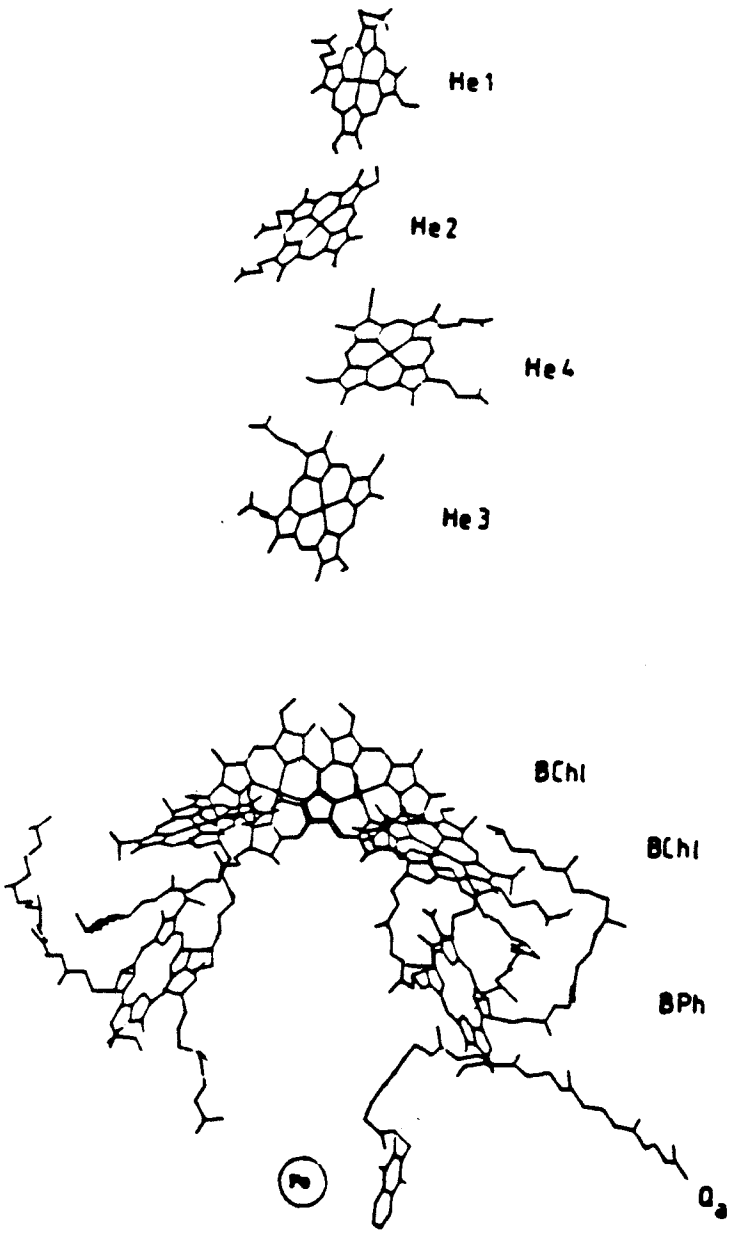

Figure 49. Arrangement of the cofactors in the reaction center protein complex of the photosynthetic bacteria *Rhodopseudomonas viridis*.[24]

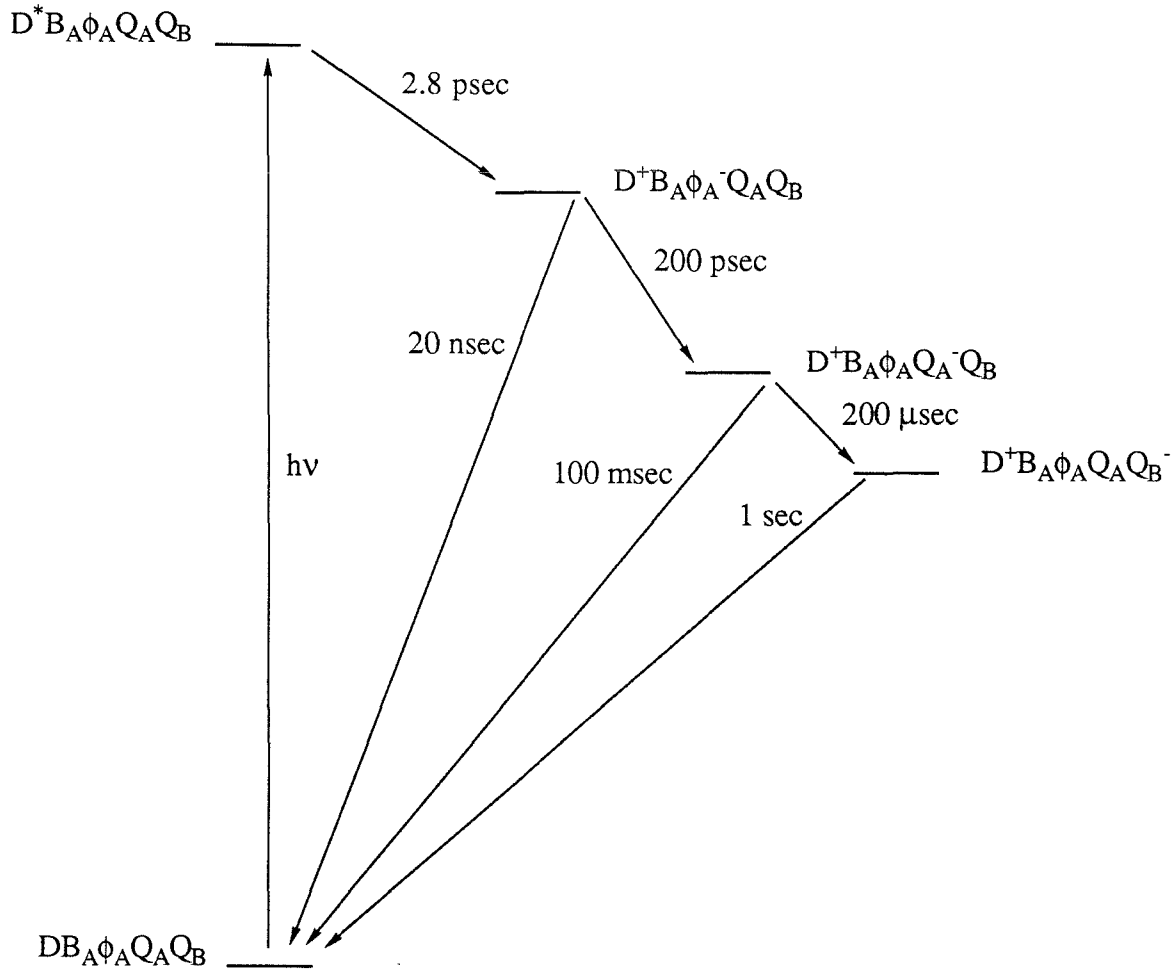

Figure 50. Kinetics of electron transfer events in bacterial photosynthetic reaction centers.[30]

Many of the electron transfer reactions in the bacterial reaction center display unusual temperature dependencies. Among the first examples to be observed was the reduction of the oxidized donor by cytochrome *c* in the bacterium *Chromatium vinosum*.[31] This reaction shows normal activated behavior from 300 to 100 K, but becomes temperature independent below 100 K. The electron transfer from the reduced bacteriopheophytin to the primary quinone is one of several reactions that show negative

activation, that is , the rate increases with decreasing temperature.[32] This reaction also has a different temperature dependence when studied in D_2O rather than H_2O. The negative activation has usually been explained in terms of quantum mechanical electron transfer theory, invoking tunnelling coupled to slow, low energy modes of the protein matrix. These modes should be fully activated at room temperature, and if there is better overlap for tunnelling from the zero level, then an increase in rate with decreasing temperature (increasing zero level population) should be observed. Figure 51 shows the temperature dependence of some photosynthetic electron transfer reactions.

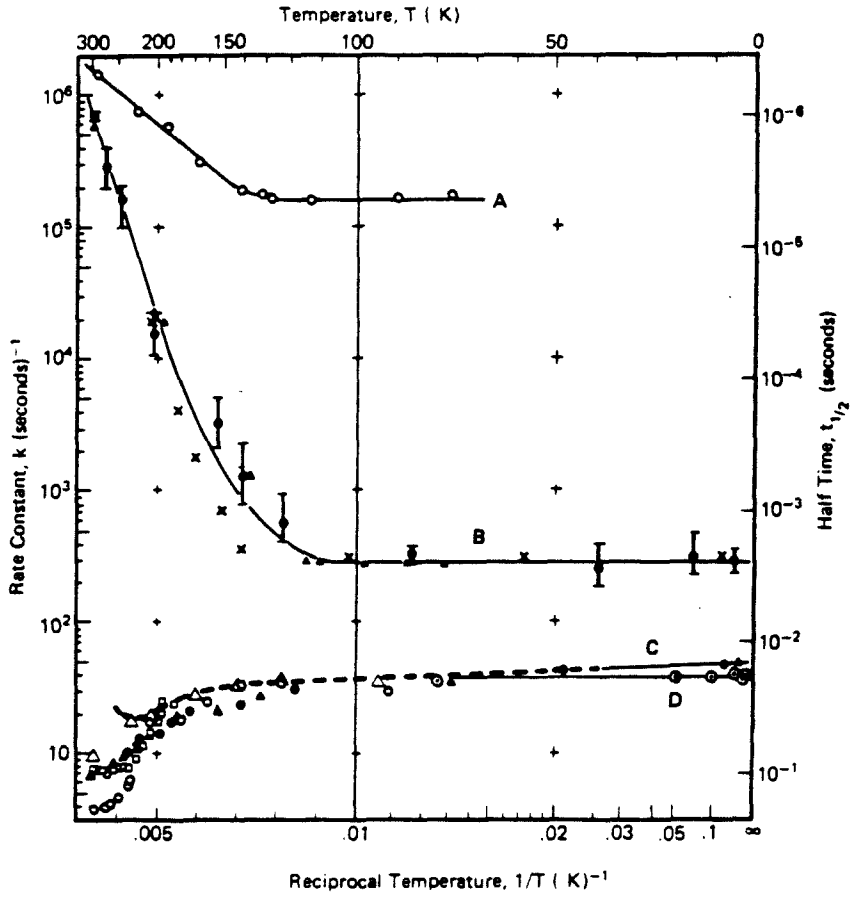

Figure 51. Temperature dependence of electron transfer reactions in bacterial photosynthetic reaction centers. Curve A: Cytochrome oxidation in *R. sphaeroides*. Curve B: Cytochrome oxidation in *C. vinosum*. Curve C: Back transfer in *R. rubrum*. Curve D: Back transfer in *R. sphaeroides*.[1a]

Dutton and co-workers recently performed a study on reaction centers from *Rb. sphaeroides* which is closely related to the experiments reported in the following chapters.[33] The quinones were removed from these reaction centers, and the primary quinone (Q_A) site filled with twenty-two other quinones of varying redox potential. The kinetics of electron transfer from the reduced bacteriopheophytin to the new Q_A (charge

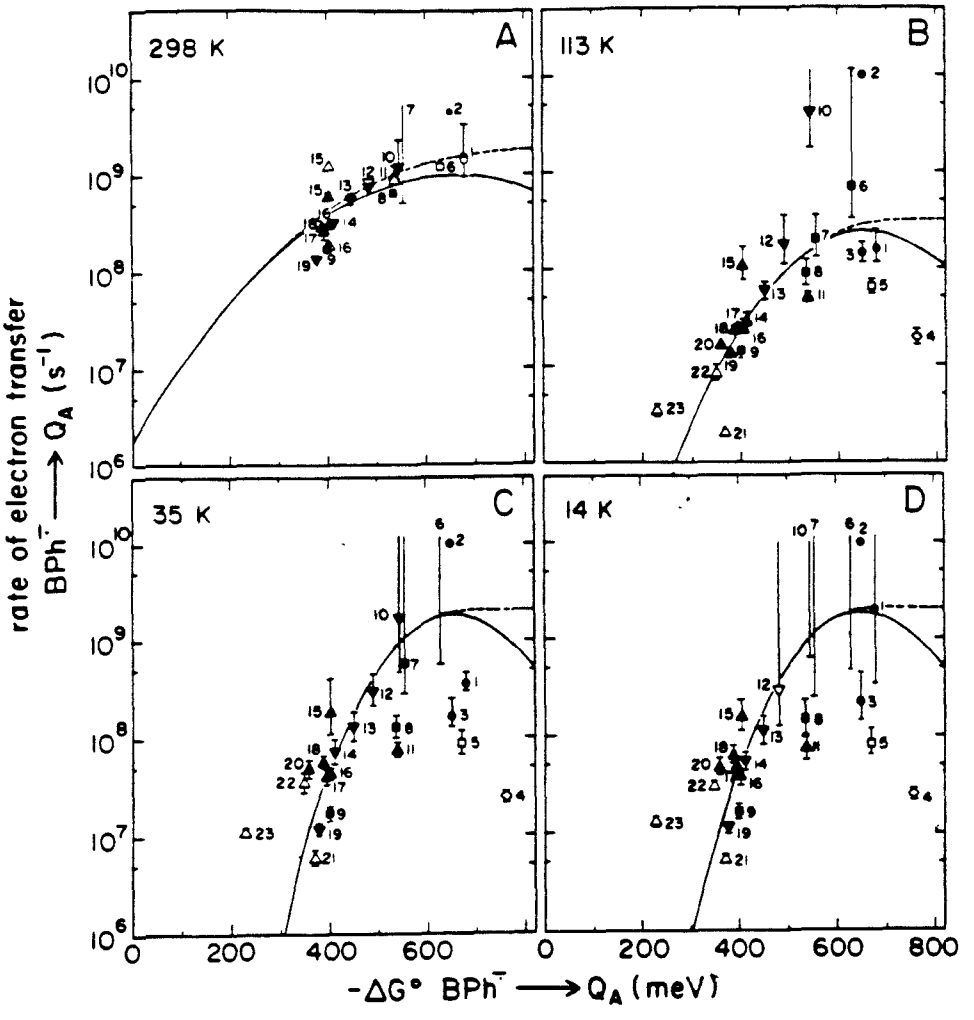

Figure 52. Electron transfer rates for the reaction $\phi_A^- Q_A \rightarrow \phi_A Q_A^-$ in bacterial photosynthetic reaction centers from *R. sphaeroides* with Q_A replaced by various synthetic quinones.[33]

shift) and from Q_A back to the oxidized donor (charge recombination) were measured at various temperatures for these modified reaction centers. This allowed tests of theoretical predictions of the dependence of the electron transfer rate on thermodynamic driving force and temperature to be made. Recall that electron transfer theory predicts a generally quadratic dependence of the rate on driving force with stronger temperature dependence for the slower rates on the legs of the parabola and the possibility of negative activation for the fastest rates. The room temperature results for the charge shift reaction show only increasing rates with driving force, but the low temperature results are basically quadratic. The charge recombination reaction appears to be fairly insensitive to driving force at all temperatures. The temperature dependence of electron transfer does not show a strong correlation with driving force, and many of the low driving force reactions show negative activation. Figure 52 shows the charge shift rates as a function of driving force at four temperatures.

2. Electron Transfer in Synthetic Systems.

There have been a number of experimental efforts to determine the dependence of electron transfer rates on variables such as thermodynamic driving force, distance, and orientation in totally synthetic systems. Many of these studies sought to confirm the predictions of theoretical treatments of electron transfer, especially the Marcus inverted region. The early work of Rehm and Weller was among the first of these studies.[34] They measured the fluorescence quenching of a number of donors and acceptors in solution. For low driving forces, the rates increased with driving force, then reached a plateau. No decline was observed at high driving forces (Figure 53). Bimolecular studies such as this suffer from problems with diffusion limited behavior and with the possibility of pre-association of donors and acceptors at high driving forces.

The most complete experimental evidence for the Marcus inverted region to date is the work of Closs and Miller.[35] In these experiments, pulse radiolysis was used to observe electron transfer from a biphenyl radical anion to a variety of acceptors linked to the donor by a steroid bridge. Since this reaction is unimolecular, the distance between donor and acceptor is a constant, and there is no diffusional component to the reaction. Plotting the electron transfer rate as a function of $-\Delta G^{o}$ gave a nearly parabolic curve (Figure 54). Some recent theoretical work suggests that charge shift reactions such as this are best for observation of both normal and inverted regions, while charge separation reactions tend to fall on the normal side of the curve and charge recombination reactions tend to be inverted.[36]

The most complete study of the distance dependence of intramolecular electron transfer is the work of Paddon-Row and Verhoeven.[37] The rate of electron transfer from a

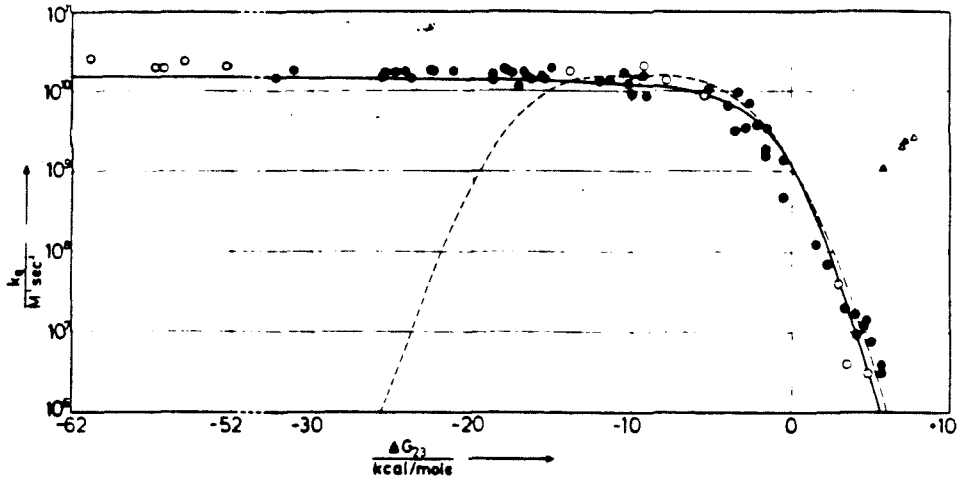

Figure 53. Intramolecular fluorescence quenching of donors and acceptors as a function of thermodynamic driving force.

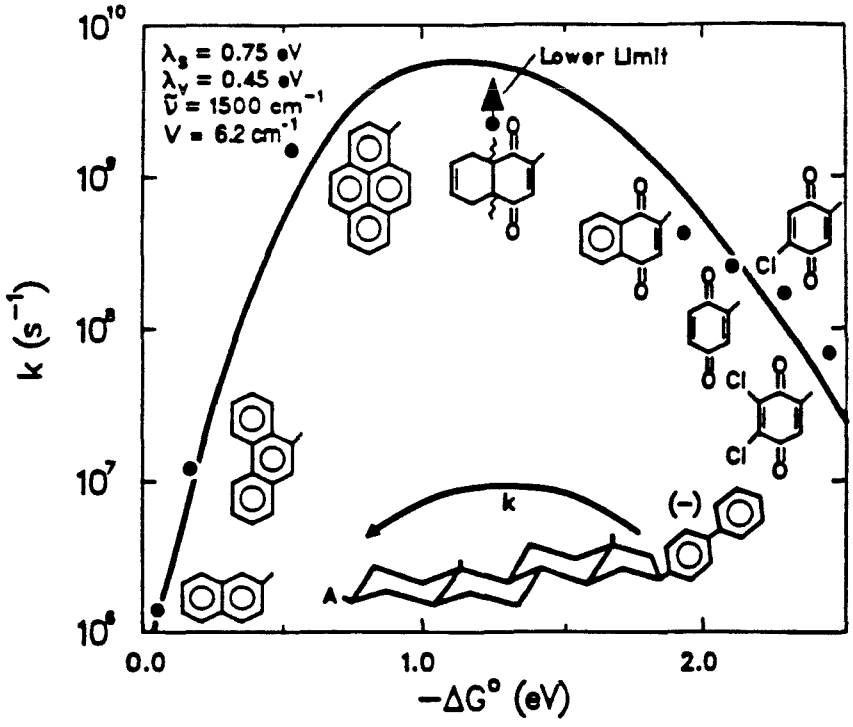

Figure 54. Electron transfer rates as a function of driving force in steroid linked donor-acceptor molecules.

photoexcited dimethoxynaphthalene donor to a dicyanoethylene acceptor linked by a rigid polycyclic hydrocarbon bridge was studied by fluorescence quenching of the donor. The molecules used in this study are shown in Figure 55. For the shortest bridges (edge to edge distance R_e=4.6 and 6.8 Å) electron transfer was so fast that fluorescence was entirely quenched ($k_{ET} > 10^{11}$ sec^{-1}). The electron transfer rates for the longer bridges were measured in a number of solvents. The distance dependence of the electron transfer in ether solvents was found to be

$$k_{ET}(opt) = k_o \exp [-0.85R_e] \qquad (35)$$

where R_e is the edge to edge distance, k_o is 2.5 x 10^{15} sec^{-1} (assumed to be the rate when

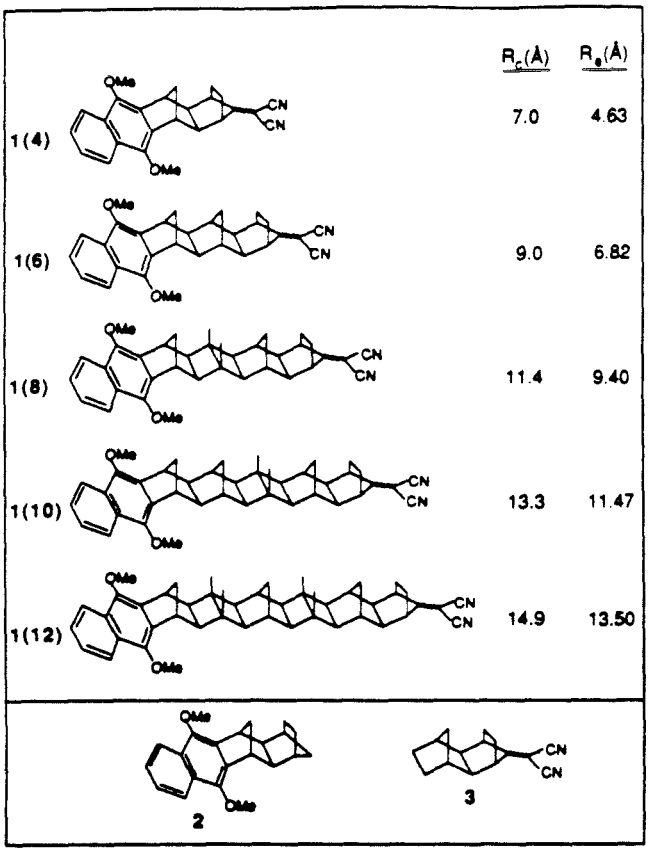

Figure 55. Donor-acceptor molecules used in studies of distance dependence of intramolecular electron transfer.[37]

R_e is zero), and k_{ET}(opt) is the observed rate constant corrected for the distance dependence of the driving force due to separation of charges. The fitted rates are shown in Figure 56. It is interesting to note that the electron transfer rate appears to show a stronger distance dependence in both more polar (acetonitrile) and less polar (cyclohexane) solvents.

In cyclohexane, no fluorescence quenching was observed for the two longest distances (R_e = 11.47 and 13.50 Å) signifying very slow electron transfer rates ($k_{ET} < 10^7$ sec^{-1}).

There have been a numbe. of reports of experiments designed to explore the theoretically predicted dependence of electron transfer on solvent dynamics. Most have focussed on systems with a significant geometry change between the neutral and charge

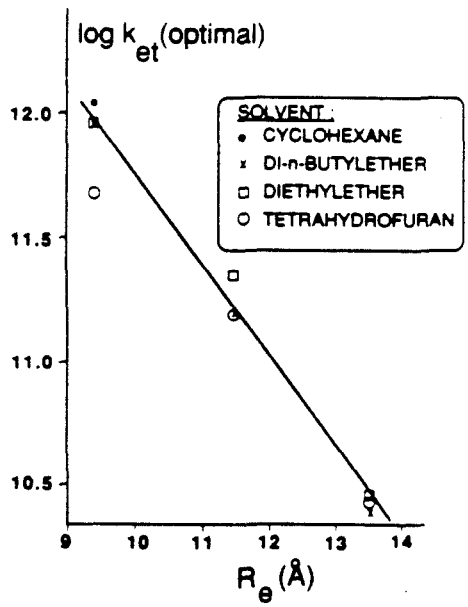

Figure 56. Distance dependence of intamolecular electron transfer rates for molecules from Figure 55 in several solvents.[37]

separated states in alcohol solvents. Kosower's group has studied the electron transfer dynamics in molecules with a twisted intramolecular charge transfer (TICT) state such as 6-N-4-methylphenylamino-2-naphthalenesulfonic acid N,N-dimethylamide (TNSDMA). A temperature study in propanol showed that the changes in the electron transfer rates

correlated with the dielectric relaxation times or with the viscosity, as shown in Figure 57.[38] A study in a number of *n*-alkanols (methanol to decanol) showed a nearly linear correlation of the fluorescence lifetime with τ_L (Figure 58).[39] Simon and Su found a similar relationship between τ_{ET} (k_{ET}^{-1}) and τ_L in bis-(4-dimethyl-aminophenyl)sulfone, which also has a TICT state.[40] Barbara's group has shown that the relevant relaxation time may not be τ_L (which is based on dielectric continuum theory),[41] but rather an experimentally measured solvation time τ_S.[42] They determined this latter relaxation time by measuring the time dependent shift in the λ_{max} of fluorescence spectra in the various

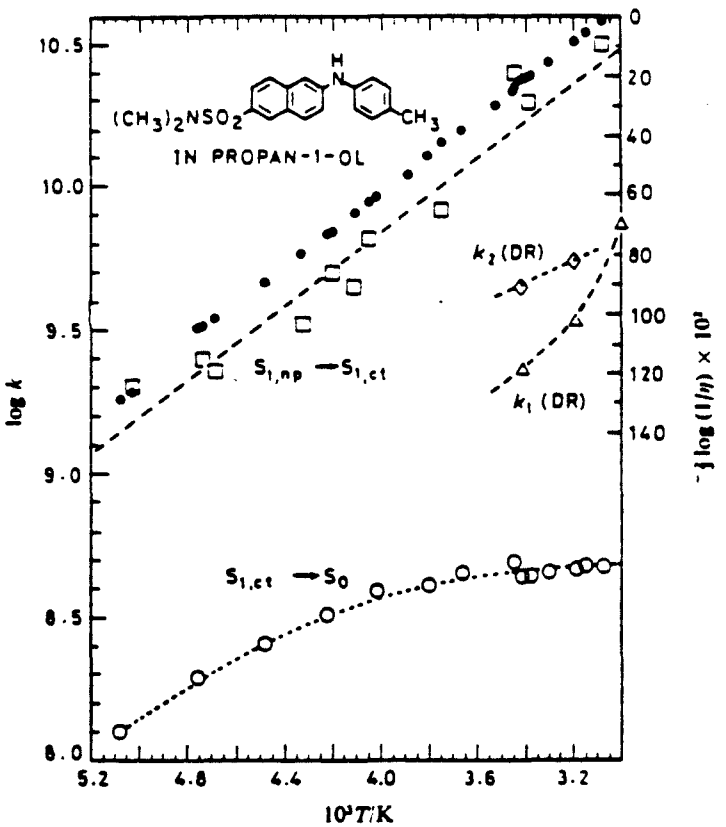

Figure 57. Semilogarithmic plot of electron transfer rate constants (open squares and open circles) for TNSDMA in 1-propanol and the function 2/3 log (1/η) (solid circles).[38]

solvents. Experiments by Heitele, Michel-Beyerle, and Finckh measured electron transfer rates as a function of temperature for a dimethylaniline donor linked to an anthracence acceptor in propionitrile and propylene glycol.[43] The rates in propylene glycol were non-Arrhenius and strongly dependent on temperature, while the rates in propionitrile were only weakly temperature dependent. Weaver's group has used electrochemical techniques to determine the role of solvent dynamics in electron exchange reactions.[44]

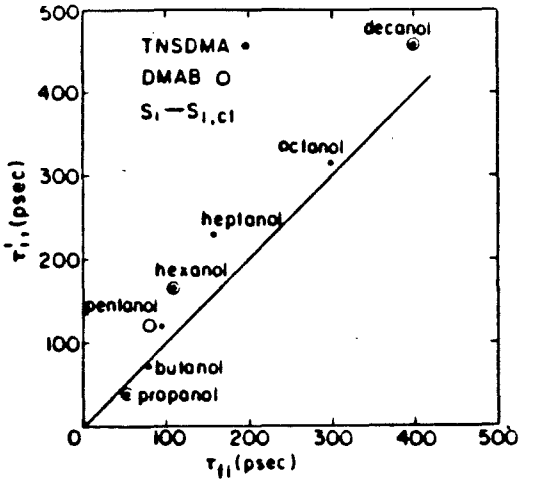

Figure 58. Plot of corrected longest dielectric relaxation times for linear alcohols τ_l' vs. the fluorescence lifetimes τ_{fl} for TNSDMA and N,N-dimethylaminobenzonitrile DMAB.[39]

3. Previous Studies on Rigid Porphyrin-Quinone Compounds.

The experiments of Joran[45] and Leland[46] (which this work continues) are unique in being the only study where electron transfer within one molecular framework has been studied as a function of more than one variable. A photoexcited zinc(II) porphyrin was employed as the donor with a quinone acceptor, as in the bacterial reaction center. To provide strict control of the donor-acceptor distance, a rigid linker consisting of a phenyl ring and a number of bicyclo[2.2.2]octane units was used as a bridge. Electron transfer rates were measured by time-resolved fluorescence quenching. In the absence of an electron acceptor, the excited porphyrin chromophore is deactivated by intersystem crossing, internal conversion, and fluorescence; and fluoresces with a lifetime τ_o, where

$$\tau_o = \frac{1}{k_{rad} + k_{ic} + k_{isc}} \quad . \tag{36}$$

In the presence of an acceptor, the singlet excited state is also deactivated by electron transfer and the observed fluorescence lifetime is τ, where

$$\tau_o = \frac{1}{k_{rad} + k_{ic} + k_{isc} + k_{ET}} \quad . \tag{37}$$

The electron transfer rate can then be calculated as

$$k_{ET} = \frac{1}{\tau} - \frac{1}{\tau_0} \quad . \tag{38}$$

The photophysics of the electron transfer active compounds are shown in Figure 59. The lifetimes of the compounds were measured using time-correlated single photon counting techniques on the picosecond time scale.

The first experiments on these porphyrin-quinone compounds sought to establish the distance dependence of the electron transfer rate.[47] The fluorescence lifetimes of three derivatives with zero, one, and two bicyclo[2.2.2]octane spacers (ZnP0Q **1**, ZnPLQ **2**, and ZnP2LQ **3**) were measured, along with the lifetime of a porphyrin with no quinone

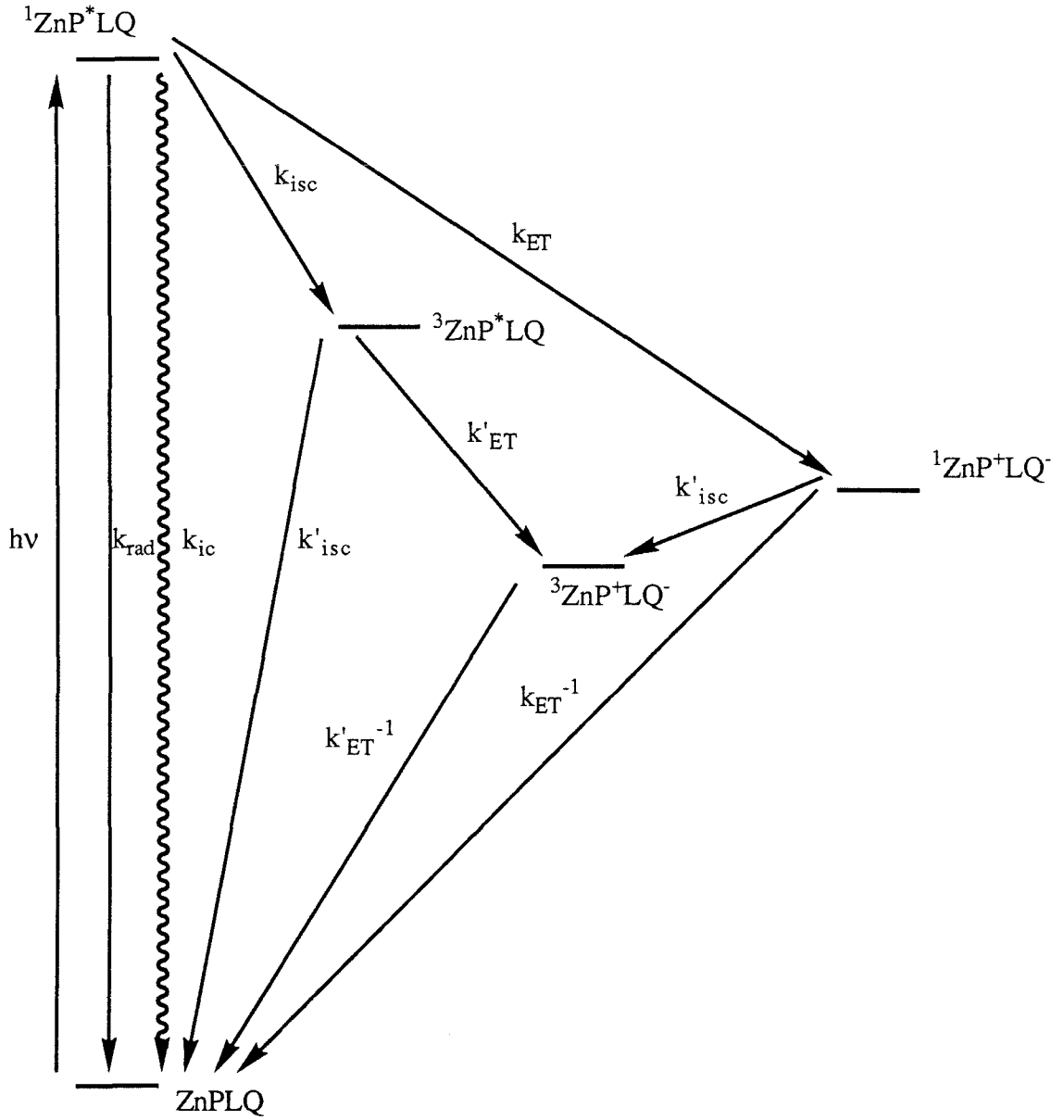

Figure 59. Jablonski diagram showing the photophysics of porphyrin-quinone compounds such as ZnPLQ **2**.

acceptor (ZnP-*t*-Bu **4**) as the reference lifetime τ_0 (Figure 60). The fluorescence of ZnP0Q **1** was highly quenched in intensity, but the observed fluorescence lifetime was identical to that of the reference porphyrin ZnP-*t*-Bu **4**. This observed fluorescence was attributed to a small fraction of molecules with reduced quinone acceptors (hydroquinone form), where electron transfer is energetically impossible. Since no shortened fluorescence lifetime was observed, only a lower limit of ~10^{11} sec^{-1} to the electron transfer rate could be established based on the time resolution of the apparatus used in the measurement. The observed fluorescence decay from ZnPLQ **2** was biexponential, giving one lifetime quite similar to ZnP-*t*-Bu **4** and one shortened lifetime. The long component was responsible for <5% of the observed fluorescence, and again was attributed to molecules with reduced acceptors. The short component was considered to be the quenched lifetime τ. The electron transfer rate was measured in this way for ZnPLQ **2** in a number of different solvents of varying polarity, from benzene to dimethylformamide (DMF). The rates were slower in more polar solvents, and were initially reported as ranging from 3.7 x 10^9 sec^{-1} in DMF to 1.25 x 10^{10} sec^{-1} in benzene. More recent measurements have shown these rates to be incorrect. New rate data is not available for all of the solvents used in the original study, but the correct rates range from 1.3 x 10^9 sec^{-1} in acetonitrile to 3.0 x 10^9 sec^{-1} in benzene. These revised rates have been checked by performing the lifetime measurements on three different laser systems and by establishing the purity and correctness of the compounds by analytical techniques. The problem with the original measurements may have been the result of an incorrect calibration of the time-correlated single photon counting apparatus or of impurities in the samples (strong ligands such as pyridine can cause large changes in the electron transfer rate). The observation that the reported lifetimes are always shorter by a factor of ~3 suggests that calibration may have been the source of the error. The fluorescence of ZnP2LQ **3** was not quenched within

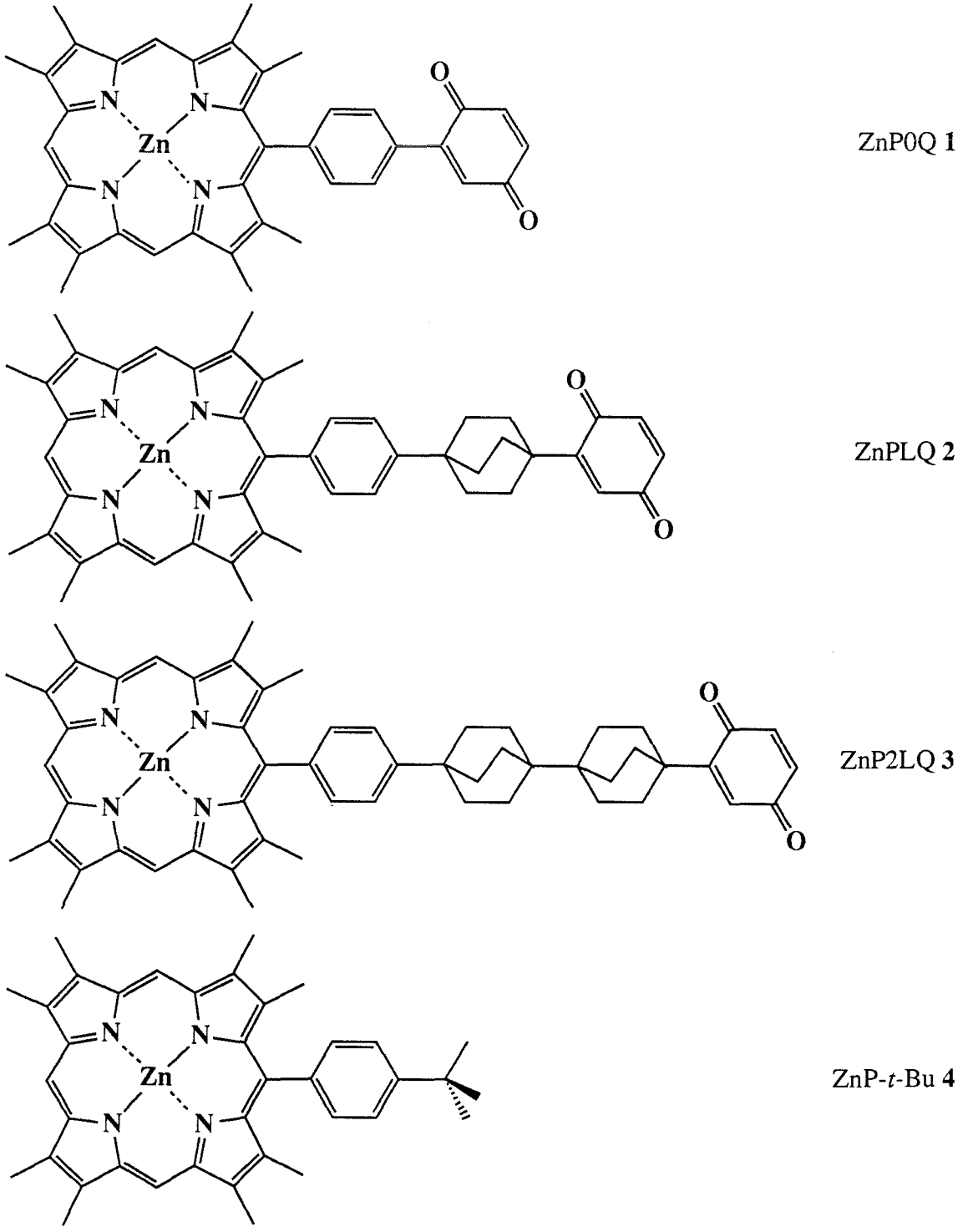

Figure 60. Porphyrin-quinone compounds **1-4**.

experimental error, nor was the lifetime observed to be shortened. This indicates that electron transfer is slow compared to other deactivation processes of the excited porphyrin.[48] An upper limit of 10^7 sec^{-1} can be established for the electron transfer rate in this compound. Further attempts to establish a rate in this compound by using platinum rather than zinc derivatives (platinum porphyrins phosphoresce rather than fluoresce, and the emission lifetime is in the μsec rather than the nsec regime)[49] were also unsuccessful in observing quenching. For the zinc derivatives, a lower limit for the distance dependence could be established from the one known rate and the two limiting values. If the rate depends exponentially on distance as

$$k_{ET} = k_o \exp [-\alpha R_e] \quad , \tag{39}$$

then α is 1.15 $Å^{-1}$ for a k_o of 1.4 x 10^{14} in benzene. The distance dependence may be stronger than this (that is, α is larger), although this value of α is slightly larger than those found by Verhoeven and Paddon-Row.[37]

Adding substituents to the quinone acceptor varies the thermodynamic driving force of the electron transfer reaction. Seven ZnPLQ derivatives with a 570 mV range of driving forces (Figure 61) were synthesized to investigate the rate as a function of ΔG^o.[50] The measured electron transfer rates for these compounds increased with increasing driving force up to the last point, which was slower than the fastest rates. Fits of the rate data to the Marcus equation (equation 4) gave values of near 6 cm^{-1} for H_{RP}, with λ varying from 1.32 eV for acetonitrile to 1.02 eV for benzene (Figure 62). Note that these fits were made with incorrect rates for the unsubstituted compound. This is the best evidence for inverted region behavior in a charge separation reaction. Several of these compounds were also studied in a 2-methyltetrahydrofuran (2MTHF) glass at 77 K.[45-47] The fluorescence decays were non-exponential, but could be fit to a distribution of ten exponentials designed to simulate the dependence of H_{RP} on the angle between the porphyrin and quinone

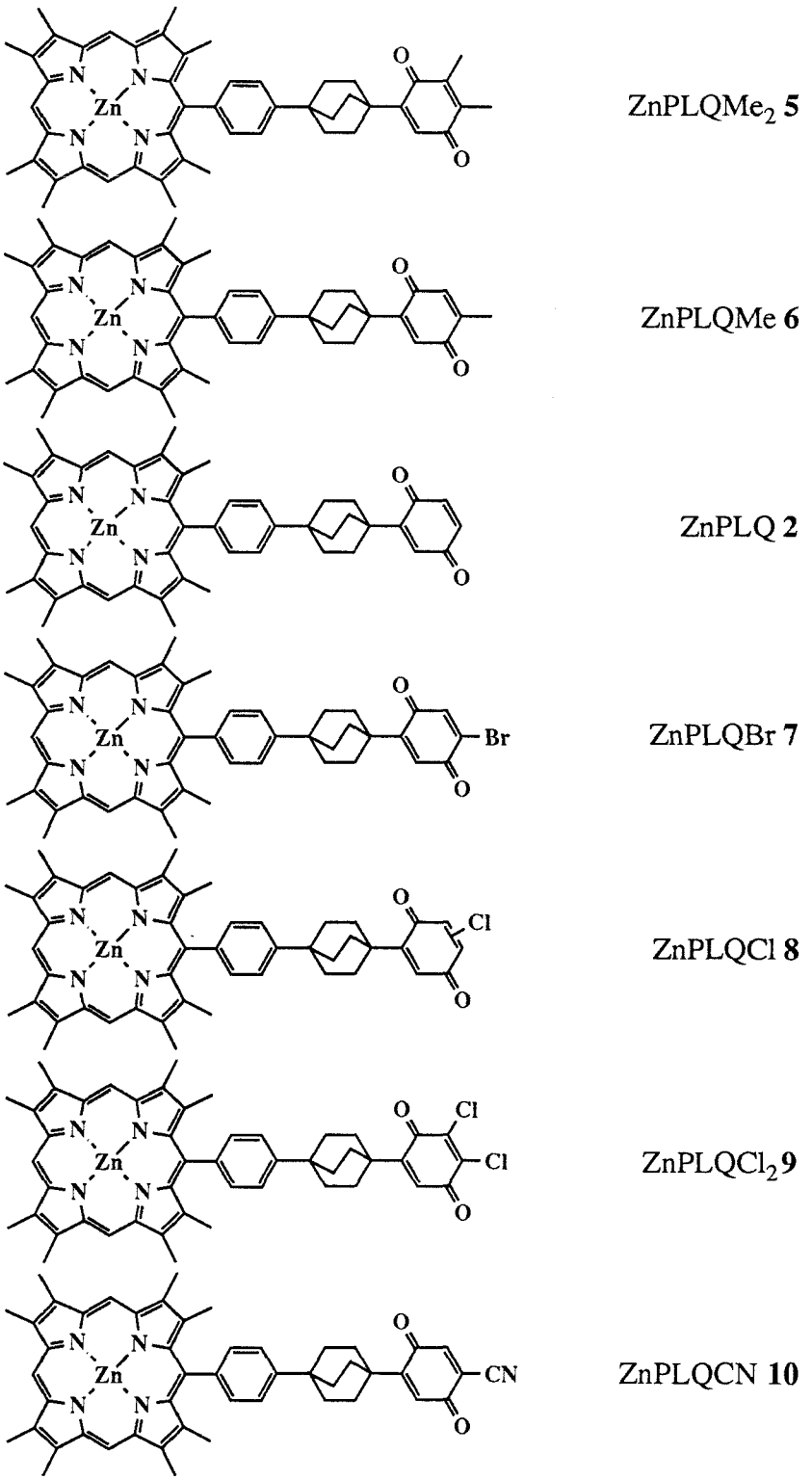

Figure 61. Porphyrin-quinone compounds used in driving force dependence study.

planes.[51] The fastest rates were not much different from those measured at room temperature. This "angle modulated" fit is probably not very accurate in describing the actual conformers of the porphyrin-quinone molecule, since molecular mechanics calculations predict that there should be only two non-equivalent conformers, yet it might

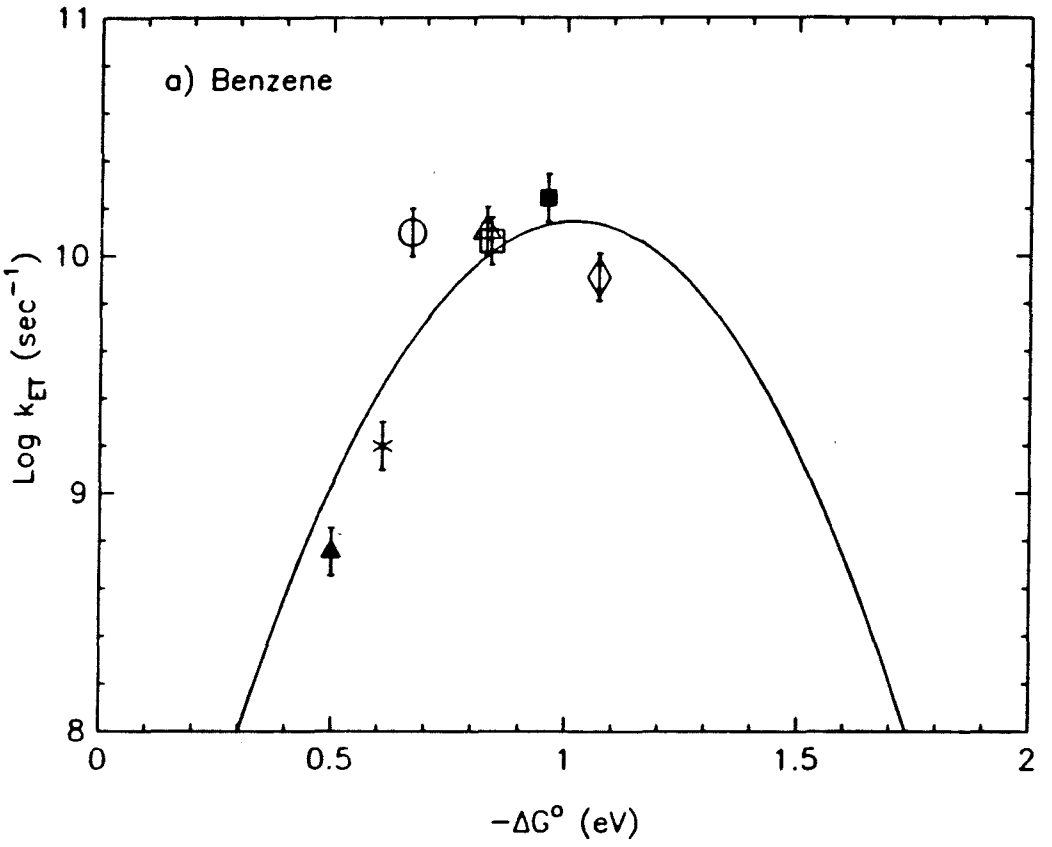

Figure 62. Semilogarithmic plot of electron transfer rates versus driving force for porphyrin-quinone compounds in Figure 61 in benzene. Solid line is least squares fit to equation 4.[46] Note that the rate represented by the open circle is incorrect and should be slower (log k_{ET} = 9.48:see text).

be a reasonable model for the distribution of rates predicted by Sumi and Marcus for the "non-diffusing" case.[17]

In the next two chapters, further studies of these porphyrin-quinone molecules are described. The distance (or orientation) dependence is further addressed by the synthesis of a new porphyrin-quinone derivative. The temperature dependence for this new molecule and the three lowest driving force members of the driving force series is also investigated in detail.

Chapter 7

Distance Dependence of Electron Transfer

The results obtained from the porphyrin-quinone molecules with zero, one, and two bicyclo[2.2.2]octane spacer units gave a limiting value to the distance dependence of the electron transfer rate. To further investigate the distance dependence, and also to investigate orientation effects on electron transfer rates, a modified porphyrin-quinone molecule, ZnPmLQ **11**, was synthesized. This molecule also has one bicyclo-[2.2.2]octane spacer unit, but it is attached *meta* (rather than *para*) to the porphyrin on the linking phenyl group. This modification has the advantage of potentially addressing several issues concerning electron transfer apart form the distance dependence. Since the porphyrin and quinone planes are skew, they cannot become coplanar. This relative orientation might not have good overlap of the two interacting wavefunctions, leading to a smaller matrix element, and therefore a slower electron transfer rate.[7] Furthermore, the difference in distance is significantly different depending on whether the electron transfer is through space or through the bonding framework. If electron transfer is through space, the rate should change dramatically, but only slightly for a through bond mechanism. Furthermore, if the π system of the phenyl ring is part of the electron transfer pathway, then the estimated matrix element should be considerably smaller for the *meta* linked compound.[52]

A. Synthesis.

The synthesis of ZnPmLQ **11** was accomplished in fourteen steps using a modification of the route utilized by Joran in the synthesis of ZnPLQ **2**, and is shown in scheme 19. Addition of methyl acrylate to 3-methylbenzylcyanide gives diester **12**, which can be cyclized to cyclohexanone **13** with sodium hydride. Decarbomethoxylation to **14**,

Scheme 19. Synthesis of ZnPmLQ **11**.

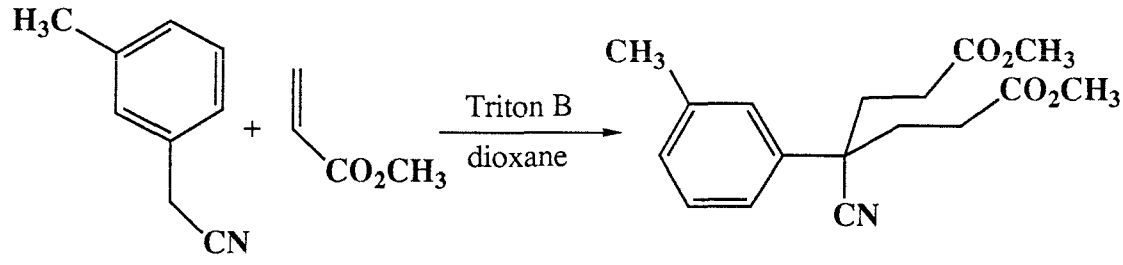

12

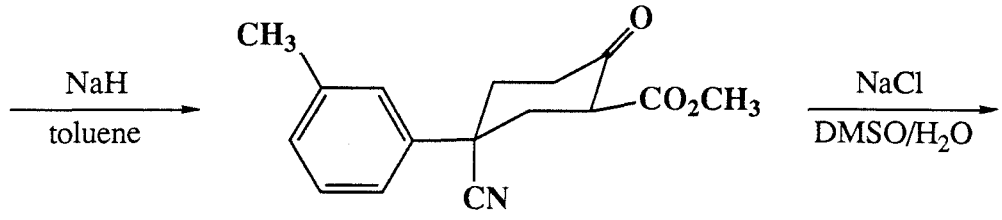

13

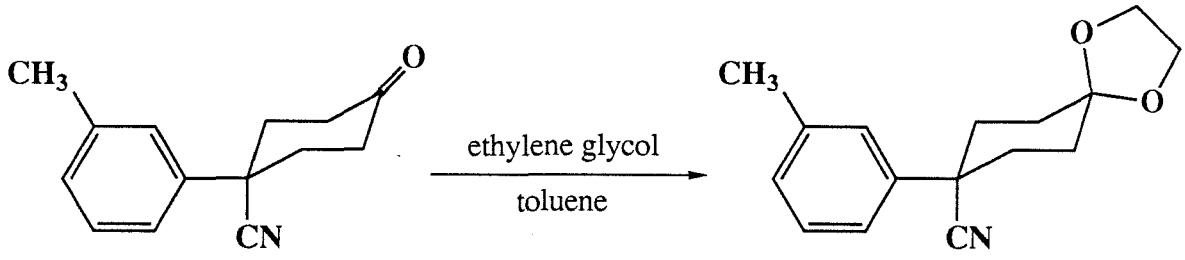

14 **15**

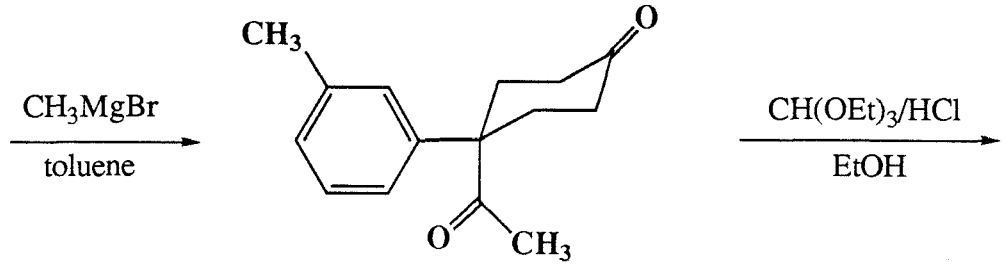

16

Scheme 19. (continued)

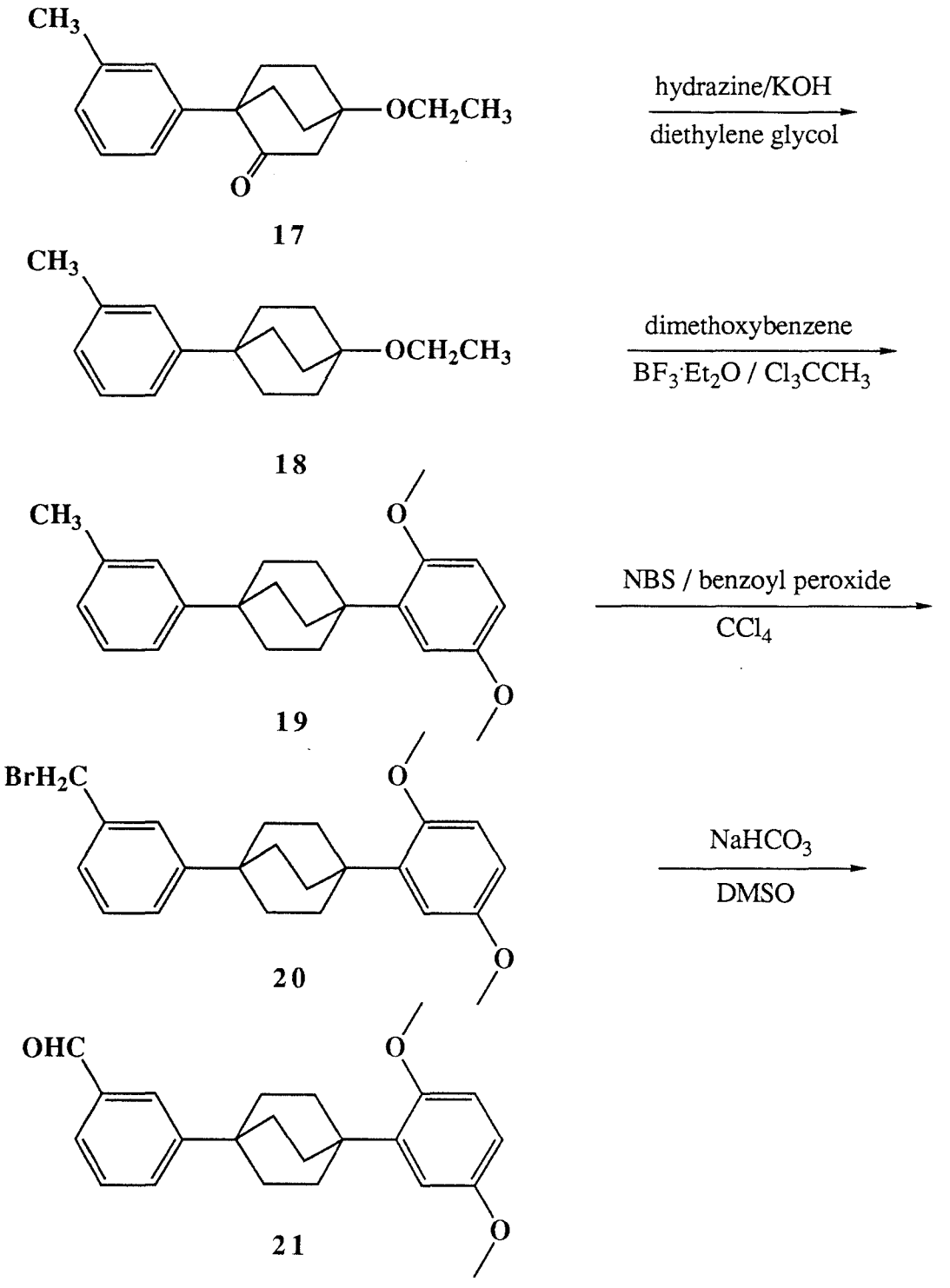

Scheme 19. (continued)

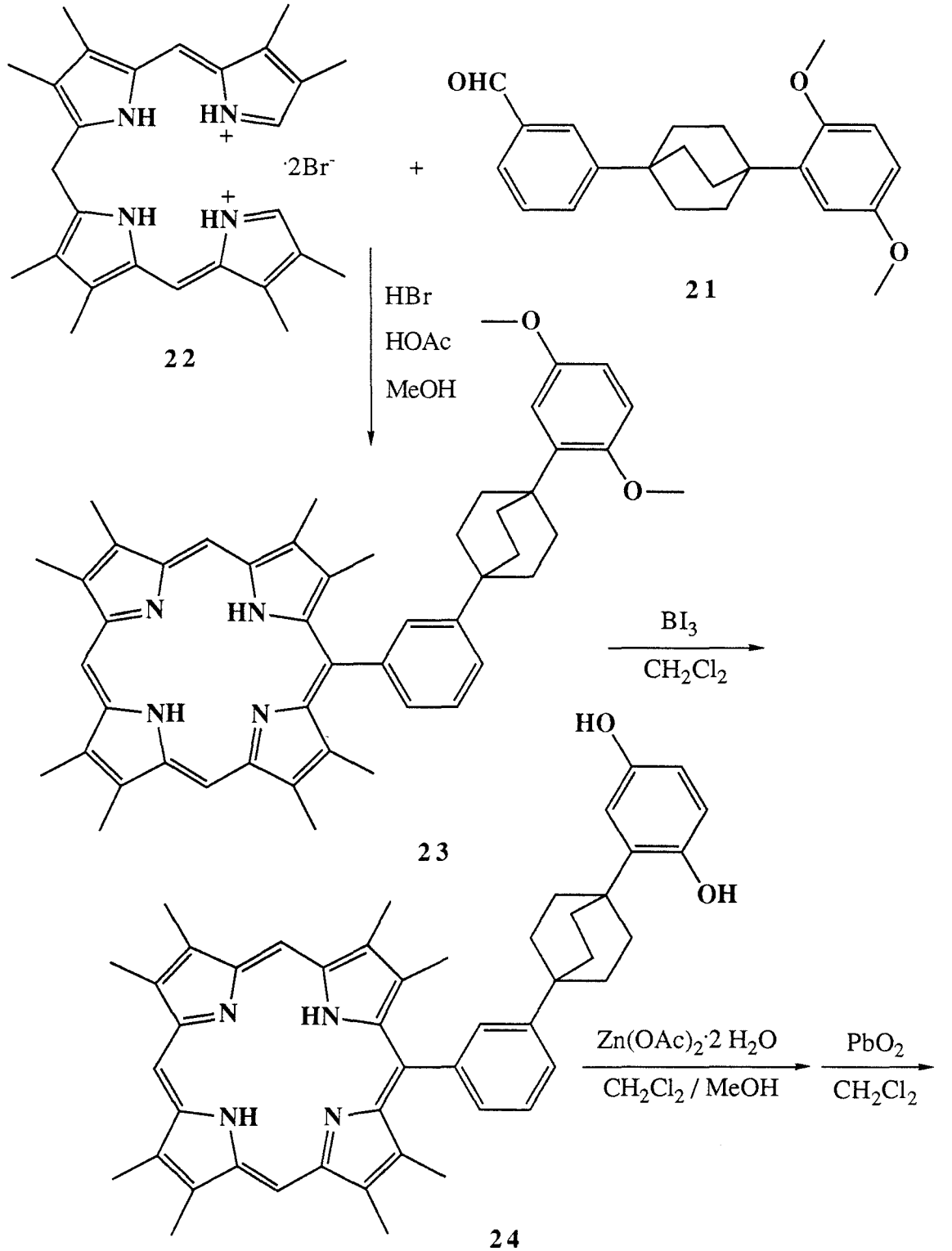

Scheme 19. (continued)

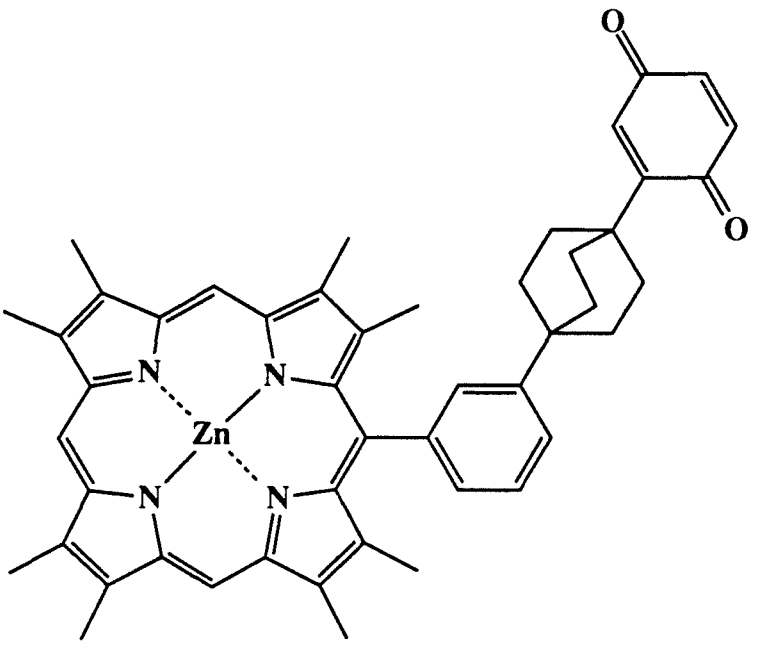

11

protection of the ketone as ketal **15**, and reaction with methylmagnesium bromide gives acetylcyclohexanone **16**. Bicyclo[2.2.2]octanone **17** is produced by acid cyclization of **16**, and Wolff-Kishner reduction gives bicyclo[2.2.2]octane **18**. Reaction with dimethoxybenzene under Friedel-Crafts conditions gives diphenylbicyclo[2.2.2]octane **19**. Treatment with N-bromosuccinimide gives benzylbromide **20**, which is transformed to the target aldehyde **21** with sodium bicarbonate. Condensation of this aldehyde with a,c-biladiene hydrobromide **22**[45] gives the protected free base porphyrin H_2PmLDMB **23**. Demethylation with boron tri-iodide generates porphyrin-hydroquinone H_2PmLQH_2 **24**. The final product, metalloporphyrin ZnPmLQ **11**, is produced by metallation of **24** with zinc acetate followed by oxidation with lead (IV) oxide. The porphyrin compounds were

purified by chromatography and characterized by UV-Vis, NMR, and mass spectra. The electronic absorption spectrum of ZnPmLQ **11** is shown in Figure 63.

B. Electron Transfer Rates.

Electron transfer rates in ZnPmLQ **11** were measured by the time-resolved fluorescence quenching technique used earlier for porphyrin-quinone molecules **1-10**. The photophysical diagram shown for ZnPLQ **2** in Figure 59 is also applicable to ZnPmLQ **11**. Fluorescence decays at 630 nm were collected on a picosecond laser system[53] set up for time-correlated single photon counting.[54] The detection wavelength was at the second maximum in the porphyrin emission spectrum for ZnPmLQ **11**, as shown in Figure 64. That this emission was due to the porphyrin chromophore was established by the fluorescence excitation spectrum, shown in Figure 65. Fluorescence decays were measured in four solvents: benzene, toluene, 2MTHF, and acetonitrile. Room temperature decays are shown in Figures 66-69. The decays fit to the sum of two exponentials. The long-lived minor component had a fluorescence lifetime similar to that of reference porphyrin ZnP-*t*-Bu **4** and was attributed to a fraction of the sample with reduced quinone acceptors. The fitted lifetimes (τ) and calculated electron transfer rates (using equation 38) for ZnPmLQ **11** and ZnPLQ **2** are listed in Table XXII. The rates for ZnPmLQ **11** are slightly faster than those for ZnPLQ **2** in each solvent.

The *through bond* edge to edge donor-acceptor distances (R_e) in ZnPLQ **2** and ZnPmLQ **11** were measured as 9.9 and 9.3 Å respectively, using Dreiding models. The *through space* distance (R_s) for ZnPmLQ **11** is measured as 8.5 Å. (For ZnPLQ **2**, R_e and R_s are necessarily equal.) The zero and two linker compounds ZnP0Q **1** and ZnP2LQ **3**, for which only limiting values of the electron transfer rate can be determined, measure 5.8 and 14.0 Å for R_e respectively. Semilogarithmic plots of the electron transfer rates (or the limiting values to those rates) vs. R_e for these four compounds in the different solvents are

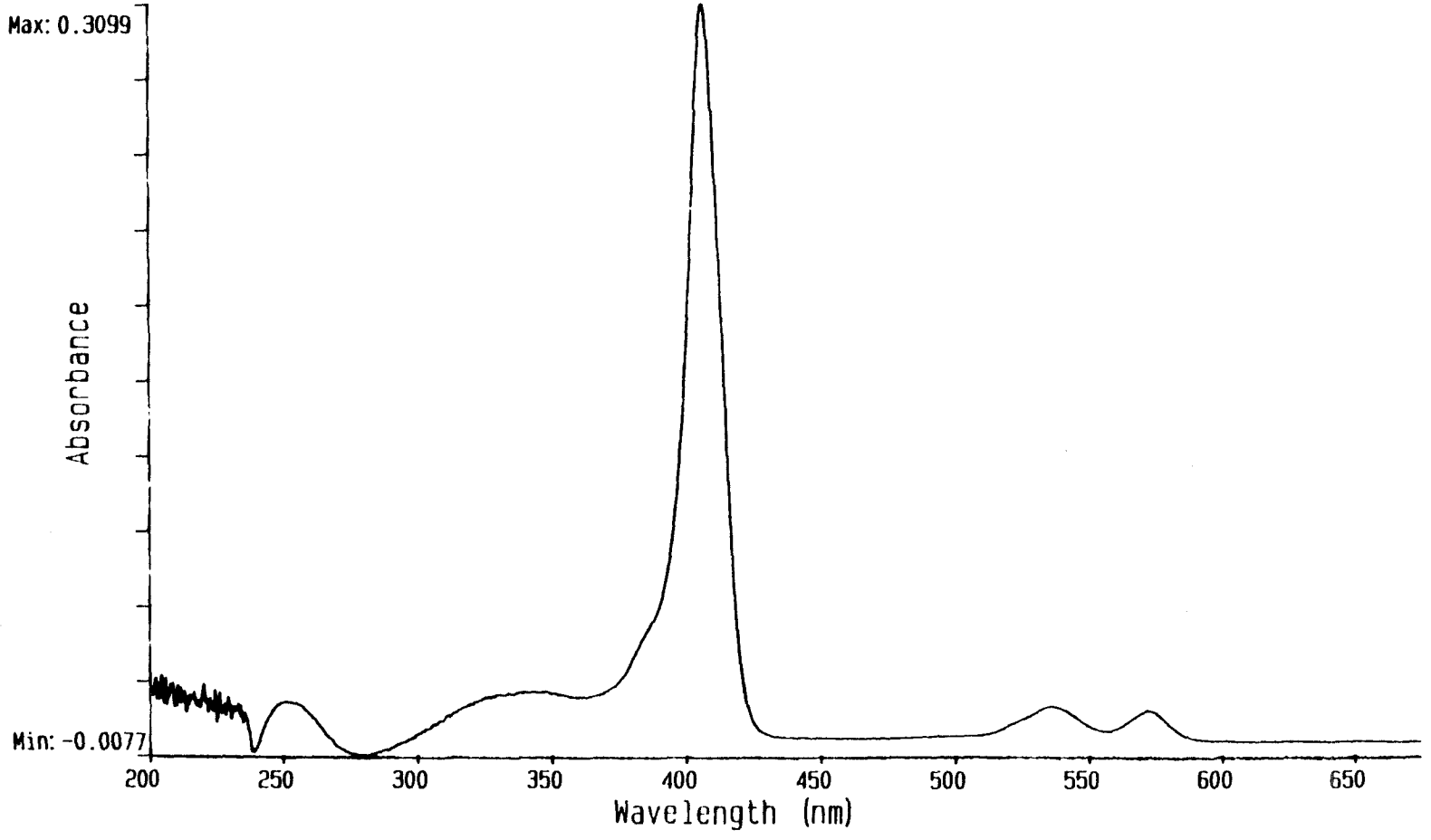

Figure 63. Electronic spectrum of porphyrin quinone molecule ZnPmLQ **11** (CH_2Cl_2).

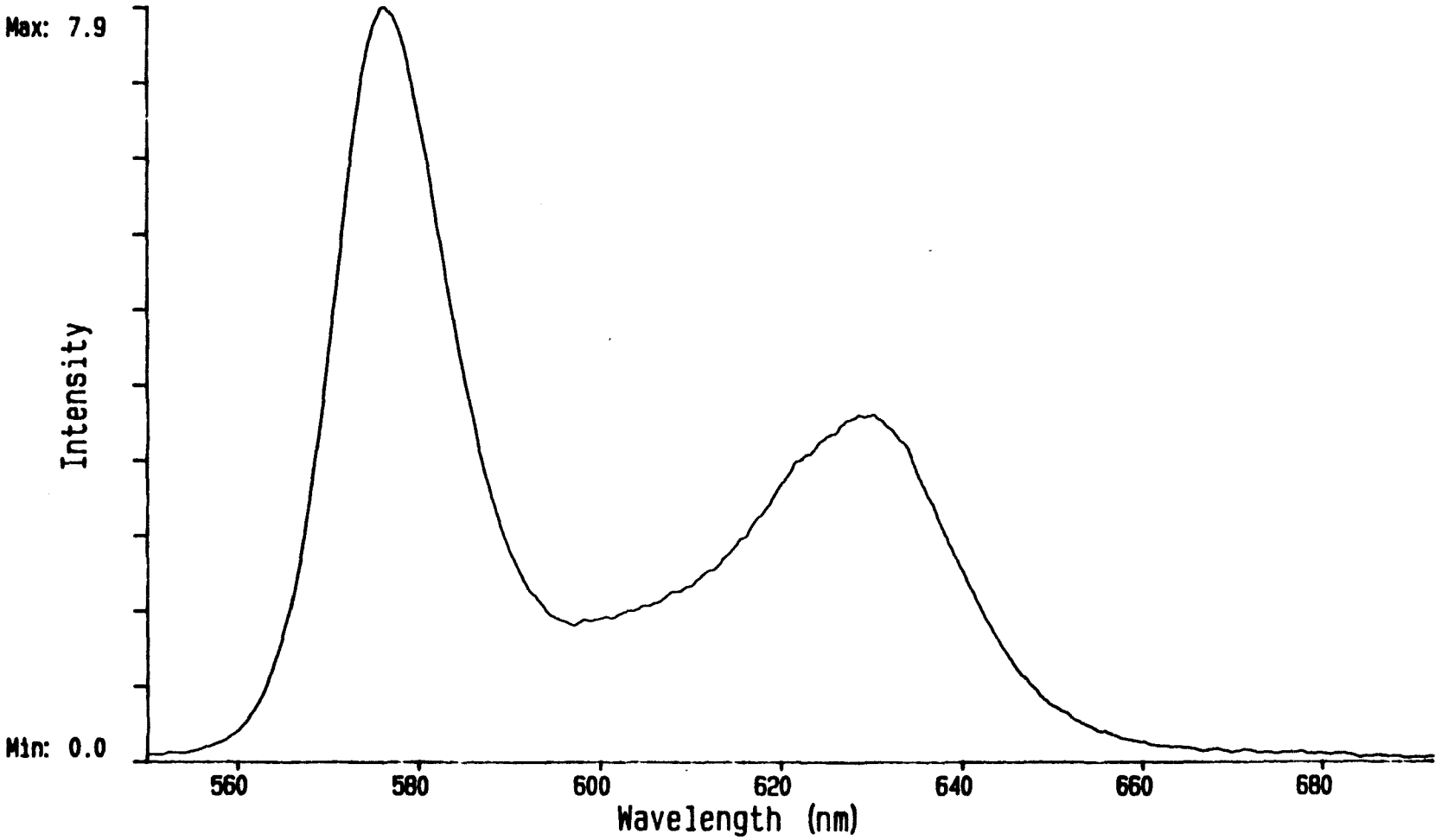

Figure 64. Emission spectrum of porphyrin-quinone compound ZnPmLQ **11** (benzene, excitation at 404 nm).

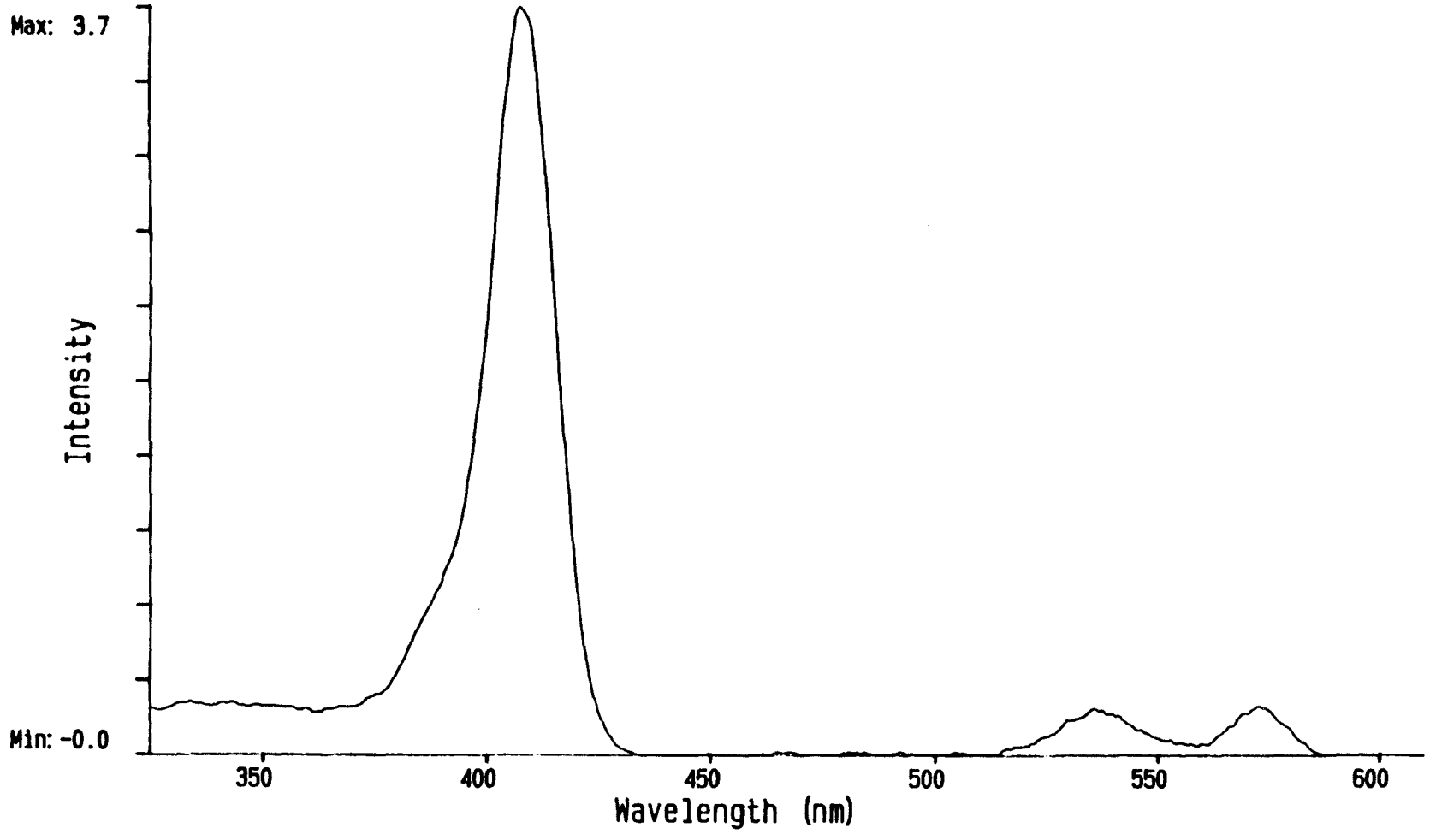

Figure 65. Fluorescence excitation spectrum of porphyrin-quinone compound ZnPmLQ **11** (benzene, detect at 632 nm).

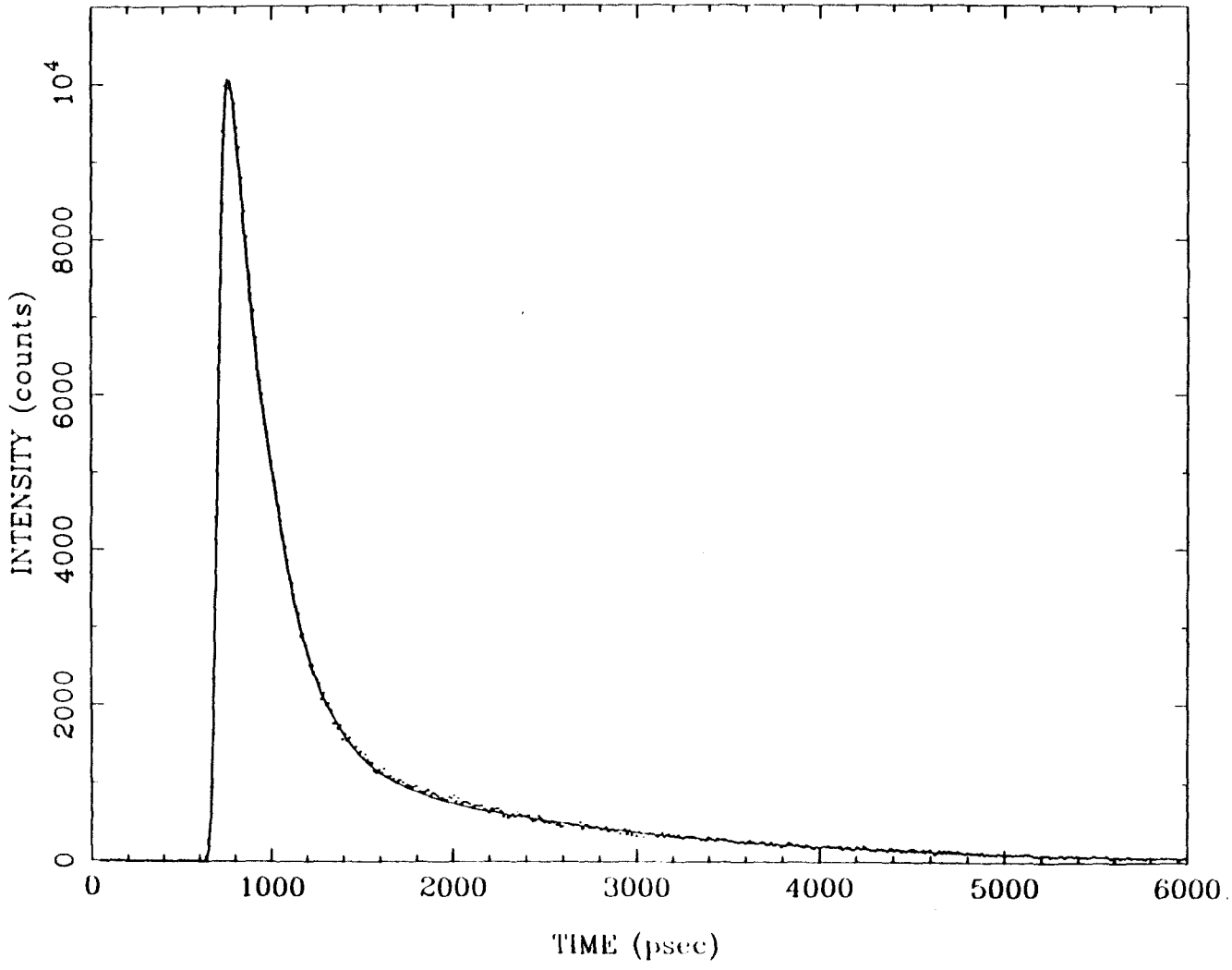

Figure 66. Fluorescence decay of porphyrin-quinone compound ZnPmLQ **11** in benzene with biexponential fit (solid line).

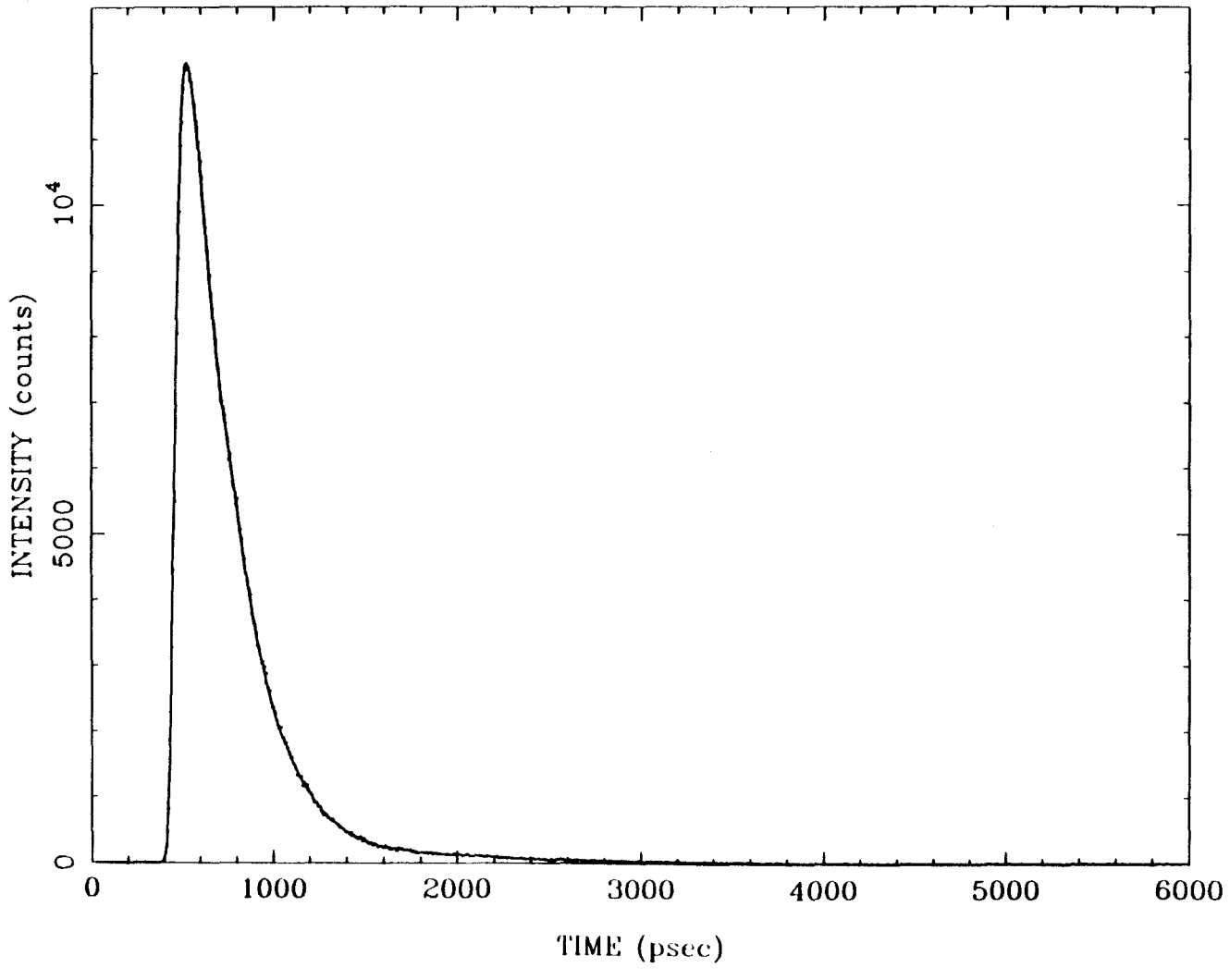

Figure 67. Fluorescence decay of porphyrin-quinone compound ZnPmLQ **11** in toluene with biexponential fit (solid line).

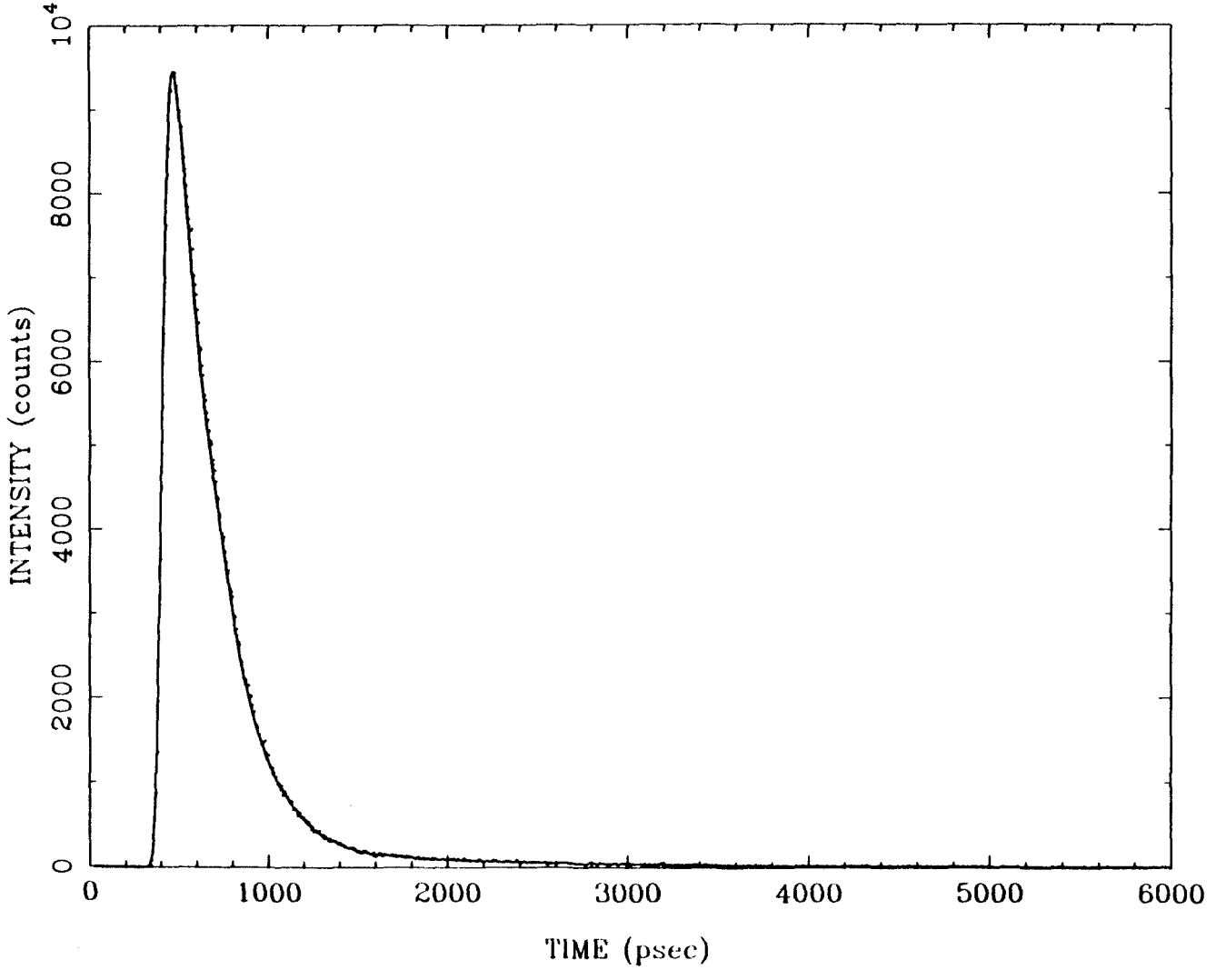

Figure 68. Fluorescence decay of porphyrin-quinone compound ZnPmLQ **11** in 2MTHF with biexponential fit (solid line).

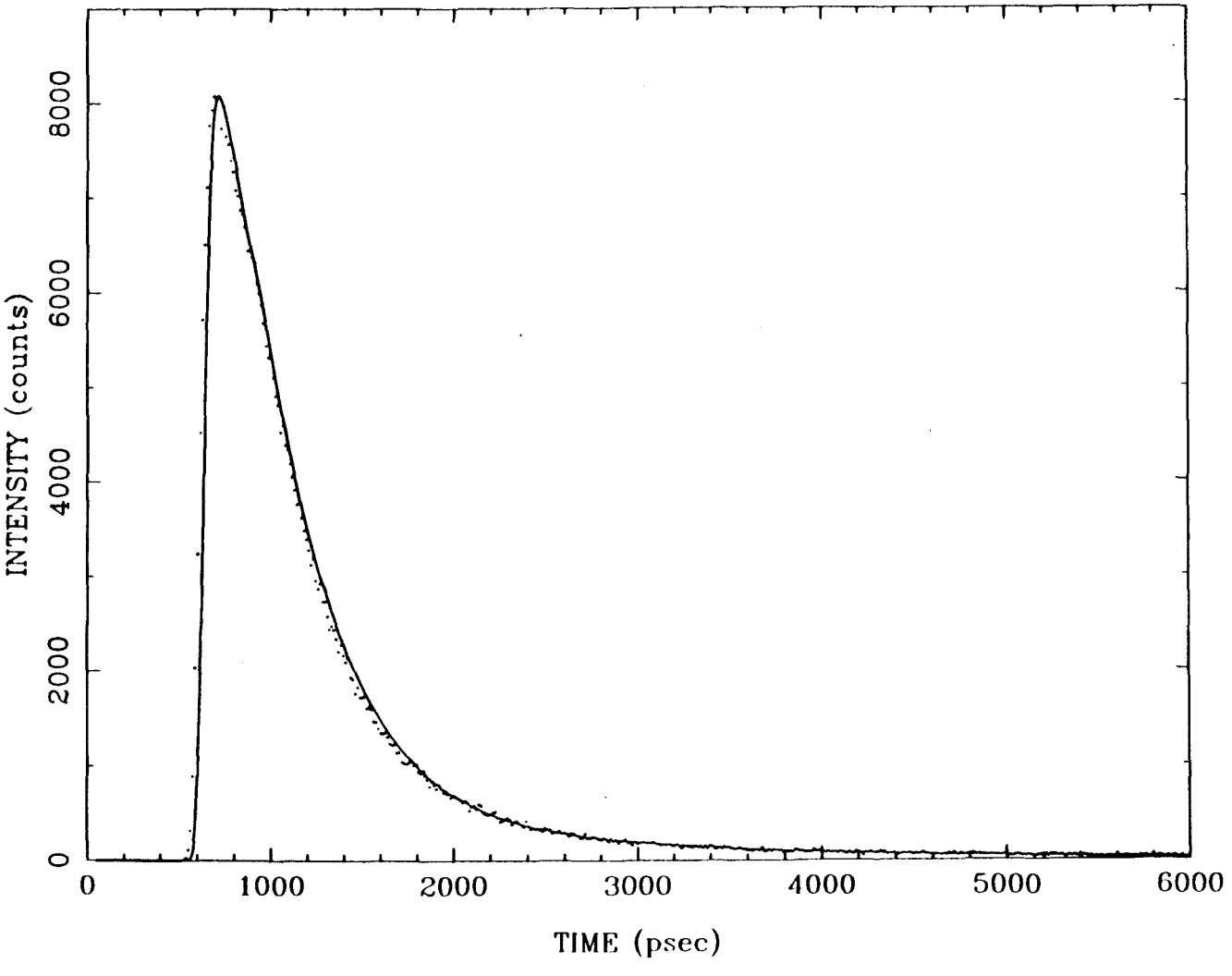

Figure 69. Fluorescence decay of porphyrin-quinone compound ZnPmLQ **11** in acetonitrile with biexponential fit (solid line).

Table XXII. Fluorescence lifetimes τ and electron transfer rates k_{ET} for ZnPLQ **2** and ZnPmLQ **11**.

solvent	τ (**2**)(psec)	k_{ET}(**2**)(sec^{-1})	τ (**11**)(psec)	k_{ET} (**11**)(sec^{-1})	τ_o (psec)
benzene	275	2.97×10^9	192	4.54×10^9	1500
toluene	303	2.64×10^9	215	4.00×10^9	1525
2MTHF	283	2.95×10^9	194	4.57×10^9	1725
acetonitrile	518	1.31×10^9	399	1.89×10^9	1620

shown in Figure 70. These plots can be seen to be reasonably linear. Similar plots of electron transfer rates vs. R_S are shown in Figure 71, and these plots are significantly less linear. This is evidence that electron transfer in these porphyrin-quinone molecules follows a through bond mechanism and is not simple "hopping" of the electron through space. A more complex picture of the through space mechanism would involve the orientational dependence of electron transfer rates as discussed by Siders et al.[7] If this model described these porphyrin-quinone compounds, then the electron transfer rate in ZnPmLQ **11** should be slower than in ZnPLQ **2** due to less favorable overlap of the porphyrin and quinone π systems. The opposite is observed.[55]

The model most consistent with the data is electron transfer by superexchange involving the σ orbitals of the phenyl ring and bicyclo[2.2.2]octane spacer. If the plane of the phenyl ring is nearly perpendicular to the plane of the porphyrin, as suggested by the crystal structures of tetraphenylporphyrin derivatives,[56] only the σ orbitals have the correct

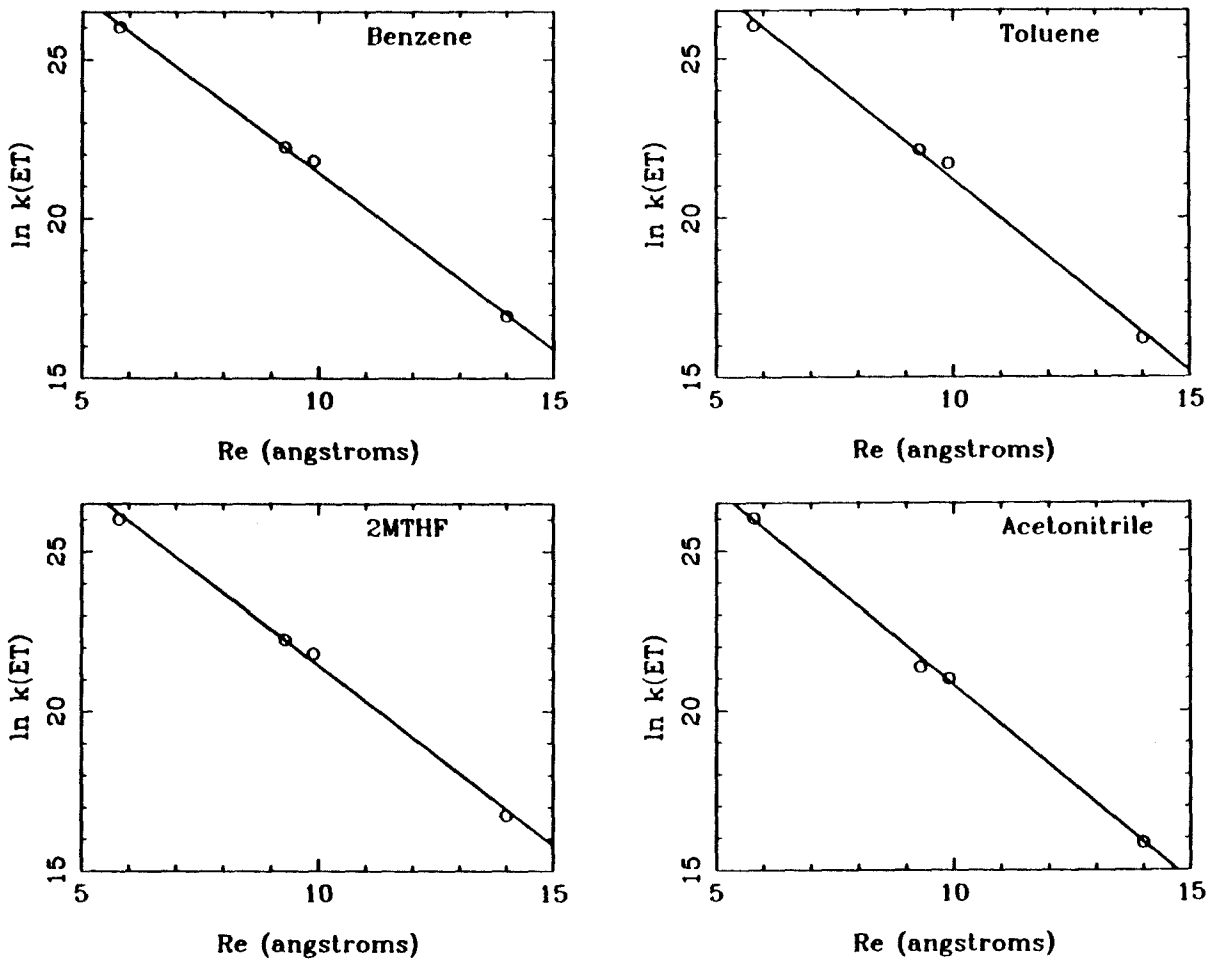

Figure 70. Semilogarithmic plots of electron transfer rates in ZnPLQ compounds as a function of through bond edge-to-edge distance R_e with least squares fit to give exponential decay constant α.

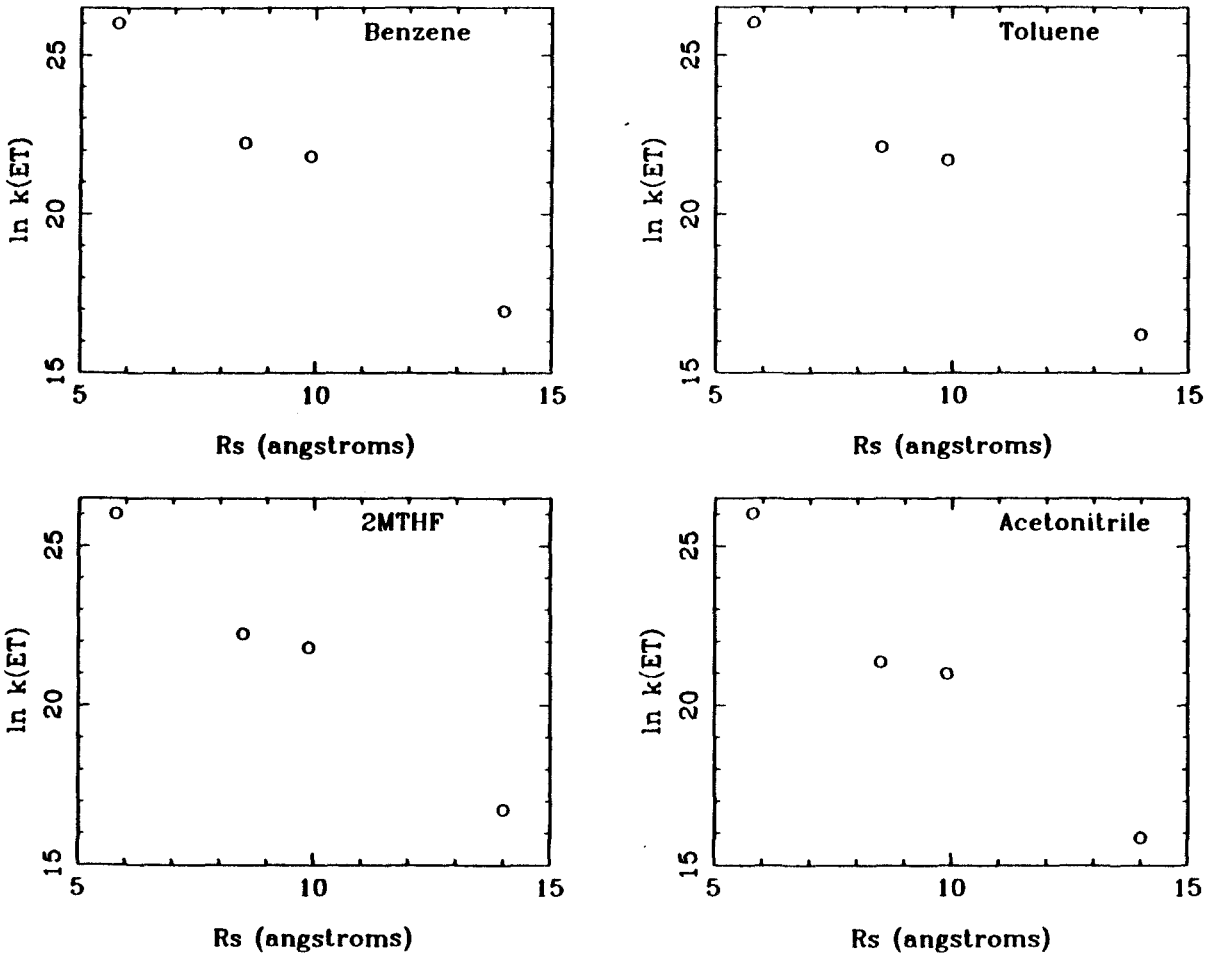

Figure 71. Semilogarithmic plots of electron transfer rates in ZnPLQ compounds as a function of through space edge-to-edge distance R_S.

symmetry to mix with the porphyrin π system. The coupling should be attenuated exponentially with distance, leading to a decrease in the electron transfer rates as

$$k_{ET} = k^{o}_{ET} \exp [-\alpha R_e] \ . \qquad (40)$$

The best values of the exponent α and k^{o}_{ET} in the various solvents are listed in Table XXIII. These values are not corrected for possible coulombic effects on the rates. These coulombic effects arise from the extra energy required to separate charges over a greater distance, and can be calculated as

$$W_p = \left[\frac{1}{4\pi\varepsilon\varepsilon_o} \right] \frac{e^2}{R} \qquad (41)$$

where R is the center to center distance between the charges, e is the amount of charge separated, ε is the solvent dielectric, and ε_o the dielectric of a vacuum. Even in vacuum (with $\varepsilon=\varepsilon_o=1$), the coulombic correction for the difference in ΔG^o for ZnPmLQ **11** and ZnPLQ **2** is only 40 mV. In acetonitrile, the correction is 1 mV. These corrections are most relevant to the benzene and toluene data, yet this data seems to correlate as well as the

Table XXIII. Best fit parameters for distance dependence of k_{ET}.

solvent	k^{o}_{ET} (sec^{-1})	α ($Å^{-1}$)
benzene	1.36×10^{14}	1.11
toluene	2.57×10^{14}	1.20
2MTHF	1.66×10^{14}	1.13
acetonitrile	2.35×10^{14}	1.23

data in the more polar solvents 2MTHF and acetonitrile. These values of α are slightly larger than those calculated by Paddon-Row and Verhoeven for their series of electron transfer model compounds.[37] This suggests that the limiting values assigned as rates to ZnP0Q and ZnP2LQ are not too far from correct. The distance dependence measured by Gray and co-workers in modified myoglobins is much stronger, with an α of 1.4.[57] The theoretical work of Beratan shows that α will depend on the type of bonds involved in the bridge and also on the connectivity.[6] Since the Paddon-Row and Verhoeven compounds have a "double bridge" structure while the ZnPLQ compounds have only a "single bridge," the stronger distance dependence (larger α) in the ZnPLQ compounds is qualitatively in agreement with Beratan's calcualtions. The modified protein systems have even lower connectivity (the shortest path is not through the bonding framework, since the protein backbone is highly folded); therefore, the very strong distance dependence for the modified proteins is also in qualitative agreement with theory.

Chapter 8

Temperature Dependence of Electron Transfer and the Role of Solvent Dynamics

Temperature dependence is an important part of any investigation of chemical reaction rates. The Arrhenius rate law and transition state theory have been used for many years to successfully interpret the temperature dependence of chemical kinetics in terms of activation energies and pre-exponential factors.[3,10,58] These activation parameters are useful guides in developing an understanding of the detailed mechanics of the reaction under investigation.

The temperature dependence of electron transfer rates is an important aspect that has seldom been addressed in synthetic model systems. Most of the temperature dependence data in the literature is concerned with biological electron transfer reactions, particularly in the bacterial photosynthetic reaction center.[31-33] These investigations have been crucial in understanding biological electron transfer and have provided impetus to the development of electron transfer theory. The temperature independence observed by DeVault and Chance for electron transfer in *Chromatium vinosum* at low temperatures emphasized the importance of tunneling in electron transfer reactions.[31] The inverse activated behavior observed for other electron transfers in bacterial photosynthetic reaction centers remains a poorly understood phenomenon.[32] One of the few reports of temperature dependence in a synthetic electron transfer system is that of Lindsey and Mauzerall.[59] Their system is complicated by conformational effects, but they observed that the electron transfer rates are nearly independent of temperature for both conformers from 290 to 124 K in 1:1 dimethylacetamide/ethanol. The conformational problems experienced by Lindsey and Mauzerall are relatively minor, but many synthetic systems have low energy conformations which are very unfavorable for electron transfer.[60] These systems commonly become

inactive for electron transfer at relatively high temperatures (above 200 K). The biological systems, where geometry is rigidly controlled by a protein matrix, are usually active down to near absolute zero.[1,32] Since ZnPLQ **2** is a relatively rigid system, these compounds should be good candidates for studying the temperature dependence of electron transfer in a well-constrained synthetic system. The observation of fluorescence quenching for ZnPLQ **2** and several of its derivatives in 2MTHF glass at 77 K confirmed the viability of low temperature electron transfer in these compounds.[45-47] What remained to be done was a careful study of the electron transfer rates over a broad range of temperatures.

A. Temperature Studies.

Electron transfer rates were measured as a function of temperature for four compounds (ZnPLQ **2**, ZnPLQMe2 **5**, ZnPLQMe **6**, and ZnPmLQ **11**) in three solvents (2MTHF, toluene, and toluene-d_8). Rates for ZnPLQ **2** and ZnPmLQ **11** were also measured in acetonitrile. The rates were established by time resolved fluorescence quenching using the techniques described earlier, with full details given in the experimental section. Temperature control was provided by a liquid helium cooled continuous flow cryostat, which gave temperature control to within ±1 K. At higher temperatures, the fluorescence decays could be fit to biexponentials, as was true for the room temperature results shown earlier. At lower temperatures (near the glass or liquid/solid transition of the solvent) the decays became more complex. A reasonable fit could usually be obtained using three exponentials, but the appearance of the decays suggested a distribution of exponentials.[61] Representative decays for ZnPLQ **2** in both intensity format and semilogarithmic format are shown as a function of temperature in Figures 72-77. The change in rates and the appearance of nonexponentiality at the lowest temperatures in 2MTHF and toluene are more easily seen in the semilog plots. Non-exponential behavior

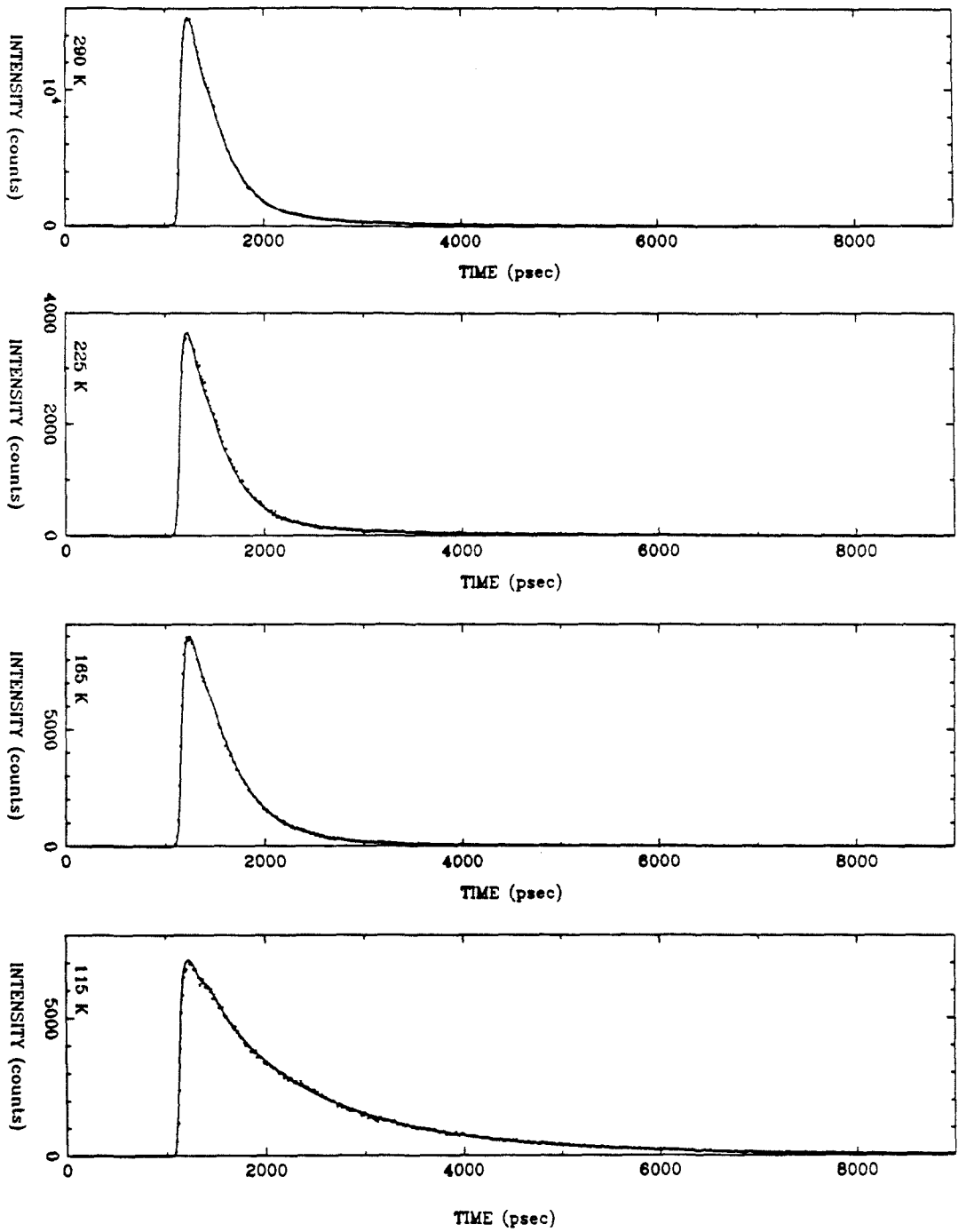

Figure 72. Fluorescence decay of ZnPLQ **2** in 2MTHF at 290, 225, 165, and 115 K with multiexponential fit (solid line).

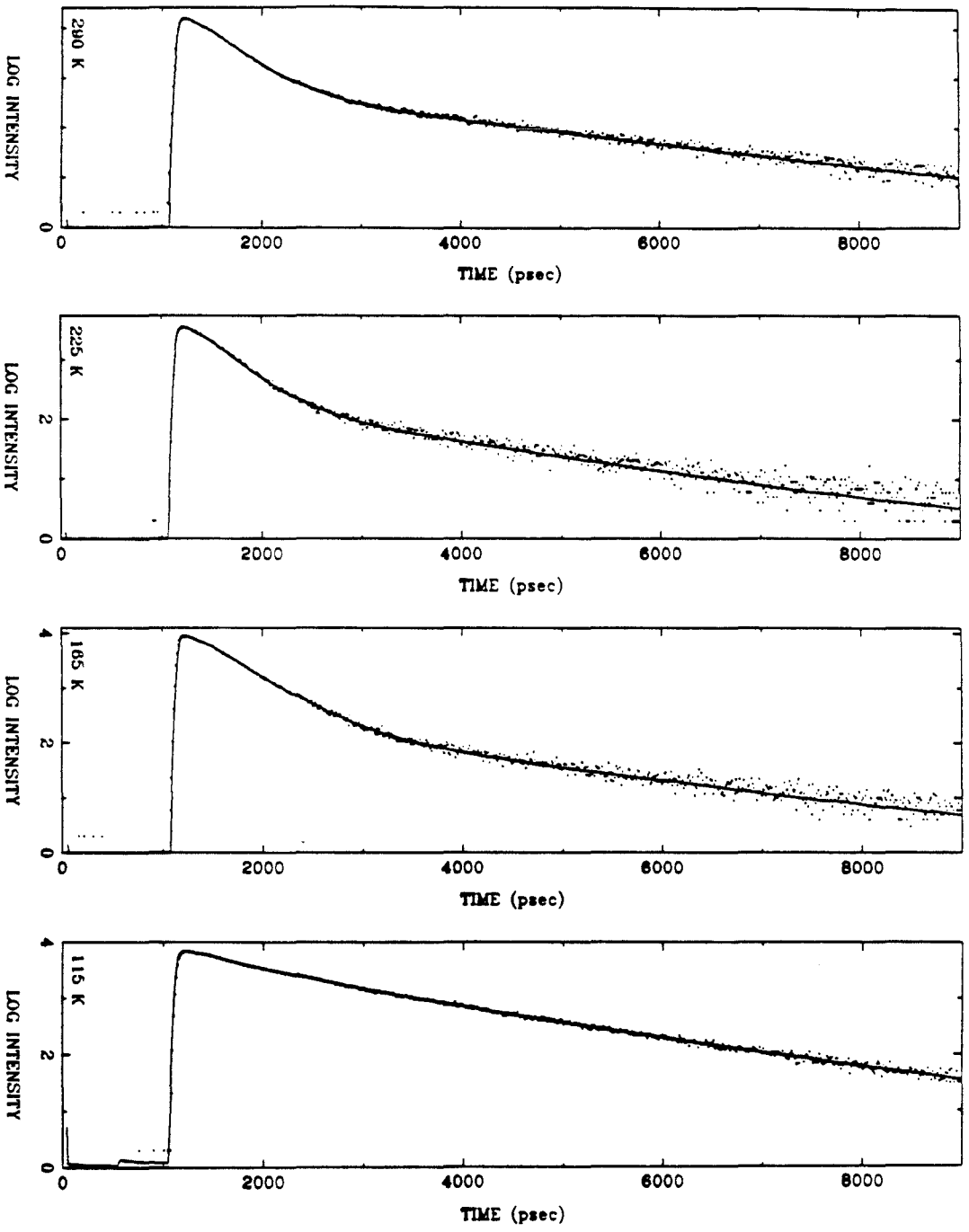

Figure 73. Fluorescence decay of ZnPLQ **2** in 2MTHF at 290, 225, 165, and 115 K in semilog format with multiexponential fit (solid line). Data at 115 K could not be fit to a biexponential, but would fit to a triexponential.

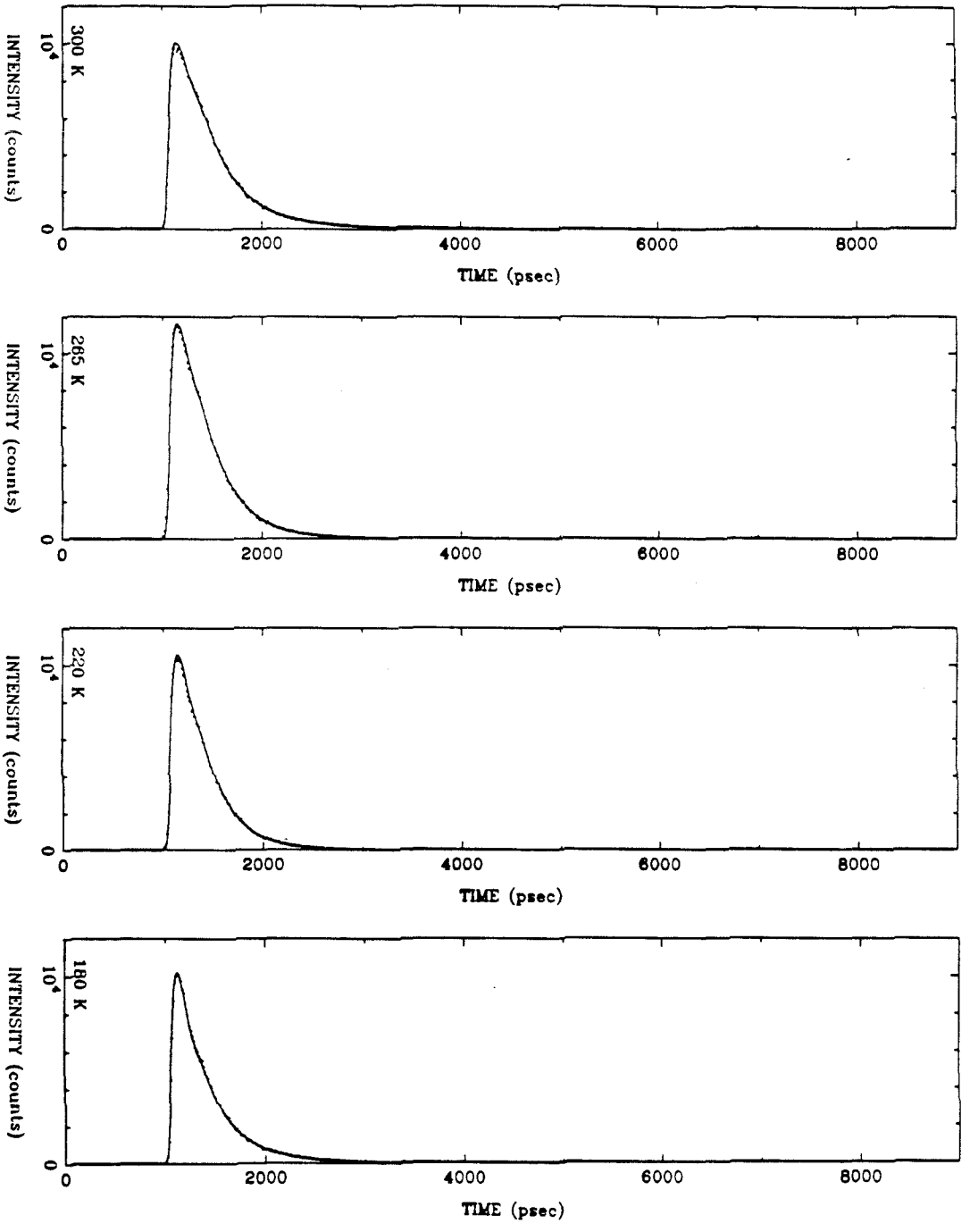

Figure 74. Fluorescence decay of ZnPLQ **2** in toluene at 300, 265, 220, and 180 K with multiexponential fit (solid line).

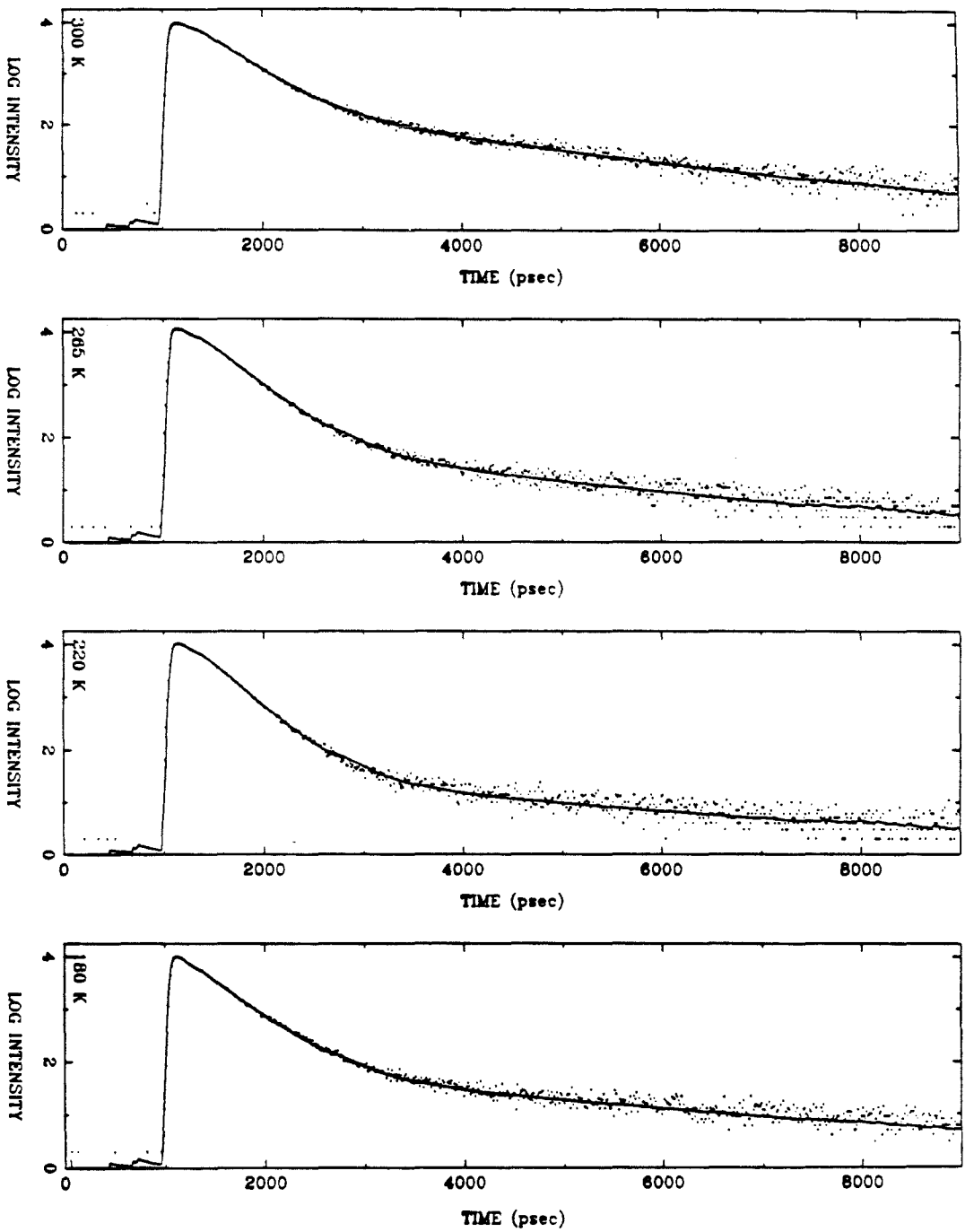

Figure 75. Fluorescence decay of ZnPLQ 2 in toluene at 300, 265, 220, and 180 K in semilog format with multiexponential fit (solid line). Data at 180 K could not be fit to a biexponential, but would fit to a triexponential.

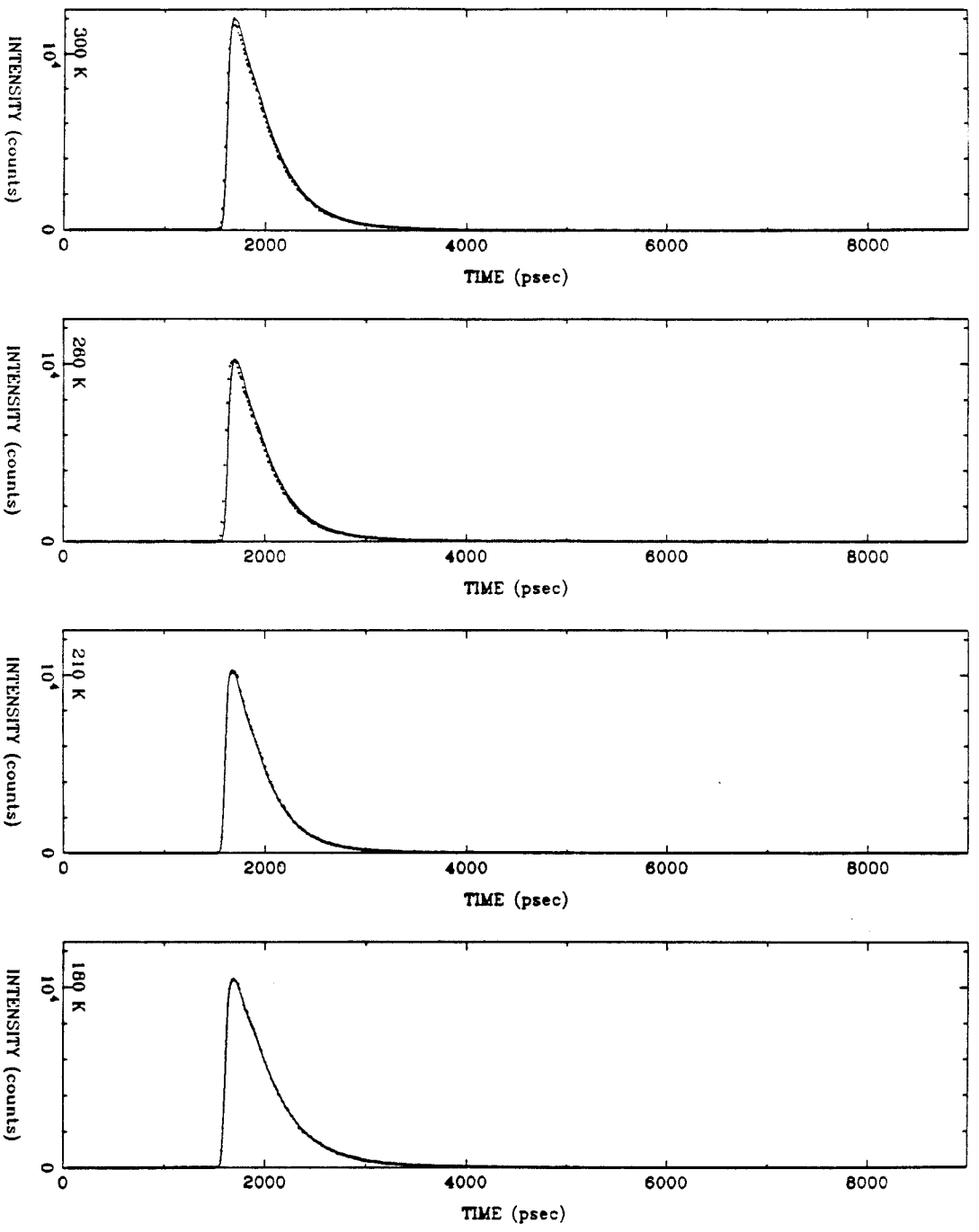

Figure 76. Fluorescence decay of ZnPLQ **2** in toluene-*d*8 at 300, 260, 210, and 180 K with biexponential fit (solid line).

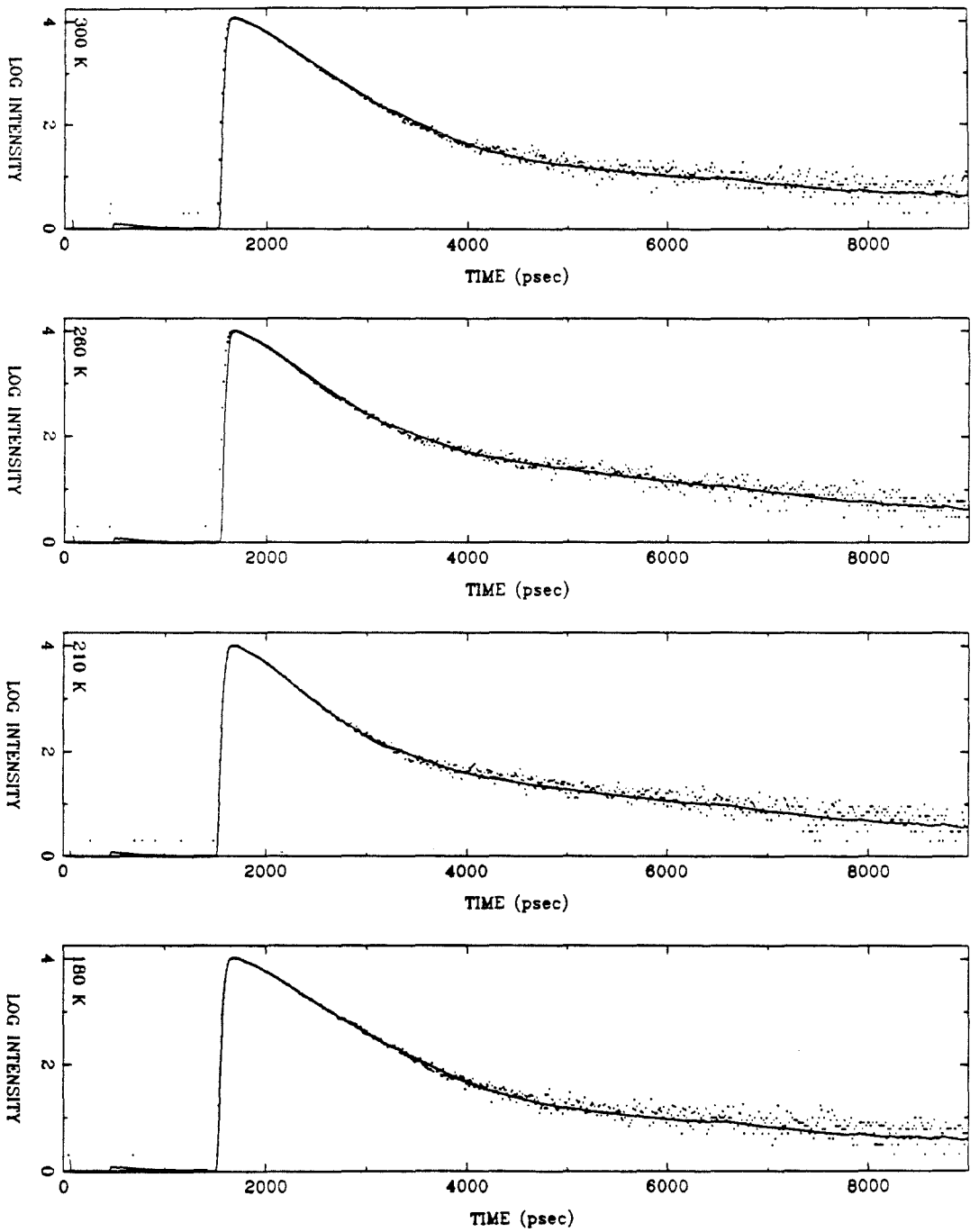

Figure 77. Fluorescence decay of ZnPLQ **2** in toluene-d_8 at 300, 260, 210, and 180 K in semilog format with biexponential fit (solid line).

began to be seen in 2MTHF near 130 K, in toluene near 200 K, and in toluene-d_8 near 190 K. The multi-exponential decays are probably the result of a distribution of electron transfer rates. This makes interpretation of the temperature dependence difficult, since any intrinsic temperature dependence is convoluted with the temperature dependence of the distribution. Only the temperature ranges where the fluorescence decays can be described well by biexponentials will be dealt with in detail.

Semilogarithmic plots of the electron transfer rates against T^{-1} are shown in Figures 78-81. Tables XXIV-XXVII list the values used for these plots. The Arrhenius rate law and transition state theory predict that such plots should be linear with a slope defined by the activation energy. The observed electron transfer rates in 2MTHF are essentially temperature independent at high temperatures, then begin to decrease with decreasing temperature around 200 K. In toluene, the electron transfer rates *increase* with decreasing temperature down to the lowest temperatures where biexponentials could describe the data. In toluene-d_8, the rates initially increase with decreasing temperature, go through a maximum between 210 and 220 K, then decrease. The different behavior in toluene and toluene-d_8, a *solvent* isotope effect, can be seen quite clearly in Figure 82, where the data for ZnPLQMe **6** in both solvents is plotted on the same graph. In acetonitrile, the electron transfer rates are relatively insensitive to temperature but show a slight decrease with decreasing temperature.

It is readily apparent that the activated behavior expected under Marcus electron transfer theory does not describe the data in Figures 78-81. The semiclassical theory of Hopfield, which predicts temperature independence at low temperature, also fails to describe the data. A fully quantum mechanical treatment could probably be made to fit the data in one solvent, but a different set of modes would be required to fit the data in the other solvents. The 2MTHF data might also be described by a scenario where at low

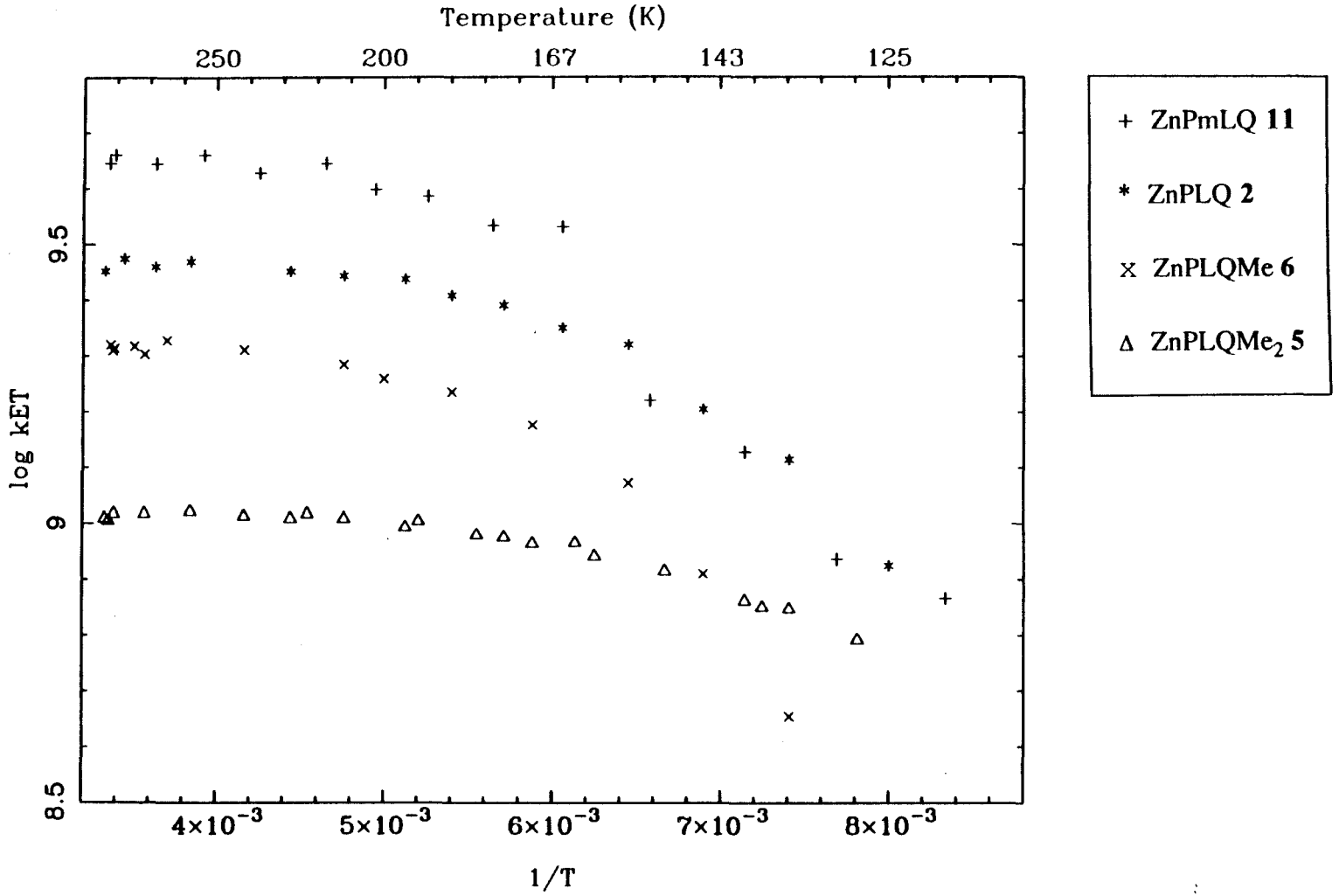

Figure 78. Semilogarithmic plot of electron transfer rates for ZnPLQ **2**, ZnPLQMe$_2$ **5**, ZnPLQMe **6**, and ZnPmLQ **11** in 2MTHF as a function of inverse temperature.

Table XXIV. Fluorescence lifetimes τ (in psec), calculated electron transfer rates k_{ET} (sec^{-1})[b], and goodness of fit parameters χ^2 for porphyrin-quinone compounds **2**, **5**, **6**, and **11** in 2MTHF as a function of temperature.

ZnPmLQ **11**				ZnPLQ **2**				ZnPLQMe **6**				ZnPLQMe2 **5**			
T	τ	χ^2	k_{ET}	T	τ	χ^2	k_{ET}	T	τ	χ^2	k_{ET}	T	τ	χ^2	k_{ET}
298	200	1.188	4.42×10^9	300	293	1.254	2.83×10^9	297	374	1.401	2.09×10^9	300	624	1.330	1.02×10^9
295	194	1.251	4.58×10^9	290	281	1.238	2.98×10^9	296	382	1.263	2.04×10^9	295	616	1.232	1.04×10^9
275	200	1.093	4.42×10^9	275	289	1.314	2.88×10^9	285	376	1.135	2.08×10^9	280	619	1.387	1.04×10^9
255	194	1.288	4.58×10^9	260	283	1.158	2.95×10^9	280	386	1.111	2.01×10^9	260	614	1.393	1.05×10^9
235	207	1.264	4.25×10^9	225	293	1.110	2.83×10^9	270	369	1.442	2.13×10^9	240	620	1.501	1.03×10^9
215	200	1.496	4.42×10^9	210	298	1.025	2.78×10^9	240	380	1.218	2.05×10^9	225	625	1.648	1.02×10^9
202	220	1.412	3.97×10^9	195	301	1.246	2.74×10^9	210	399	1.335	1.93×10^9	220	617	1.379	1.04×10^9
190	225	1.401	3.86×10^9	185	318	1.123	2.56×10^9	200	404	1.237	1.89×10^9	210	625	1.176	1.02×10^9
177	250	1.316	3.42×10^9	175	329	1.241	2.46×10^9	185	435	1.343	1.72×10^9	192	631	1.150	1.01×10^9
165	251	1.404	3.40×10^9	165	354	1.178	2.24×10^9	170	480	1.334	1.50×10^9	180	652	1.212	9.54×10^8
152[a]	447	0.902	1.66×10^9	155	374	1.372	2.09×10^9	155	567	1.157	1.18×10^9	170	666	1.342	9.22×10^8
140[a]	521	0.937	1.34×10^9	145	449	1.234	1.65×10^9	145[a]	718	1.135	8.13×10^8	160	688	1.167	8.74×10^8
130[a]	693	1.045	8.63×10^8	135[a]	544	1.090	1.26×10^9	135[a]	970	1.285	4.51×10^8	150	709	1.322	8.31×10^8
120[a]	761	1.041	7.34×10^8	125[a]	703	1.101	8.43×10^8	125[a]	1158	1.398	2.84×10^8	140	766	1.158	7.26×10^8
												135	780	1.025	7.02×10^8
												128	835	0.926	6.18×10^8

a. Fit to three exponentials. The lifetime τ listed here is the second longest of the three lifetimes.

b. Calculated with equation 37; $\tau_o = 1725$ psec

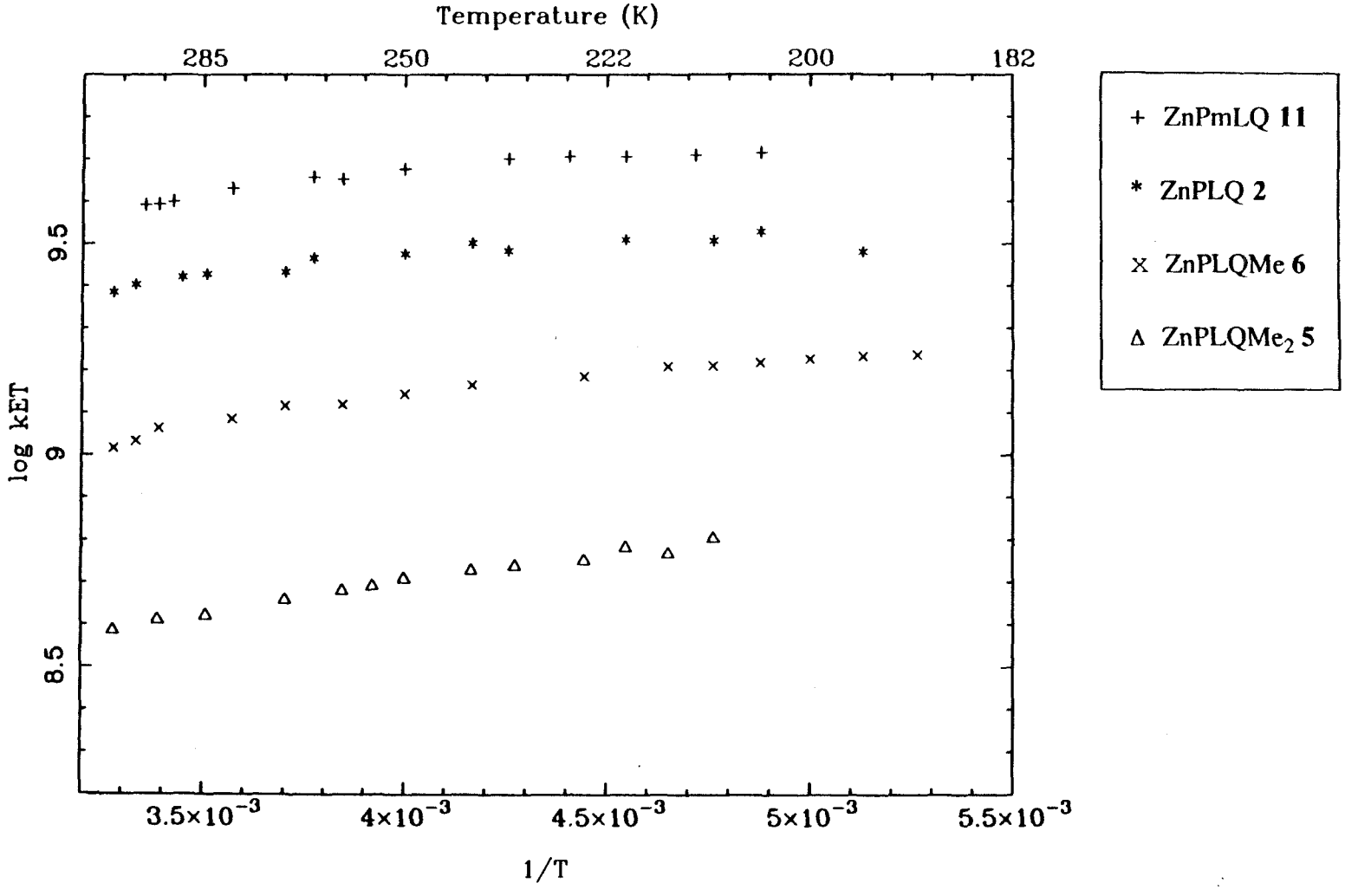

Figure 79. Semilogarithmic plot of electron transfer rates for ZnPLQ **2**, ZnPLQMe$_2$ **5**, ZnPLQMe **6**, and ZnPmLQ **11** in toluene as a function of inverse temperature.

Table XXV. Fluorescence lifetimes τ (in psec), calculated electron transfer rates k_{ET} (sec^{-1})[a], and goodness of fit parameters χ^2 for porphyrin-quinone compounds **2**, **5**, **6**, and **11** in toluene as a function of temperature.

ZnPmLQ **11**				ZnPLQ **2**				ZnPLQMe **6**				ZnPLQMe2 **5**			
T	τ	χ^2	k_{ET}	T	τ	χ^2	k_{ET}	T	τ	χ^2	k_{ET}	T	τ	χ^2	k_{ET}
298	219	1.632	3.91×10^9	305	324	1.304	2.43×10^9	305	590	1.248	1.04×10^9	305	960	1.218	3.86×10^8
295	218	1.718	3.93×10^9	300	314	1.217	2.53×10^9	300	577	1.363	1.08×10^9	295	940	1.242	3.98×10^8
292	215	1.301	3.99×10^9	290	303	1.544	2.64×10^9	295	545	1.150	1.18×10^9	285	931	1.178	4.18×10^8
280	197	1.100	4.42×10^9	285	300	1.193	2.68×10^9	280	532	1.311	1.22×10^9	270	900	1.267	4.55×10^8
265	192	1.236	4.55×10^9	265	279	1.223	2.93×10^9	270	509	1.299	1.31×10^9	260	881	1.138	4.79×10^8
250	181	1.218	4.87×10^9	250	268	1.134	3.08×10^9	260	507	1.221	1.32×10^9	255	871	1.382	4.92×10^8
235	176	1.257	5.03×10^9	240	261	1.322	3.18×10^9	250	487	1.320	1.40×10^9	250	856	1.167	5.12×10^8
227	174	1.272	5.09×10^9	235	270	1.242	3.05×10^9	240	470	1.173	1.47×10^9	240	839	1.194	5.36×10^8
220	174	1.233	5.09×10^9	220	252	1.263	3.31×10^9	225	456	1.015	1.54×10^9	234	830	1.265	5.49×10^8
212	173	1.278	5.12×10^9	220	261	0.979	3.18×10^9	215	440	1.015	1.62×10^9	225	819	1.178	5.65×10^8
205	171	1.452	5.19×10^9	210	258	1.146	3.22×10^9	210	437	0.985	1.63×10^9	215	805	1.149	5.86×10^8
				205	248	1.087	3.38×10^9	205	431	1.045	1.66×10^9	210	773	1.362	6.38×10^8
								200	427	1.022	1.69×10^9	200	690	1.253	7.94×10^8
								195	421	1.137	1.72×10^9	195	598	1.176	1.02×10^9
								190	420	1.251	1.73×10^9	190	571	1.147	1.10×10^9

a. Calculated with equation 37; $\tau_0 = 1525$ psec.

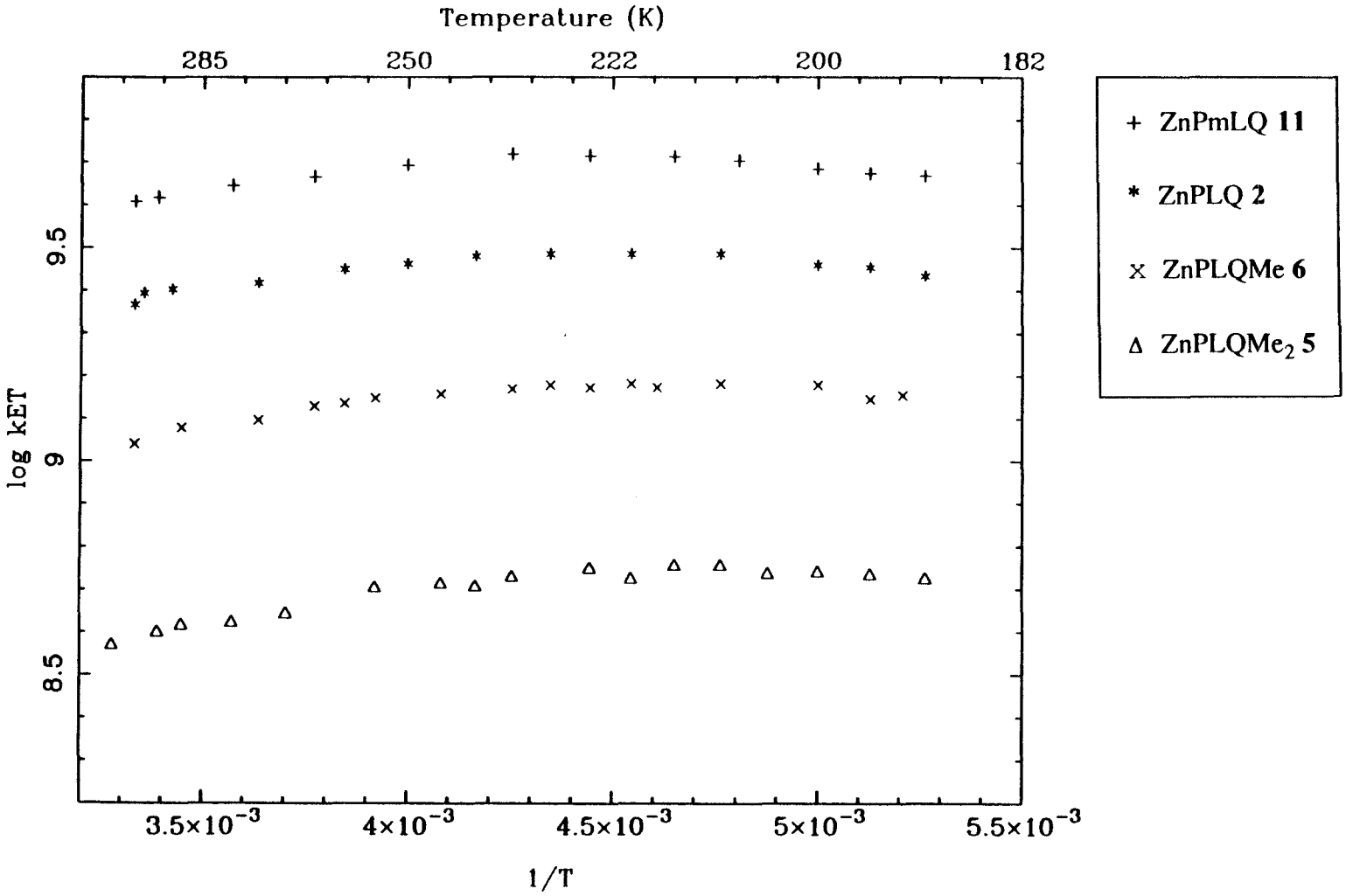

Figure 80. Semilogarithmic plot of electron transfer rates for ZnPLQ **2**, ZnPLQMe$_2$ **5**, ZnPLQMe **6**, and ZnPmLQ **11** in toluene-d_8 as a function of inverse temperature.

Table XXVI. Fluorescence lifetimes τ (in psec), calculated electron transfer rates k_{ET} (sec^{-1})[a], and goodness of fit parameters χ^2 for porphyrin-quinone compounds **2**, **5**, **6**, and **11** in toluene-d_8 as a function of temperature.

ZnPmLQ **11**				ZnPLQ **2**				ZnPLQMe **6**				ZnPLQMe2 **5**			
T	τ	χ^2	k_{ET}	T	τ	χ^2	k_{ET}	T	τ	χ^2	k_{ET}	T	τ	χ^2	k_{ET}
300	212	1.42	4.06×10^9	300	335	1.305	2.33×10^9	300	568	1.375	1.10×10^9	305	975	1.203	3.70×10^8
295	208	1.27	4.15×10^9	298	319	1.355	2.48×10^9	290	538	1.324	1.20×10^9	295	950	1.297	3.97×10^8
280	197	1.52	4.42×10^9	292	314	1.445	2.53×10^9	275	526	1.314	1.25×10^9	280	931	1.241	4.18×10^8
265	189	1.58	4.64×10^9	275	310	1.365	2.57×10^9	265	498	1.344	1.35×10^9	270	914	1.240	4.38×10^8
250	179	1.48	4.93×10^9	260	289	1.231	2.80×10^9	260	494	1.162	1.37×10^9	255	862	1.449	5.04×10^8
235	170	1.69	5.23×10^9	250	281	1.484	2.90×10^9	255	485	1.245	1.41×10^9	240	860	1.160	5.07×10^8
225	171	1.67	5.19×10^9	240	272	1.630	3.02×10^9	245	476	1.100	1.44×10^9	235	840	1.128	5.35×10^8
215	172	1.77	5.16×10^9	230	270	1.337	3.05×10^9	235	468	1.352	1.48×10^9	225	823	1.505	5.59×10^8
208	175	1.72	5.06×10^9	220	267	1.291	3.09×10^9	230	461	0.969	1.51×10^9	220	844	1.258	5.29×10^8
200	182	1.83	4.84×10^9	210	269	1.326	3.06×10^9	225	466	1.285	1.49×10^9	215	817	1.364	5.68×10^8
195	186	2.15	4.72×10^9	200	278	1.239	2.94×10^9	220	459	1.169	1.54×10^9	210	817	1.358	5.68×10^8
190	188	2.19	4.66×10^9	195	285	1.342	2.85×10^9	217	467	1.493	1.49×10^9	205	834	1.251	5.43×10^8
				190	296	1.269	2.72×10^9	210	455	1.065	1.54×10^9	200	831	1.326	5.48×10^8
				180	344	1.155	2.25×10^9	200	462	0.983	1.51×10^9	195	836	1.317	5.40×10^8
								195	486	0.952	1.40×10^9	190	851	1.373	5.19×10^8
								190	565	1.153	1.11×10^9	185	866	1.364	4.99×10^8

a. Calculated using equation 37; $\tau_0 = 1525$ psec

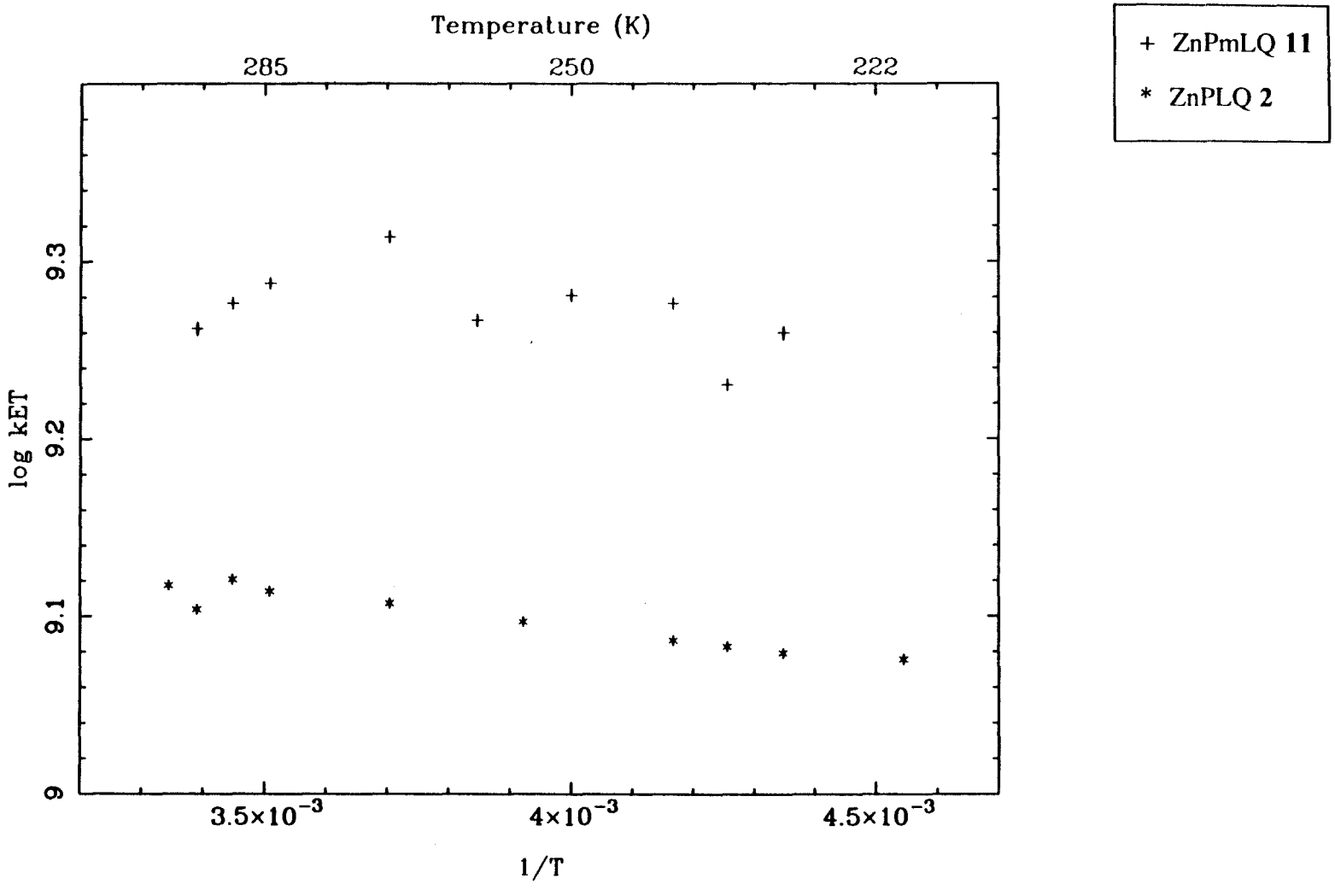

Figure 81. Semilogarithmic plot of electron transfer rates for ZnPLQ 2 and ZnPmLQ **11** in acetonitrile as a function of inverse temperature.

Table XXVII. Fluorescence lifetimes τ (in psec), calculated electron transfer rates k_{ET} (sec^{-1})[a], and goodness of fit parameters χ^2 for porphyrin-quinone compounds **2** and **11** in acetonitrile as a function of temperature.

ZnPmLQ **11**				ZnPLQ **2**			
T	τ	χ^2	k_{ET}	T	τ	χ^2	k_{ET}
295	409	1.468	1.83×10^9	299	519	1.201	2.33×10^9
290	399	1.101	1.89×10^9	295	531	1.156	2.48×10^9
285	391	1.033	1.94×10^9	290	516	1.104	2.53×10^9
270	374	1.271	2.06×10^9	285	521	1.125	2.57×10^9
260	406	1.378	1.85×10^9	270	528	1.149	2.80×10^9
250	396	1.052	1.91×10^9	262	569	1.574	2.90×10^9
240	399	1.143	1.89×10^9	255	535	1.192	3.02×10^9
235	432	1.497	1.70×10^9	240	543	1.131	3.05×10^9
230	410	1.260	1.82×10^9	235	548	1.069	3.09×10^9
				230	549	1.136	3.06×10^9
				220	552	1.094	2.94×10^9

a. Calculated using equation 37; $\tau_o = 1620$ psec.

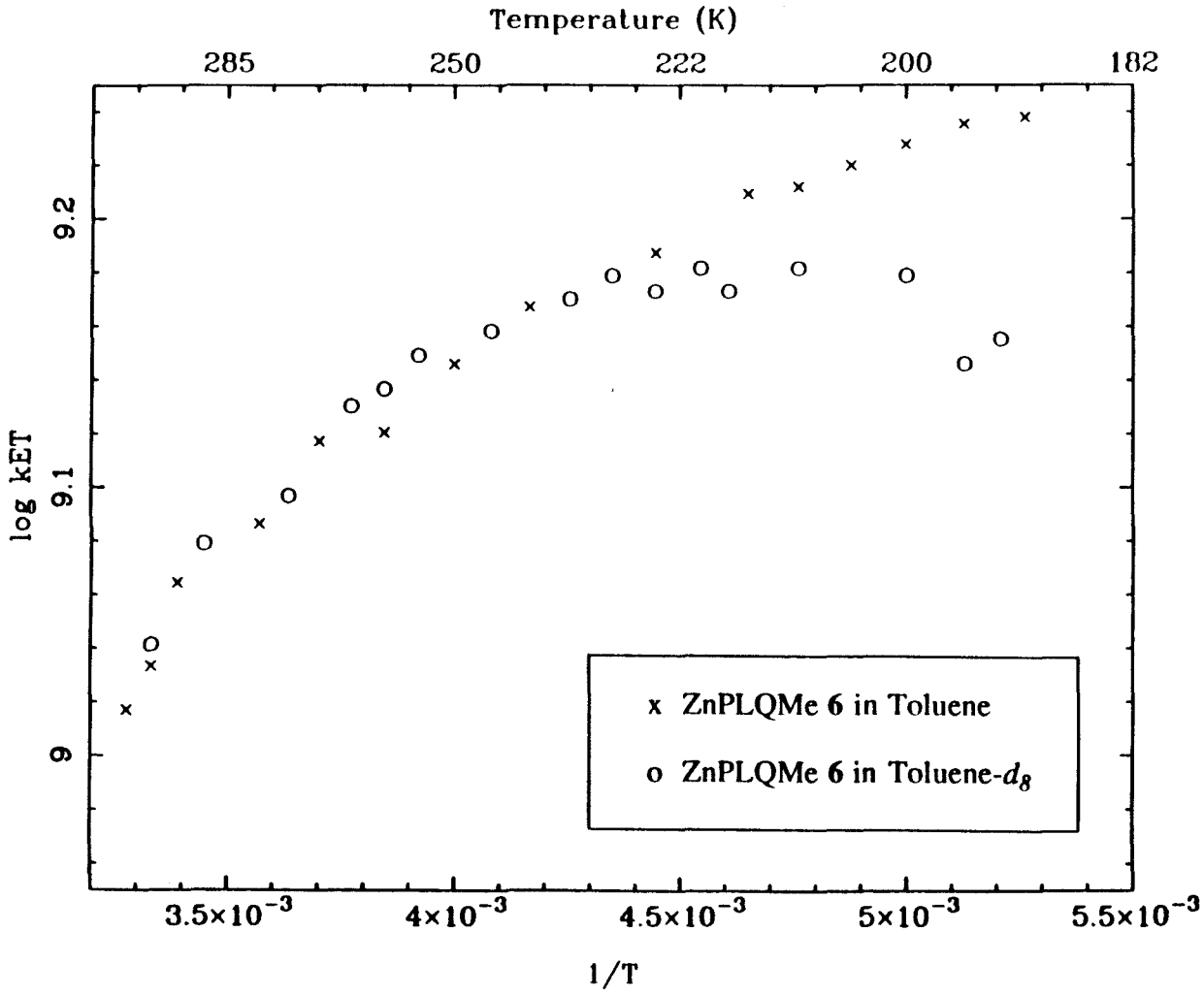

Figure 82. Semilogarithmic plot of electron transfer rates for ZnPLQMe **6** in toluene and toluene-d_8 as a function of inverse temperature.

temperatures internal rotation of the porphyrin and quinone relative to each other is rate limiting. The smallest rotation barrier in the bridge is associated with the bond connecting the phenyl ring to the bicyclo[2.2.2]octane spacer. Previous NMR studies have shown rapid rotation (~10^{11} - 10^{12} rad/sec) about this type of bond at room temperature,[62] and molecular mechanics calculations project a barrier slightly less than 1.0 kcal/mol for this rotation. The temperature dependent regime of the 2MTHF data corresponds to an activation energy of ~1.0 kcal/mol. This model cannot describe the toluene and toluene-d_8 data, however, and so must be considered inadequate.

The predictions of solvent dynamics studies based on the work of Kramers, as described in Chapter 6, show a strong resemblance to the temperature dependence data in Figures 78-80. The solvent friction should increase with decreasing temperature. At very low friction (underdamped), the Kramers theory predicts rates should increase with increasing friction (decreasing temperature). The rates should go through a maximum, then decrease with increasing friction at high friction (overdamped).[12] This model could describe the temperature dependence observed in all three solvents by considering that the different solvents have different amounts of damping (friction). In alcohol solvents, electron transfer rates have been shown to correlate with solvent dynamics as predicted for the overdamped regime.[38-43] The longitudinal relaxation time (τ_L) has been shown to be a good measure of solvent friction for electron transfer reactions.[39]

The temperature dependence of τ_L for 2MTHF and toluene was calculated from data in the literature. τ_L can be related to the Debye relaxation time τ_D by the expression

$$\tau_L = \tau_D \left(\frac{n^2}{\varepsilon} \right) \tag{42}$$

where n is the index of refraction and ε is the static dielectric constant.[41] The Debye time depends on temperature and viscosity η as

$$\tau_D = \frac{4\pi\eta a^3}{k_B T} \tag{43}$$

where $4\pi a^3$ is the effective volume of a solvent molecule.[63] What is needed to calculate τ_L as a function of temperature is a value for τ_D at a known temperature, plus the temperature dependence of η, n, and ε. The solvents were assumed to have a constant molar refractivity, so the index of refraction n should scale with the density. Experimental data exists in the literature to establish all of these properties for 2MTHF and toluene except for τ_D and viscosity for 2MTHF. The viscosity has been studied near the glass transition, but not at the higher temperatures needed here. The known viscosity dependence of THF was used as a reasonable approximation for the viscosity dependence of 2MTHF. For 2MTHF, values of η,[64] n,[65] and ε[66] were calculated as:

$$\ln \eta = -3.635 + 896.8\ T^{-1}$$
$$n = 1.915 - (1.816 \times 10^{-3})\ T + (4.204 \times 10^{-7})\ T^2$$
$$\varepsilon = 18.63 - (4.529 \times 10^{-2})\ T + (3.427 \times 10^{-5})\ T^2. \tag{44}$$

The measured value of 3.0 psec for τ_D of THF at 273 K was used to establish the volume factor of $4\pi a^3$ for calculating τ_D as a function of temperature.[67] The calculated τ_L's can be fit to an exponential function of temperature such that:

$$\tau_L = (1.55 \times 10^{-2}) \exp\left[\frac{1048.1}{T}\right]. \tag{45}$$

For toluene, the following expressions were used to calculate the values of η,[68] n,[67,68] and ε:[69]

$$\ln \eta = -5.878 + (1.287 \times 10^{3})\ T^{-1} + (4.575 \times 10^{-3})\ T - (4.499 \times 10^{-6})\ T^2$$
$$n = 1.981 - (1.628 \times 10^{-3})\ T$$
$$\varepsilon = -6.752 + (1.042 \times 10^{-1})\ T - (3.833 \times 10^{-4})\ T^2 + (4.575 \times 10^{-7})\ T^3. \tag{46}$$

The known value of 5.0 psec for τ_D at 298 K was used to establish the volume factor $4\pi a^3$.[70] The calculated τ_L's fit to an exponential function of temperature such that:

$$\tau_L = (2.77 \times 10^{-2}) \exp\left[\frac{1525.6}{T}\right] . \quad (47)$$

For toluene-d_8, the ratio of the moments of inertia for toluene and toluene-d_8 was used to scale τ_L. The calculated values of τ_L for toluene were multiplied by 1.60 to give τ_L values for toluene-d_8. The calculated values of τ_L are plotted vs T^{-1} in Figure 83.

The work of Rips and Jortner, as discussed in Chapter 6 (equations 24-30), showed that an equation of the form:

$$k_{ET} = \frac{k_{NA}}{1 + \kappa_A} , \quad (48)$$

where κ_A is a function of τ_L, should describe electron transfer rates in the moderate to high friction regime.[18-20] If τ_L is the appropriate measure of friction for both underdamped and overdamped regimes, the method of Skinner and Wolynes[21] suggests that both regimes could be described by a general equation such as:

$$k_{ET} = \frac{k_{NA}\,\tau_L}{A + B\,\tau_L + C\,\tau_L^2} = \frac{k_{NA}}{A\,\tau_L^{-1} + B + C\,\tau_L} = \frac{k_{NA}}{\frac{\alpha}{k_{NA}\,\tau_L} + B + \gamma\,k_{NA}\,\tau_L} \quad (49)$$

It was found that an equation of this type, with B=1.00, could be used to fit the data reasonably well for three of the solvents, as shown in Figures 84-86. The data set in acetonitrile was judged to be too incomplete and too weakly dependent on temperature to warrant fitting. Values for k_{NA} and the coefficients α and γ were determined by plotting the data for each compound in each solvent with k_{ET}^{-1} as a function of τ_L, and fitting by least squares to a quadratic. These quadratic fits were very good, with correlation coefficients greater than 0.990 in all cases. The average values for α and γ were then used with the k_{NA} derived from this fit to produce the fitted curves in Figures 84-86. As a result of this, the fits are better in the middle (ZnPLQ **2** and ZnPLQMe **6**) than at the extremes (ZnPmLQ **11** and $ZnPLQMe_2$ **5**), especially for the toluene isotopomers. Different values of the maximum rate k_{NA} and the coefficients α and γ were required for 2MTHF and the

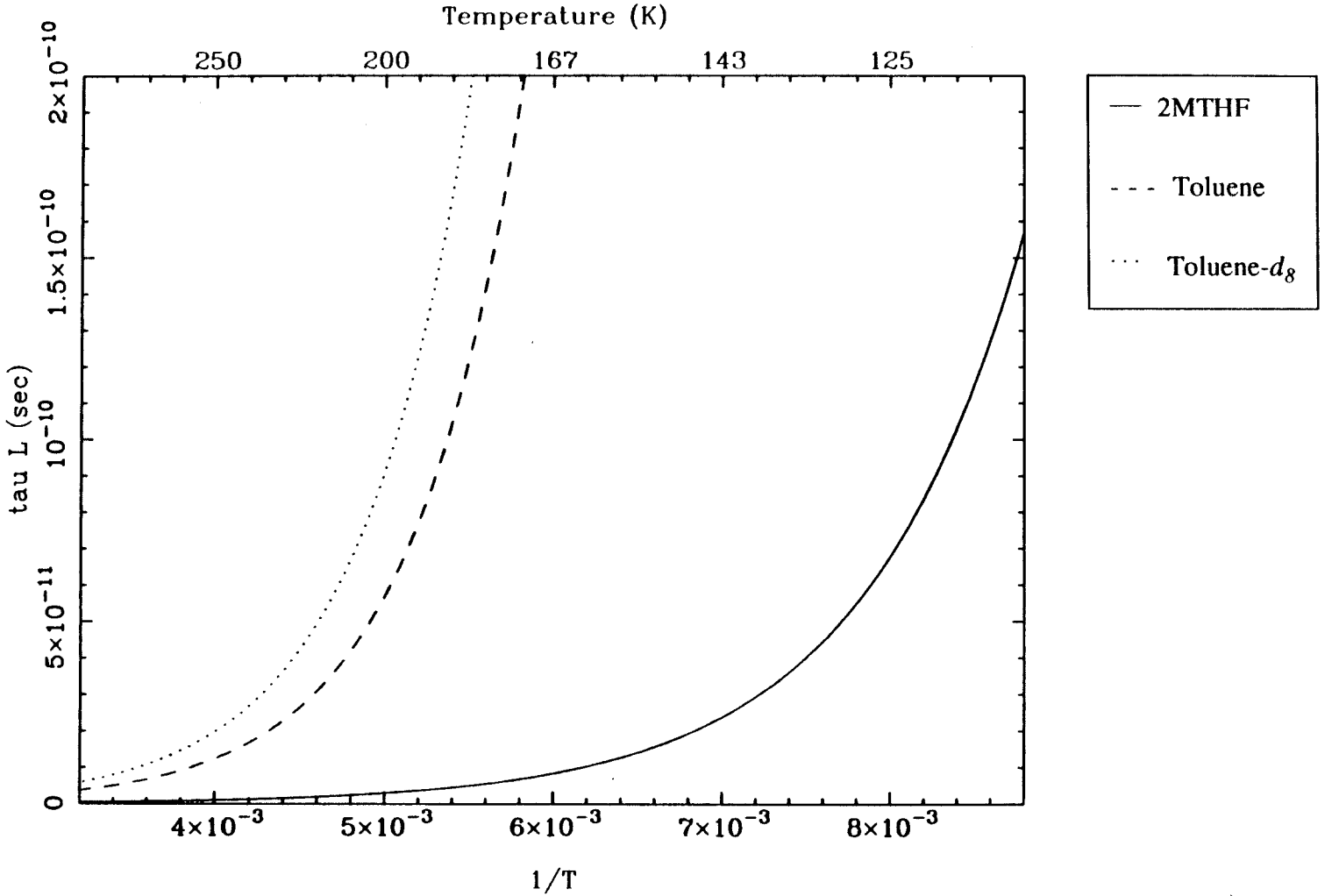

Figure 83. Plot of calculated values for the longitudinal relaxation time τ_L for 2MTHF, toluene, and toluene-d_8 as a function of inverse temperature.

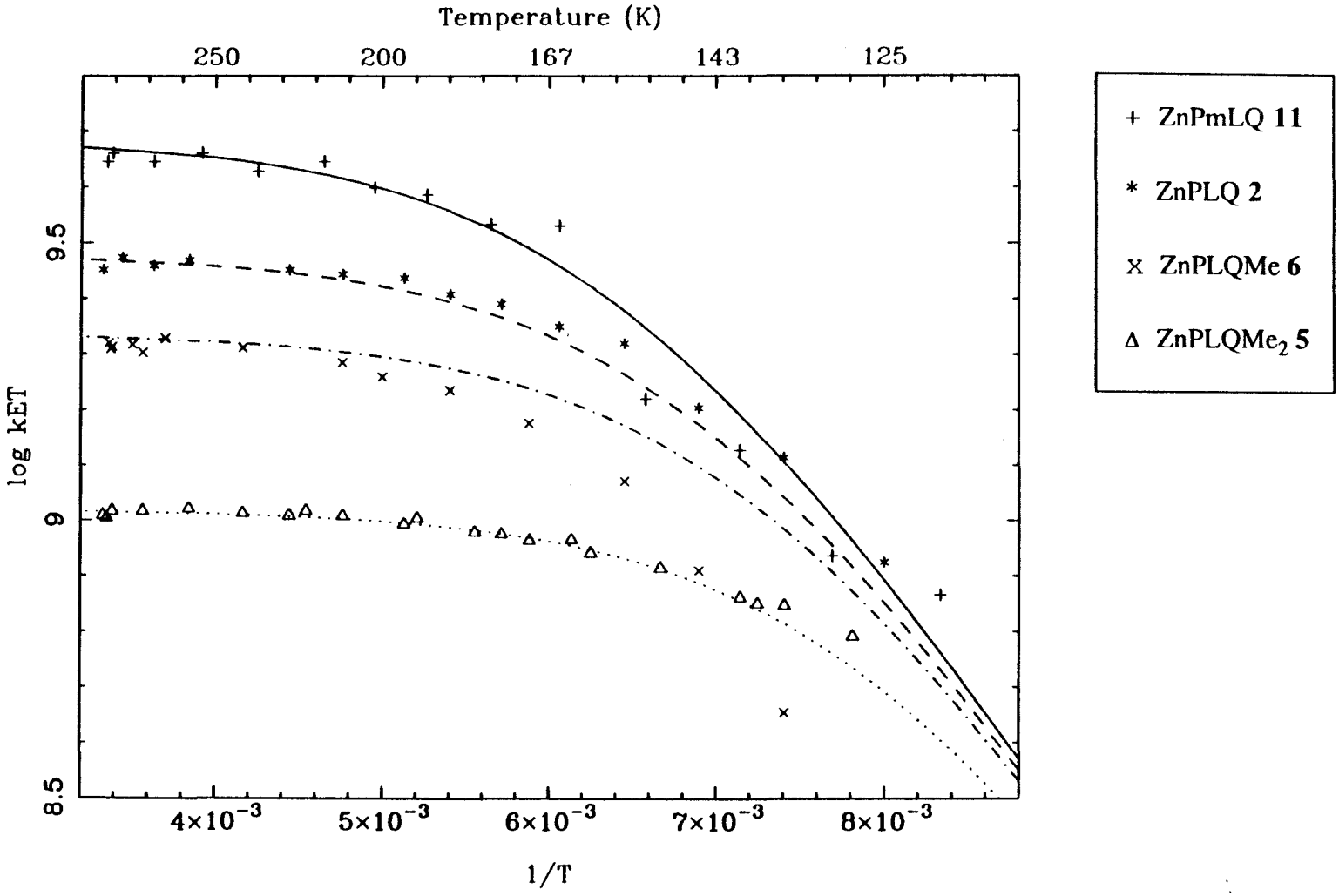

Figure 84. Semilogarithmic plot of electron transfer rates for ZnPLQ **2**, ZnPLQMe$_2$ **5**, ZnPLQMe **6**, and ZnPmLQ **11** in 2MTHF as a function of inverse temperature with fits (solid lines) based on solvent dynamics control of electron transfer rates.

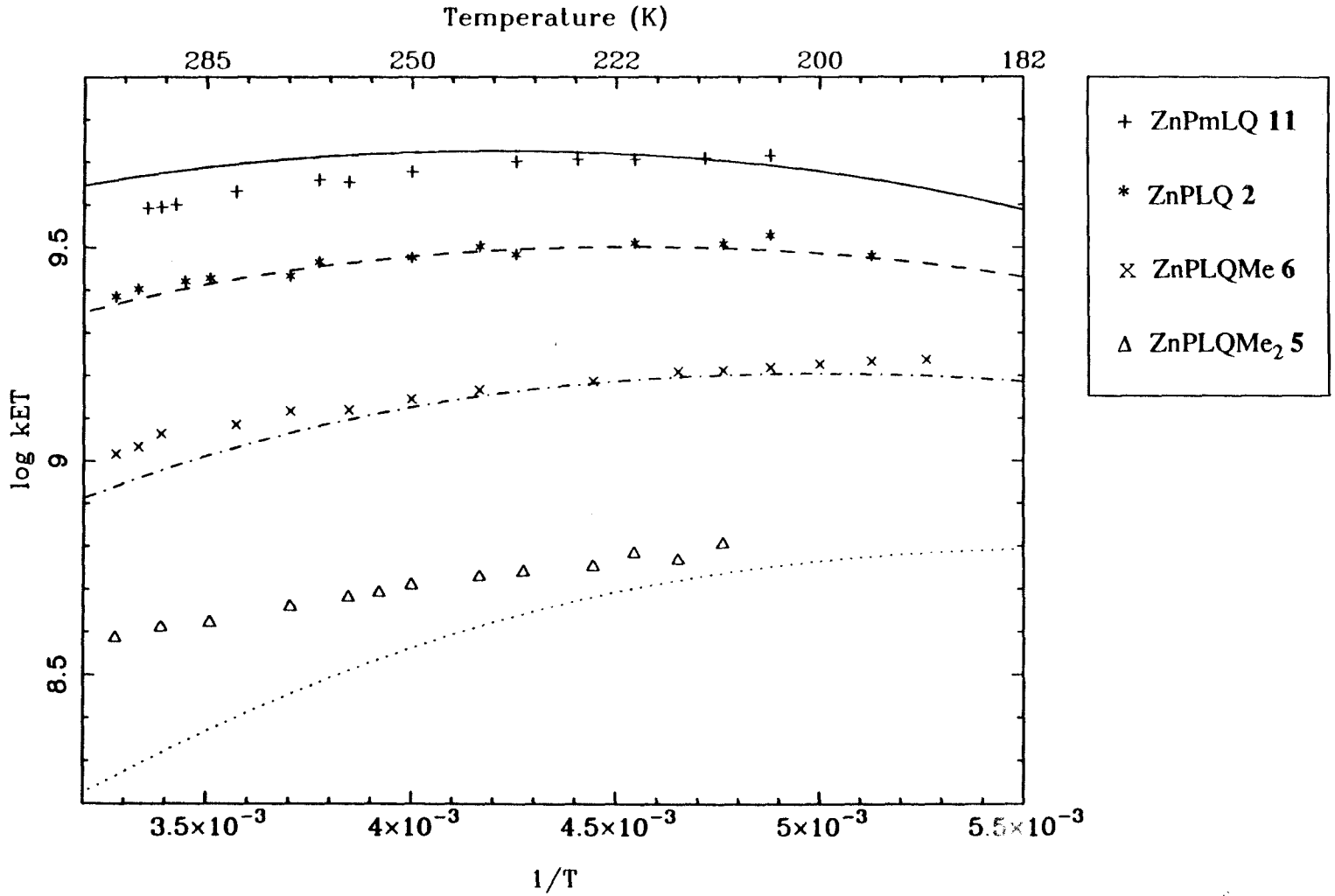

Figure 85. Semilogarithmic plot of electron transfer rates for ZnPLQ **2**, ZnPLQMe$_2$ **5**, ZnPLQMe **6**, and ZnPmLQ **11** in toluene as a function of inverse temperature with fits (solid lines) based on solvent dynamics control of electron transfer rates.

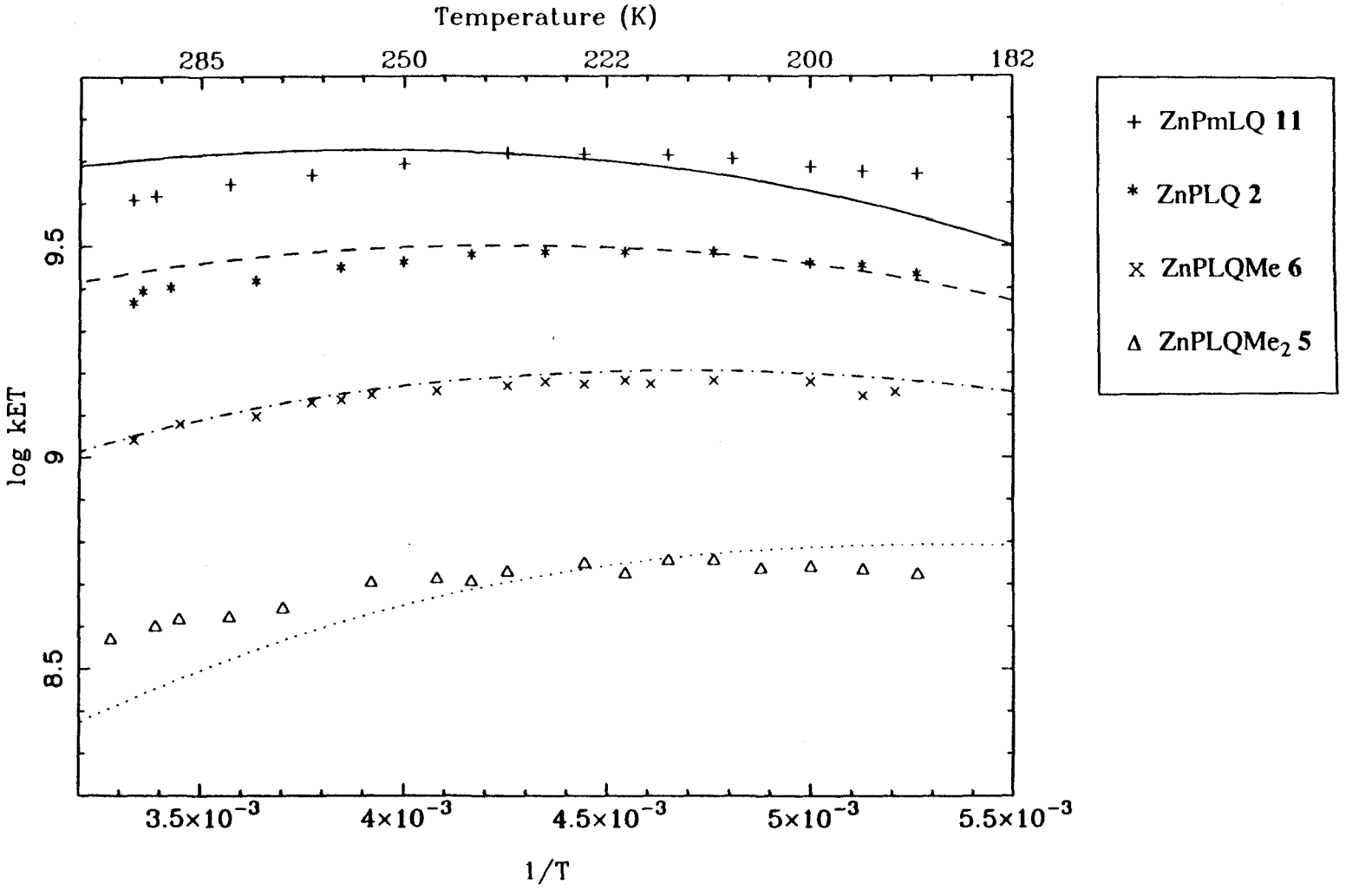

Figure 86. Semilogarithmic plot of electron transfer rates for ZnPLQ **2**, ZnPLQMe$_2$ **5**, ZnPLQMe **6**, and ZnPmLQ **11** in toluene-d_8 as a function of inverse temperature with fits (solid lines) based on solvent dynamics control of electron transfer rates.

Table XXVIII. Best fit parameters for temperature (solvent dynamics) dependence of k_{ET}.

	2MTHF	Toluene/Toluene-d_8
α	0.00	8.768×10^{-3}
γ	15.83	7.823×10^{-1}
k_{NA} ZnPLQ **2**	3.01×10^{9}	3.70×10^{9}
k_{NA} ZnPLQMe$_2$ **5**	1.04×10^{9}	7.25×10^{8}
k_{NA} ZnPLQMe **6**	2.17×10^{9}	1.87×10^{9}
k_{NA} ZnPmLQ **11**	4.84×10^{9}	6.20×10^{9}

toluene isotopomers, but both toluene and toluene-d_8 could be fit reasonably well using the same k_{NA} and coefficients. The values of k_{NA}, α, and γ used for the fits are listed in Table XXVIII. The ability to fit such diverse data with a similar equation based on a simple model is quite remarkable. The success of this model in fitting the data is evidence that solvent dynamics is the dominant factor in the temperature dependence of the electron transfer rates in these molecules. A more elaborate treatment, for example, one taking into account the frequency dependence of the friction with respect to the dielectric dispersion behavior of the solvent,[12] should generate better fits. Better fits might also be achieved by treating the dependence of the friction coefficients on the barrier height and shape. Theoretical treatments have shown the nature of the barrier to be quite critical in solvent dynamics limited reactions.[14-16] Measurement of the temperature dependence of experimentally determined solvation times[42] should also give better fits.

The picture of the electron transfer process in ZnPLQ **2** and its derivatives that emerges from the temperature studies is as follows. The intramolecular part of the electron

transfer does not seem to have much influence on the temperature dependence, but serves to determine the maximum rate, giving similar trends for all of the compounds. One possible explanantion for this is that the intramolecular barrier crossing is not activated even at 300 K, but the transition from the reactant surface to the product surface is by nuclear tunnelling. In non-polar solvents such as toluene, the rate is limited by the ability of the solvent to deactivate the system by removing excess vibrational energy after it has traversed the barrier to the product surface. This vibrational energy transfer is more efficient at lower temperatures; therefore, the rate increases with decreasing temperature. The higher efficiency reflects stronger coupling between the system and the solvent bath, rather than a change in the occupation of vibrational energy levels. In toluene-d_8, a point is eventually reached where the solvent reorganization required to accommodate the charge separated state is rate limiting, and the rate begins to decrease with decreasing temperature and increasing τ_L. The "nonadiabatic plateau"[23] region in toluene-d_8 is quite small. Unfortunately, ZnPLQ compounds are nearly insoluble in aliphatic hydrocarbons, where dielectric friction should be even lower than in aromatics. In 2MTHF, a relatively polar solvent, the system is already in the "nonadiabatic plateau" region at 300 K, and the rate is limited by the intramolecular barrier crossing. As the temperature is decreased, a point is reached where the solvent reorganization barrier is rate limiting, and the rate tracks the longitudinal relaxation time. If rates were measured in 2MTHF at higher temperatures, up to 400 or 500 K, the vibrational deactivation limit should be reached at some point, and the rates would decrease with increasing temperature. The acetonitrile data is difficult to interpret due to the very weak temperature dependence and small temperature range, but the 2MTHF results suggest that this regime should be part of the "nonadiabatic plateau" for this solvent, since the high dielectric makes τ_L very short. At extremely low temperatures (near a phase transition) in both polar and non-polar solvents, non-exponential decays are observed. This probably corresponds to Marcus and Sumi's "narrow window" or "non-

diffusing" limits, where non-exponential decays are a result of a time-dependent rate constant or a distribution of initial conditions.[17] Fluorescence quenching can be observed down to 25 K in these molecules,[71] but electron transfer can no longer be described by a single rate. A different type of model will be required to adequately fit this extremely low temperature data. Further investigations of the temperature dependence in this very low temperature regime are planned, and the results of these studies should reveal more about the controlling factors in electron transfer under these extreme conditions.

Chapter 9

Conclusions

The investigations of intramolecular electron transfer rates in porphyrin-quinone compounds detailed in the previous chapters have provided some new insights into electron transfer reactions. The studies described in Chapter 7 support the distance dependence model of Beratan, which predicts an exponential decay of electron transfer rates as a function of distance, with the decay constant determined by the nature of the bridge.[6] The temperature dependence investigations described in Chapter 8 are in accord with other work, both experimental and theoretical, which shows electron transfer rates should depend on the dielectric relaxation of the solvent. The unique nature of the work described here, however, is the apparent observation of the "Kramers turnover" and a solvent isotope effect in the toluene and toluene-d_8 data. This observation should spur further investigations which will further illumine the nature of the coupling between electron transfer reactions and solvent dynamics.

Chapter 10

Experimental Section

General.

Infrared spectra were recorded on a Shimadzu IR-435 spectrophotometer. Proton NMR spectra were recorded on a Varian Associates EM-390 or a JEOL GX-400 spectrometer. Chemical shifts are recorded in parts per million (ppm) downfield from tetramethylsilane (TMS) in δ units and coupling constants are in Hertz. NMR data are reported in this order: chemical shift, multiplicity (s=singlet, d=doublet, t=triplet, q=quartet, m=multiplet), number of protons, coupling constants. Electronic spectra were recorded on a Perkin-Elmer Lambda 4 spectrophotometer. Fluorescence spectra were recorded on a Perkin-Elmer Lambda 9 fluorimeter. Mass spectra (MS) of porphyrins were obtained at the Midwest Center for Mass Spectrometry (NSF Regional Instrumentation Facility) by fast atom bombardment (FAB) techniques. Other mass spectra were obtained at the MS Center at UC Riverside. Chemical analyses were performed at the Caltech Microanalytical Laboratory. All reactions were run under a positive pressure of argon unless otherwise noted. All reagents were used as received from standard suppliers with the following exceptions. 2-Methyltetrahydrofuran was distilled from calcium hydride, then stored under vacuum over sodium/benzophenone ketyl or over calcium hydride and redistilled by vacuum transfer immediately before use. Toluene-d_8 for time resolved spectroscopy (99.6+ atom% D) was obtained from Aldrich Chemical Co. or Cambridge Isotope Laboratories and distilled under vacuum before use. Other solvents for time-resolved spectroscopy (toluene, benzene, acetonitrile) were obtained as HPLC grade solvents packed under nitrogen in "Sure-Seal" bottles from Aldrich Chemical Co. These solvents were removed from the bottle by syringe, then vacuum transferred onto the sample.

Synthesis.

5-{4'-[4''-(2''',5'''-benzoquinone)bicyclo[2.2.2]octyl]phenyl}-2,3,7,8,12,13,17,18-octamethylporphyrinato Zinc(II) (2).[45] Free base porphyrin-hydroquinone **26** was dissolved in 40 ml CH_2Cl_2 and treated 0.8 g (3.3 mmol) PbO_2. The mixture was stirred in the dark for 30 minutes, then filtered to remove the oxidant. The resulting free base porphyrin-quinone was then treated with 4 ml methanol saturated with $Zn(OAc)_2 \cdot 2H_2O$. The mixture was stirred in the dark for 1 hour, then washed with H_2O (3 x 50 ml) and dried over Na_2SO_4. The drying agent was removed by filtration and the solvent was removed *in vacuo*, and the remaining metalloporphyrin-quinone was purified by chromatography (CH_2Cl_2; silica gel).

UV-Vis (CH_2Cl_2): 246.6, 336.3, 404.5, 533.8, 570.7 nm.

NMR ($CDCl_3$): δ 10.08 (s, 2H); 9.91 (s, 1H); 7.93 (d, 2H); 7.65 (d, 2H); 6.72 (s, 2H); 6.64 (s, 1H); 3.58 (s, 12H); 3.49 (s, 6H); 2.40 (s, 6H); 2.24 (m, 6H); 2.15 (m, 6H).

MS: m/e = 776; exact mass for $C_{48}H_{48}N_4O_2Zn$: calculated 776.3068, found 776.3065.[72]

5-(4'-*tert*-Butyl-phenyl)-2,3,7,8,12,13,17,18-octamethylporphyrinato Zinc(II) (4). Free base porphyrin **29** was dissolved in 15 ml CH_2Cl_2 and treated with 3 ml methanol saturated with $Zn(OAc)_2 \cdot 2H_2O$. The mixture was stirred for 1 hour, then washed with H_2O (2 x 75 ml) and dried over Na_2SO_4. The drying agent was removed by filtration and the solvent removed *in vacuo*. The porphyrin was purified by chromatography (CH_2Cl_2; silica gel).

UV-Vis (CH_2Cl_2): 332.1; 403.4; 534.2; 570.5 nm.

NMR ($CDCl_3$): δ 10.10 (s, 2H); 9.88 (s, 1H); 7.90 (d, 2H, J=8.1); 7.70 (d, 2H, J=8.1); 3.58 (s, 6H); 3,55 (s, 6H); 3.49 (s, 6H); 2.42 (s, 6H); 1.59 (s, 9H).

5-{4'-[4''-(3''',4'''-dimethyl-2''',5'''-benzoquinone)bicyclo[2.2.2] octyl]phenyl}-2,3,7,8,12,13,17,18-octamethylporphyrinato Zinc(II) (5). Free base porphyrin-hydroquinone **28** was dissolved in 100 ml CH_2Cl_2 and treated with 0.5 g (2.1 mmol) PbO_2. The mixture was stirred for 45 minutes, then filtered. The porphyrin solution was then treated with 2 ml methanol saturated with $Zn(OAc)_2 \cdot 2H_2O$. The mixture was stirred in the dark for 1 hour, then washed with H_2O (4 x 50 ml) and dried over Na_2SO_4. The drying agent was removed by filtration, and the solvent was removed *in vacuo*. The pure porphyrin-quinone was obtained by chromatography (CH_2Cl_2, silica gel).

UV-Vis (CH_2Cl_2): 260.5, 325.9, 403.8, 533.8, 570.0 nm.

NMR (CD_2Cl_2): δ 10.18 (s, 2H); 10.05 (s, 1H); 7.95 (d, 2H); 7.74 (d, 2H); 6.60 (s, 1H); 3.60 (s, 12H); 3.55 (s, 6H); 2.42 (s, 6H); 2.24 (m, 6H); 2.16 (m, 6H); 2.09 (s, 3H); 2.01 (s, 3H).

5-{4'-[4''-(4'''-methyl-2''',5'''-benzoquinone)bicyclo[2.2.2]octyl] phenyl}-2,3,7,8,12,13,17,18-octamethylporphyrinato Zinc (II) (6). This compound was the gift of A.D. Joran. The material was re-purified by chromatography (CH_2Cl_2, silica gel).

UV-Vis (CH_2Cl_2): 255.6, 404.6; 533.6; 570.4 nm.

NMR ($CDCl_3$): δ 10.10 (s, 2H); 9.95 (s, 1H); 7.96 (d, 2H); 7.65 (d, 2H); 6.62 (s, 1H); 6.58 (s, 1H); 3.59 (s, 12H); 3.49 (s, 6H); 2.40 (s, 6H); 2.24 (m, 6H); 2.11 (m, 6H); 2.04 (s, 3H).

5-{3'-[4''-(2''',5'''-benzoquinone)bicyclo[2.2.2]octyl]phenyl}-2,3, 7,8,12,13,17,18-octamethylporphyrinato Zinc (II) (11). A solution of free base-hydro-quinone **24** in 20 ml CH_2Cl_2 was treated with 2 ml methanol saturated with $Zn(OAc)_2 \cdot 2H_2O$ and stirred for 1 hour in the dark. The solution was washed with H_2O (3 x 75 ml) and saturated Na_2CO_3 (1 x 75 ml), then dried over Na_2SO_4. The drying agent

was removed by filtration and 0.5 g (2.1 mmol) PbO_2 was added. The mixture was stirred for 1 hour, then the oxidant was removed by filtration. The solvent was removed *in vacuo*, and the pure metalloporphyrin-quinone **11** was obtained by chromatography (CH_2Cl_2; silica gel).

UV-Vis (CH_2Cl_2): 248.7, 331.4, 404.5, 533.8, 570.0 nm.

NMR (CD_2Cl_2): δ 10.18 (s, 2H); 9.99 (s, 1H); 8.10 (s, 1H); 7.82 (m, 2H); 7.70 (m; 1H); 6.68 (s, 2H); 6.62 (s, 1H); 3.60 (s, 12H); 3.56 (s, 6H); 2.40 (s, 6H); 2.20 (m; 6H); 2.05 (m, 6H)

MS: m/e = 776; Exact mass for $C_{48}H_{48}N_4O_2Zn$: calculated 776.3068; found 776.3050

Dimethyl-4-cyano-4-(3'-methyl)phenylheptanedioate (12).[73] A solution of 2.0 g (12 mmol) Triton B (N-benzyltrimethylammonium hydroxide) in 20 ml dry dioxane was added dropwise over 30 minutes to a solution of 25.0 g (191 mmol) 3-methylbenzylcyanide and 35.0 g (406 mmol) freshly distilled methyl acrylate in 100 ml dry dioxane. When addition was complete, the mixture was brought to reflux for three hours. The mixture was allowed to cool, and 120 ml of anhydrous diethyl ether was added. The solution was washed with 0.1 M HCl (2 x 30 ml), water (2 x 30 ml), and 10% aqueous Na_2CO_3 (2 x 50 ml), then dried over Na_2SO_4. The drying agent was removed by filtration and the solvent was removed *in vacuo* to give a white solid. Recrystallization from diethyl ether/hexane gave 48.0 g (158 mmol, 83% yield) of (**12**) as white crystals.

NMR ($CDCl_3$): δ 7.220-7.067 (m, 4H); 3.55 (s, 6H); 2.47-2.02 (m, 8H), 2.31 (s, 3H).

IR (KBr): 2980, 2960, 2920, 2230, 1720, 1600, 1440, 1400, 1365, 1300, 1275, 1200, 1178, 1160, 1020, 880, 790, 715 cm^{-1}.

Analysis ($C_{17}H_{21}NO_4$): calculated C 67.31; H 6.98; N 4.62
found C 67.44; H 7.00; N 4.52.

MS: m/e = 303 (M+).

2-Carbomethoxy-4-cyano-4-(3'-methyl)phenylcyclohexanone (13).[74] A solution of 53.24 g (175.6 mmol) of diester (**12**) in 230 ml toluene with 1.5 ml methanol was added dropwise to a well-stirred slurry of 11.18 g (373 mmol) sodium hydride (80% in mineral oil) in 240 ml toluene with 1.5 ml methanol. When addition was complete, the mixture was brought to reflux for four hours, then allowed to cool. The sodium hydride was quenched by addition of 30 ml glacial acetic acid, and the reaction mixture was worked up in two 300 ml portions. Each was washed with water (2 x 150 ml), 10% aqueous Na_2CO_3 (100 ml), and saturated NaCl (100 ml). The portions were dried over Na_2SO_4. The drying agent was removed by filtration, and the solvent was removed *in vacuo* to give 45.95 g (169.4 mmol, 96.5% yield) of **13** as white crystals.

NMR ($CDCl_3$): δ 7.264-7.094 (m, 4H); 3.71 (s, 3H); 2.95-2.112 (m, 7H); 2.33 (s, 3H).

IR (KBr): 3050, 2990, 2970, 2875, 2210, 1660, 1620, 1440, 1410, 1390, 1370, 1300, 1285, 1240, 1220, 1190, 1060,820, 790,710 cm^{-1}.

Analysis ($C_{16}H_{17}NO_3$): calculated C 70.83; H 6.32; N 5.16

found C 72.13; H 6.93; N 4.74.

MS: m/e=271; exact mass for $C_{16}H_{17}NO_3$: calculated 271.1208, found 271.1222.

4-cyano-4-(3'-methyl)phenylcyclohexanone (14).[75] A mixture of 33.73 g (125.8 mmol) cyclohexanone **13** and 38.00 g (649.6 mmol) sodium chloride in 465 ml 85% aqueous dimethylsulfoxide was refluxed for four hours then allowed to cool. The mixture was poured into 250 ml ice water, then extracted with toluene (4 x 100 ml). The combined organics were washed with water (50 ml) and saturated NaCl (50 ml) then dried over Na_2SO_4. The drying agent was removed by filtration and the solvent was removed *in vacuo* to give a yellow oil that crystallized on standing. Recrystallization from diethyl ether gave 13.30 g (62.4 mmol, 49.6% yield) **14** as white crystals.

NMR (CDCl3): δ 7.311-7.148 (m, 4H); 2.935-2.228 (m, 8H); 2.372 (s, 3H).

IR (KBr): 3050, 2980, 2970, 2900, 2210, 1710, 1482, 1458, 1438, 1412, 1380, 1350, 1180, 1128, 960, 785, 700 cm^{-1}.

Analysis ($C_{14}H_{15}NO$): calculated C 78.84; H 7.09; N 6.57

found C 78.89; H 7.17; N 6.55.

MS: m/e = 213; exact mass for $C_{14}H_{15}NO$: calculated 213.1154, found 213.1160.

8-Cyano-8-(3'-methyl)phenyl-1,4-dioxaspiro[4.5]decane (15).[76] A solution of 13.08 g (61.4 mmol) cyclohexanone **14** and 0.82 g (4.8 mmol) *p*-toluenesulfonic acid in 40 ml toluene and 65 ml ethylene glycol was distilled azeotropically. The azeotopic distillate was collected in a Dean-Stark distillation head and distillation continued until 30 ml of distillate had been collected. The reaction was allowed to cool, and 100 ml 10% aqueous Na_2CO_3 and 200 ml diethyl ether were added. The organic phase was separated and washed with water (80 ml) and saturated NaCl (80 ml) then dried over Na_2SO_4. The drying agent was removed by filtration and the solvent was removed *in vacuo* to give 15.17 g (59.0 mmol, 96% yield) **15** as a pale yellow oil.

NMR (CDCl3): δ 7.305-7.101 (m, 4H); 4.015-3.931 (m, 4H); 2.355 (s, 3H), 2.166-1.829 (m, 8H).

4-Acetyl-4-(3'-methyl)phenylcyclohexanone (16).[76] To a well stirred solution of 15.17 g (59.0 mmol) spirodecane **15** in 200 ml toluene in an oven dried flask under argon was added dropwise 79 ml of a 3.0 M solution of methylmagnesium bromide in diethyl ether. After addition was complete, the mixture was refluxed for forty-five hours, then allowed to cool. After dropwise addition of 250 ml 2.0 N HCl, the mixture was refluxed an additional five hours then allowed to cool again. The organics were separated and the aqueous phase extracted with toluene (3 x 75 ml). These toluene extracts were combined with the other organics and then washed with 10% aqueous Na_2CO_3 (2 x 75 ml), water (75 ml), and saturated NaCl (75 ml). The combined organics were dried

over Na_2SO_4, filtered, and the solvent removed *in vacuo* to give a brown oil. Vacuum distillation (bp 145° C; 5 torr) gave 10.40 g (45.2 mmol, 76% yield) of **16** as a clear oil.

NMR ($CDCl_3$): δ 7.266-7.035 (m, 4H); 2.588-2.251 (m, 8H), 2.343 (s, 3H); 1.978 (s, 3H)

Analysis ($C_{15}H_{18}O_2$): calculated C 78.23; H 7.88

found C 78.47; H 8.47.

MS: m/e = 230; exact mass for $C_{15}H_{18}O_2$: calculated 230.1307, found 230.1304.

1-Ethoxy-4-(3'-methyl)phenylbicyclo[2.2.2]octan-3-one (17).[77] A solution of 10.40 g (45.2 mmol) cyclohexanone **16** and 21.50 g (145 mmol) triethylorthoformate in 100 ml absolute ethanol was cooled to 0° C. Anhydrous hydrogen chloride was bubbled through the solution for 15 minutes, leaving the solution a deep reddish brown. The solution was refluxed for 1 hour then the solvents were removed *in vacuo*. Water (100 ml) was added, and the mixture was extracted with diethyl ether (5 x 50 ml). The combined organic extracts were washed with saturated $NaHCO_3$ (2 x 40 ml) and saturated NaCl (40 ml) then dried over $MgSO_4$. The drying agent was removed by filtration, and the solvent was removed *in vacuo* to give 8.62 g (33.4 mmol, 73.9% yield) **17** as a light brown oil. Crystallization from diethyl ether gave white crystals of **17**.

NMR ($CDCl_3$): δ 7.278-6.996 (m, 4H); 3.518 (q, 2H); 2.632 (s, 2H); 2.372 (s, 3H); 2.296-1.913 (m, 8H); 1.236 (t, 3H).

IR (KBr): 2950, 2850, 1720, 1380, 1105, 780, 695 cm^{-1}.

Analysis ($C_{17}H_{22}O_2$): calculated C 79.03; H 8.58

found C 78.96; H 8.55.

MS: m/e = 258; exact mass for $C_{17}H_{22}O_2$: calculated 258.1620, found 258.1606.

1-Ethoxy-4-(3'-methyl)phenylbicyclo[2.2.2]octane (18).[78] A mixture of 3.00 g (11.6 mmol) bicyclo[2.2.2]octanone **17**, 4.00 g (71.3 mmol) potassium hydroxide, and 3.8 ml (3.7 g; 74 mmol) hydrazine hydrate in 75 ml bis-(2-hydroxyethyl)-

ether was refluxed for 5 hours. The mixture was allowed to cool, then filtered through celite, and rinsed through with 100 ml diethyl ether and 75 ml dichloromethane. The organic filtrate was washed with water (2 x 50 ml) and saturated NaCl (50 ml) and dried over Na_2SO_4. The drying agent was removed by filtration and the solvent was removed *in vacuo* to give a brown oil. Recrystallization from methanol gave 1.32 g (5.4 mmol, 47% yield) of **18** as white crystals.

NMR ($CDCl_3$): δ 7.183-6.961 (m, 4H); 3.416 (q, 2H, J=7.0); 2.313 (s, 3H); 1.956-1.754 (m, 12H); 1.153 (t, 3H, J=7.0).

IR (KBr): 3050, 2940, 2910, 2860, 1605, 1492, 1454, 1382, 1355, 1105, 787, 700 cm^{-1}.

Analysis ($C_{17}H_{24}O$): calculated C 83.55; H 9.90

found C 83.34; H 9.75.

MS: m/e = 244; exact mass for $C_{17}H_{24}O$: calculated 244.1827, found 244.1817.

2',5'-Dimethoxy-3''-methyl-1,4-diphenylbicyclo[2.2.2]octane (19). A solution of 0.99 g (4.05 mmol) bicyclo[2.2.2]octane **18**, 12 mg (0.070 mmol) *p*-toluenesulfonic acid, and 5.01 ml (5.78 g; 40.7 mmol) boron trifluoride etherate in 80 ml trichloroethylene was refluxed for one hour. A solution of 3.0 g (21.7 mmol) 1,4-dimethoxybenzene in 20 ml trichloroethylene was then added dropwise and the mixture refluxed for 27 hours. The mixture was allowed to cool and then poured into 200 ml 10% Na_2CO_3. The organic layer was separated and the aqueous layer extracted with dichloromethane (2 x 50 ml). The combined organics were washed with water (2 x 50 ml) and saturated NaCl (2 x 50 ml), and dried over Na_2SO_4. The drying agent was removed by filtration, and the solvent was removed *in vacuo*. Chromatography (95:5 toluene-dichloromethane, silica, R_f=0.8) gave 0.72 g (2.1 mmol, 52% yield) **19** as a pale yellow gum which crystallized on standing.

NMR ($CDCl_3$): δ7.215-6.977 (m, 4H); 6.842-6.663 (m, 3H); 3.774 (s, 3H); 3.743 (s, 3H); 2.343 (s, 3H); 2.324-1.903 (m, 12H).

IR (KBr): 2940, 2860, 1605, 1585, 1492, 1459, 1383, 1220, 1042, 1022, 868, 794, 777, 723, 699 cm^{-1}.

Analysis ($C_{23}H_{28}O_2$): calculated C 82.10; H 8.39

found C 82.18; H 8.42

MS: m/e = 336; exact mass for $C_{23}H_{28}O_2$: calculated 336.2089 , found 336.2075.

2',5'-Dimethoxy-3''-bromomethyl-1,4-diphenylbicyclo[2.2.2]octane (20). A solution of 260 mg (0.77 mmol) diphenylbicyclo[2.2.2]octane **19**, 180 mg (1.01 mmol) N-bromosuccinimide, and 50 mg (0.21 mmol) benzoyl peroxide in 30 ml carbon tetrachloride was refluxed for nine hours. The mixture was allowed to cool and the solids were removed by filtration. The solvent was removed *in vacuo*, and the crude product was used without further purification.

NMR ($CDCl_3$): δ 7.5-7.0 (m, 4H); 6.62 (m, 2H); 6.52 (m, 1H); 4.37 (s, 2H); 3.70 (s, 3H); 3.60 (s, 3H); 1.96 (m, 6H); 1.80 (m, 6H).

2',5'-Dimethoxy-3''-formyl-1,4-diphenylbicyclo[2.2.2]octane (21).[79] A mixture of 80 mg (0.19 mmol) benzylbromide **20** and 125 mg (1.49 mmol) sodium bicarbonate in 15 ml dimethylsulfoxide was refluxed for four hours, then poured into 100 ml ice water. The solution was extracted with ethyl acetate (4 x 50 ml) and dichloromethane (2 x 50 ml) and the combined organics were washed with saturated NaCl (2 x 40 ml). The organics were dried over Na_2SO_4, filtered, and the solvent was removed *in vacuo*. Chromatography (1:1 ether-hexane, silica, R_f=0.6) gave 28 mg (0.080 mmol, 42% yield) **21** as a pale yellow oil.

NMR ($CDCl_3$): δ 10.00 (S, 1H); 8.08-7.50 (m, 4H); 6.80 (s, 2H); 6.70 (s, 1H); 3.80 (s, 3H); 3.76 (s, 3H); 2.09 (m, 6H); 1.95 (m, 6H).

1,19-Dideoxy-2,3,7,8,12,13,17,18-octamethyl-a,c-biladiene dihydrobromide (22). This compound was synthesized by the method of Joran.[45] A mixture of 123 mg (1.29 mmol) 3,4-dimethylpyrrole (the gift of B.A.Leland) and 101 mg (0.391

mmol) 5,5′-diformyl-3,3′,4,4′-tetramethyldipyrrylmethane (the gift of A.D.Joran) in 10 ml methanol in a foil-wrapped Ehrlenmeyer flask was treated with 1 ml of 48% hydrobromic acid. The mixture was swirled for several minutes in a 95° C water bath, covered with foil to exclude light, and set aside to stand at room temperature for 3 hours. The precipitated red-brown solid was filtered and washed with a solution of methanol and 48% hydrobromic acid, then with anhydrous diethyl ether to give 166 mg (0.289 mmol, 73.9%) of a,c-biladiene hydrobromide **22**. The powdery product was used immediately or stored under argon at -20° C.

NMR ($CDCl_3$): δ 7.64 (s ,2H); 7.23 (s, 2H); 5.24, (s, 2H); 2.31 (s, 6H); 2.26 (s, 6H); 2.09 (s, 6H); 1.95 9s, 6H)

5-{3′-[4″-(2‴,5‴-dimethoxyphenyl)bicyclo[2.2.2]octyl]phenyl}-2,3,7,8,12,13,17,18-octamethylporphyrin (23).[80] A mixture of 60 mg (0.104 mmol) a,c-biladiene hydrobromide **22** and 28 mg (0.080 mmol) aldehyde **21** in 8 ml methanol was treated with several drops of glacial acetic acid saturated with anhydrous HBr. The mixture was gently refluxed in the dark for 45 hours, then quenched with $NaHCO_3$. The resulting mixture was filtered and rinsed through with numerous 10 ml portions of CH_2Cl_2. The resulting red-brown solution was concentrated and chromatographed (98:2 CH_2Cl_2:CH3CN; silica gel) to give the pure porphyrin.

UV-Vis (CH_2Cl_2): 229.2, 401.7, 501.1, 533.8, 570.7, 622.8 nm.

NMR ($CDCl_3$): δ 10.12 (s, 2H); 9.87 (s, 1H); 8.12 (s, 1H); 7.80 (m, 2H); 7.65 (m, 1H); 6.80 (m, 2H); 6.68 (m, 1H); 3.82 (s, 3H); 3.77 (s, 3H); 3.60 (s, 6H); 3.57 (s, 6H); 3.50 (s, 6H); 2.42 (s, 6H); 2.18 (m, 12H); -3.17 (s, 1H); -3.32 (s, 1H).

5-{3′-[4″-(2‴, 5‴-dihydroxyphenyl)bicyclo[2.2.2]octyl]phenyl}-2,3,7,8,12,13,17,18-octamethylporphyrin (24). A solution of free base porphyrin-dimethoxybenzene **23** in 50 ml CH_2Cl_2 in a 3-neck flask was cooled to 0° C

under argon. A solution of 1.4 g (3.6 mmol) boron tri-iodide in 5 ml CH_2Cl_2 was added dropwise via syringe. The mixture was stirred for 90 minutes, then poured into 50 ml dilute ammonium hydroxide. The organic layer was separated and washed with 2 x 50 ml saturated $NaCO_3$, then dried over Na_2SO_4. The drying agent was removed by filtration, and the solvent was removed *in vacuo*. The free base porphyrin-hydroquinone was purified by chromatography (95:5 CH_2Cl_2:CH_3CN; silica gel).

UV-Vis (CH_2Cl_2): 247.2, 401.7, 501.1, 533.8, 570.7, 622.8 nm.

NMR (CD_2Cl_2): δ 10.18 (s, 2H); 9.97 (s, 1H); 7.85 (m, 1H); 7.70 (m, 2H); 7.57 (m, 1H); 6.68 (s, 2H); 6.57 (s, 1H); 3.62 (s, 6H); 3.59 (s, 6H); 3.50 (s, 6H); 2.42 (s, 6H); 2.28 (m, 6H); 2.17 (m, 6H).

5-{4'-[4''-(2''',5'''-dimethoxyphenyl)bicyclo[2.2.2]octyl]phenyl}-2,3,7,8,12,13,17,18-octamethylporphyrin (25).[45] A mixture of 68.8 mg (0.20 mmol) 1,4-(2',5'-dimethoxy-4''-formyl)diphenylbicyclo[2.2.2]octane (the gift of A.D. Joran) and 120 mg (0.21 mmol) a,c-biladiene hydrobromide **22** in 13 ml methanol was treated with a few drops of acetic acid saturated with anhydrous HBr then gently refluxed in the dark for 38 hours. The mixture was neutralized with $NaHCO_3$, then filtered and rinsed with methanol and CH_2Cl_2. The solvent was removed *in vacuo* and the porphyrin-dimethoxybenzene was purified by chromatography (98:2 CH_2Cl_2:CH_3CN; silica gel).

UV-Vis (CH_2Cl_2): 332.0, 403.3, 501.0, 533.5, 571.1, 625.3 nm.

NMR ($CDCl_3$): δ 10.10 (s, 2H); 9.88 (s, 1H); 7.89 (d, 2H, J=8.3); 7.67 (d, 2H, J=8.1); 6.93 (d, 1H, J=3.2); 6.85 (d, 1H, J=8.8); 6.73 (m, 1H); 3.87 (s, 3H); 3.81 (s, 3H); 3.58 (s, 6H); 3.55 (s, 6H); 3.49 (s, 6H); 2.40 (s, 6H); 2.24 (m, 12H); -3.2 (s, 1H); -3.4 (s, 1H).

5-{4'-[4''-(2''',5'''-dihydroxyphenyl)bicyclo[2.2.2]octyl]phenyl}-2,3,7,8,12,13,17,18-octamethylporphyrin (26). A solution of free base porphyrin-dimethoxybenzene 25 in 30 ml CH_2Cl_2 in a 3-neck flask was cooled to 0^o C

under argon. A solution of 0.3 g (0.77 mmol) boron tri-iodide in 2 ml CH_2Cl_2 was added dropwise via syringe. The mixture was stirred at 0^o C for 40 minutes, then poured into 70 ml dilute ammonium hydroxide. The organic layer was separated and washed with H_2O (2 x 50 ml), then dried over Na_2SO_4. The drying agent was removed by filtration, and the solvent removed *in vacuo*. The free base porphyrin-hydroquinone was purified by chromatography (95:5 CH_2Cl_2:CH_3CN; silica gel).

NMR ($CDCl_3$): δ 10.10 (s, 2H); 9.90 (s, 1H); 7.93 (d, 2H); 7.67 (d, 2H); 6.72 (m, 2H); 6.63(m, 1H); 3.59 (s, 6H); 3.55 (s, 6H); 3.48 (s, 6H); 2.40 (s, 6H); 2.23 (m, 6H); 2.15 (m, 6H); -3.25 (s, 2H)

5-{4'-[4''-(3''',4'''-dimethyl-2''',5'''-dimethoxyphenyl)bicyclo [2.2.2]octyl]phenyl}-2,3,7,8,12,13,17,18-octamethylporphyrin (27).[45] A mixture of 70 mg (0.18 mmol) of the appropriate aldehyde (the gift of A.D. Joran) and 97.6 mg (0.17 mmol) a,c-biladiene hydrobromide **22** in 12 ml methanol was treated with a few drops of glacial acetic acid saturated with anhydrous HBr, then gently refluxed in the dark for 38 hours. The mixture was neutralized with $NaHCO_3$, then filtered. The filtrate was washed with methanol, then with CH_2Cl_2. The solvent was removed *in vacuo*, and the porphyrin-dimethoxybenzene was purified by chromatography (95:5 CH_2Cl_2:CH_3CN; silica gel).

UV-Vis: 284, 404, 502, 534, 570, 623 nm.

NMR ($CDCl_3$): δ 10.12 (s, 2H); 9.89 (s, 1H); 7.91 (d, 2H); 7.69 (d, 2H); 6.77 (s, 1H); 3.81 (s, 3H); 3.77 (s, 3H); 3.59 (s, 6H); 3.55 (s, 6H); 3.48 (s, 6H); 2.40 (s, 6H); 2.22 (m, 12H); 2.18 (s, 3H); 2.15 (s, 3H); -3.20 (s, 1H); -3.37 (s, 1H).

5- {4'- [4''- (3''', 4'''-dimethyl-2''', 5'''- dihydroxyphenyl)bicyclo [2.2.2]octyl]phenyl}-2,3,7,8,12,13,17,18-octamethylporphyrin (28). A

solution of free base porphyrin-dimethoxybenzene **27** in 50 ml CH_2Cl_2 in a 3-necked flask was cooled to 0^o C in an ice bath while under argon. A solution of 0.60 g (1.5 mmol) boron tri-iodide in 2 ml CH_2Cl_2 was added by syringe while stirring vigorously. The solution was stirred at 0^o C for 1 hour, then poured into 50 ml dilute ammonium hydroxide. The organic layer was separated and washed with 2 x 25 ml saturated $NaCO_3$ then 2 x 25 ml H_2O. The porphyrin solution was dried over Na_2SO_4, filtered, and the solvent was removed *in vacuo*. The free base porphyrin-hydroquinone **28** was purified by chromatography (9:1 CH_2Cl_2:CH_3CN; silica gel).

5-(4'-*tert*-Butylphenyl)-2,3,7,8,12,13,17,18-octamethyl porphyrin (29).[45] A mixture of 0.5 ml (3 mmol) 4-*tert*-butylbenzaldehyde and 71.8 mg (0.125 mmol) a,c-biladiene hydrobromide **22** in 15 ml methanol was treated with 5 drops glacial acetic acid saturated with anhydrous HBr then gently refluxed in the dark for 45 hours. The mixture was neutralized with $NaHCO_3$, then filtered and washed with methanol and CH_2Cl_2. The solvent was removed *in vacuo*, and the porphyrin was purified by chromatography (98:2 CH_2Cl_2:CH_3CN; silica gel).

UV-Vis (CH_2Cl_2): 280, 402, 500, 534, 570, 623 nm.

NMR ($CDCl_3$): δ 10.10 (s, 2H); 9.88 (s, 1H); 7.90 (d, 2H, J=8.1); 7.70 (d, 2H, J=8.1); 3.58 (s, 6H); 3,55 (s, 6H); 3.49 (s, 6H); 2.42 (s, 6H); 1.59 (s, 9H); -3.26 (s, 2H).

Time-Resolved Spectroscopy.

Samples for time-correlated single photon counting were repurified by chromatography immediately prior to measurement. For room temperature measurements, an aliquot of the chromatographed solution was filtered through 0.5 micron Millipore filters into a special sample cell with a Teflon stopcock and sidearm for degassing. The chromatography solvent was removed by pumping on a vacuum line trapped with liquid N_2

for several hours. The spectroscopy solvent was then filtered (or vacuum transferred) into the cell, and the solution degassed through 3 freeze-pump-thaw cycles. For variable temperature measurements, an aliquot of the chromatographed porphyrin solution was pipetted into a sample holder with a septum inlet and the chromatography solvent was removed by pumping on a vacuum line trapped with liquid nitrogen for several hours. The spectroscopy solvent was then vacuum transferred onto the porphyrin sample. The solution was then filtered through 0.5 micron Millipore filters into a low temperature cuvette (Starna) and deaerated by bubbling with ultra high purity helium for ten minutes. The cuvette was sealed with Teflon tape and a Teflon stopper, and placed in the cuvette holder for the Oxford continuous flow low temperature spectroscopy dewar. The sample was allowed to equilibrate at the initial temperature for 15 minutes, and at each subsequent temperature for at least 10 minutes. Liquid helium was used as the cryogenic liquid. Temperature control was provided to within 0.1 K with an Oxford ITC4 temperature control unit. The sample was checked for demetallation by electronic absorption spectroscopy after each low temperature run.

The laser system used for single photon counting (Figure 87) consisted of a cavity dumped dye laser (Coherent; Rhodamine 6G laser dye) synchronously pumped by the doubled output from a mode-locked cw Nd:YAG laser (Quantronix 416; Coherent mode locker). The pulse widths from the dye laser were consistently less than 60 psec FWHM. The dye laser beam was attenuated with neutral density filters and focused through the cell with a 25 cm lens. Fluorescence from the sample was collected after passing through a dichroic sheet polarizer set at 54.7^{o} to the excitation polarization to minimize rotational depolarization effects, then a 610 nm cut-off filter (Schott RG610) and a 10 nm bandpass monochromator (ISA) set at 630 nm to exclude scatter from the laser excitation pulse, and

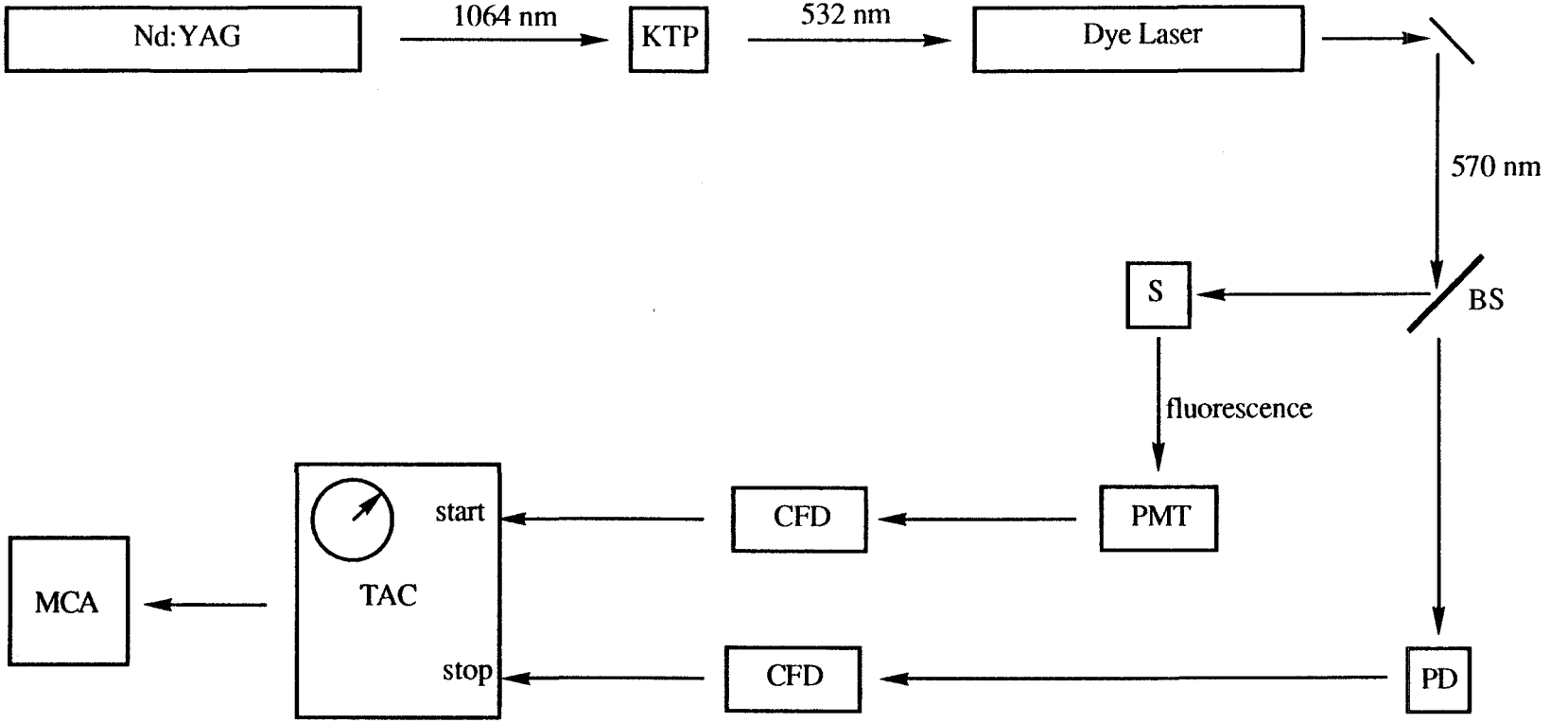

Figure 87. Picosecond laser spectroscopy apparatus for single photon counting. Nd:YAG=pump laser; KTP= doubling crystal; BS= beamsplitter; PD=photodiode; S=sample; PMT=photomultiplier tube; CFD= constant fraction discriminator; TAC=time to amplitude converter; MCA= multichannel analyzer.

the emission was detected by a Hamamatsu R-1564U multichannel plate photomultiplier tube. The output signal from the MCP-PMT was amplified (Hewlett Packard 8447 amplifier, 0.1-1300 MHz bandwidth) and sent through a constant fraction discriminator (Tennelec 455) to generate a start pulse for the time to amplitude converter (Ortec 457). The stop pulse for the TAC was generated by detecting part of the excitation pulse (split off before reaching the sample) with a photodiode (Hamamatsu) and passing the amplified signal from the diode through a constant fraction discriminator and appropriate electronic delay ciricuits (Ortec 475A). The pulses from the TAC were collected on a Ortec-Norland 5600 multichannel analyzer set up for peak height analysis. Decays were collected until the maximum channel was in the 8000 to 10000 count range to give good statistics.

Fluorescence decays were fit using an iterative non-linear least squares program written by B.A. Leland.[46] This program fit up to three exponential components with iterative reconvolution with a system response function. This system response function was acquired by detecting scattered light from the excitation pulses using a colloidal suspension in water. Most of the fits converged to a goodness of fit parameter (χ^2) less than 1.200, but with the low temperature optical dewar (with 6 extra windows to distort the optical quality of the excitation and fluorescence) in place, fits with higher χ^2 were accepted.

References and Notes

1. a) DeVault, D. "Quantum Mechanical Tunnelling in Biological Systems," 2nd ed., Cambridge University Press, Cambridge: 1984. b) Sutin, N. *Acc. Chem. Res.* **1982**, *15*, 275-282. c) Newton, M.D.; Sutin, N. *Ann. Rev. Phys. Chem.* **1984**, *35*, 437-480. d) Mauzerall, D.; Ballard, S.G. *Ann. Rev. Phys. Chem.* **1982**, *33*, 377-407. e) Gust, D.; Moore, T.A. *Science* **1989**, *244*, 35-41.
2. a) Marcus, R.A. *J. Chem. Phys.* **1956**, *24*, 966-978. b) Marcus, R.A. *J. Chem.Phys.* **1965**, *43*, 679-701. c) Marcus, R.A. in "Tunnelling in Biological Systems", Chance, B.; DeVault, D.; Frauenfelder, H.; Marcus, R.A.; Schrieffer, J.R.; Sutin, N. eds. Academic Press, New York: 1979, 109-127.
3. a) Eyring, H. *J. Chem. Phys.* **1935**, *3*, 107-115. b) Eyring, H. *Chem. Rev.* **1935**, *17*, 65-77.
4. a) Landau, L. *Phys. Z. Sowj. U.* **1932**, *1*, 88-98. b) Zener, C. *Proc. R. Soc. Lond.* **1932**, *A137*, 696-702.
5. Sutin, N. in "Supramolecular Photochemistry," Balzani, V. ed., D. Reidel Publishing, Dordrecht: 1987.
6. a) Beratan, D.N. *J. Am. Chem. Soc.* **1986**, *108*, 4321-4326. b) Onuchic, J.N.; Beratan, D.N. *J. Am. Chem. Soc.* **1987**, *109*, 6771-6778.
7. Siders, P.; Cave, R.J.; Marcus, R.A. *J. Chem. Phys.* **1984**, *81*, 5613-5624.
8. Hopfield, J.J. *Proc. Nat. Acad. Sci. USA* **1974**, *71*, 3640-3644.
9. Jortner, J. *J. Chem. Phys.* **1976**, *64*, 4860-4867.
10. For recent reviews of transition state theory, see: a) Pechukas, P. *Ann. Rev. Phys. Chem.* **1981**, *32*, 159-177. b) Truhlar, D.G.; Hase, W.L.; Hynes, J.T. *J. Phys. Chem.* **1983**, **87**, 2664-2682.
11. Kramers, H.A. *Physika* **1940**, *7*, 284-304.
12. a) Hynes, J.T. *Ann. Rev. Phys. Chem.* **1985**, *36*, 573-597. b) Hynes, J.T. *J. Stat.*

Phys. **1986**, *42*, 149-168. c) Maroncelli, M.; MacInnis, J.; Fleming, G.R. *Science*, **1989**, *243*, 1674-1681. d) Hanggi, P. *J. Stat. Phys.* **1986**, *42*, 105-148.

13. Van der Zwan, G.; Hynes, J.T. *J. Chem. Phys.* **1982**, *76*, 2993-3001.
14. Morillo, M.; Cukier, R.I. *J. Chem. Phys.* **1988**, *89*, 6736-6743.
15. Calef, D.F.; Wolynes, P.G. *J. Phys. Chem.* **1983**, *87*, 3387-3400.
16. Calef, D.E.; Wolynes, P.G. *J. Chem. Phys.* **1983**, **78**, 470-482.
17. Sumi, H.; Marcus, R.A. *J. Chem. Phys.* **1986**, *84*, 4894-4914.
18. Rips, I.; Jortner, J. *J. Chem. Phys.* **1987**, *87*, 2090-2104.
19. Rips, I.; Jortner, J. *J.Chem. Phys.* **1987**, *87*, 6513-6519.
20. Rips, I.; Jortner, J. *J. Chem. Phys.* **1988**, *88*, 818-822.
21. Skinner, J.L.; Wolynes, P.G. *J. Chem. Phys.* **1978**, *69*, 2143-2150.
22. "The Pade´ Approximant in Theoretical Physics," Baker, G.A.; Gammel, J.L. eds., Academic Press, New York, NY: 1970.
23. Onuchic, J.N.; Wolynes, P.G. *J. Phys. Chem.* **1988**, *92*, 6495-6503.
24. a) Deisenhofer, J.; Epp, O.; Miki, K.; Huber, R.; Michel, H. *J. Mol. Biol.* **1984**, *180*, 385-398. b) Deisenhofer, J.; Epp., O.; Miki, K.; Huber, R.; Michel, H. *Nature* **1985**, *318*, 618-624. c) Michel, H.; Epp, O.; Deisenhofer, J. *EMBO J.* **1986**, *5*, 2445-2451. d) Michel, H.; Deisenhofer, J. *Chem. Scr.* **1987**, *27B*, 173-180. e) Michel, H.; Deisenhofer, J. *Biochemistry* **1988**, *27*, 1-7.
25. a) Allen, J.P.; Feher, G.; Yeates, T.O.; Komiya, H.; Rees, D.C. *Proc. Nat. Acad. Sci. (USA)* **1987**, *84*, 5730-5734. b) Allen, J.P.; Feher, G.; Yeates, T.O.; Komiya, H.; Rees, D.C. *Proc. Nat. Acad. Sci. (USA)* **1987**, *84*, 6162-6166. c) Yeates, T.O.; Komiya, H.; Rees, D.C.; Allen, J.P.; Feher, G. *Proc. Nat. Acad. Sci. (USA)* **1987**, *84*, 6438-6442.
26. The *Rps. viridis* structure also includes a bound cytochrome which serves to reduce the special pair after photo-oxidation.

27. Only one of the quinones was found in the *Rps. viridis* structure, the other presumably having been lost during purification.

28. A bacteriochlorophyll (the accessory bacteriochlorophyll B_A) lies approximately between the special pair and the bacteriopheophytin acceptor. Although there have been some reports of observing electron transfer to this bacteriochlorophyll (Shuvalov, V.A.; Klevanik, A.V. *FEBS Lett.* **1983**, *160*, 51-55.) the consensus is that the state $D^+B_A^-$ does not exist as a resolvable intermediate.

29. In some species, this cytochrome is bound to the reaction center protein complex; in other species, the cytochrome is a diffusing species.

30. a) "The Photosynthetic Bacterial Reaction Center: Structure and Dynamics,: Breton, J.; Vermeglio, A. eds. Plenum, New York, NY: 1987. b) "Antennas and Reaction Centers of Photosynthetic Bacteria," Michel-Beyerle, M.E. ed., Springer-Verlag, Berlin: 1985. c) "New Comprehensive Biochemistry Volume 15: Photosynthesis," Amesz, J. ed., Elsevier, Amsterdam: 1987. d) "The Photosynthetic Bacteria," Clayton, R.K. ed., Plenum, New York, NY: 1978. e) Blankenship, R.E.; Parson, W.W. in "Photosynthesis in Relation to Model Systems," Barber, J. ed., Elsevier, Amsterdam: 1979.

31. DeVault, D.; Chance, B. *Biophys. J.* **1966**, *6*, 825-847.

32. a) Kirmaier, C.; Holten, D.; Parson, W.W. *Biochim. Biophys. Acta* **1985**, *810*, 34-48. b) Kirmaier, C.; Blankenship, R.E.; Holten, D. *Biochim. Biophys. Acta* **1986**, *850*, 275-285. c) Kirmaier, C.; Holten, D.; Debus, R.J.; Feher, G.; Okamura, M.Y. *Proc. Nat. Acad. Sci. (USA)* **1986**, *83*, 957-961. d) Kirmaier, C.; Holten, D. in "The Photosynthetic Bacterial Reaction Center: Structure and Dynamics," Breton, J.; Vermeglio, A. eds., Plenum, New York, NY: 1987.

33. a) Gunner, M.R.; Robertson, D.E.; Dutton, P.L. *J. Phys. Chem.* **1986**, *90*, 3783-3795. b) Gunner, M.R.; Dutton, P.L. *J. Am. Chem. Soc.* **1989**, *111*, 3400-3412.

34. Rehm, D.; Weller, A. *Isr. J. Chem.* **1970**, *8*, 259-271.

35. a) Calcaterra, L.T.; Closs, G.L.; Miller, J.R. *J. Am. Chem. Soc.* **1983**, *105*, 670-671. b) Miller, J.R.; Calcaterra, L.T.; Closs, G.L. *J. Am. Chem. Soc.* **1984**, *106*, 3047-3049.

36. Kakitani, T.; Mataga, N. *J. Phys. Chem.* **1986**, *90*, 993-995.

37. a) Oevering, H.; Paddon-Row, M.N.; Heppener, M.; Oliver, A.M.; Cotsaris, E.; Verhoeven, J.W.; Hush, N.S. *J. Am. Chem. Soc.* **1987**, *109*, 3258-3269. b) Warman, J.M.; deHaas, M.P.; Paddon-Row, M.N.; Cotsaris, E.; Hush, N.S.; Oevering, H.; Verhoeven, J.W. *Nature* **1986**, *320*, 615-616. c) Hush, N.S.; Paddon-Row, M.N.; Cotsaris, E.; Oevering, H.; Verhoeven, J.W.; Heppener, M. *Chem. Phys. Lett.* **1985**, *117*, 8-11. d) Verhoeven, J.W. *Pure and Appl. Chem.* **1986**, *58*, 1285-1290.

38. Huppert, D.; Kanety, H.; Kosower, E.M. *Faraday Disc. Chem. Soc.* **1982**, *74*, 161-175.

39. a) Kosower, E.M.; Huppert, D. *Chem. Phys. Lett.* **1983**, *96*, 433-435. b) Kosower, E.M.; Huppert, D. *Ann. Rev. Phys. Chem* . **1986**, *37*, 127-156.

40. Simon, J.D.; Su, S.-G. *J. Phys. Chem.* **1988**, *92*, 2395-2397.

41. a) Hubbard, J.; Onsager, L. *J. Chem. Phys.* **1977**, *67*, 4850-4857. b) Hubbard, J. *J. Chem. Phys.* **1978**, *68*, 1649-1664.

42. a) Kahlow, M.A.; Kang, T.J.; Barbara, P.F. *J. Phys. Chem.* **1987**, *91*, 6452-6455. b) Kang, T.J.; Kahlow, M.A.; Giser, D.; Swallen, S.; Nagarajan, V.; Jarzeba, W.; Barbara, P.F. *J. Phys. Chem.* **1988**, *92*, 6800-6807.

43. Heitele, H.; Michel-Beyerle, M.E.; Finckh, P. *Chem. Phys. Lett.* **1987**, *138*, 237-243.

44. a) Gennett, T.; Milner, D.F.; Weaver, M.J. *J. Phys. Chem.* **1985**, *89*, 2787-2794. b) McManis, G.E.; Weaver, M.J. *Chem. Phys. Lett.* **1988**, *145*, 55-60.

45. Joran, A.D., Doctoral Dissertation, California Institute of Technology, Pasadena CA: 1986.

46. Leland, B.A., Doctoral Dissertation, California Institute of Technology, Pasadena CA: 1987.

47. a) Joran, A.D.; Leland, B.A.; Geller, G.G.; Hopfield, J.J.; Dervan, P.B. *J. Am. Chem. Soc.* **1984**, *106*, 6090-6092. b) Leland, B.A.; Joran, A.D.; Felker, P.M.; Hopfield, J.J.; Zewail, A.H.; Dervan, P.B. *J. Phys. Chem.* **1985**, *89*, 5571-5573.

48. The fluorescence lifetime of zinc (II) porphyrins is determined mostly by the rate of intersystem crossing. a) Seybold, P.G.; Gouterman, M. J. *J. Mol. Spect.* **1969**, *31*, 1-13. b) Dilung, I.I.; Kapinus, E.I. *Russ. Chem. Rev.* **1978**, *47*, 43-53.

49. a) Ponterini, G.; Serpone, N.; Bergkamp, M.A.; Netzel, T.L. *J. Am. Chem. Soc.* **1983**, *105*, 4639-4645. b) Callis, J.B.; Gouterman, M.; Jones, Y.M.; Henderson, B.H. *J. Molec. Spect.* **1971**, *39*, 410-420.

50. Joran, A.D.; Leland, B.A.; Felker, P.M.; Zewail, A.H .; Hopfield, J.J. ; Dervan, P.B. *Nature* **1987**, *327*, 508-511.

51. Specifically, the time-dependent fluorescence intensity I(t) was fit to a biexponential such that

$$I(t) = \sum_{i=1}^{N} \frac{1}{N} \exp\left[-t\left(\cos^2\theta/\tau_1 + 1/\tau_2\right)\right] + \frac{b_o}{a_o} \exp\left[-t/\tau_2\right]$$

where N is the number of angles (usually 10), τ_1 and τ_2 the lifetimes of the two exponential components, and b_o/a_o is the ratio of the two exponential components.

52. Beratan, D.N; Goldman, C.. personal communication.

53. The picosecond spectroscopy was done in the laboratory of Dr. J. W. Perry at

Caltech's Jet Propulsion Laboratory, with the assistance of Dr. L. R. Khundkar. The system is a conventional single-photon counting apparatus, and is described further in chapter 10.

54. O'Connor, D.V.; Phillips, D. "Time Correlated Single Photon Counting," Academic Press, New York NY: 1984.

55. The observed slight (factor of 1.5) increase in the rate *could* be due to a decrease due to orientation effects combined with an increase due to distance and distance dependent driving force effects. The observed rates are in accord with the previously observed distance dependence as calculated for R_e; therefore, by Occam's Razor, this simpler model is preferred.

56. a) Silvers, S.J.; Tulinsky, A. *J. Am. Chem. Soc.* **1964**, *86*, 927-928. b) Fuhrhop, J.-H. *Struct. Bonding (Berlin)* **1974**, *18*, 1-67.

57. a) Axup, A.W.; Albin, M.; Mayo, S.L.; Crutchley, R.J.; Gray, H.B. *J. Am. Chem. Soc.* **1988**, *110*, 435-439. b) Mayo, S.L.; Ellis, W.R.; Crutchley, R.J.; Gray, H.B. *Science*, **1986**, *233*, 948-952. c) Crutchley, R.J.; Ellis, W.R.; Gray, H.B. *J. Am. Chem. Soc.* **1985**, *107*, 5002-5004.

58. a) Arrhenius, S. *Z. Phys. Chem.* **1889**, *4*, 226-248. b) Moelwyn-Hughes, E.A. "The Chemical Statics and Kinetics of Solutions," Academic Press, New York NY: 1971.

59. Lindsey, J.S.; Delaney, J.K.; Mauzerall, D.C.; Linschitz, H. *J. Am. Chem. Soc.* **1988**, *110*, 3610-3621.

60. a) Overfield, R.E.; Scherz, A.; Kaufmann, K.J.; Wasielewski, M.R. *J. Am. Chem. Soc.* **1983**, *105*, 5747-5752. b) Gust, D.; Moore, T.A.; Makings, L.R.; Liddell, P.A.; Nemeth, G.A.; Moore, A.L. *J. Am. Chem. Soc.* **1986**, *108*, 8028-8031. c) Gust, D.; Moore, T.A.; Liddell, P.A.; Nemeth, G.A.; Makings, L.R.; Moore, A.L.; Barrett, D.; Pessiki, P.J.; Bensasson, R.V.; Rougee, M.;

Chachaty, C.; DeSchryver, F.C.; Van der Auweraer, M.; Holzworth, A.R.; Connolly, J.S. *J. Am. Chem. Soc.* **1987**, *109*, 846-856.

61. There is some variation of the fraction of the two exponential components with temperature which suggests that some of the long lived component may be due to dielectric dispersion in the solvent even at room temperature. In support of this, extreme measures to exclude water from the solvent (sample preparation under argon) and addition of an oxidizing agent to the sample did not eradicate the long lived component.

62. Craik, D.J.; Adcock, W.; Levy, G.C. *Magn. Res. Chem.* **1986**, *24*, 783-791.

63. Bottcher, C.J.F. "Theory of Electric Polarization," Elsevier, Amsterdam: 1952.

64. Engler, B.P.; Harrah, L.A. *Sandia Report*, # **78-1414**.

65. Shinsaka, K.; Gee, N.; Freeman, G.R. *J. Chem. Thermodyn.* **1985**, *17*, 1111-1119.

66. Gee, N.; Shinsaka, K.; Dodelet, J.-P.; Freeman, G.R. *J. Chem. Thermodyn.* **1986**, *18*, 221-234.

67. Buckley, F.; Maryott, A.A. *Tables of Dielectric Dispersion Data for Pure Liquids and Dilute Solutions*, U.S. Dept. of Commerce, National Bureau of Standards Circular 589, Washington D.C. 1958.

68. a) Ritzoulis, G.; Papadopoulos, N.; Jannakoudakis, D. *J. Chem. Eng. Data* **1986**, *31*, 146-148. b) Geist, J.M.; Cannon, M.R. *Ind. Eng. Chem. Anal. Ed.* **1946**, *18*, 611-613.

69. Mopsik, F.I. *J. Chem. Phys.* **1969**, *50*, 2559-2569.

70. a) Reimschussel, W.; Abramczyk, H.; Baranska, H.; Labudzinska, A. *Chem. Phys.* **1982**, *72*, 313-319. b) Levy, C.; D'Arrigo, G. *Mol. Phys.* **1983**, *50*, 917-934. c) Samios, D.; Dorfmuller, T. *Chem. Phys. Lett.* **1985**, *117*, 165-170.

71. Time resolved emission studies have been done in *n*-butylbenzene down to 23 K for

ZnPLQ **2**. The temperature dependence of the rates above the glass transition in this solvent resembles that for toluene, but *n*-butylbenzene will glass (toluene freezes) and so allow optical studies to be performed down to very low temperatures. The decays become strongly non-exponential below the glass transition, but fluorescence quenching continued down to the lowest temperature the optical dewar could maintain.

72. The mass spectral data are for the reduced quinone. Reduction occurs during ionization under FAB conditions, a common occurrence for quinones.

73. Bruson, H.A.; Riener, T.W. *J. Am. Chem. Soc.* **1942**, *64*, 2850-2858.

74. Irie, H.; Tsuda, Y.; Uyeo, S. *J. Chem. Soc.* **1959**, 1446-1459.

75. Krapcho, A.P.; Long, A.J. *Tet. Lett.* **1973**, 957-960.

76. Swenton, J.S.; Blankenship, R.M.; Sanitra, R. *J. Am. Chem. Soc.* **1975**, *97*, 4941-4847.

77. Morita, K.-I.; Kobayashi, T. *J. Org. Chem.* **1966**, *31*, 229-232

78. Suzuki, Z.; Morita, K. *J. Org. Chem.* **1967**, *32*, 31-34.

79. Nace, H.R.; Monagle, J.J. *J. Org. Chem.* **1959**, *24*, 1792-1793.

80. Harris, D.; Johnson, A.W.; Gaete-Holmes, R. *Bioorganic Chem.* **1980**, *9*, 63-70.